THE UNIVERSITY OF
WARWICK

University of Warwick institutional repository: http://go.warwick.ac.uk/wrap

A Thesis Submitted for the Degree of PhD at the University of Warwick

http://go.warwick.ac.uk/wrap/3065

This thesis is made available online and is protected by original copyright.

Please scroll down to view the document itself.

Please refer to the repository record for this item for information to help you to cite it. Our policy information is available from the repository home page.

ACOUSTIC NOISE FROM SMALL ELECTRONICALLY COMMUTATED MOTORS

Mark Brackley

Thesis submitted for the examination for the degree of Doctor of Philosophy

School of Engineering

University of Warwick

Coventry CV4 7AL

May 2001

This copy of the thesis has been supplied on condition that anyone who consults it is understood to recognise that the copyright rests with its author and that no quotation from the thesis and no information derived from it may be published without the prior written consent of the author or the University (as may be appropriate).

TABLE OF CONTENTS

LIST OF FIGURES AND TABLES

CHAPTER 6

GLOSSARY OF SYMBOLS

ξ	Damping ratio
ω_n	Undamped natural frequency
ϕ_f	Field flux
a	Acceleration of a stator
ψ_a	Armature Flux Linkage
B	Resultant Flux Density
B_x	Flux Density in the direction x
B_y	Flux Density in the direction y
c	Viscous damping coefficient
E_a	Induced armature voltage
ψ_f	Field Flux Linkage
F	Resultant Maxwell Stress Force
F_n	Radial force
F_x	Maxwell Stress Force in the direction x
F_y	Maxwell Stress Force in the direction y
I	Sound intensity
I_0	Threshold of hearing intensity
I_a	Armature current
I_f	Field current
i_f	Instantaneous value of field current
i_t	instantaneous value of armature current
J	Current Density
k_c	Coupling coefficient
k	Stiffness coefficient
L'_{pA}	Surface averaged A-weighted sound pressure level
L'_{pAi}	A-weighted sound pressure level measured at the *i*th microphone position
m	Equivalent mass of stator
N	Number of microphone positions
N_a	Number of armature turns
N_f	Number of field turns
N_r	Number of rotor poles

N_s	Number of stator poles
P	Sound pressure level
P_0	Threshold of hearing (reference atmospheric pressure)
P_{in}	Input power
P_{out}	Output power
p_t	Instantaneous output power
P_{iron}	Iron losses
R_a	Resistance of armature winding
$\Re_n$	Reluctance of magnetic circuit
R_f	Resistance of field winding
ω	Rotor speed
T_{av}	Average electromechanical torque
T	Period of a resonant frequency
Δt	Small time step
t	Time interval between commutation edges
T_c	One half of a period of a resonant frequency
V_s	Supply voltage
v_a	Instantaneous voltage applied to an armature winding
x	Displacement of stator

ACKNOWLEDGEMENTS

Thanks are due to Vent-Axia Ltd and Sifan-Torin Ltd for the supply of fan components and test equipment, and to all the members of the Centre for Advanced Electronically Controlled Drives. My sincere thanks also extend to Professor Charles Pollock for his consistent supervision, to my colleagues in the Power Electronics and Drives Research Group, and to Rebecca Shaw for her support and encouragement throughout.

ABSTRACT

An analysis of acoustic noise in electronically controlled variable speed drives is presented. The causes of vibration and acoustic noise in switched reluctance motors are discussed and it is shown that brushless d.c. motors can produce resonant vibration and acoustic noise by similar mechanisms.

The flux switching motor is introduced. This new class of reluctance motor is an advance on the established switched reluctance motor, retaining many of its benefits, but with a simpler and cheaper power electronic converter. The phase windings and method of flux control are different and tests are performed to quantify the effect on the acoustic noise produced. Measurements of acoustic noise are made on one flux switching motor and one 2-phase switched reluctance motor, made from the same laminations and mechanical components. It is shown that the flux switching motor produced 2dB less acoustic noise under the same conditions. Finite element analysis is used to calculate the radial force profiles of the two motors during normal rotation, and further analysis of this data provides evidence to support the experimental results. The experimental results go on to show how the acoustic noise from a second flux switching drive was found to be comparable to that of a split phase induction motor.

CHAPTER 1

INTRODUCTION

1.1 Introduction

Acoustic noise is an environmental issue, which is becoming increasingly important in the modern world. Noise is considered to be a pollutant and reducing it has been the focus of attention for some time. It is a problem in many parts of industry, because of its effects on the workforce, and its effects on the local community. Because of the high public profile of environmental issues, low acoustic noise is now a marketing feature for many products. Given the choice between a quiet and noisy product, the customer will almost certainly chose the quiet one.

The main focus of this thesis is on the production of acoustic noise from brushless motors. Many applications are particularly sensitive to acoustic noise. A good example of such an application is ventilation equipment using fans and blowers, which may be situated in quiet places such as the home or office. They may be operating continuously or automatically switched on and off as required. As well as considering the total noise emitted by such an appliance, the frequency content of the noise must be considered also. A motor which emits a single tone noise, as is the trend with reluctance motors, will probably be considered unacceptable in this application.

Acoustic noise in a work or home environment can have adverse effects on people [1]. Fatigue and loss of concentration are symptoms of exposure to acoustic noise. In more serious cases, hearing loss is experienced. This can happen in a number of

ways. High intensity sounds (such as explosions) can cause the eardrum to rupture, resulting in irreversible damage. Exposure to a loud noise for a limited time causes a short term loss of sensitivity. The ear recovers relatively quickly after this type of exposure and no long-term damage occurs. However, exposure to noisy environments for long periods of time, such as people at work may experience, can cause permanent hearing loss over a period of years.

Clearly there is a need for low acoustic noise motors in industrial, commercial and domestic products. There is also a demand for longer lifetime, higher efficiencies, lower weight and variable speed control from drives. There are many motor technologies available, each with advantages and disadvantages. As is often the case in engineering, trade offs and compromises are needed to best suit a motor to an application.

Understanding and reducing acoustic noise from brushless electronically controlled drives such as switched reluctance, flux switching and brushless d.c. drives allows the potential advantages of each to be exploited. Because these motors are not generally commutated with sine wave current, they are more susceptible to acoustic noise than, say, the induction motor. The characteristics of acoustic noise in common motor technologies are discussed in chapter 2.

1.2 Objectives

The main objectives of this thesis are to:

- Review the topic of acoustic noise relating to electric motors
- Report on advances by the author in the reduction of acoustic noise from switched reluctance drives.
- Report on advances in brushless d.c. motor acoustic noise reduction
- Introduce the new flux switching motor technology
- Evaluate the acoustic noise produced by two flux switching motors
- Compare the acoustic noise production of a flux switching motor with a switched reluctance motor.
- Identify by simulation any similarity or differences between the radial force and vibration production of the flux switching motor and the switched reluctance motor.

Initially, a brief introduction to the format of this thesis will be given, followed by an introduction to sound and sound measurement.

1.3 Format of Thesis

This thesis has eight chapters, including this introductory chapter, and a list of references.

Chapter two reviews the electromagnetic, mechanical and aerodynamic sources of vibration and acoustic noise in some common types of electric motor. These include induction motors, brushed d.c. machines, universal motors, switched reluctance and brushless d.c. motors. Known acoustic noise reduction methods are also described.

Chapter three provides an introduction to the structure and operation of the switched reluctance motor. It goes on to describe the main source of acoustic noise in this type of machine, and reviews the existing electronic cancellation techniques for reducing acoustic noise from the machine stator. Further to this, the chapter describes new work by the author that extends the application of the acoustic noise cancellation technique from the stator of the motor, to any coupled component that has resonances excited by motor commutation. A fan application driven by a single phase switched reluctance motor is described and results from the reduction of vibration and acoustic noise from the fan housing are presented.

The fourth chapter describes the structure and operation of the brushless d.c. motor. A case study is presented which shows that the brushless d.c. motor can be susceptible to discrete frequency acoustic noise problems, similar to those experienced in switched reluctance machines, when commutated with trapezoidal current. A technique is proposed for altering the commutation of the motor in the time domain to avoid exciting mechanical resonances, and a low cost implementation

scheme is given. Experimental results showing the reduction of acoustic noise and vibration are presented and discussed.

Chapter five introduces a new class of electric motor known as the flux switching motor. This motor is a combination of the switched reluctance motor and the inductor alternator. Its construction and method of operation are described, and typical converter topologies presented. The chapter goes on to investigate the detailed design of an external rotor flux switching motor, for a low acoustic noise application, using finite element analysis (FEA). Particular attention is paid to the torque and radial force profiling by the geometric design of the lamination. Simple electromagnetic equations are solved to predict the performance of the motor for a particular winding design. Some experimental measurements of flux are made and compared with those predicted by the FEA simulation method, to validate the model.

Following this, chapter six briefly presents the design of a 2-phase external rotor switched reluctance machine, to be compared to the external rotor flux switching motor designed in chapter 5. Both machines are constructed from the same laminations and mechanical parts. The natural resonant frequencies associated with the motors, and the acoustic noise they produce when driving a fan are measured. The electrical performance and the levels of acoustic noise recorded are compared and discussed.

In the latter part of this chapter, the design of an internal rotor flux switching motor is presented. This motor has been constructed from spare parts (including the stator stack) from a split phase induction motor. Its electrical performance and acoustic

noise produced are measured and compared against the induction motor it originated from. Again, a fan application was used to test the motors.

Chapter 7 describes a finite element simulation of the radial forces in the external rotor two-phase switched reluctance motor and the external rotor flux switching motor using measured current excitation waveforms. The simulation shows how the second differential of total radial force, which is the impulse to the vibration equation, differs between the two machines. An analysis of the effects of the lamination geometry on the radial force profile is also given, and suggestions made as to how the rotor and stator pole geometries could be improved.

The final chapter draws together conclusions reached throughout the thesis and reiterates the main achievements. The author's contribution to knowledge in the analysis and reduction of acoustic noise in switched reluctance motors, brushless d.c. motors and flux switching motors is highlighted, and areas for future work suggested.

Chapter 1 now concludes with an introduction to sound, vibration and sound measurement.

1.4 Sound and Vibration

Sound is a phenomenon that surrounds us every day, yet the basic physics of sound were not understood at all two hundred years ago. The first measurement of the speed of sound in air was made by French mathematician Marin Mersenne around 1640, but it wasn't until the pioneering work by early physicists such as Helmholtz

(1821-1894) and Lord Rayleigh (1842-1919) that sound was explained by defining it as a wave motion. Effects such as echoes and diffraction were explainable using wave motion theory and analogies were made with light and other forms of electromagnetic radiation.

A sound wave in air is made up of variations in pressure above and below that of the undisturbed gas. If a point source produces a disturbance, under normal conditions it will propagate as a spherical wave at a speed of around $330ms^{-1}$ (increasing with temperature). The sound *intensity* falls by the square of the distance from the source.

1.4.1 Sound Quantities

There are two widely adopted quantities in the measurement of sound - sound *intensity* and sound *pressure*. Sound intensity is defined as the sound power per unit area. Most sound intensity measurements are made relative to a standard threshold of hearing I_0, at a frequency of 1kHz, where

$$I_0 = 1x10^{-12}\ Wm^{-2} \tag{1.1}$$

This value has a wide acceptance as a nominal standard threshold (minimum sound that can be heard) and corresponds to 0dB. Sound measurements are usually quoted using the dB scale and so a measurement of sound intensity is calculated from the relationship:

$$I(dB) = 10\log_{10}\left[\frac{I}{I_0}\right] \tag{1.2}$$

Where I Sound intensity in Wm^{-2}

I_0 Threshold of hearing intensity in Wm^{-2}

The sound power associated with a constant source is the amount of energy released, as sound, to the surroundings per second. However the surrounding environment is very important in shaping what happens to the sound wave once it has left the source. Sound reflection, refraction and diffraction all affect the resultant sound waves and the characteristics of the sound will change with listening position. Another measurement unit is therefore needed to take the effects of the surroundings into account. The second standard unit of measurement is sound pressure level (SPL).

Sound pressure is defined as the amount of pressure variation relative to atmospheric pressure. Atmospheric pressure is the standard threshold of hearing and is quoted as:

$$P_0 = 2\text{x}10^{-5}\ \text{Nm}^{-2} \tag{1.3}$$

As with sound intensity, sound pressure level is usually quoted in decibels and therefore a measurement of sound pressure level (dB) can be calculated from the following relationship.

$$P(dB) = 10\log_{10}\left[\frac{P^2}{P_0^{\,2}}\right] \tag{1.4}$$

Where P Sound pressure level in Nm^{-2}

P_0 Threshold of hearing in Nm^{-2} (reference atmospheric pressure)

Sound pressure level is an instantaneous value at a position in space. Because the surroundings of a sound source affect the SPL, a system of sampling and averaging is used to obtain a value of SPL for a source.

1.4.2 Weighting Functions

The human ear can hear sounds at a range of frequencies, usually quoted as 20Hz – 20kHz. With age this range narrows, starting with the higher frequencies. The human ear does not possess a uniform sensitivity across its hearing frequency range, thus some frequencies will sound louder than others. Most sound measurements are taken to determine the effects of a sound on the human ear. To compensate for the ear's non-uniform sensitivity a set of frequency weighting curves have been compiled. When these are applied to measurements of SPL, they make the measuring device behave like the human ear. Most measuring instruments do this internally by means of electronic filters that emphasise certain frequencies. Because the sensitivity of the ear also changes with SPL, different weightings are used depending on the range of SPL's being measured. Figure 1.1 shows the internationally recognised weighting functions, A, B, C and D.

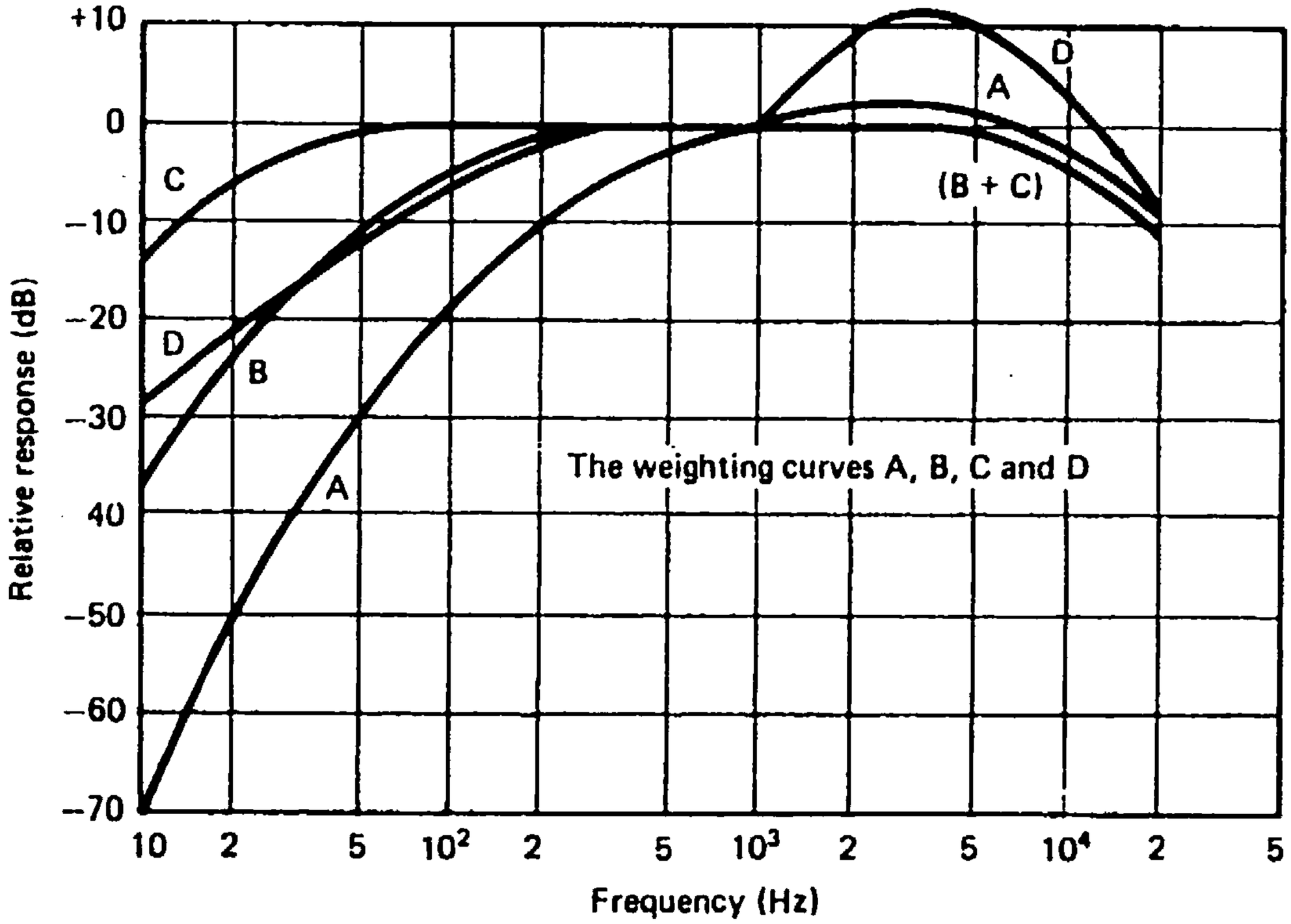

Figure 1.1: A, B, C and D weighting functions[1]

The 'A' weighting, although intended for SPL's of below 55dB, provides the best correlation with perceived loudness for most applications, and is the most common form of weighting function. The 'B' weighting function is designed for use with SPL measurements in the ranges 55-85dB, and 'C' weighting for SPL's above this. Occasionally a combination of both is applied to high SPL's. The 'D' function is specifically for measuring the noise of an aircraft at takeoff and during flight.

[1] Taken from: JD Turner and AJ Pretlove, *Acoustics for Engineers*, Macmillan,1991

1.4.3 Vibration

Vibration is the response of a surface to a force. Characteristics of the surface and the forcing determine the vibration produced and ultimately the acoustic noise radiated. Such surface characteristics are mass, damping coefficient, stiffness coefficient, and undamped natural frequency (natural resonant frequency). Essentially, the response of a surface to a forcing is dependent on three things:

- The magnitude of the forcing
- The proximity of the forcing frequency to a resonant frequency
- The level of correlation between the force distribution and the distribution of modal deflections.

1.4.4 Radiation Efficiency

When a surface is vibrating, the acoustic noise it produces depends on its radiation efficiency. Radiation efficiency is a measure of how much acoustic noise a surface can produce from a given vibration input. A large surface will usually have better radiation efficiency than a smaller one. As well as this, acoustic noise is also related to the surface velocity. Taking the two simple, extreme cases - when the natural wavelength of sound in air is much smaller than the typical wavelength of normal surface vibration, the sound power radiated is effectively proportional to the mean-square normal velocity. When the natural wavelength of sound in air is much greater than the typical wavelength of normal surface vibration, the sound power radiated is effectively proportional to the mean square normal acceleration. For most small motors, it can be assumed that the sound power is effectively proportional to the velocity of the vibrating surface.

1.4.5 Measuring Sound

Different methods of sound measurement are used in different circumstances. There are many instruments available, from a simple hand held device to fully computerised capture and processing hardware and software. The quality of the transducer and processing power dictate the accuracy of results obtainable. To obtain a detailed analysis of a sound, the magnitude of different frequencies must be measured. The Fast Fourier Transform (FFT) is used to transpose the sound, which is in the time domain, into a spectrum of frequencies, in the frequency domain. A simplified diagram of the measurement process is given in figure 1.2.

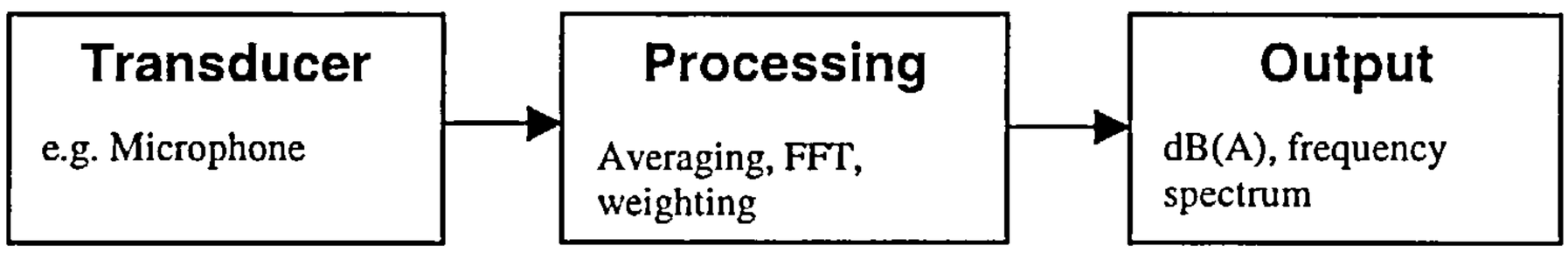

Figure 1.2: Sound measurement process

The output usually takes the form of a graphical display, which easily enables peak frequencies to be identified. The weighted average SPL (unit dBA) is generally used as a measure of how loud a sound is. Before embarking on sound measurement, it is useful to see a scale of common sounds and their dBA levels. Table 1.1 shows some examples:

Table 1.1: Sound Pressure Levels of various common sounds

SPL (dBA)	**Example of sound / *Comment***
194	*Maximum possible without going below a vacuum*
140	Gunfire at gunners ear
130	*Threshold of pain*
120	Pneumatic breaker
100	Heavy industry
80	Inside a bus
62	12" Ventilation fan (with single phase induction motor)
60	Normal conversation
50	Average office environment
30	Library
0	*Threshold of hearing (average young person)*

This clearly shows that in some situations, acoustic noise from electric motors may be insignificant in comparison with the surroundings. However, it also shows that if for example, an electric motor is employed in an office or library where the background acoustic noise is very low, any acoustic noise produced by motor will be highly significant. Thus matching a type of electric motor to an application, and an environment, is important.

CHAPTER 2

SOURCES OF ACOUSTIC NOISE AND VIBRATION IN ELECTRIC MOTORS

2.1 Introduction

The analysis and reduction of acoustic noise and vibration from electric motors has been the subject of publications over many years. Considerable knowledge has been gained in the sources of acoustic noise from a variety of different types of electric motor. These sources can be classified into three categories: 1) Electromagnetic, 2) Mechanical, 3) Aerodynamic. This chapter will review the sources of acoustic noise for some common types of electric motor. The analysis and measurement of acoustic noise in electric machines is a detailed topic and is summarised comprehensively by Yang and Ellison [2].

Initially the link between *acoustic noise* and *vibration* will be explored. Sound is generated by a moving surface causing a disturbance in air. This disturbance radiates out as a wave and, if it is within a certain frequency range, can be detected by the ear. In an electric motor, a surface must be moving or vibrating to initiate the disturbance. The movement of these surfaces will be referred to as the *vibration*. The resultant sound propagated by these surfaces will be referred to as the *acoustic noise*. In most cases, the frequencies of a vibration will match the frequencies of the acoustic noise it generates, sometimes with harmonics. Also, reducing the magnitude of the vibration of a surface reduces the acoustic noise it produces.

2.2 Mechanical Behaviour of a Stator

The stator of a machine can be subject to three types of vibration - torsional, axial and radial. Torsional vibration is caused by imbalanced forces, in the direction of rotation, around the airgap of a motor with salient poles. Pole skew, or the small variations in rotor speed caused by torque ripple are examples of how this type of vibration can exist. Axial vibration is usually an issue of greater importance in larger machines, particularly generators, where axial forces can be out of phase. The production of airborne acoustic noise is generally as a result of radial vibration of the stator surface. [3,4]

This chapter will highlight many sources of vibration and acoustic noise in electric motors. How these sources combine to produce a resultant vibration depends on the characteristics of the force and the characteristics of the stator structure. The mechanical stiffness, natural resonant frequency and vibration mode set the characteristics of the stator. Figure 2.1 shows the radial vibration modes M=0 to M=5 around the circumference of a stator. A vibration mode can be thought of as the number and spread of points on the stator circumference that move inward, move outward, or do not move at all. The various combinations of these movements are referred to as orders of vibration modes. Higher mode orders give rise to higher frequencies of vibration, but are harder to excite. Generally, for smaller machines, mode orders greater than 4 can be ignored [5].

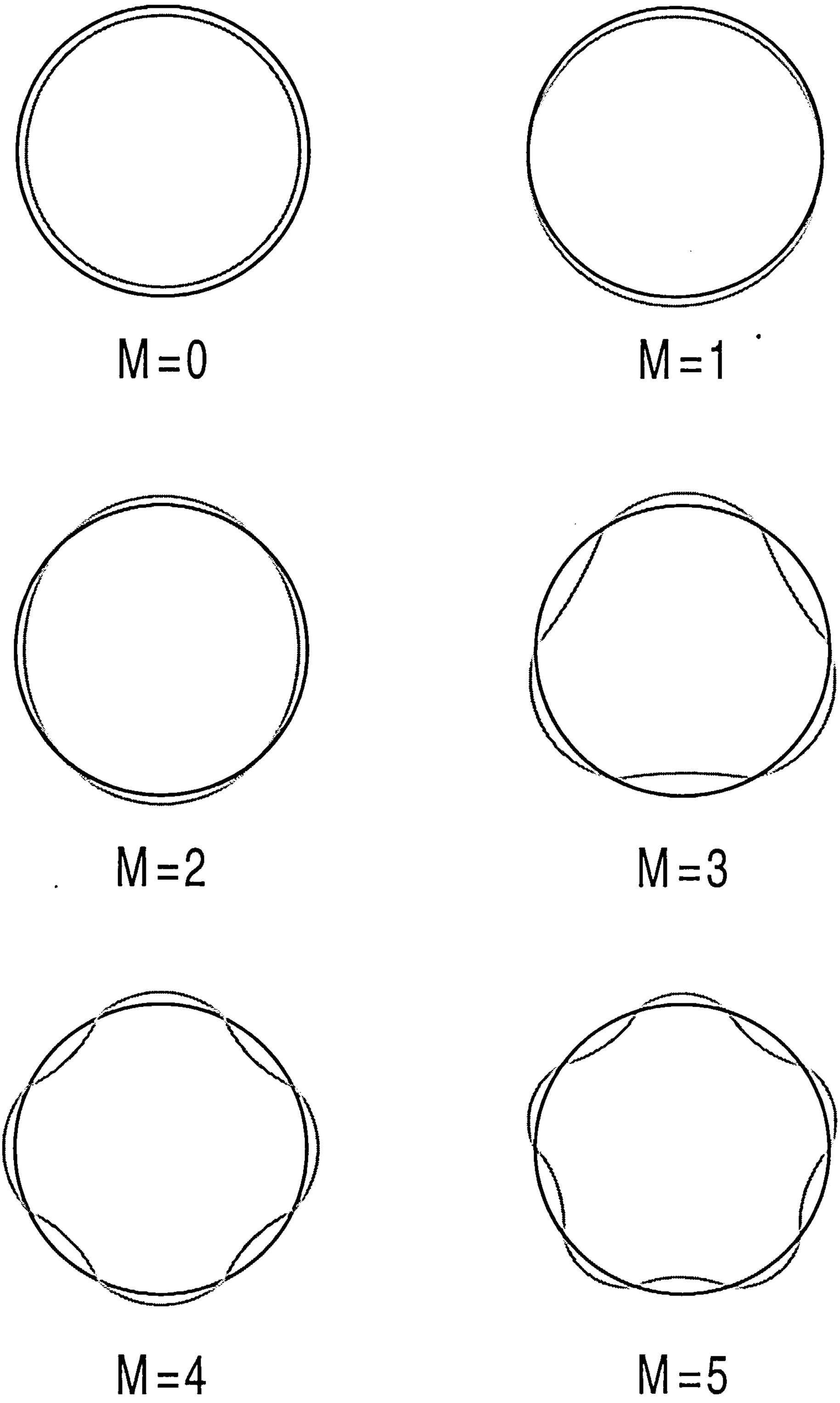

Figure 2.1: Radial vibration modes around the circumference of a motor stator

Much work has been done on the modelling and experimental analysis of vibrations in electric machines to gain a better understanding of their behaviour. Motor frame, laminations, stack length, teeth, and windings all affect the vibration response of a stator [6, 7, 8]. Prediction of stator resonant frequencies and vibration responses can help designers produce quieter machines. However, understanding the fundamental sources of vibration in a machine can help in reducing the excitation of those vibrations.

2.3 Vibration and Acoustic Noise of Electromagnetic Origin

There are many types of electric motor, each having its own merits and disadvantages. One factor common to them all, is the reliance on magnetic sheer stress to provide rotation. There are two methods of supplying this magnetic sheer stress. The first is produced when current flows through motor windings. The windings may be concentrated in one part of the motor, or evenly distributed around it. Further to this, the current supplied (therefore the torque produced) can vary with time in different ways. Common time variations include sinusoidal, constant, square-wave etc.. The second method of producing magnetic sheer stress is by the use of permanent magnets. Again, these can be distributed around the geometry of the motor in various ways, and their interaction depends heavily on this. The magnetic sheer stress produced by permanent magnets is dependent on reluctance and is therefore not necessarily constant.

The different methods of producing magnetic flux, give rise to different vibration and acoustic properties [9]. The remainder of this section will discuss the

electromagnetically induced vibration and acoustic noise produced by some common types of electric motor.

2.3.1 Three-Phase Induction Motor

The three-phase induction motor is widely used in industry. The stator is non-salient i.e. the stator teeth provide a constant airgap around the circumference, ignoring the small separations to allow the windings into the slots. It has a distributed three phase winding in the slots, providing a near sinusoidal space distribution of magnetic flux. The rotor can take two forms. The squirrel cage rotor and the wound rotor. A motor with the cage rotor shall be examined. If the stator windings are supplied with an a.c. sinusoidal current, having 120° phase shift per phase, a rotating magnetic field of constant amplitude is produced which will induce currents in the rotor to produce torque. The fundamental component of magnetic flux in the airgap is sinusoidally distributed around it and at any point will be varying sinusoidally with time. In small machines this produces little stator vibration and acoustic noise, as the low frequency gives rise to a low surface velocity, and is usually well below the first resonant frequency.

In the non-salient structure, the slots affect the uniformity of the airgap and therefore the reluctance of the magnetic circuit changes periodically with rotation. Also, magnetic saturation has a similar effect, causing fluctuations in the permeance of the airgap. Both these effects, which are not limited to the induction motor, cause harmonics in the sinusoidal flux, which causes increased acoustic noise and vibration at the harmonic frequencies.

When speed (frequency) control is applied to the three phase motor using an inverter, the currents produced are not perfectly sinusoidal and this can induce vibrations and acoustic noise at the carrier or mean carrier frequency. The effect is reduced if the carrier frequencies are made ultrasonic. Research into electronic control of induction motors is the subject of continuing work [10-14].

2.3.2 Single-Phase Induction Motor

The single-phase induction motor takes three common forms – split phase, capacitor run and shaded pole machines. They exist as different methods of starting the single phase motor. Each type has a cage rotor. The stator of the split phase and capacitor run motors has distributed windings, and the stator of the shaded pole machine has concentrated windings. By way of example, the capacitor run motor has a main winding and an auxiliary winding which is physically displaced by 90°. A capacitor ensures the winding currents have a phase displacement. Both windings are fed with a sinusoidal a.c. voltage, which sets up an alternating flux. This flux induces an alternating current in the rotor conductors, which in turn induces its own alternating flux, which opposes that from the stator. A resultant torque is developed as the motor speed increases because the flux induced in the rotor decreases and the flux produced by the stator increases. Instantaneous power pulsates at twice the stator supply frequency, consequently there are torque pulsations at double the stator frequency. These are in addition to the resultant torque described above. They arise from interactions between the time varying fluxes and MMF's in the motor rotor and stator. The pulsating torque does not add to the average torque, but rather causes small speed fluctuations. These, along with the effects of pulsating flux, produce an acoustic humming effect that is not present in polyphase machines [15].

Even with the effects described above, the level of stator vibration produced by sine wave fed induction machines is very small, because the fundamental component of magnetic flux varies smoothly. The application of electronic speed control causes greatly increased levels of acoustic noise. The triac converter, commonly used in low cost speed control for the single-phase induction motor, distorts the sinusoidal voltage waveforms applied to the stator windings. This in turn produces distorted flux patterns and results in increased acoustic noise at harmonic frequencies.

2.3.3 D.C. Machine

The stator of a d.c. machine carries a field winding which provides a symmetrical airgap flux along the pole axis. There are many individual windings on the rotor, which make up the armature of the machine, and the terminals are brought out to a mechanical commutator. Carbon brushes, in contact with the commutator, connect and disconnect a d.c. supply such that the MMF produced by the armature current is fixed in space, and therefore with respect to the stator. When the sides of an armature coil pass the centre of the region between stator poles, the commutator is set such that the current direction in that coil will reverse. As a consequence, the conductors under one stator pole all carry current in one direction and will produce MMF along the quadrature axis. If compensation for the armature reaction is applied, and ignoring other factors, then the resultant flux distribution in the airgap is constant between the stator poles, and zero outside them. This distribution of airgap flux does not vary with time and does not therefore induce any stator vibration. The torque produced by a d.c. machine is constant, and therefore no acoustic noise is induced in a load by torque production. The main source of acoustic noise and vibration in small d.c. machines is the action of the brushes on the armature

commutator. As the brushes wear, the acoustic noise becomes worse and sparking occurs. This also has an impact on the life of the machine. Further discussion is given in [16].

2.3.4 Single-Phase Universal Motor

The single-phase universal motor comprises a stator and rotor of the same form as the d.c. machine described above. It can be used with either a d.c. or a.c. source, but is most commonly used in domestic appliances with a single phase a.c. supply. Consider the case when an a.c. supply is connected to the motor windings. The field winding is connected in series with the commutator. Current flows through the field and armature windings, the field producing the pole flux, and the armature producing the quadrature flux. Although the a.c. current reverses in alternate half cycles, the instantaneous torque is unidirectional. If the effects of eddy currents are ignored, the instantaneous torque varies sinusoidally, between a positive value and zero, at twice the supply frequency [15]. This fluctuating torque induces acoustic noise from the machine system. The mechanical commutator provides the same disadvantages as described above. The speed of the series motor can be varied using a triac controller, which distorts the sinusoidal waveforms. As with the single-phase induction motor, this causes increased acoustic noise at harmonic frequencies.

2.3.5 Brushless D.C. Motor

The brushless d.c. motor comprises a non-salient rotor, often with surface mounted permanent magnets, and a stator which can either have concentrated or distributed phase windings. A common, low cost form of this machine is a three-phase motor fed with trapezoidal current. The constant flux provided by the permanent magnets

is the dominant airgap flux and this is little affected by armature current. The distribution of flux around the airgap of the motor is approximately rectangular, and rotates with the rotor. Fringing effects cause this rectangular shape to be more rounded at the edges. The fundamental component of flux varies smoothly and therefore does not induce much vibration of the stator. However torque ripple is produced by the switching of phase currents, and this may cause increased levels of acoustic noise. Some work has been done on the reduction of torque ripple and acoustic noise from the brushless d.c. motor by overlapping the switching of the phase currents [17]. The introduction of lamination skew for the reduction of radial forces is covered in a paper by Hanselman [18]. Further to this, the author has shown that the brushless d.c. motor is susceptible to a similar acoustic noise production mechanism as is present in the switched reluctance motor and this is described in Chapter 4 and in [19].

2.3.6 Switched Reluctance Motor

The switched reluctance motor comprises a stator and rotor which both have salient poles. The stator has concentrated phase windings which are the only source of MMF in this type of motor. The motor requires a power electronic converter to commutate the phase currents. When a phase current is flowing, the rotor will move to align its poles with the energised stator poles. Before this alignment position is reached, the phase must be switched off and the current rapidly decreased to zero. When the phase current is on, and the rotor poles are moving toward the stator poles, the reluctance of the airgap is decreasing, and the airgap flux increases. When the phase is switched off, the airgap flux decays to zero. The variation of flux in the airgap is therefore very large, and the radial force involved is approximately an order

of magnitude larger than the torque producing force, and so stator vibrations of comparatively large magnitudes are generated. In 1989, Cameron *et al.* showed that these stator vibrations were the most significant cause of acoustic noise from the switched reluctance motor [20]. The torque ripple in a single-phase machine, which is also a source of vibration, is very large although this decreases with increasing phase number. Cameron et al also showed that torque ripple was not a significant source of vibration and acoustic noise in the switched reluctance motor. In 1993, Pulle *et al.* showed that the instant of peak torque did not coincide with the instant peak radial force, and that by advancing the firing angle, the time between them could be extended further [21]. This coupled with rapid current decay and pole shaping reduced the acoustic noise produced. Physical techniques such as lamination skewing have also been shown to reduce stator deformation and therefore be beneficial to the reduction of acoustic noise [22]. An electronic cancellation technique exists to reduce stator vibration [23-25]. Chapter 3 looks in more detail at acoustic noise from the switched reluctance motor and the electronic cancellation of acoustic noise.

2.4 Mechanical Sources

2.4.1 Bearings

All electric motors produce some acoustic noise generated by mechanical sources. Bearings, of whatever type, produce acoustic noise due to friction between the moving and stationary parts. Sleeve bearings are considered to produce a low magnitude of acoustic noise. Rolling ball bearings produce considerably more acoustic noise and this may be significant in small, low power, high speed machines [5]. As bearings wear with use, the acoustic noise they produce increases. The

quality of ball-race bearings can vary considerably and factors such as lubricant selection, matched balls, polished raceways and shielding can increase the life, and decrease the acoustic noise produced. The housing of bearings is also important in the acoustic noise they produce. Bearings can be easily damaged during assembly. Pre-load must be applied to ball race bearings and thrust washers used with sleeve bearings to prevent axial movement. Oil impregnated sleeve bearings must not be allowed to dry out.

2.4.2 Concentricity

Concentricity of the rotor and stator parts is vital to maintaining a uniform permeance of the airgap around a motor of any type. Some types of motor will be less tolerant to misalignment than others. Because of the high radial forces present in the switched reluctance motor, any misalignment of the rotor and stator causes large increases in its acoustic noise production. The radial forces in an induction motor are smaller and vary smoothly making it slightly more tolerant to misalignment.

2.4.3 Rotor and Load Imbalance

Any imbalance of a rotating body will result in vibration. The primary cause of an imbalance is when there is a mismatch between the geometric centre of a body, and its centre of gravity. This will result in vibration from a machine, even if it is rotated by external means (i.e. not energised). An imbalance can cause the airgap in the motor to vary due to the centrifugal force, which will cause an increase in vibration from the motor's electromagnetic sources. If the shaft is not sufficiently stiff this can cause an imbalance when rotating due to the sagging effect in the centre which gives

rise to increased vibration and stress on the rotor material. It is also important to consider the balance of the rotating load as well as that of the rotor.

2.4.4 Resonance and Critical Speeds

A motor structure has a set of natural resonant frequencies. Some frequencies may lie within a range where their excitation could occur by the rotation of the rotor. Electromagnetic forces produced by commutation may excite others. Resonance occurs when an excitation force is provided which matches the resonant frequency or a multiple of it. This results in a greatly increased magnitude of vibration at this frequency.

The critical speed of a rotor is the speed at which the rotational frequency (revolutions per second) matches the rotor resonant frequency. At this speed a greatly increased magnitude of vibration is caused by the rotor 'wobbling' in a radial direction between its bearings. It is important that the critical speed of a machine is known, and that it is not within the operating speed range. Operation at, or near, the critical speed will not only cause increased vibration and acoustic noise, but will severely reduce the life of the bearings and could result in a rotor material failure.

Resonance, of one form or another, is the cause of much acoustic noise from electric motors because a relatively small excitation results in large magnitudes of vibration. Studies into the prediction of resonant frequencies of motor components (particularly stators) help machine designers avoid resonant frequencies that could be excited by motor commutation or speed range [2,26].

2.4.5 Brush and Commutator Noise

The main source of acoustic noise in the d.c. machine is the sliding friction and sparking between the stationary brushes and the rotating commutator surface [15]. A mechanical commutator is a considerable disadvantage compared with brushless motors because it also limits the life of the machine. As brushes become worn and the commutator surface degrades, the acoustic noise produced increases.

2.4.6 Simple Vibration Reduction Techniques

Vibration of an electric motor stator radiates acoustic noise from its surface. However such vibrations can cause acoustic noise from other surfaces if they are allowed to transmit through a structure. An example of this is an electric motor mounted on a bracket or base plate. If the method of mounting allows the transmission of vibration, the large surface area of the bracket or plate will radiate acoustic noise, which may be greater than that from the stator of the machine. Many products exist to dampen the transmission of vibration. Resilient mountings, flex-loc™, rubber bearing sleeves and filling compounds all dampen vibration, or isolate components with damping material. In commercial products, it is often easier and cheaper to stop the transmission of vibration, or at least dampen it, than to eliminate it at source.

2.5 Aerodynamic Sources

Acoustic noise from aerodynamic sources is airborne rather than structure borne. It will not result in vibration of the stator, unlike electromagnetic and mechanical sources. The profile of the noise contains discrete frequency components, which are related to motor speed, caused by the periodic disturbance of air by a rotating

member. This can be a salient rotor or a motor cooling fan. In non-salient machines, the only significant windage noise will be caused by the presence of a cooling fan, which will itself generate acoustic noise, and generate further acoustic noise if there are stationary objects in the air stream. In salient machines such as the switched reluctance motor the fan action of the rotating poles, particularly when rotating within salient stator poles, will be the main source of windage noise. Minimising this can be achieved by filling the rotor slots with a non-magnetic material, such as epoxy resin, to create a smooth cylindrical rotating surface. The windage noise generated by a motor is heavily speed dependent and if the speed is constant will not vary significantly with load [9].

2.6 Conclusion

There are many possible sources of acoustic noise in electric motors, some of which are easier to eliminate or minimise than others. In all cases it is the variation and distribution of magnetic flux in the machine airgap that determines the radial force exerted on the machine stator, and the instantaneous torque production. Generally, distributed windings and sinusoidal excitation currents cause less acoustic noise and vibration than concentrated windings and pulsed excitation, although each type of motor should be judged on its merits.

As the switched reluctance motor is considered to be one of the more noisy motor technologies, the next chapter will provide more detail of the acoustic noise production mechanisms, which are caused by virtue of its operation.

CHAPTER 3

THE SWITCHED RELUCTANCE MOTOR

3.1 Structure of the Switched Reluctance Motor

The switched reluctance motor comprises a stator and rotor, usually made from laminated steel, each having salient poles. The stator has phase coils placed around each pole. The currents in the phase coils are commutated electronically and there are no brushes or permanent magnets involved. The rotor and stator are aligned concentrically with a small airgap between them (in small machines typically 0.3-0.5mm). The switched reluctance motor can be designed with many phase and pole number combinations and investigations into the design choices and constraints have been published [27]. Figure 3.1 shows a simple diagram of a 4 stator pole, 4 rotor pole single phase switched reluctance lamination structure, with an internal rotor.

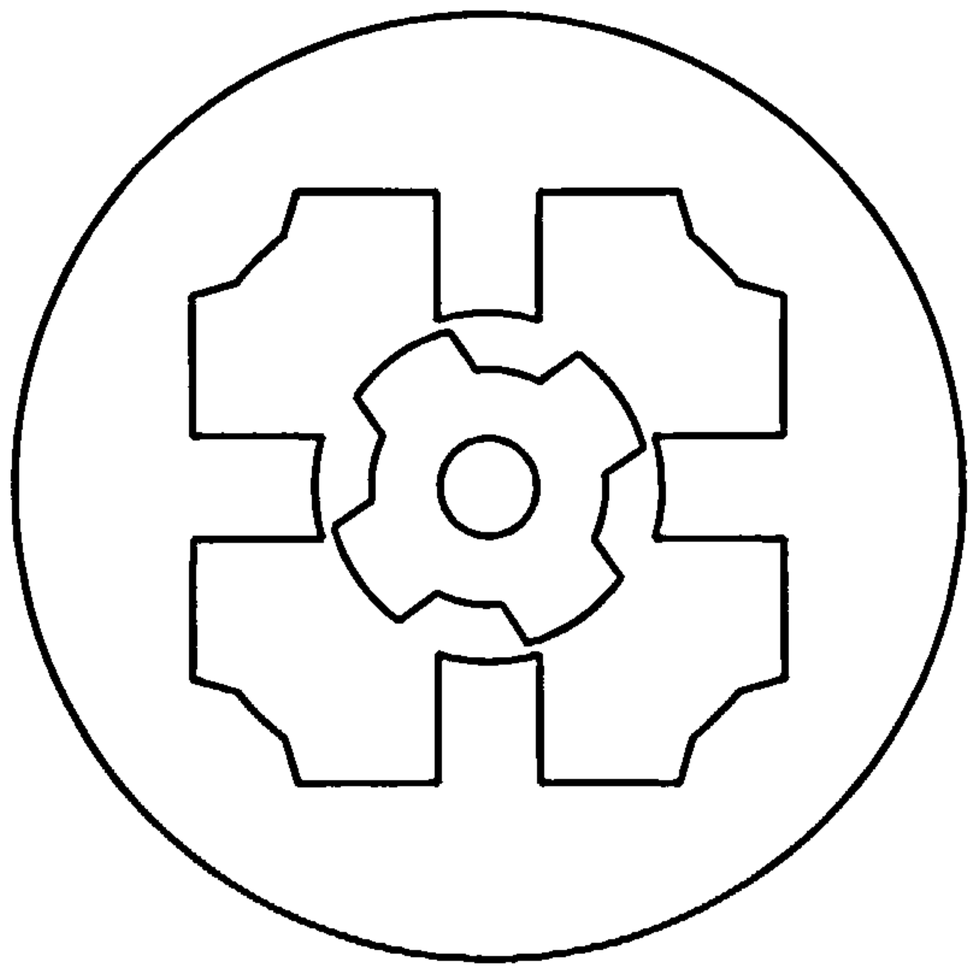

Figure 3.1: Simple 4/4 single phase switched reluctance lamination

The design of the rotor and stator pole geometry's [28] is the subject of many publications, but the general principles are covered by Miller [29]. The shape of the pole faces in the airgap changes motor operation. It has been shown that by grading the airgap between rotor and stator poles benefits in starting can be obtained [30,31]. This is because the range of rotor angles over which torque is produced in a particular direction is extended, at the cost of a lower average torque. Other pole designs may be aimed at producing high average torque, or a smoother torque output.

3.2 Principle of Operation

Figure 3.2(a) shows the 4/4 single-phase machine with a phase coil around each stator pole. When a voltage is applied to the phase coils, current flows and a magnetic flux builds up. The standard "dot and cross" convention has been used to show direction of current in each coil. The rotor will move to the position shown in figure 3.2(b) where the stator and rotor poles line up. This is known as the aligned position and is the position of minimum reluctance. Conversely, there is also a position termed "unaligned" where the rotor poles are exactly half way between stator poles, and the reluctance is maximum.

To create continuous rotation, the current in the phase coils must be supplied at the correct time such that the rotor is continuously being attracted in the direction of rotation. In order to do this, the position of the rotor relative to the stator must be known and this is most simply achieved by using a sensor. It should be noted that there is continuing work on the sensorless control of the switched reluctance motor, as the need for a sensor is considered a disadvantage [32].

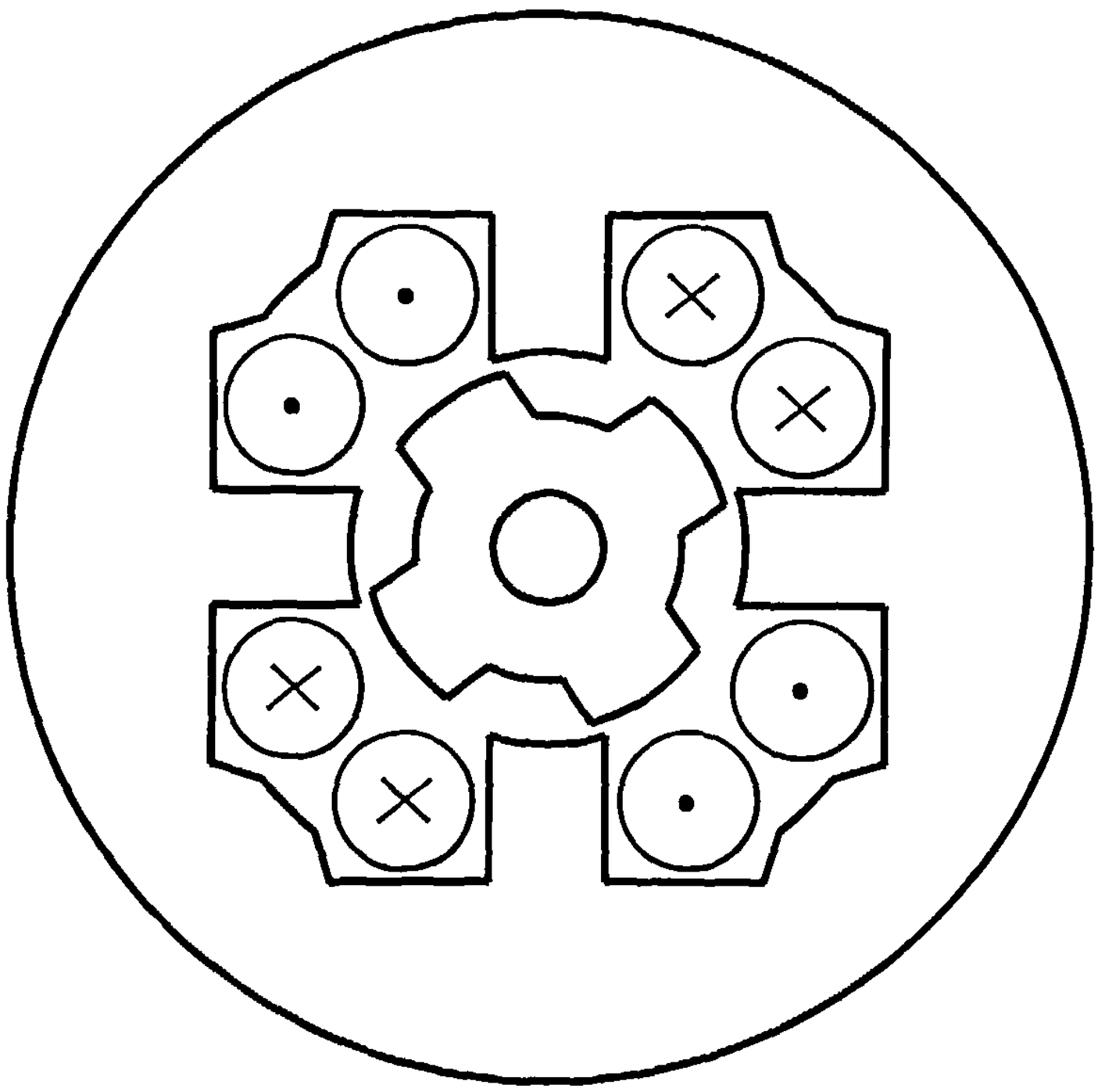

Figure 3.2(a): 4/4 machine with arbitrary rotor position

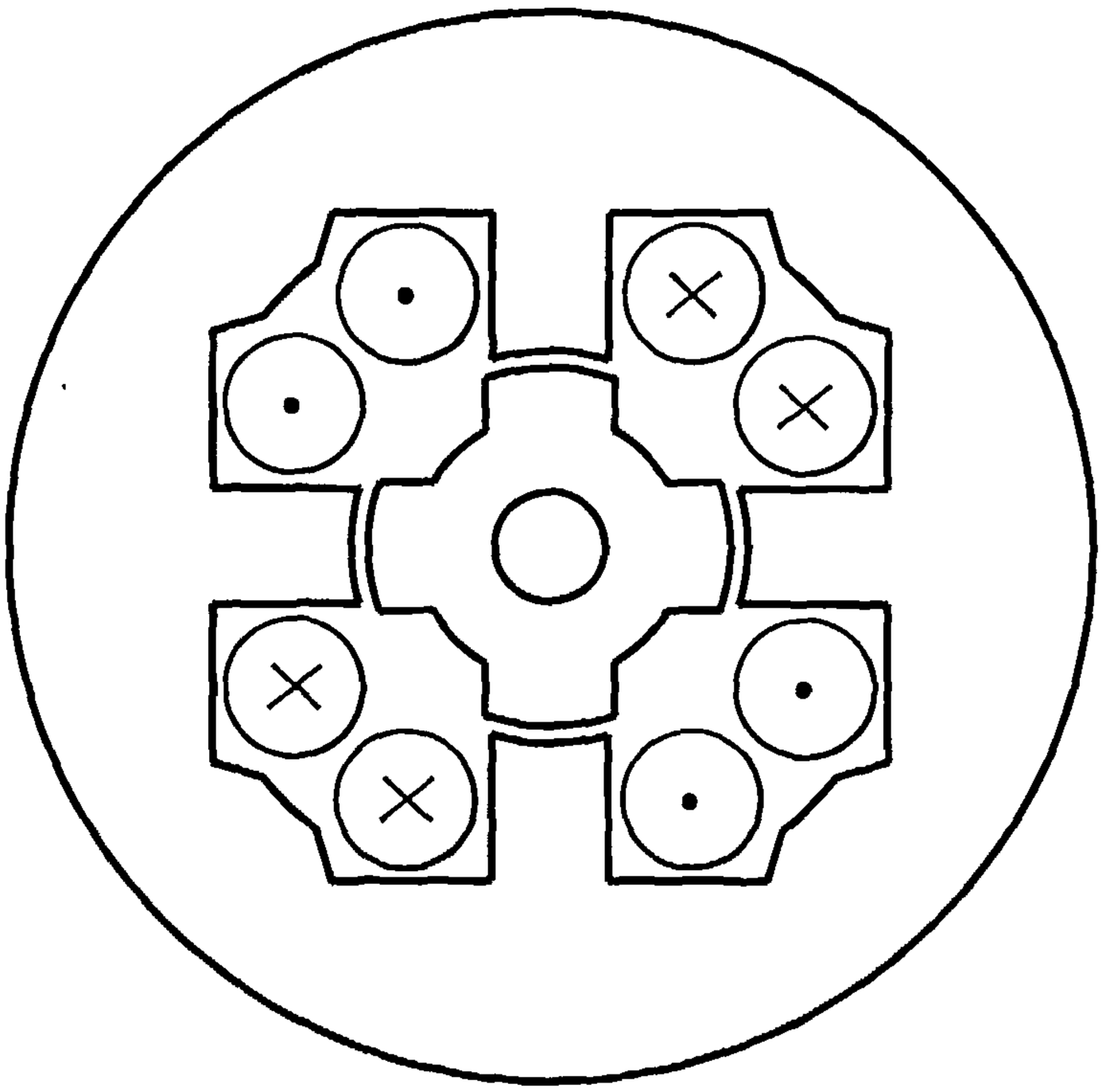

Figure 3.2(b): 4/4 machine with rotor in aligned position

3.3 Simple Converter Topology

In order to turn the phase voltage on and off at the correct times a power electronic converter is needed. The asymmetric half bridge circuit will be used to continue the single-phase example. Figure 3.3 shows the power schematic for the asymmetric half bridge circuit.

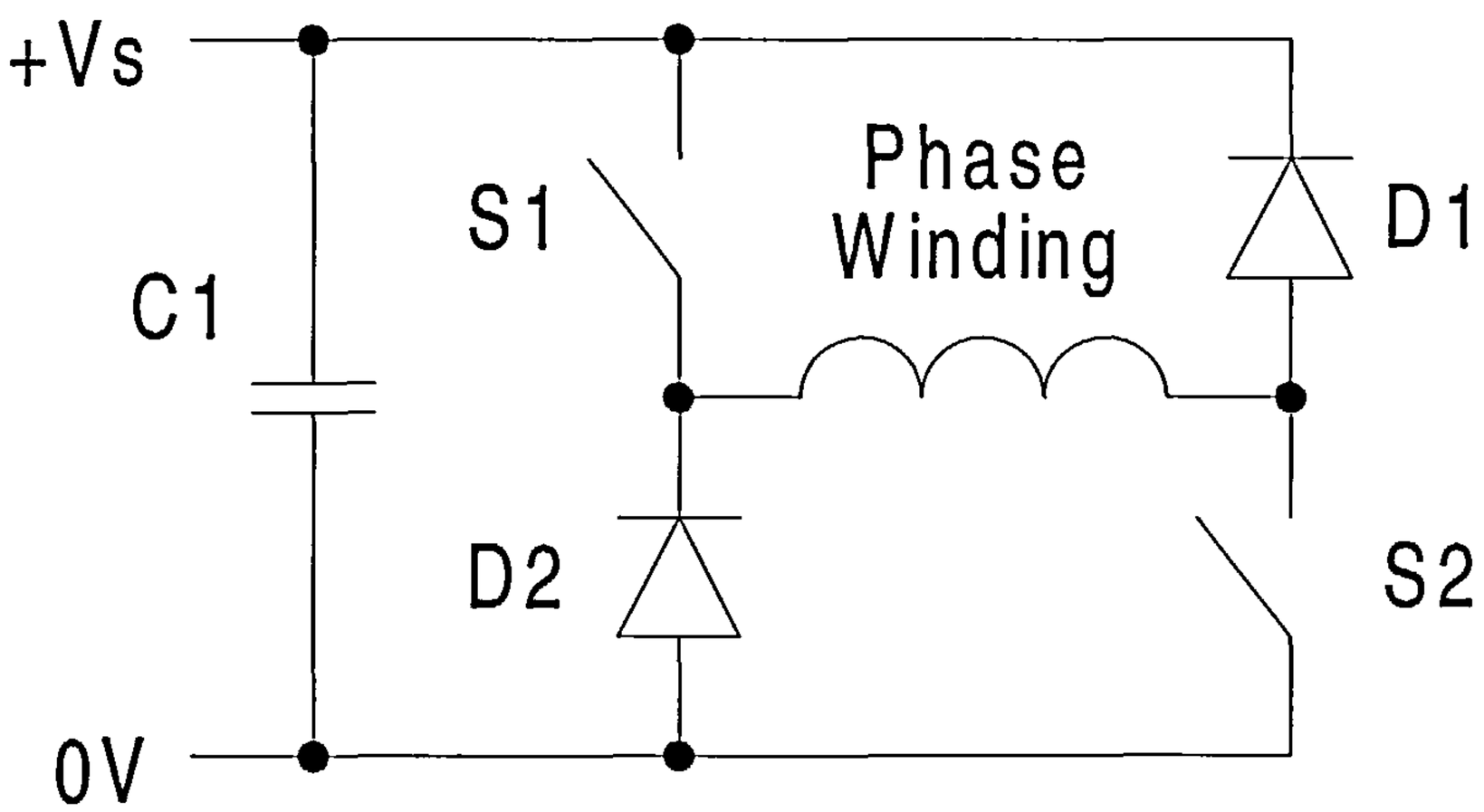

Figure 3.3: Single phase power circuit schematic

The circuit typically consists of two power switches (typically IGBT or MOSFET's) and two power diodes. The gate drives for the switches are not shown, but they decode a change in state of the position sensor and turn the power switches on or off. The circuit has three modes of operation. When both switches are turned on, supply voltage is seen across the phase winding, and phase current rapidly increases. When one switch is turned off, say S1, a zero volt loop condition is set up. The phase current continues to circulate around the freewheel path provided by the diode D2 and the other switch S2, with no energy being exchanged with the supply. When the second switch S2 turns off, the voltage across the winding reverses and the energy that is stored in the winding, due to its inductance, is transferred through the diodes

back into the d.c. supply until the phase current reaches zero. Switching techniques exist to control the phase current. As the current builds up the switches can be simultaneously opened and closed at a high (ultrasonic) frequency to apply and reverse the supply voltage to the phase, to limit the current flowing. This is known as "hard" chopping. Operating just one power switch in this way is known as soft chopping, utilising the zero volt loop capability of the circuit. There are other inverter topologies, and these are discussed in [33,34].

3.4 Forces in a Switched Reluctance Motor

When the windings are energised, there is a force of attraction between the rotor and stator poles causing the rotor to move into its preferred (aligned) position. This force of attraction can be resolved into two perpendicular components. These components shall be termed radial, acting across the airgap, and tangential, acting around it. At any time, the resultant force acting on a rotor pole is equal and opposite to that acting on a stator pole. Depending on the mechanical properties of the rotor and stator, this force may cause one or both parts to undergo a shape deformation in an attempt to close the airgap between them.

The tangential and radial forces in a switched reluctance motor will be dealt with separately, although in reality they exist together as components of a resultant force.

3.4.1 Tangential Force

The tangential force in a motor, is the torque producing force. If constant torque production at every rotor position were possible, then the tangential force would not contribute to acoustic noise at all. However in operating the switched reluctance

motor, the instantaneous torque created varies as the machine turns. This effect is known as torque ripple. If the machine is running at constant speed, the torque ripple will cause small variations in the instantaneous speed, which may induce vibration in the machine structure. The magnitude of the tangential force is an order of magnitude less than the radial force, which is responsible for producing the majority of vibration and hence acoustic noise in the switched reluctance motor.

3.4.2 Radial Force

Radial force is the undesirable effect of producing torque. It does not contribute to the torque producing force or act to improved performance of the motor. Common switched reluctance machines will have a rotor turning inside the stator. Because of its cylindrical shape, the stator structure is less stiff in the radial direction, than the rotor. Section 2.2 refers to the behaviour of a stator with respect to its various modes of radial vibration. Depending on the number of poles in the machine, the radial force associated with commutation can cause deformation of the stator shape by one or more modes. A motor with a higher number of poles will undergo a higher mode of deformation, which is harder to excite. The excitation of modes of vibration is the dominant cause of acoustic noise in the switched reluctance machine.

The theory of this type of stator deformation usually assumes that the radial forces around the machine are balanced i.e. each rotor and stator pole pair have the same force of attraction between them as the next pair. This relies on the assumption that the airgap of the motor is of constant width between the poles. In practice, perfect concentricity of rotor and stator is hard to achieve. This results in an asymmetric airgap where perhaps, one pole pair has a smaller airgap than a diagonally opposite

pole pair. The force between the first pole pair would be greater than that between the second, and the deformation that occurs may not be symmetrical. In the experience of the author, if the support structure (which holds rotor and stator together) is weak, the stator and rotor will move together to try and close the smallest airgap. Rather than exciting a mode of vibration, the stator moves as a whole causing a vibration at a different frequency, which can be the dominant source of acoustic noise.

3.5 Acoustic Noise and Vibration

There are many publications concerned with the analysis of acoustic noise from the switched reluctance machine [19, 35-38]. Cameron, Lang and Umans published one of the first studies into acoustic noise in 1989 [20]. They showed that the dominant source of vibration in a switched reluctance motor was caused by stator deformation. Mode M=1 and M=3 (refer to figure 2.1, Chapter 2) were excited in their tests, and were described as single ovalisation and double ovalisation. The stator vibration produced by these modes radiated acoustic noise at distinct resonant frequencies.

The normal operation of the switched reluctance motor is conducive to exciting vibration in one or more mode shapes. As current builds up in the phase winding, the rotor turns towards a position of alignment. During this time the radial component of force is increasing. As the point of commutation is reached, the radial force is at a maximum in the working stroke, and deformation of the stator geometry can occur. At the point of commutation, the rate of change of radial force reverses and releases the stator from its inward attraction. This induces a damped oscillation, causing the outer surface of the stator to radiate acoustic noise at a resonant

frequency linked to the mode of excitation. This occurs every working stroke and is probably considered the main disadvantage of the switched reluctance motor. Increasing the thickness of the stator back iron to improve the stiffness of the structure is one method of reducing the magnitude of deformation. Another is to select a machine with a higher number of poles which is less likely to exhibit the low mode orders of deformation which are easily excited. With the large radial forces involved in reluctance motor technology, concentricity and mechanical strength are important design requirements.

3.6 Stator Vibration Cancellation Technique

A technique has been developed by Wu and Pollock [23,24] to reduce the vibration and hence acoustic noise caused by ovalisation of the stator of a switched reluctance motor. Their early work determined that motor commutation caused vibration of the stator, at its natural resonant frequency. More specifically they discovered that it was a step change in the voltage applied to the phase windings, such as occurs to bring the current to zero, that caused the most significant magnitude of vibration. This is because the radial force between rotor and stator poles is high when this occurs, near the aligned position. The proposed technique electronically alters the motor commutation to reduce the vibration and acoustic noise radiated from the stator due to ovalisation.

To initiate phase winding commutation the voltage across the phase reverses. This causes the rate of change of force to reverse and the stator poles retreat causing the stator to undergo a damped oscillation. This oscillation occurs at a natural resonant frequency of the stator structure in accordance with its mode of vibration excitation

(section 2.2). The principle of active cancellation reverses the voltage across the phase winding in two controlled stages rather than one. This creates two damped vibrations of the stator which are arranged to be opposite in phase. The vibrations have a cancelling effect and therefore reduce the net vibration of the stator and its associated acoustic noise.

The 2 stage reversal of phase voltage is achieved by controlling the turn off of the two power switches in the asymmetric half bridge circuit. Figure 3.4 shows the gate control signals for normal operation and with active cancellation applied.

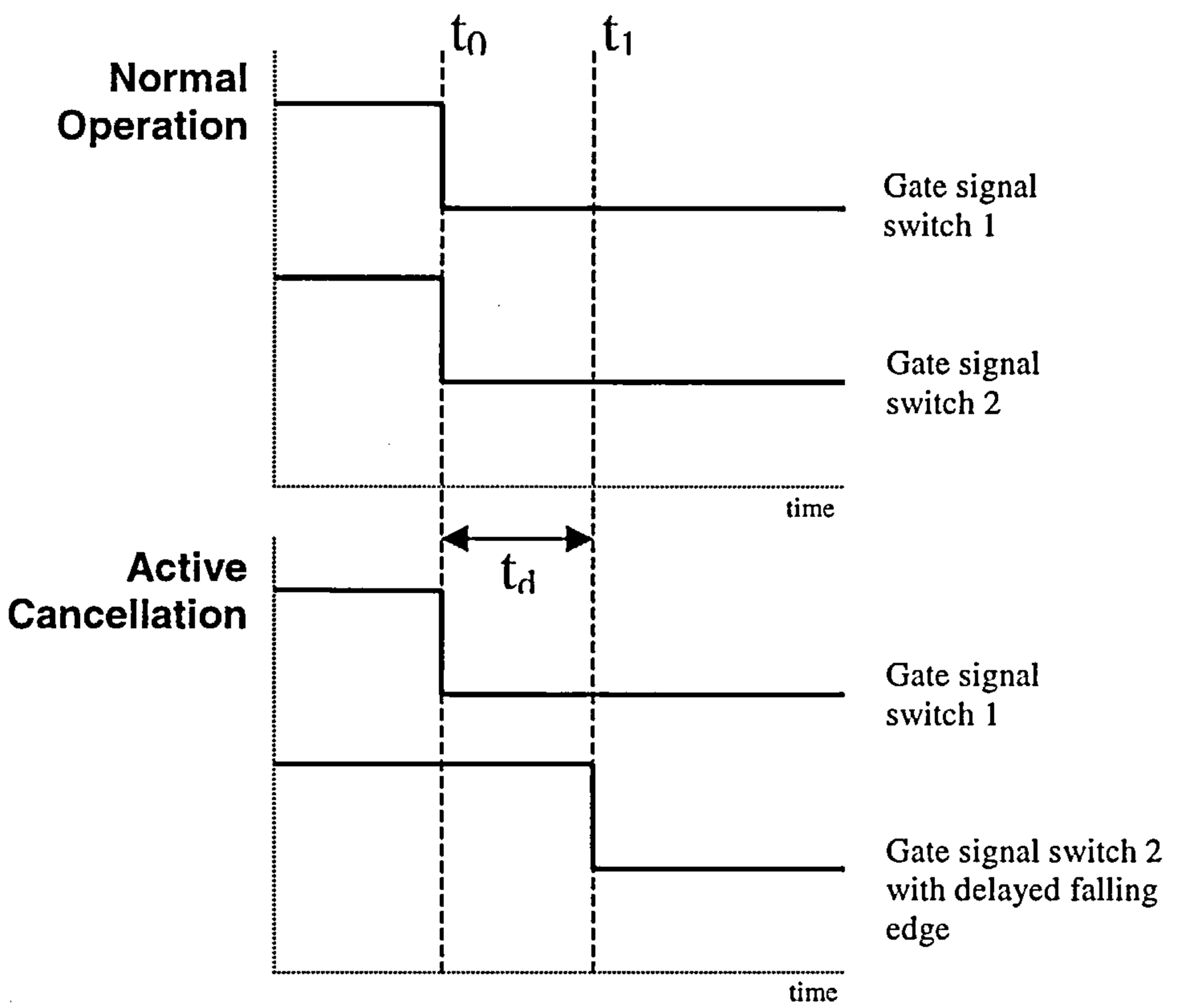

Figure 3.4: Gate control signals under normal operation and with Active Cancellation implemented

Let V_s be the supply voltage to the asymmetric half bridge. Under normal operating conditions, switches 1 and 2 turn off at t_0 simultaneously and the voltage across the phase windings changes from $+V_s$ to $-V_s$ in one step. Active cancellation turns switch 1 off at t_0 and then turns switch 2 off at t_1. The voltage across the phase winding changes from +Vs to 0V at t_0, creating the first vibration, and then from 0V to –Vs at t_1, creating the second. The two vibrations, which are at the stator natural resonant frequency, are a fixed time, t_d, apart. If t_d is set to one half of the period of the resonant frequency, the time will equate to a 180° phase shift and the two vibrations will have a cancelling effect, thus reducing the resultant vibration and acoustic noise from the stator. Figure 3.5 shows the stator vibration from a one phase switched reluctance machine (a) before and (b) after active cancellation was applied to a static, step voltage test. Also shown are the phase current and the frequency spectrum of the vibration in each case. Times t_0 andt_1 are marked.

(a)

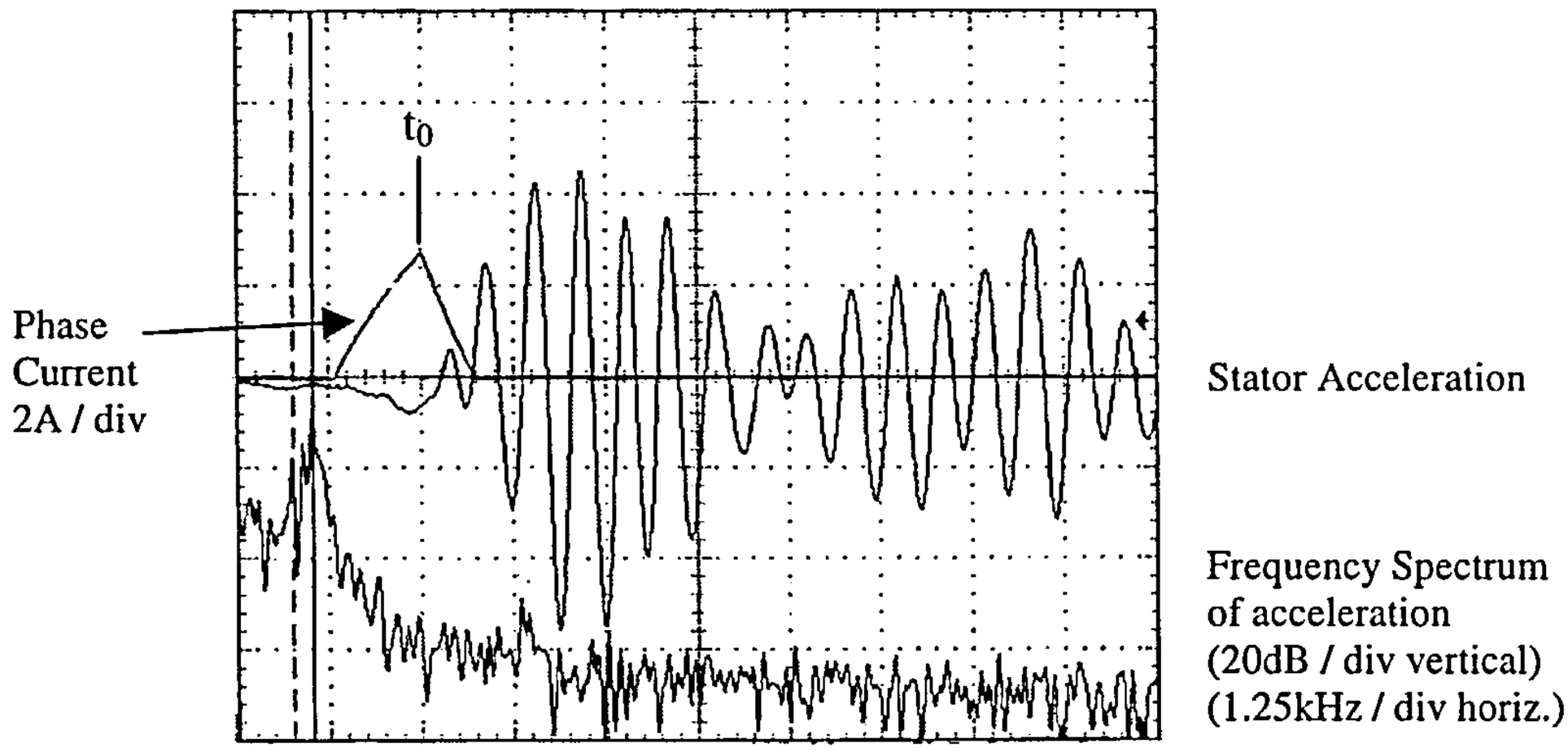

(b)

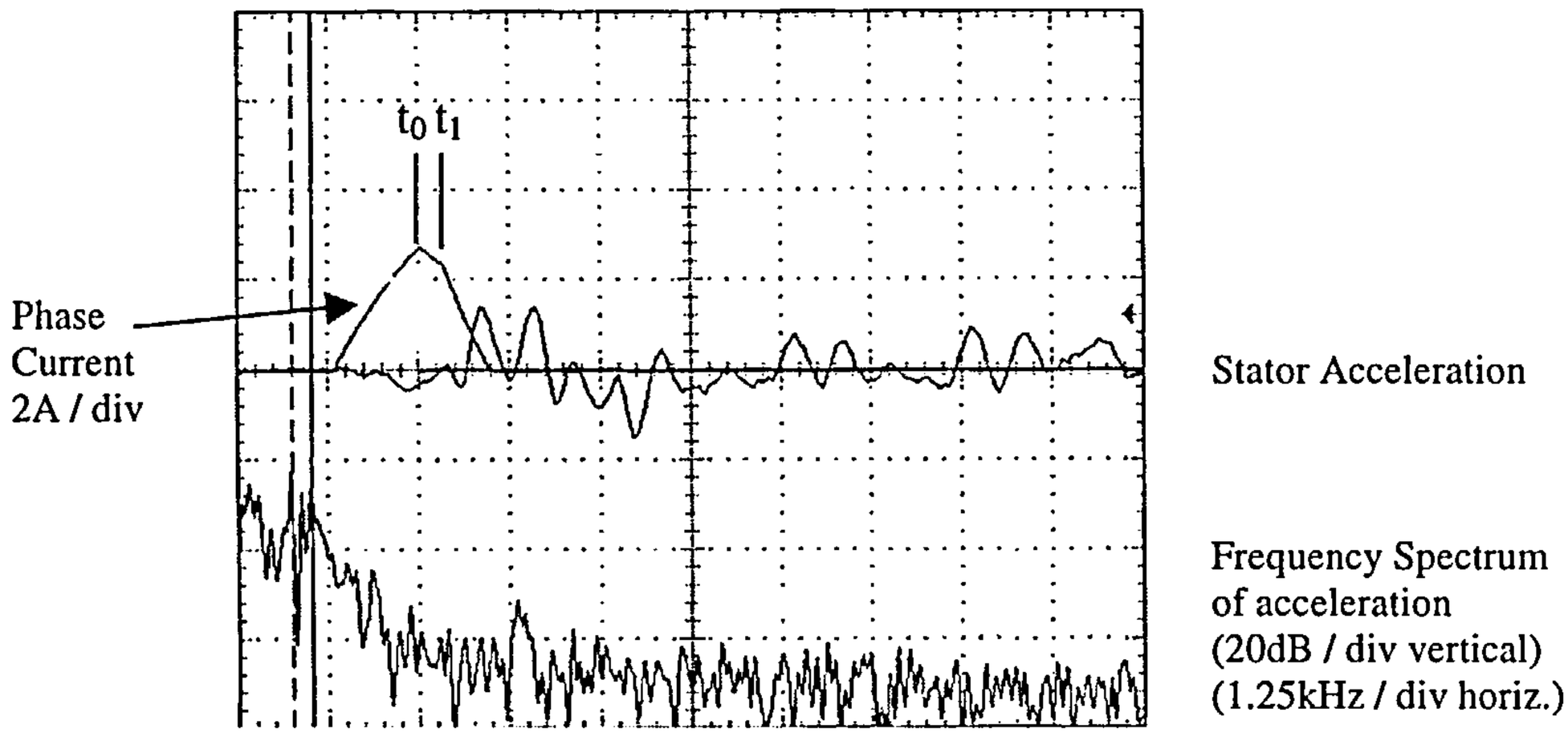

Figure 3.5: Motor current and vibration of an SR motor stator (a) without and (b) with active cancellation targeting the stator resonant frequency

Notice how the rate of decay of current is less between t_0 and t_1 as it is freewheeling around the circuit, and at t_1 it resumes a more rapid decay as the voltage across the winding is reversed.

The technique provides cancellation of stator vibration at one fixed frequency over the entire speed range of the motor. This frequency is the dominant (usually stator) natural resonant frequency, which has to be determined by external measurement as the cancellation topology does not have any measurement or feedback built in. The resonant frequency of the stator is set by its mechanical design and geometry and will only vary slightly between identical machines due to manufacturing build differences. Active cancellation is a very low cost acoustic noise reduction technique that could be implemented using just a resistor, capacitor and diode providing an RC time constant delay to the falling edge of one gate signal.

The theory outlined above was the basis for more work on acoustic noise cancellation and the technology was advanced by the development of a method of applying the technique under different converter control conditions and to circuits without zero volt loop capability. [27].

The author also extended the application of the acoustic noise reduction technology [39], using the single-phase machine described in section 3.5.1 controlled by the asymmetric half bridge circuit. This is outlined below.

3.7 New Application of Active Cancellation

Section 3.6 describes in detail the effect that motor commutation has on stator vibration and acoustic noise. When the voltage across the phase windings reverses, and the rotor - stator attraction is released, the stator oscillates at its natural resonant frequency. The release generates a force pulse which travels through the whole motor and anything mechanically coupled to it. The structure will have its own set

of natural resonant frequencies and under certain conditions can oscillate in much the same way as the stator, when excited with a force pulse. It is possible that another part of the motor or coupled system could cause a higher level of acoustic noise than that produced by the resonance of the stator.

The following sections relate to investigations carried out on a 4/4 single phase switched reluctance motor driving a fan in a hand-dryer application. The motor has a rated speed of 5000rpm and has an input power of approximately 250W. It drives a centrifugal fan, which is surrounded by a housing to duct the air flow. The motor is controlled by a standard asymmetric half bridge circuit. Figure 3.6 shows a picture of the arrangement.

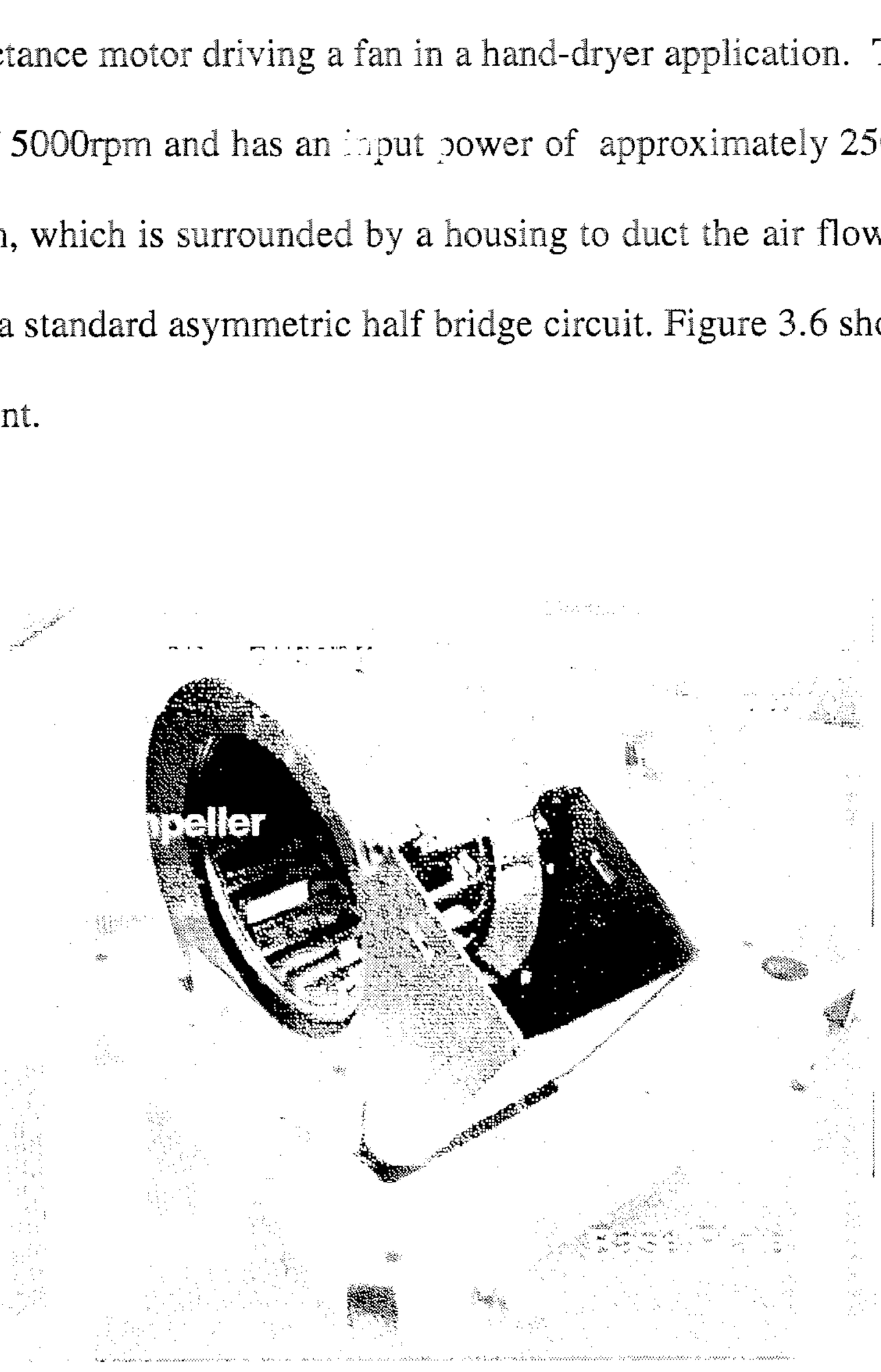

Figure 3.6: Picture of the prototype arrangement

3.7.1 Static Impulse Investigation

In an attempt to learn more about the fan system's resonant characteristics, a static pulse test was performed. Using a signal generator to supply the power electronic converter, current was pulsed, in a ramp up ramp down style, through the motor windings with the rotor stationary in the aligned position. The ensuing vibration was measured using an accelerometer. By moving the position of the accelerometer around the motor and fan system it was possible to identify resonant vibrations of the system components which were being excited by the pulsing motor current. Using a digital oscilloscope to perform an FFT on the accelerometer signal, a spectrum of its frequency content was produced. This static analysis revealed a motor stator resonant frequency of 650Hz and a fan housing resonant frequency of 976Hz. These were the only significant frequencies of vibration. The amplitude of the fan housing vibration was far greater than the vibration measured on the stator.

3.7.2 Investigation at Rated Speed

The motor was accelerated to its rated speed and the overall acoustic noise was measured with a microphone at a distance 0.3m. Figure 3.7 shows part of the frequency spectrum of the acoustic noise measured. The resonant frequencies of the stator at 650Hz and fan housing at 976Hz are marked.

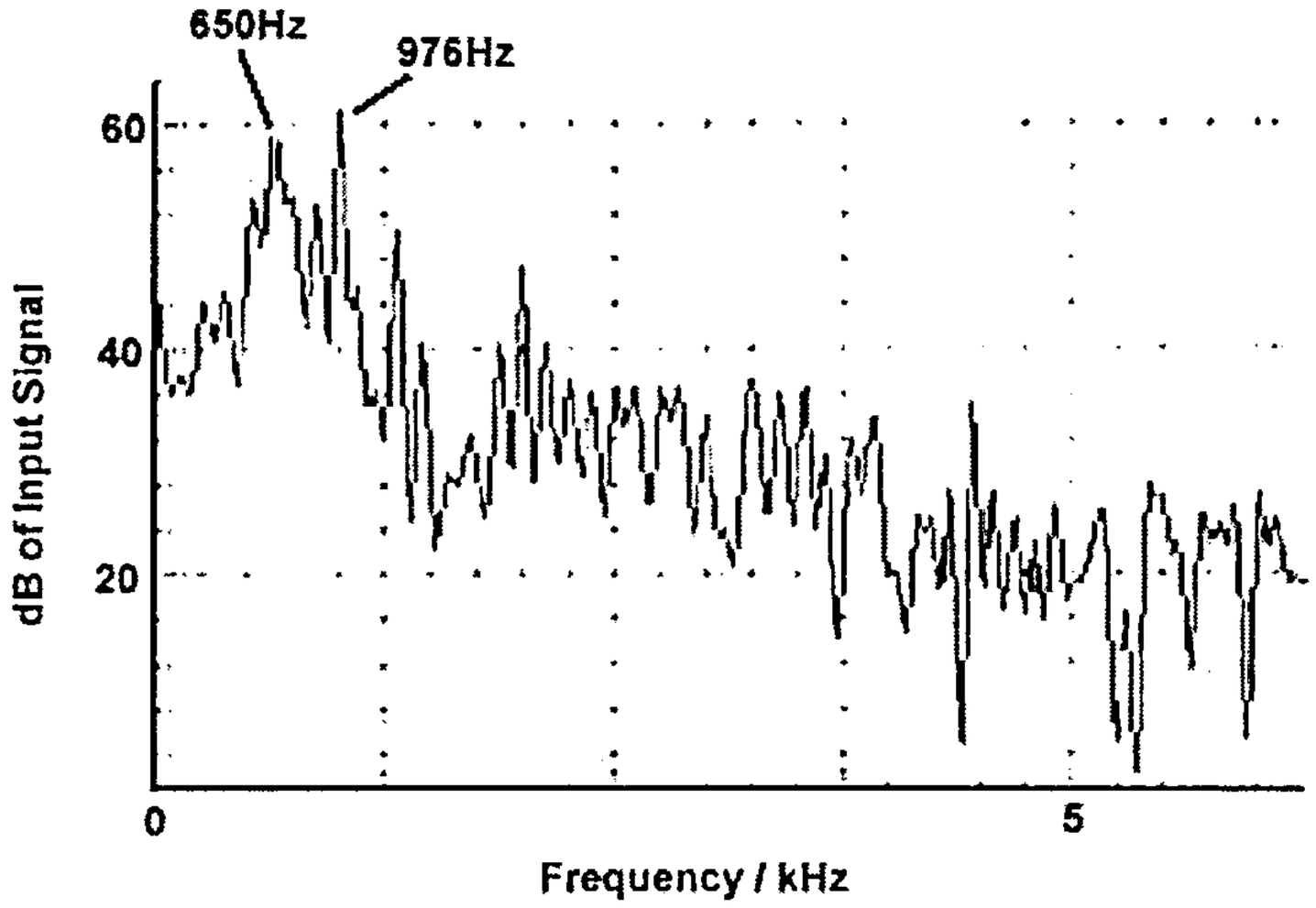

Figure 3.7: Power Spectrum of acoustic noise measured with a microphone at 0.3m

This confirms that the pure tone acoustic noise produced was attributable to the motor stator resonance, but more significantly, to the resonance of the fan housing. The motor commutation was exciting a mechanical resonance in the fan housing by the transmission of force pulses through the couplings. As this was the most significant source of acoustic noise, attention was focused on its reduction.

3.7.3 Reduction of Vibration and Acoustic Noise from the Fan Housing

As an extension of the prior art described in section 3.6, the active cancellation technique was applied to this motor. However, the target frequency for cancellation was **not** the resonant frequency of the stator (650Hz). Instead the resonant frequency of the fan housing, 976Hz, was targeted. This resonant frequency has a period T=1.025ms, thus one half of a resonant cycle, t_c = 512µs. The theory was that if a delay of t_c=512µs was introduced between the turn off of the two power switches, two forces would be pulsed through the coupled system which would set up and then cancel the vibration of the fan housing. The delay was set up such that it could be switched in and out with the motor running. Its' effect on the vibration of the fan

housing is shown in figure 3.8. Acceleration was measured with an accelerometer coupled to the fan housing. Figure 3.8 (a) is without cancellation, and (b) with cancellation.

(a)

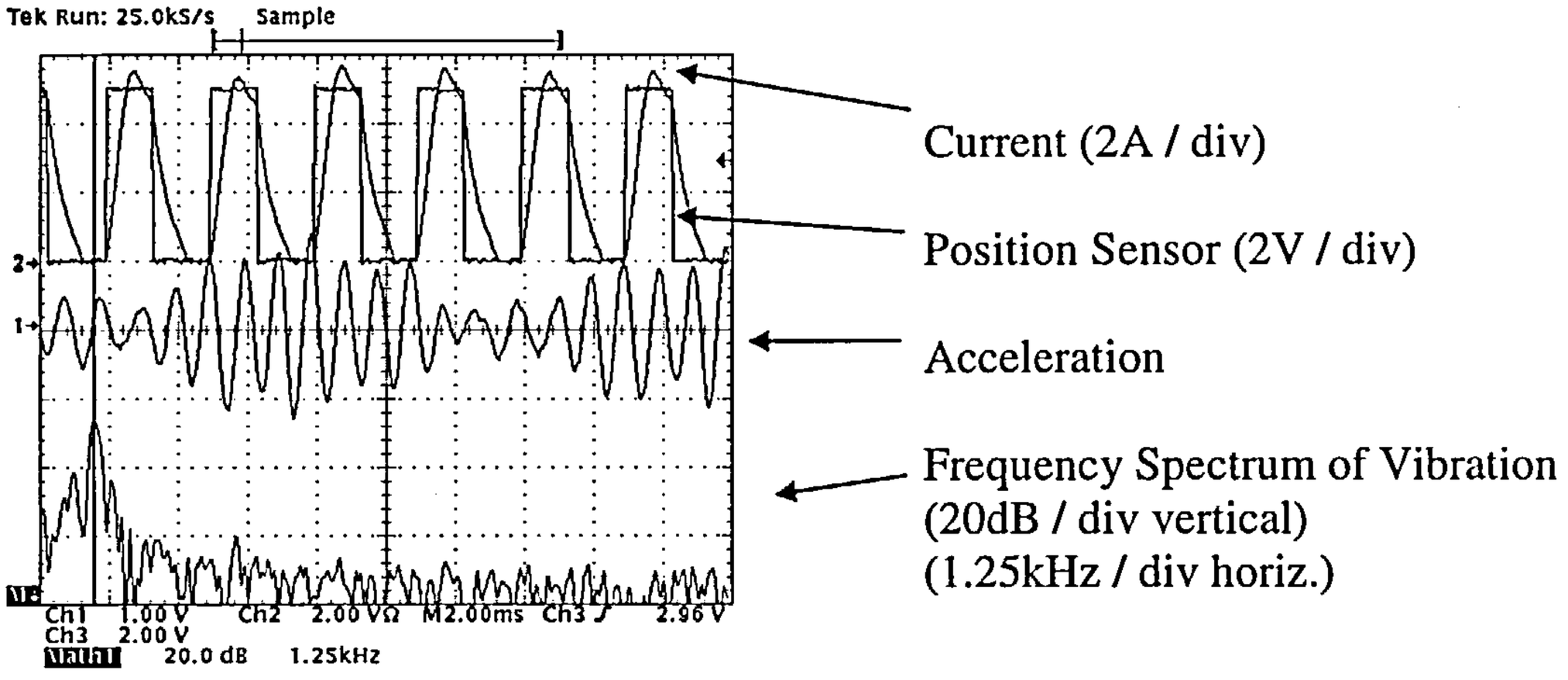

(b)

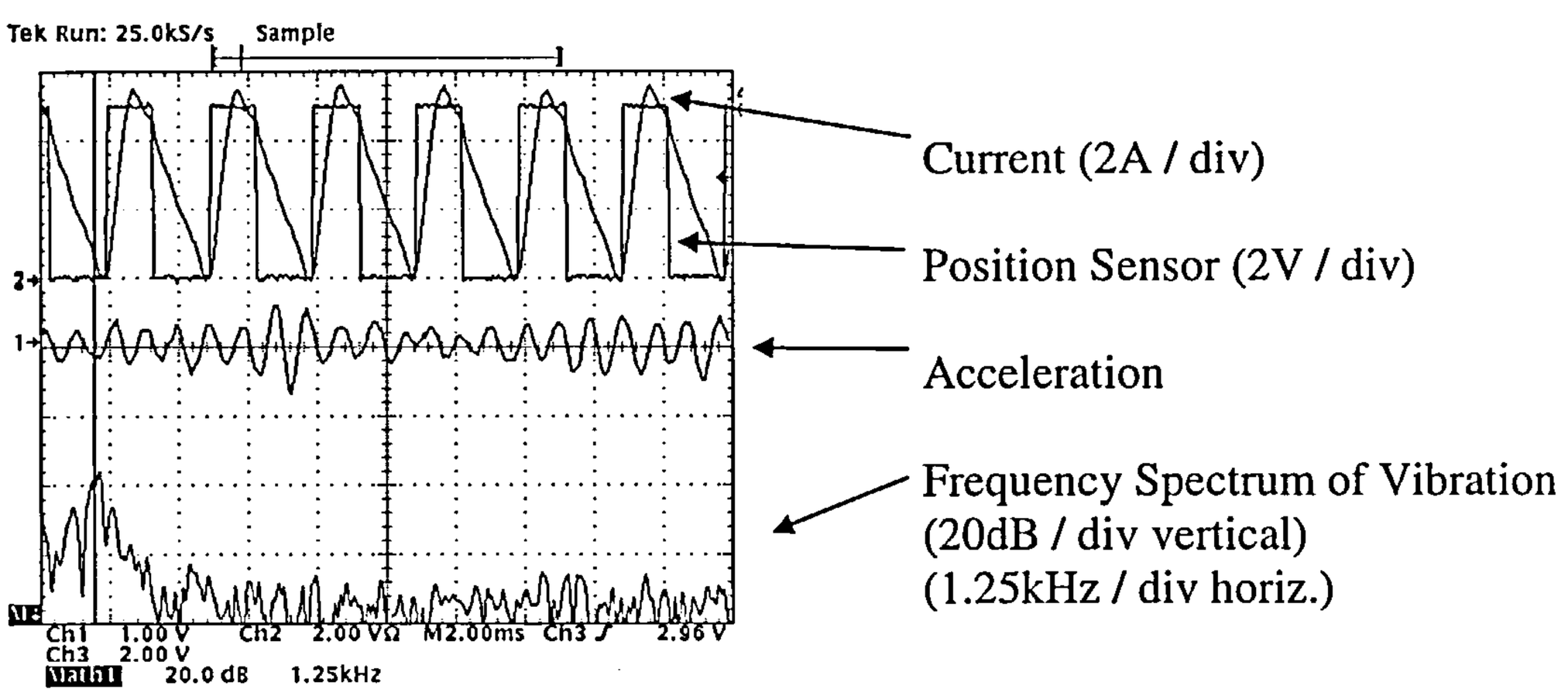

Figure 3.8: Motor current and vibration of fan housing (a) without and (b) with active cancellation targeting the fan housing resonant frequency

The resonant vibration measured on the fan housing has clearly been reduced and the harsh pure tone ringing that was present before has been suppressed. Analysis of the frequency spectrum reveals that the magnitude of the vibration of the fan housing at

the target frequency, 976Hz, has been reduced by 8-10dB. The apparent increase in magnitude of higher frequencies is created by signal noise and the sample point, and should be discounted. The significant reduction of the target vibration frequency clearly shows the power of this technique and the importance of extending its application beyond the limitations of the stator of the switched reluctance motor.

3.8 Conclusion

This chapter has explained the operation of the switched reluctance motor, using the example of a single-phase machine driven by an asymmetric half bridge converter. Switched reluctance motors are notoriously noisy and a brief description of the main cause of this acoustic noise, ovalisation of the stator, has been presented. Emphasis has also been placed on the accuracy and strength of the motor frame which can also contribute to acoustic noise.

Prior art has seen the development of an electronic noise reduction technique, for reducing the vibration and radiated acoustic noise from the stator of the motor at its natural resonant frequency. An overview of this technique, known as active cancellation, has been presented. It shows how motor commutation can be altered to create two force pulses, the second of which has a cancelling effect on the vibration induced by the first.

The final section explains the author's new work in extending the active cancellation technique. Previously, active cancellation has only been used to cancel resonant vibration of the stator of a switched reluctance motor. A fan application has been presented where the greatest source of acoustic noise was the resonant vibration of

the fan housing, caused by motor commutation force pulses. The author shows how active cancellation was applied to reduce the excitation of the fan housing resonance, thereby reducing the acoustic noise of the system.

CHAPTER 4

THE BRUSHLESS D.C. MOTOR

4.1 Introduction

The brushless d.c. motor is a well established drive used in many applications. Although acoustic noise is not considered to be an issue with this type of drive, an investigation by the author has shown that it is vulnerable to similar acoustic noise problems as the switched reluctance drive, particularly when driven with square wave current. Little work has been done on acoustic noise in brushless d.c. motors but schemes aimed at smoothing drive current to prevent torque ripple and vibration are the subject of patents [40,41]. The following sections will describe the research efforts carried out by the author, to examine the electrical excitation of mechanical resonances in a brushless d.c. motor, and the acoustic noise this produces. It also describes a low cost solution which has been implemented on a 3-phase brushless d.c. motor. This published chapter is based upon a paper [19].

4.2 The Brushless D.C. Motor

The brushless d.c. motor (with concentrated windings) comprises a stator, constructed from laminated steel, and a rotor carrying a permanent magnet ring. The stator has salient teeth and concentrated phase coils placed around each tooth. The rotor is a steel shaft carrying the permanent magnet ring. The ring is magnetised with magnetic poles (alternately North and South) around the circumference. The rotor rotates within the stator with an airgap between the stator teeth and the permanent magnet ring.

Phase coils placed around each stator tooth can be energised with bi-directional current to create either a North or South pole in that tooth. When this happens, the rotor will either be attracted toward the tooth, if the magnetic poles are different, repelled away from it, if the magnetic poles are the same, or a combination of both. This is the principle that creates rotation in the machine.

4.3 Description of the 3-Phase Brushless D.C. Drive

A 3-phase brushless d.c. motor (with 8 permanent magnet rotor poles and 12 stator teeth) driving a centrifugal boiler fan has been analysed. The motor is operated by a standard six switch 3-phase inverter with a 30V d.c. rail. Three Hall effect sensors located inside the stator of the motor provide position information to the inverter which commutates the motor. Figure 4.1 shows a schematic of this arrangement.

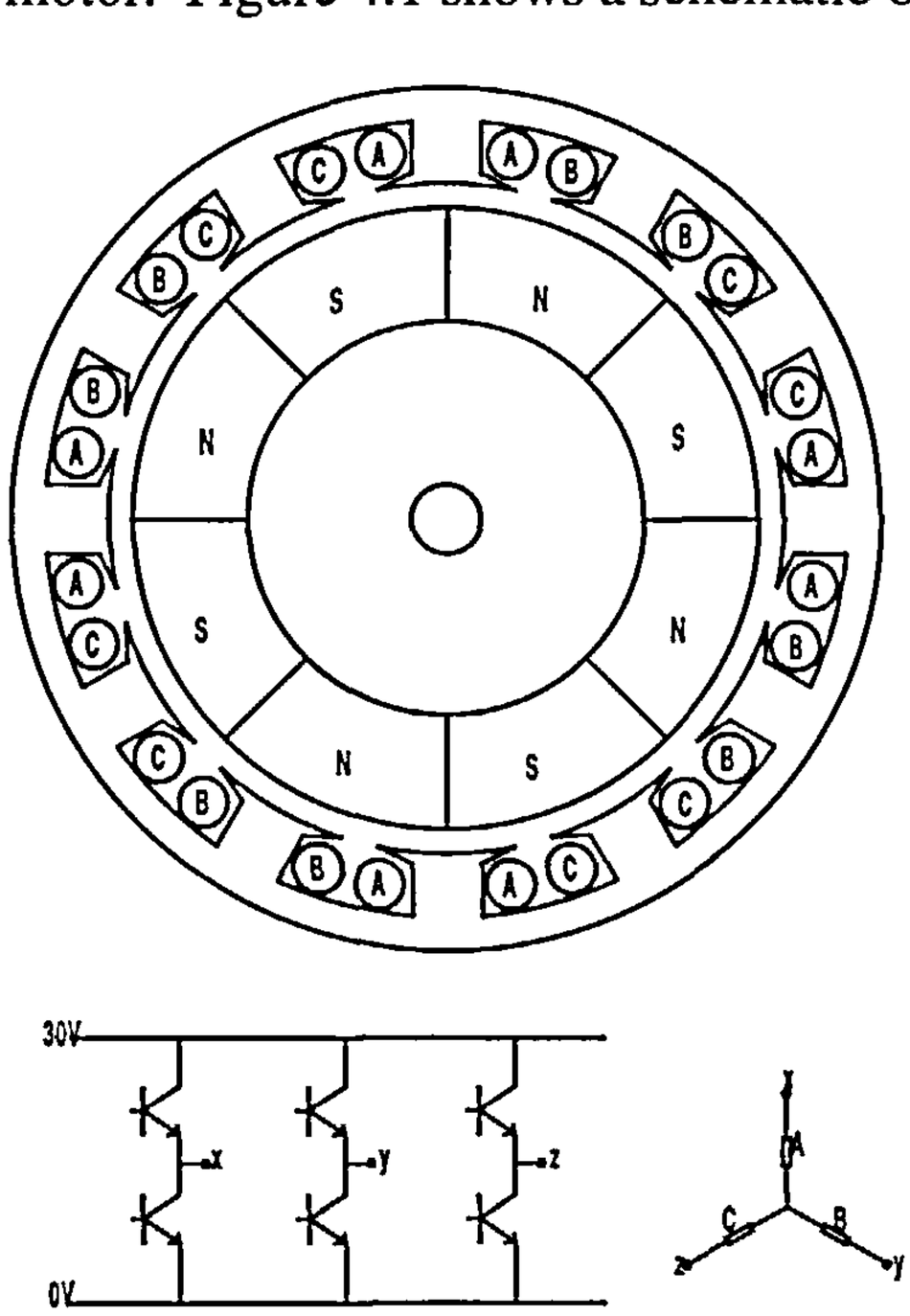

Figure 4.1: Schematic diagram of 3-phase brushless D.C. motor and inverter

As the speed range is swept, there are several speeds at which mechanical resonances are excited causing the system to emit pure tone acoustic noise. Finding cause of this was the purpose of the following investigation.

4.4 Experimental Analysis of Acoustic Noise and Vibration

4.4.1 Magnetic Shaker Test

A magnetic shaker was coupled to various components of the motor and boiler fan (whilst assembled) to measure their natural resonant frequencies. This helps to identify or eliminate components as being the source of the acoustic noise. The magnetic shaker was excited with a variable frequency sine wave via an amplifier as shown in figure 4.2.

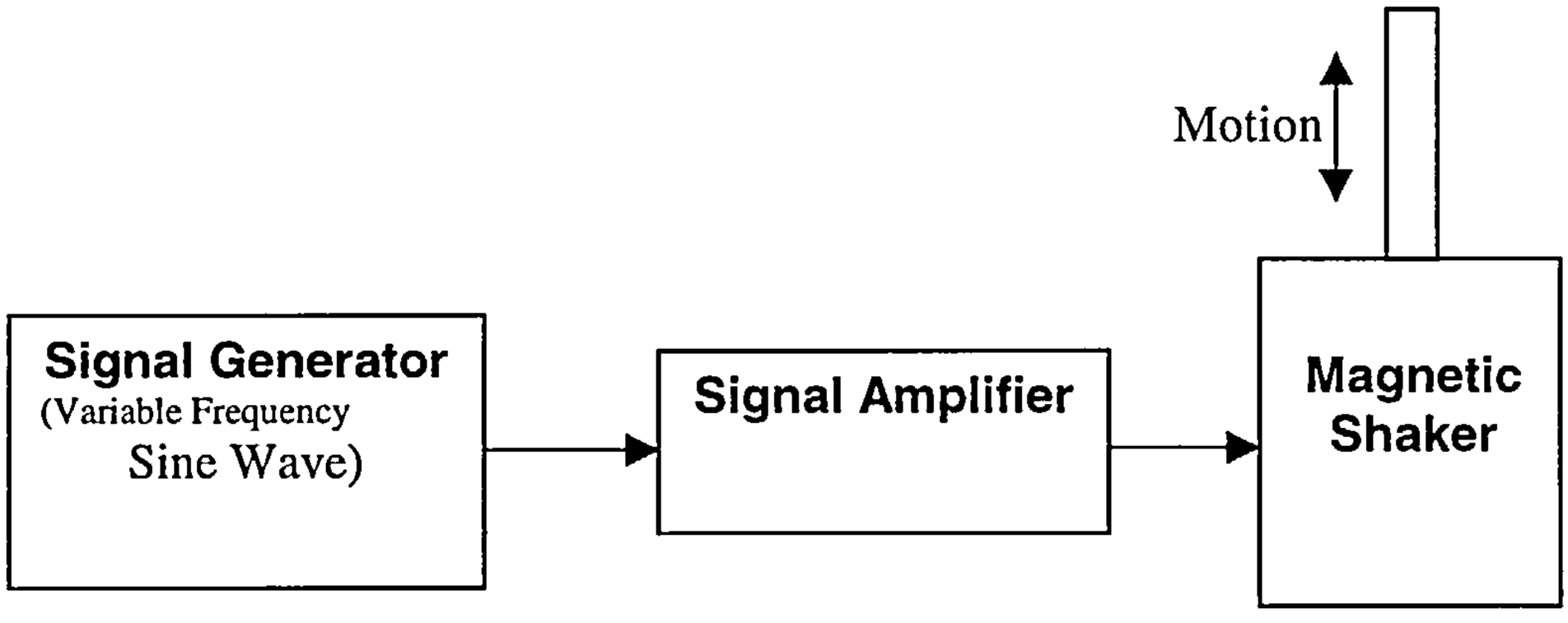

Figure 4.2: Control of the magnetic shaker

Measurements of surface vibration were made and frequencies that exhibit a high gain in vibration amplitude were noted. These frequencies are resonant frequencies and their associated harmonics. Fundamental frequencies provide the most amplitude gain. Work detailed in section 3.7 has shown that the resonance of fan housings, due to their enclosure-like structure, can be a major source of acoustic

noise in this type of assembly [39]. Table 4.1 shows the resonant frequencies of some of the components of the unit, measured whilst assembled.

Table 4.1: Resonant frequencies of system components

System Component	Resonant Frequency / Hz
Motor cooling fan blades	319
Motor Endcap	480
Fan Housing	594
Impeller surface	625

4.4.2 Static Testing

Static impulse tests were also performed to characterise the resonant properties of the assembly. Using a 2 switch drive circuit and a signal generator, current was pulsed through the phase windings of the motor in a ramp up – ramp down style. The phase windings of the motor are star connected and various phase pairs were excited, all producing very similar results.

Vibration was measured with an accelerometer at various points around the motor and was found to be greatest in magnitude at the centre of the endcap of the motor. The two dominant natural frequencies of vibration are 480Hz and 1440Hz. Other frequencies of significance were found to be 960Hz, 640Hz and 360Hz. Figure 4.3 shows the resulting vibration of the endcap of the motor when current was pulsed through two phases.

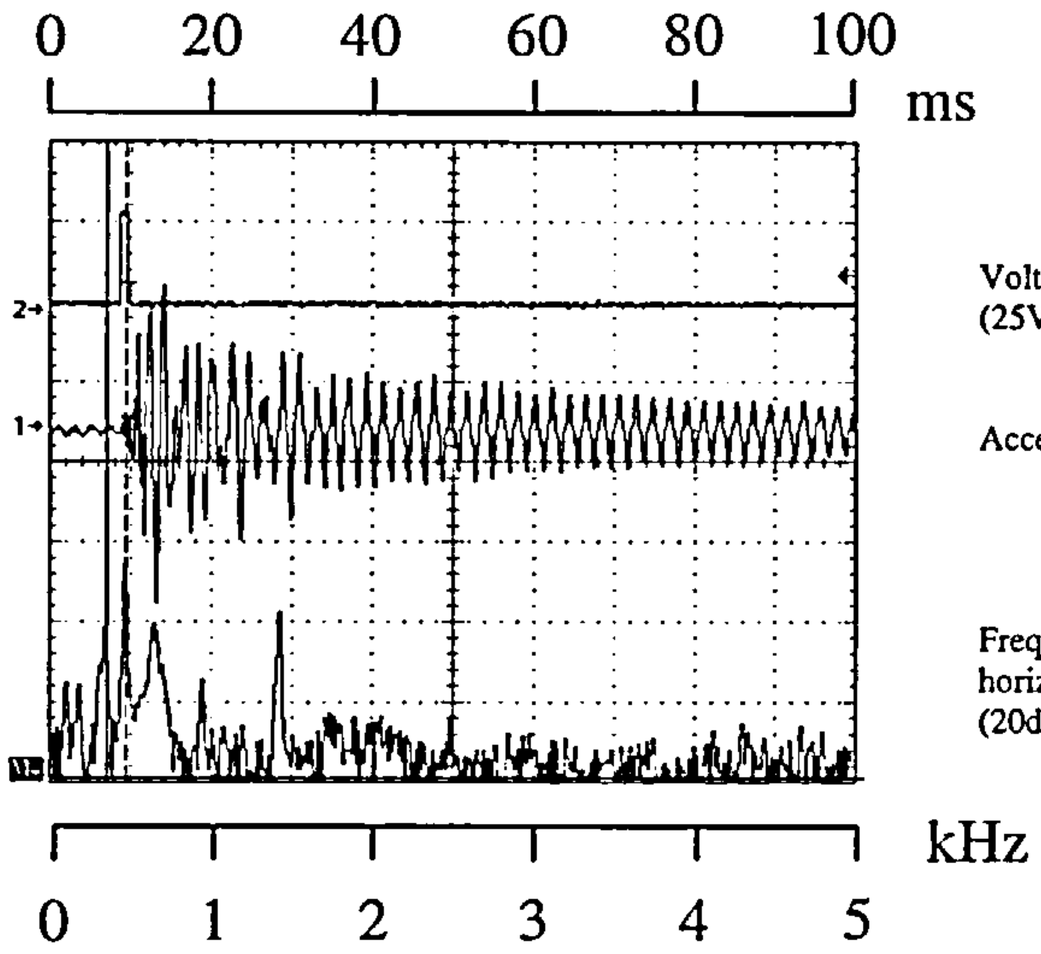

Figure 4.3: Current pulse, vibration of endcap, and frequency power spectrum during static test

4.4.3 Dynamic Tests

Using the six switch inverter the motor was accelerated to 1200rpm, the point at which the loudest acoustic noise was produced by the mechanical resonance. Measurements of vibration were made around the assembly by placing an accelerometer on a target surface. It was found that the vibration measured on the surface of the motor endcap was greater in magnitude than that measured on the side of the lamination stack, the fan housing and the fixing bracket. Fig. 4.4 shows the current in one phase, vibration, and frequency power spectrum of the vibration measured axially on the motor endcap when resonating.

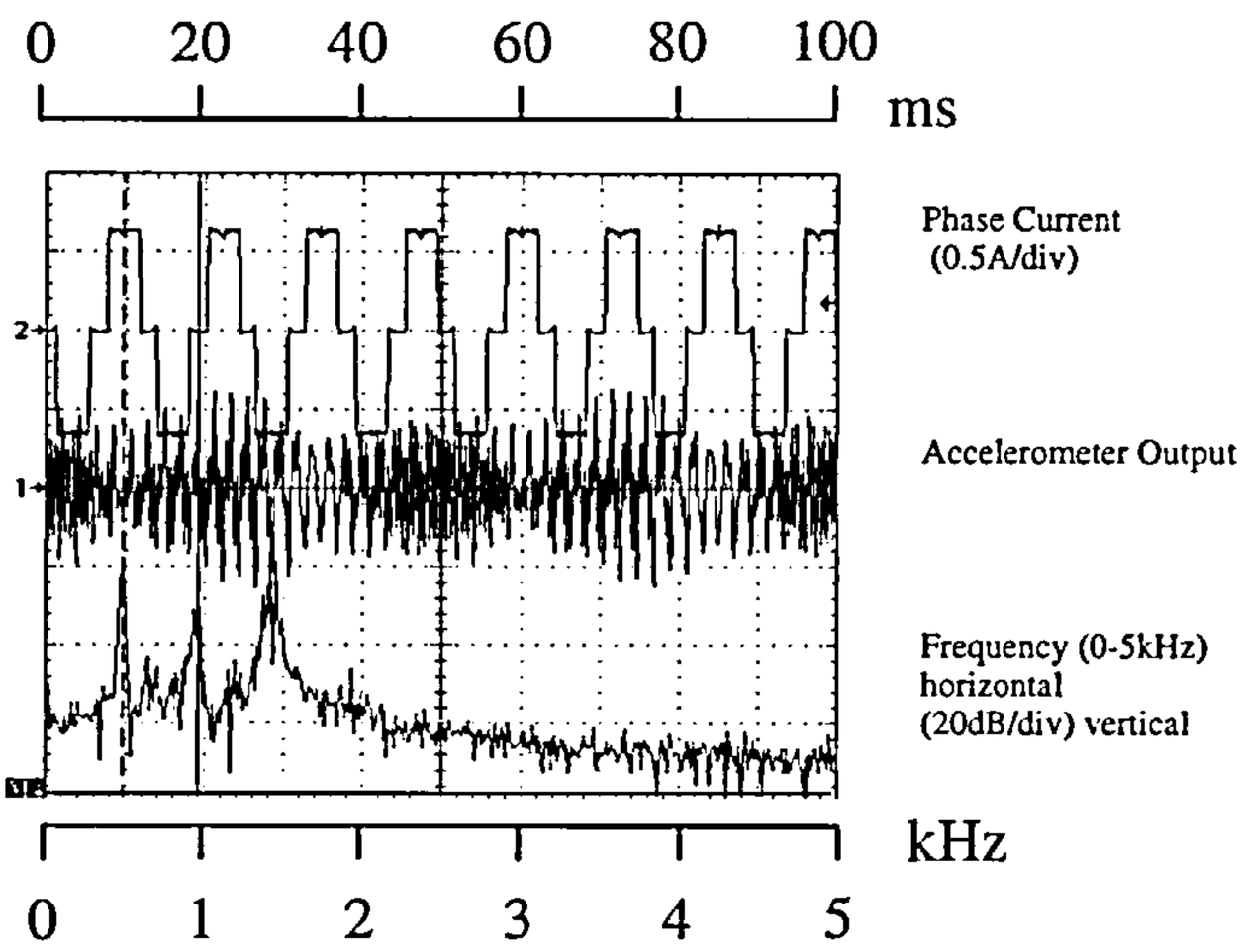

Figure 4.4: Phase current and vibration measured on motor endcap surface

A microphone measuring the overall acoustic noise output confirmed that the dominant frequencies of vibration, measured with the accelerometer, corresponded to the dominant frequencies in the acoustic noise profile. Analysis of the frequency power spectrum in figure 4.4 revealed that these dominant frequencies were 480Hz, 960Hz and 1440Hz. Unlike results presented in chapter 3, the vibration measured on the fan housing was not significant in the acoustic noise profile. The author concluded that the source of the acoustic noise was the vibration of the rotor assembly, which caused the endcap of the motor to flex and vibrate.

4.5 Experimental Analysis of Motor Commutation

In an attempt to establish whether the commutation of the motor was exciting the natural mechanical resonance described above, the motor commutation was analysed at a speed of 1200rpm corresponding to maximum resonant vibration amplitude. The 3-phase inverter uses 3 position sensor signals to generate the necessary currents in the motor windings for rotation. Figure 4.5 shows the current in one of the motor

phases, and the 3 sensor signals it was derived from, when the motor is running at 1200rpm.

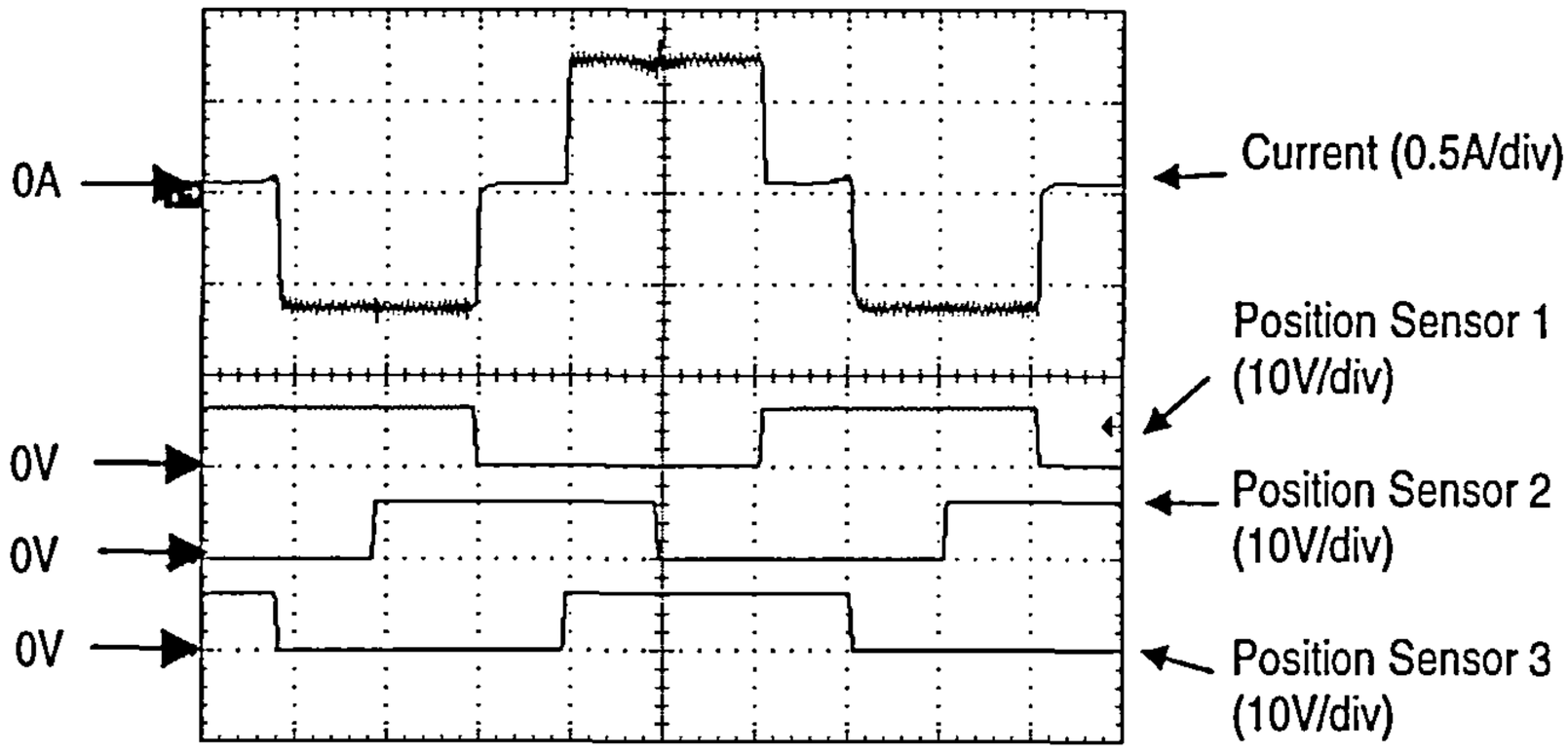

Figure 4.5: Current waveform, in one of the three phase windings and sensor signals

At a motor speed of 1200rpm the frequency of the current in each phase is 80Hz. The frequency of the individual position sensor signals is also 80Hz.

Section 3.5 showed that electronically excited acoustic noise is caused by force pulses which are created by changes in the rate of change of flux. Considering the currents in all phases of this motor it was discovered that for every complete current cycle, there are six changes in current level across the three phases, triggered by every position sensor commutation edge. These current changes generate sudden changes in the attractive and repulsive forces between rotor and stator, which happen at regular intervals within the commutation. This corresponds to six changes in the rate of change of flux. The conclusion of this is that the commutation of the motor at 1200rpm generates regular force pulses at a frequency of 480Hz.

4.5.1 Correlation Between Commutation and Acoustic Noise

Analysis of the mechanical characteristics of the fan assembly (section 4.4.1) revealed the natural mechanical resonant frequency of the rotor assembly and motor endcap was 480Hz. When the system was in mechanical resonance, the speed of the motor was 1200rpm. Analysis of the motor commutation showed that at this speed the frequency of the force pulses generated by changing current levels was 480Hz, coinciding with the natural mechanical resonant frequency. It was concluded that the resonance and associated acoustic noise was being caused by the pattern of motor currents. The commutation of the motor was exciting the mechanical resonance of the rotor assembly when the frequency of the force pulses (produced by commutation) matched the mechanical resonant frequency, or some multiple of it. At speeds where this forcing frequency does not match the mechanical resonant frequency, the resonance is not excited and the acoustic noise profile does not contain resonant frequencies of large magnitudes.

Having found the cause of the acoustic noise, methods of avoiding the excitation of the resonance were investigated. If the motor currents produced by the inverter are exciting a mechanical resonance, causing acoustic noise, previous work on switched reluctance motors has shown that it may be possible to alter the current make-up to stop the production of acoustic noise.

4.6 Reduction of Discrete Frequency Acoustic Noise

Chapter 3 shows that electronic commutation in switched reluctance motors produce force pulses which generate vibration and acoustic noise at resonant frequencies. It also shows that it is possible to reduce this effect by creating two force pulses per commutation, rather than one, with a controlled time delay between the pulses.

The proposal for the 3-phase brushless d.c. system is slightly different to the active cancellation method applied to switched reluctance motors, but uses similar principles. In this scheme, the time **between** commutations is altered such that the pattern of the force pulses counteracts the excitation of the mechanical resonance, reducing the acoustic noise generated at the resonant frequency. Having identified the resonant frequency of 480Hz, which has a period of 2.08ms, it was proposed to shift some of the commutation edges by a time equal to 1.04ms – half of one period of the mechanical resonance. This was done by adding the 1.04ms time delay to the falling edge of various combinations of the three position sensor signals before they reach the inverter, thereby changing the commutation pattern.

4.7 Application of Noise Reduction Technique to the Brushless D.C. Motor

4.7.1 Experimental Procedure

It was found that because the rotor was vibrating due to rotor resonance, the quality of the sensor signals was degraded. To investigate the effects of the noise reduction technique, the motor was controlled in an open loop fashion with the 3 sensor signals being simulated by an electronic circuit with their frequency controlled by a signal generator. For experimental purposes, the time delay was added to the falling edge of the position sensor signals by diverting the signals through a digital counter circuit. The modified signals were then fed to the inverter where the phase currents were switched appropriately. This is shown in Figure 4.6.

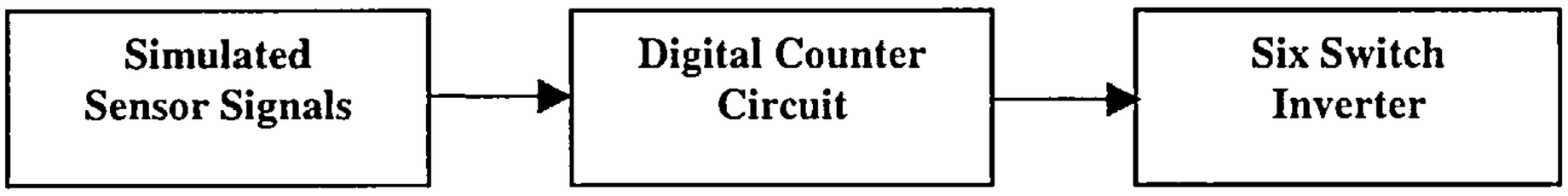

Figure 4.6: Adding time delay to the simulated position sensor signals

Adding the fixed time delay to various combinations of sensor signals was investigated to examine the effects on vibration and acoustic noise. Figure 4.7 shows how the sensor signals were altered, by analysing the time between consecutive edges. Figure 4.7(a) shows the unaltered case and figures 4.7(b-d) show the effect of adding the delay to the falling edges of one, two and all three sensor signals respectively. At 1200 rpm the time 't' is the time for one period of the resonant frequency (2.08ms).

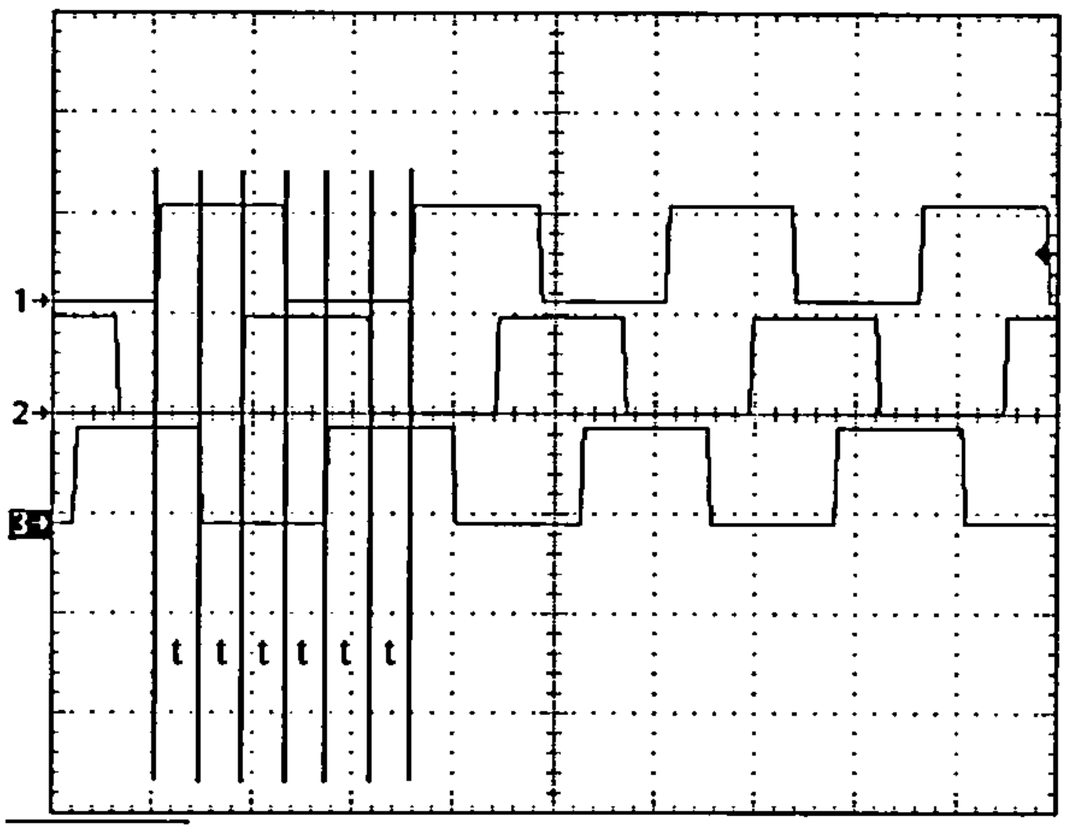

Figure 4.7(a): Unaltered sensor signals

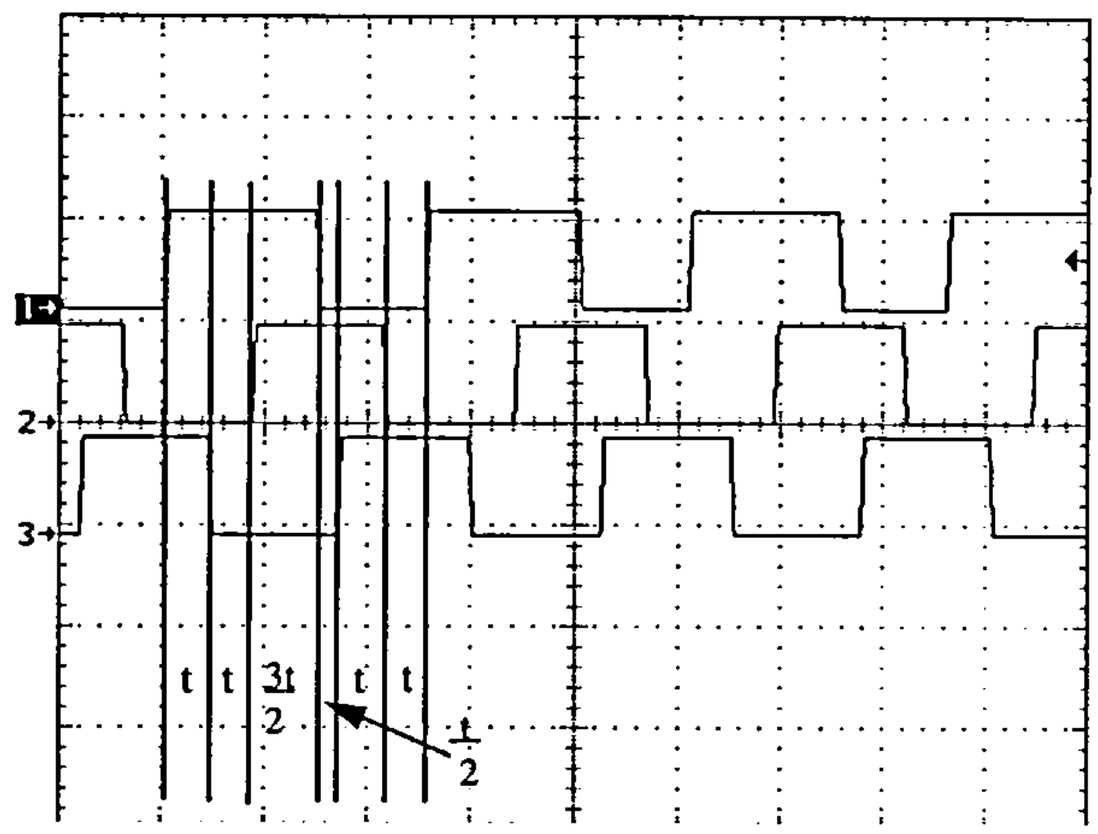

Figure 4.7(b): One sensor signal with falling edge delayed

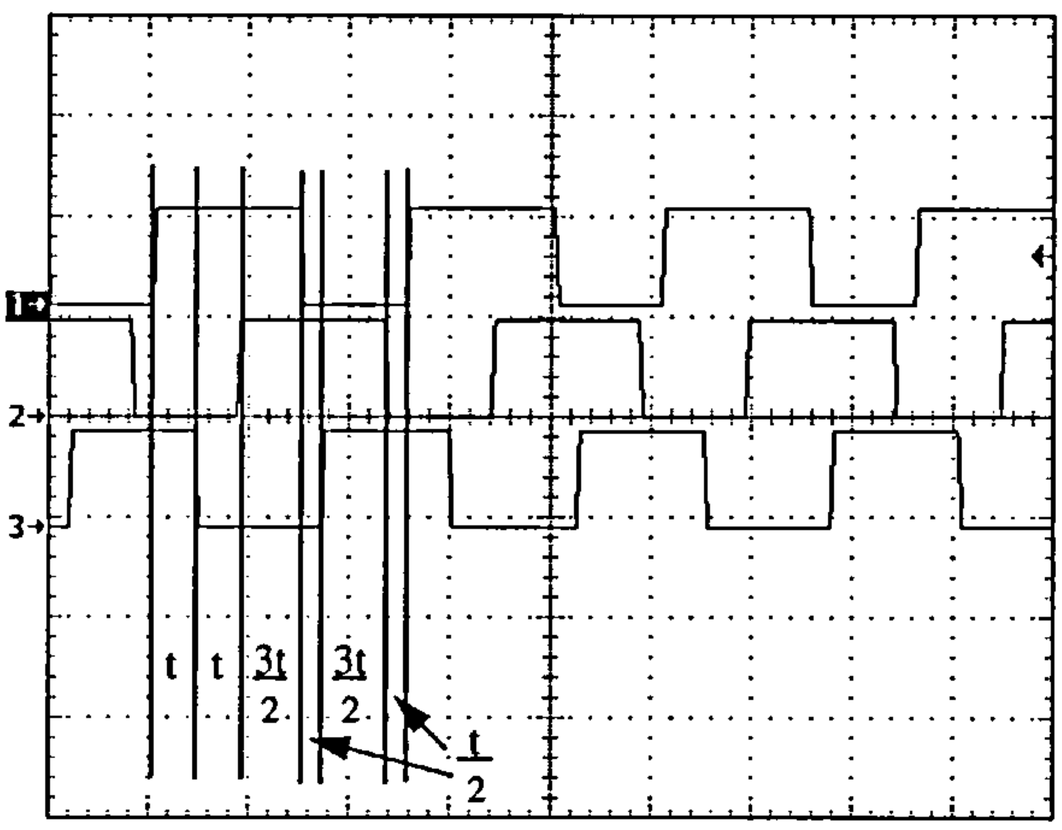

Figure 4.7(c): Two sensor signals with falling edge delayed

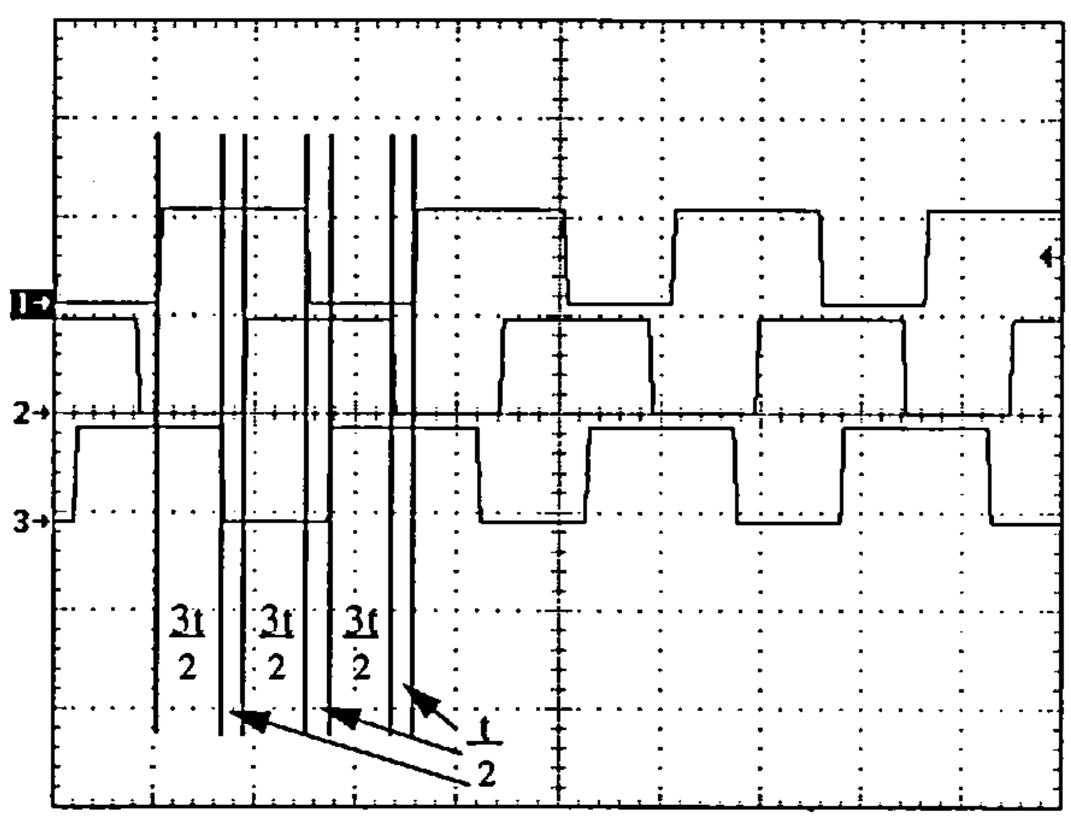

Figure 4.7(d): All three sensor signals with falling edge delayed

4.7.2 Results

Measurements of vibration of the endcap of the motor were made with an accelerometer with the delay schemes implemented using the techniques described above. It was found that there were significant changes in the vibrations produced at 1200rpm, the resonant speed. Figure 4.8(a-d) show the 3 sensor signals controlling commutation, the vibration of the motor endcap and a frequency power spectrum of

the vibration measured at a motor speed of 1200rpm, for each commutation scheme. The pulsing nature of the vibration, which is a strong indication of a natural resonance, has a period consistent with each revolution of the motor. A * indicates the phase signal that has had its falling edge delayed.

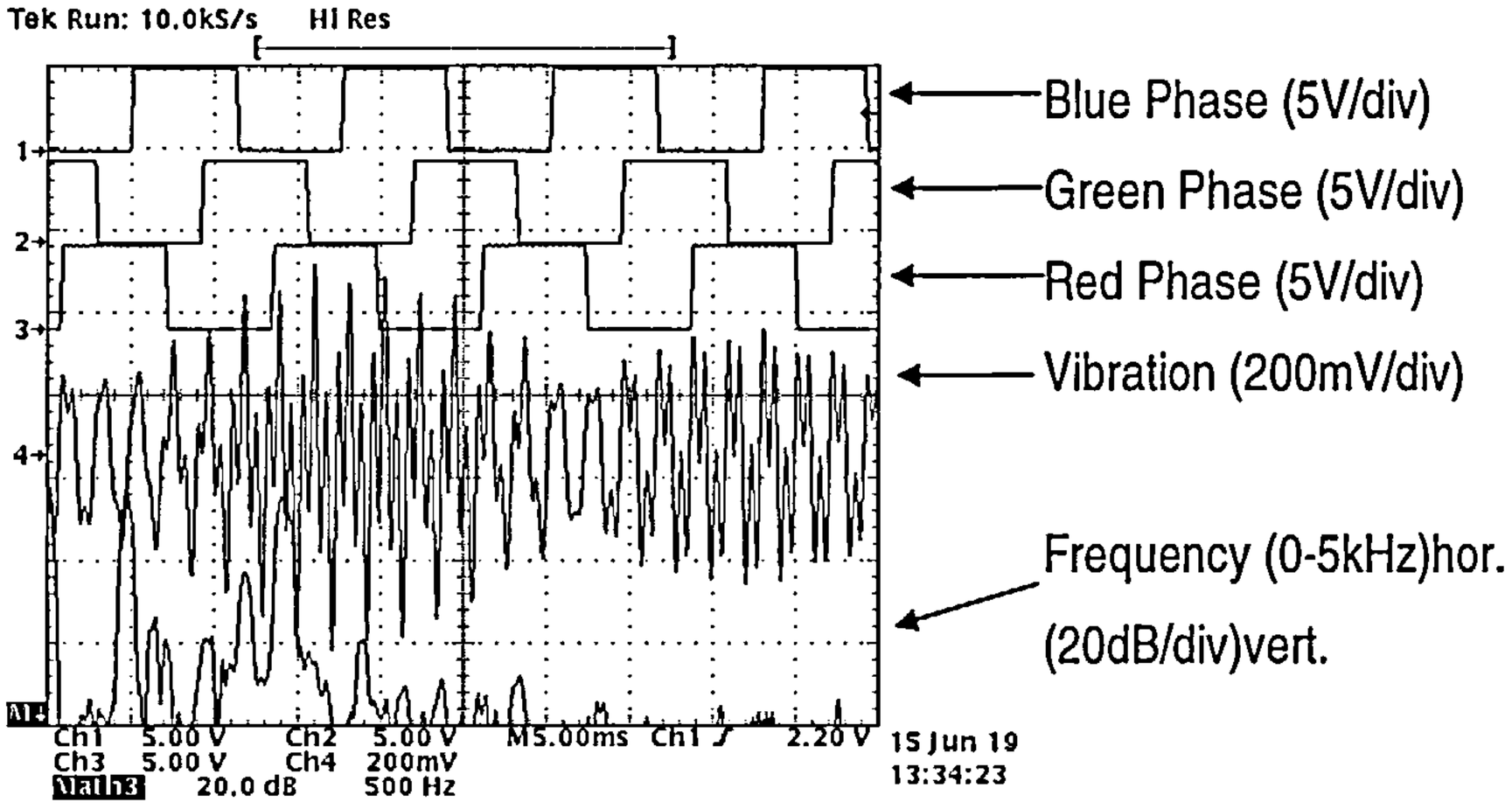

Figure 4.8(a): Unaltered sensor signals

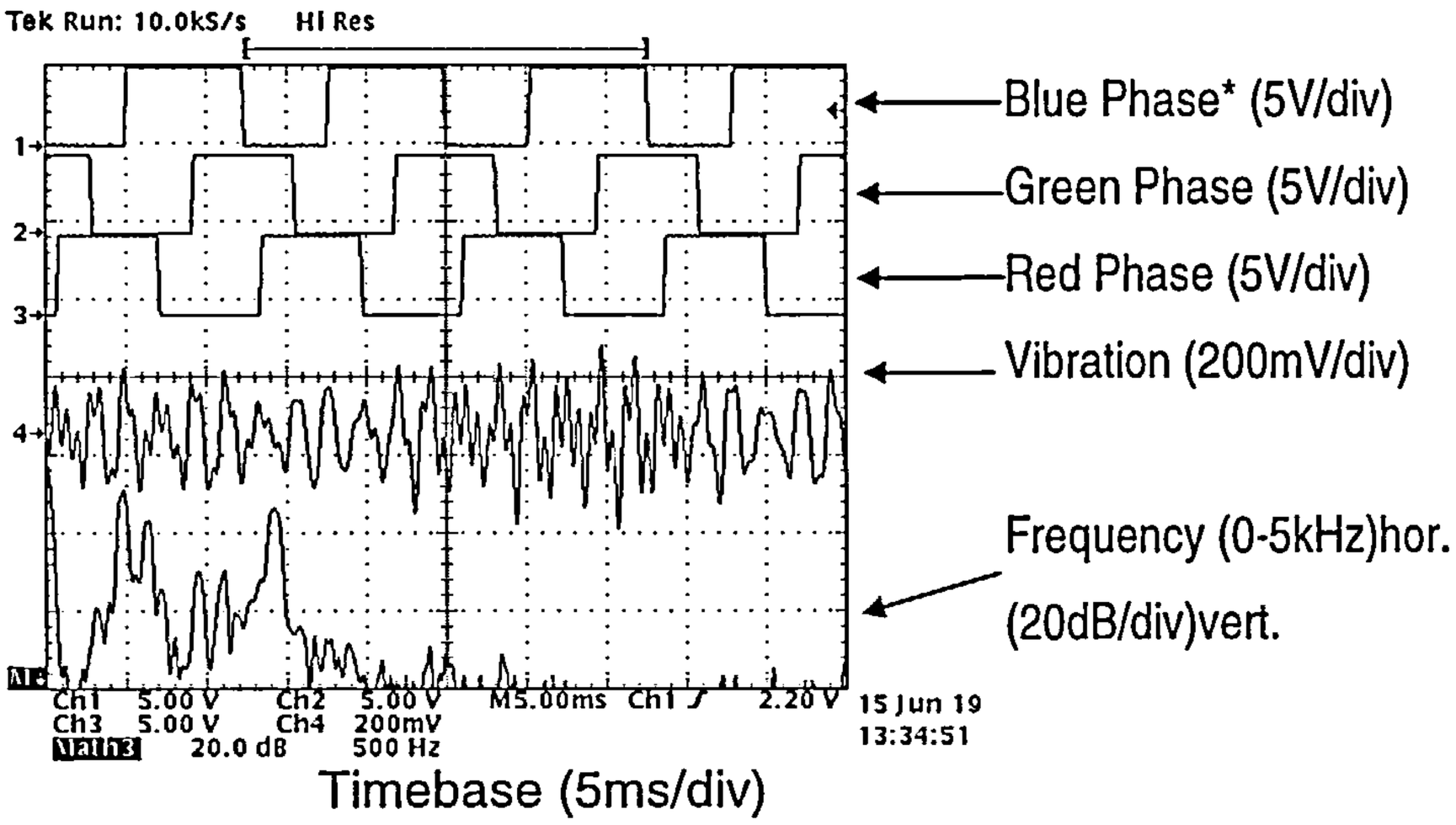

Figure 4.8(b): One altered sensor signal

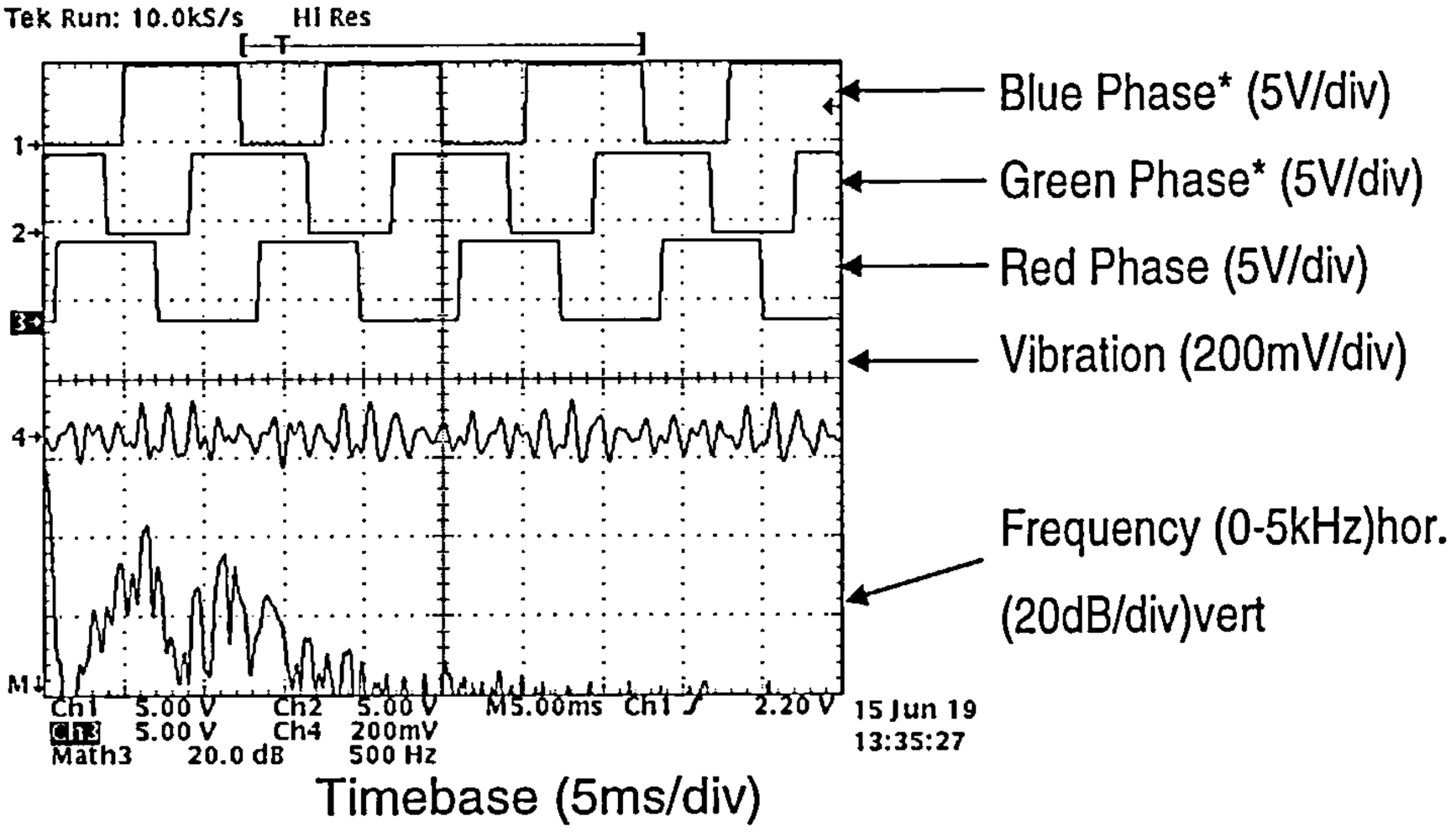

Figure 4.8(c): Two altered sensor signals

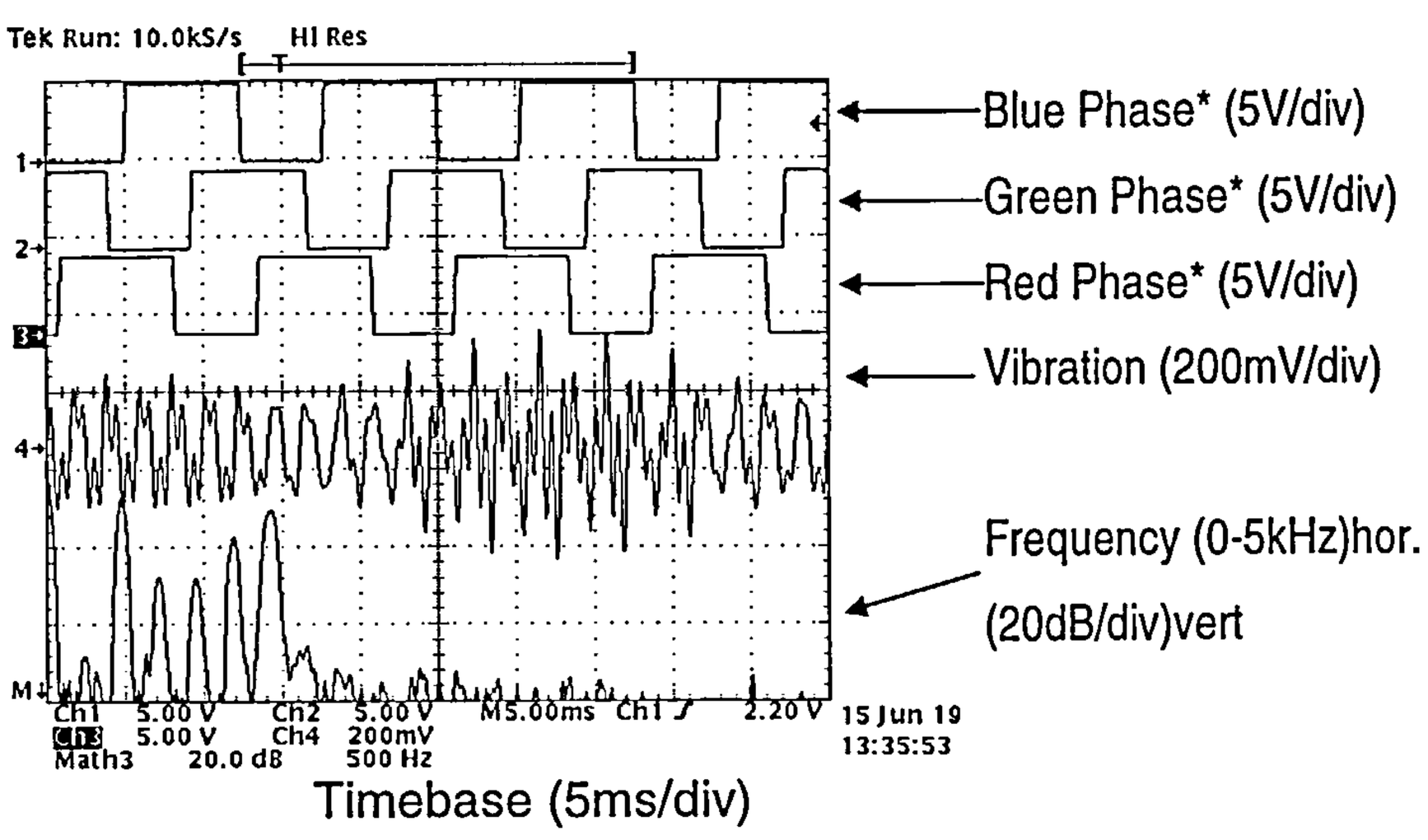

Figure 4.8(d): Three altered sensor signals

4.7.3 Analysis of Results

Comparing the acceleration displayed in figures 4.8(b-d) with 4.8(a) clearly shows that delaying the falling edges of any combination of the sensor signals reduces the magnitude of the resonant vibration. However it is also apparent that the most significant decrease in resonant vibration and acoustic noise is achieved by delaying the falling edges of any **two** of the sensor signals as shown in figure 4.8(c).

Analysis of the frequency power spectrum of the acceleration produced with unaltered sensor signals, highlights the resonant frequencies at 480Hz and 1440Hz. It has been shown that the resonance is excited by the regular commutation pattern shown in figure 4.7(a). When only one signal was altered, the commutation was changed but it still contained many commutations at interval 't'. Hence the magnitude of the vibration at these frequencies was slightly reduced, but the resonance could still be detected audibly. Delaying the falling edges of two of the signals introduced a more varied commutation pattern producing the most significant reduction in resonant vibration and, perhaps more importantly, stopped the pure tone acoustic noise at the resonant frequencies. Figure 4.8(c) clearly shows a large reduction in the power spectrum at these frequencies. When the delay was added to the falling edges of all three signals, the commutation interval t appeared to be eliminated, but another regular pattern was set up which introduced another vibration component that excited harmonics at 240Hz intervals. This produced vibration and acoustic noise at 480Hz, 620Hz, 960Hz, 1200Hz and 1440Hz.

4.8 Simple Implementation of Noise Reduction Scheme

For experimental purposes, the time delay was added to the falling edge of the sensor signals by diverting the signals through a digital counter circuit. However this would be too costly in practice and is unnecessary. With cost and volume production in mind, a simple additional stage to the motor control circuitry is proposed which would provide the delay on the falling edge of each signal. Figure 4.9 shows a schematic for a stage that could be implemented between the position sensor output and the inverter.

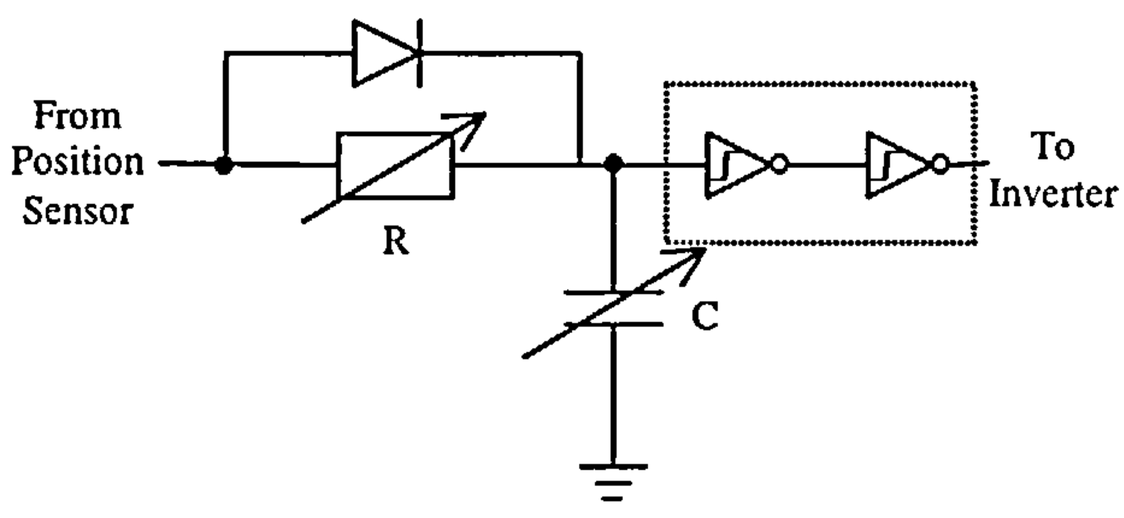

Figure 4.9: Schematic layout of additional stage providing a delay on the falling edges of a position sensor signal

The stage consists of 4 components. The resistor and capacitor provide an RC decay time constant for a falling edge. The diode allows a rising edge to bypass the RC leg and be unaffected. The inverting Schmitt trigger gates ensure the sensor signal leaves the stage with clean, straight edges before reaching the inverter. Values for resistance, R, and capacitance, C, can be altered to vary the time delay and hence target a particular resonant frequency.

The limitations of this approach are similar to those for active cancellation applied to switched reluctance motors. The target resonant frequency must be established first,

and so far only one resonant frequency can be targeted. It is also recognised that the resonant frequency may vary slightly between identical motors. The range of frequencies that can be targeted is limited and depends on the speed of the motor.

4.9 Conclusion

This work has shown that the brushless d.c. motor, particularly when commutated with square wave current, is susceptible to mechanical resonances and acoustic noise which are excited by changing motor currents. It was found that the force pulses, produced by changing current levels in a 2-phase motor, excite a mechanical rotor resonance. This happened at a particular speed where the frequency of the force pulses, coincided with the mechanical resonant frequency of the rotor assembly. This resulted in a large increase in vibration and pure tone acoustic noise at the resonant frequency and its harmonics, proving the correlation between motor excitation frequency, mechanical resonant frequency, and the frequency at which vibration and acoustic noise is emitted.

An investigation into reducing the excitation of the mechanical resonance has been described. This was achieved by delaying the falling edges of combinations of sensor signals, by a time equal to one half of the period of the resonant frequency, thereby altering the motor commutation pattern and therefore the pattern of the force pulses produced. An effective commutation pattern for reducing vibration at resonance has been highlighted and results displayed.

A simple, low cost implementation of the noise reduction technique has also been proposed by the addition of a stage between the position sensor signals and the inverter. This is to delay the falling edges of the sensor signals by a time equal to one half of a period of the mechanical resonant frequency. Adding this stage to two of the three sensor signals will ensure the commutation pattern is altered to best avoid exciting the resonance.

Overall this work has shown that the brushless d.c. motor can generate discrete frequency acoustic noise in much the same way as a switched reluctance motor. It also shows how a technique, originally designed to reduce pure tone acoustic noise from the stator of a switched reluctance motor, has been adapted and applied to the brushless d.c. motor resulting in the elimination of acoustic noise at the resonant frequency and its harmonics.

CHAPTER 5

THE FLUX SWITCHING MOTOR

5.1 Introduction

The flux switching machine is a new class of electric motor, and is a combination of the switched reluctance motor and the inductor alternator [42]. It uses the reluctance principle for rotation, but exhibits motor characteristics similar to those of a D.C. machine. The windings in this machine are fully pitched, and their method of excitation is unconventional. Benefits of winding switched reluctance motors with fully pitched windings are the subject of publications [43-46]. A full explanation and background to the new flux switching technology is given in [47].

5.2 Construction

The motor has a laminated structure, which is doubly salient, and does not employ magnets or brushes. All the motor windings are in stator slots and the rotor is a simple reluctance rotor. This makes the machine robust and easy to build. As in all doubly salient motors, torque is developed by the movement of the rotor, with respect to the stator, to a position of minimum reluctance to the flux set up by current in the motor windings. Figure 5.1 shows the simplest example of the construction of the flux switching motor, with 4 stator poles and 2 rotor poles.

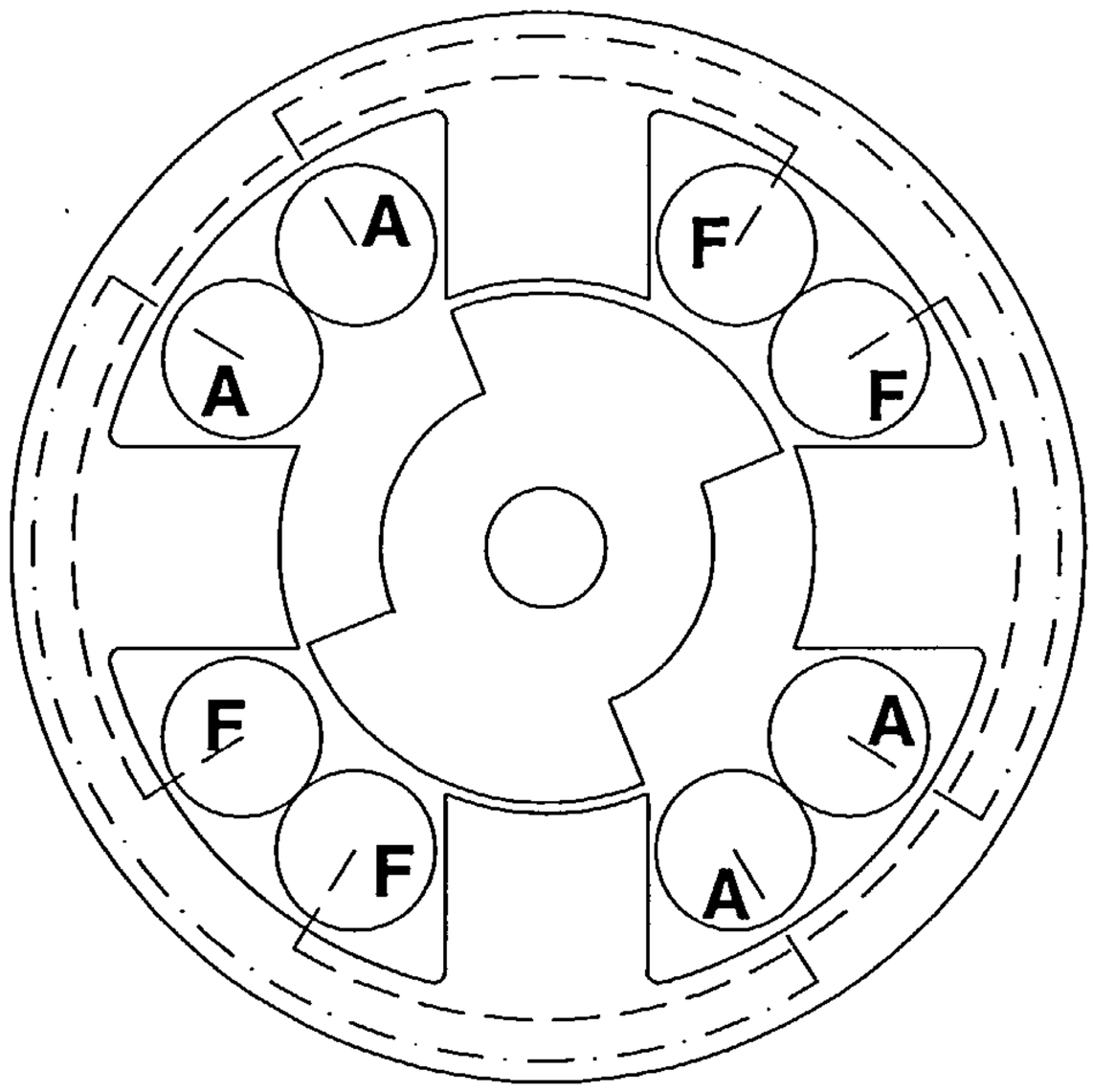

Figure 5.1: Construction of a 4/2 flux switching motor

There are two windings in this machine. These shall be termed field winding, labelled 'F', and armature winding, labelled 'A'. In figure 5.1, the windings are fully pitched across the machine. The field winding carries a unipolar d.c. current and the armature winding requires bipolar current. The field is usually wound with single strand wire, but to achieve the bipolar current in the armature, a double strand (insulated) bifilar arrangement is used. Although this only utilises half of the available armature slot area per working stroke, it saves on costly power converters that supply bipolar current to a single strand winding.

5.3 Method of Operation

Figure 5.2 shows the field and armature windings with the conventional dot and cross notation used to denote positive and negative current.

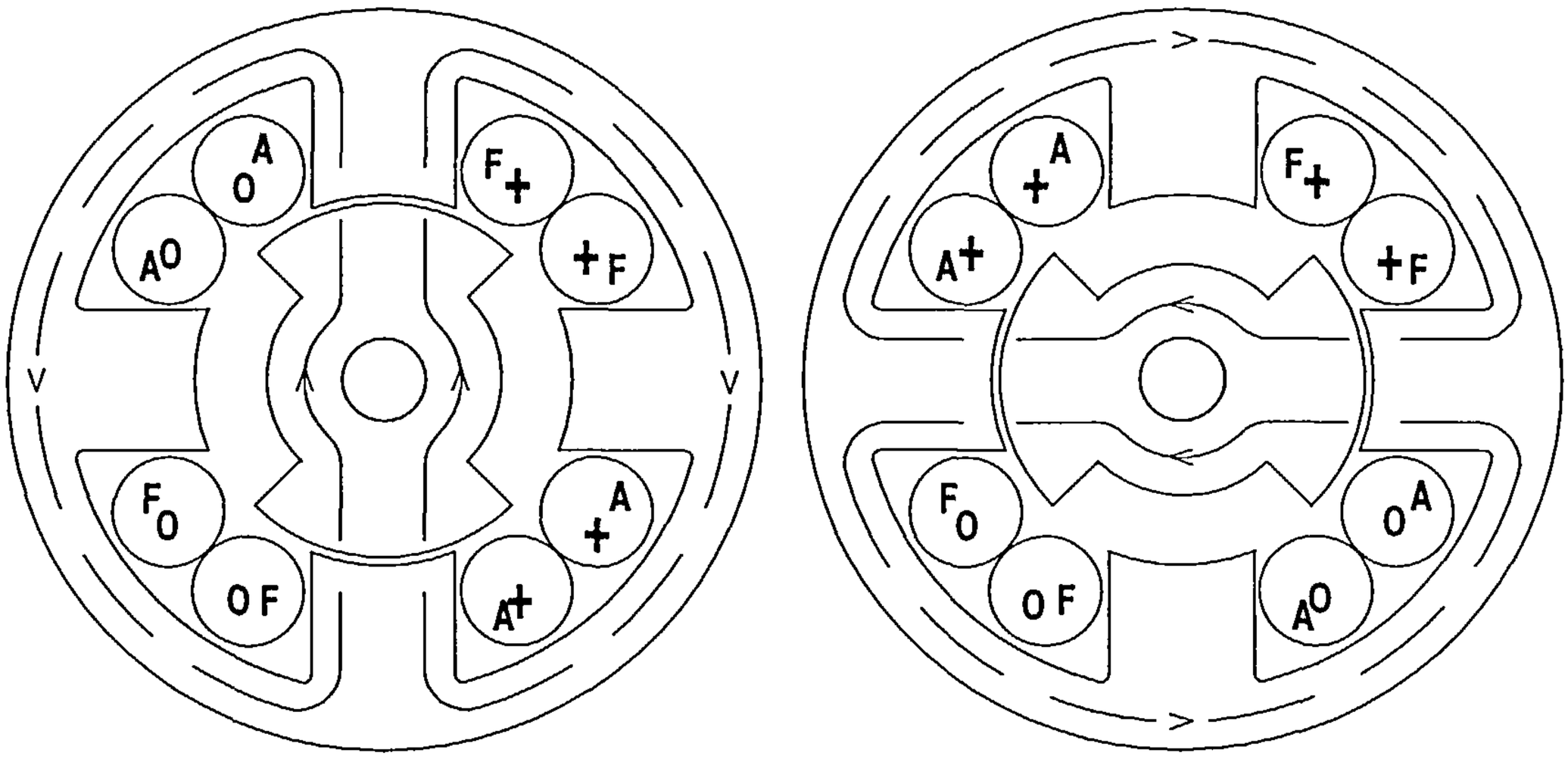

(a) Field +ve Armature +ve

(b) Field +ve Armature -ve

Figure 5.2: The two aligned positions achieved by switching polarity of armature current only

The dashed lines show the two flux paths, from which rotation is derived. In figure 5.2 (a) the field winding, F, is carrying positive current and the armature winding, A, is also carrying positive current. This energises the top and bottom stator pole pair and will pull the rotor into alignment as shown. In figure 5.2 (b) the field winding is still carrying positive current, but the armature winding now carries negative current which energises the left and right stator pole pair, bringing the rotor into the other aligned position as shown. The flux in the back iron behind the field winding is unipolar which reduces the iron losses in this part of the material.

Because the machine always carries d.c. current in the field winding, there is always flux present. The direction of the armature current, can be thought of as orientating the flux between the two paths shown, attracting the rotor to either one pole pair or the other. Even though the structure of the machine is very similar to a switched reluctance topology, the method of flux control is very different. It is for this reason

that a study of acoustic noise from this new machine has been undertaken, and presented in further chapters.

5.4 Simple Analysis

A simple analysis of the operation of this machine requires some ideal characteristics to be assumed. These have been stated where used.

The constant excitation of the field winding sets up a constant[2] flux ϕ_f. The simplified expression for this is:

$$\phi_f = \frac{N_f I_f}{\Re} \qquad \text{Wb} \qquad (5.1)$$

Where ϕ_f field flux

N_f field turns

I_f field current (A)

$\Re$ Reluctance of magnetic circuit (H^{-1})

As the rotor rotates, the field flux linking the armature windings varies linearly between positive and negative values. Not all the field flux will link the armature windings, and to compensate, a coupling coefficient, k, must be introduced. This changing armature flux produces an induced voltage (back-emf), E_a, in the armature coils of magnitude:

[2] Field flux will actually fluctuate with armature current, and rotor position.

$$E_a = \frac{2N_r k_c N_a}{\pi} \phi_f \omega \qquad \text{V} \qquad (5.2)$$

Where N_r Number of rotor poles

k_c coupling coefficient

N_a armature turns

ω rotor speed (rad s^{-1})

To obtain electromechanical energy conversion and produce motoring torque, a current must flow in the armature in opposition to the induced armature voltage. Under the idealised conditions of a square wave current, synchronous to the induced armature voltage, the electromechanical torque, T_{av}, can be expressed by:

$$T_{av} = \frac{2N_r k}{\pi \Re} N_f I_f N_a I_a \qquad \text{Nm} \qquad (5.3)$$

where I_a is the armature current (A).

It is these equations that link the simple analysis of the flux switching motor, to that of a D.C. machine. However unlike a D.C. machine, the flux switching motor has no brushes to commutate the armature and therefore requires a power electronic converter to control it.

5.5 Power Electronic Converter

One of the great benefits of the flux switching motor is the fact that the field winding carries a d.c. current, which does not have to be controlled by any power electronics. As in a D.C. machine, this field winding can be connected in shunt or in series with the armature circuit. The machines built and tested by the author have been connected in the series configuration, therefore emphasis will be placed on this circuit configuration in later analysis.

Previously the structure of the machine was described as having a double strand wound (bifilar) armature winding. The armature slots require *bipolar* mmf to produce bipolar flux. If a single strand wire was used, this *bipolar* mmf could be obtained from an inverter circuit, of which there are many configurations. Instead, due to factors such as cost, a novel circuit has been proposed [47], which utilises the bifilar winding, by alternately passing unipolar current through each half of the winding.

In low power applications, the inherent avalanche capability of MOSFET's can be utilised, removing the need for an additional snubber. With the field winding in series, a freewheel diode around the field winding or a capacitor across the armature circuit is required to capture the leakage energy. These configurations are shown in figure 5.3.

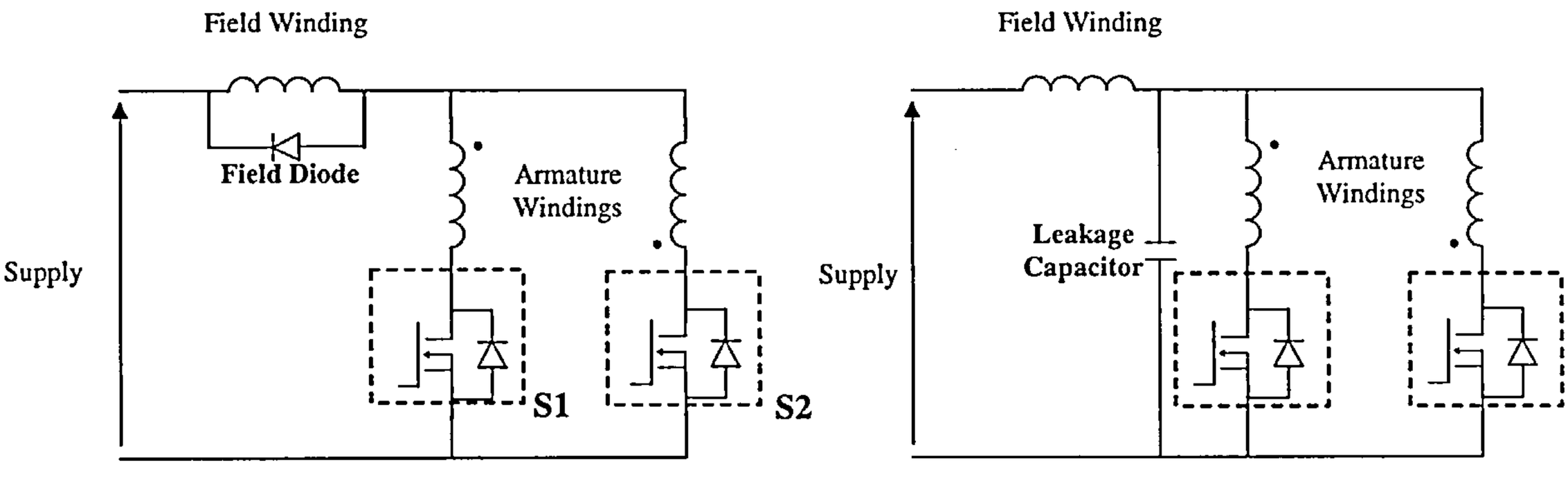

Figure 5.3: Series connected flux switching with (a) freewheel field diode, (b) armature capacitor

The converter requires the addition of a position sensor and a standard gate drive circuit to control the power switches. Because both switches are referenced to ground the complexity, and therefore cost, of the gate drive is minimised.

5.5.1 Operation of Converter

Consider the configuration shown in figure 5.3(a). When switch S1 turns on, current is drawn through the field winding and one half of the armature winding from the supply. The rotor will move to align itself with the energised stator poles. Before switch S2 can turn on, to continue the commutation, the S1 must be turned off to avoid a short circuit current. When S1 is turned off the stored energy in the first armature winding transfers across, by transformer action, to the second closely coupled armature winding. As this is connected in opposition to the first, the current now flowing in the second armature is negative and reduces to zero by flowing into the supply via the fast recovery freewheel switch diode and the field diode. When S2 is turned on, the current in the second armature reverses (becomes positive) and provides an opposite mmf to allow the motor to continue to rotate. As the two armature windings are not perfectly coupled, not all of the stored energy is transferred from one to the other. The difference is the *leakage energy,* which causes a build up in voltage across the MOSFET and is dissipated by avalanche breakdown in the MOSFET.

5.6 Design of a Low Acoustic Noise Flux Switching Motor

5.6.1 Application and Design Specification

Many applications require low acoustic noise motors, but one particularly sensitive application is low speed domestic and commercial ventilation products. As a vehicle for analysing the acoustic noise from a flux switching motor, and to allow comparisons to be made with other motors, a 9" window fan was used to house and load the motors. This constrained the overall size of the prototype machine to an OD of 90mm and a total length of 100mm. The maximum operating speed was to be 1800rpm and at this speed, the fan requires approximately 0.1Nm of torque and 20W output power from the motor.

The choice of whether to build an internal or external rotor machine was decided by parameters such as end winding length, inertia of rotor and total weight. The result of having the stator internal to the machine was much shorter end windings. As the machine was to be fairly low power and low speed, it was felt that an external rotor would be mechanically acceptable. Figure 5.5 will show an example of an external rotor arrangement. Factors such as low starting torque and no specific acceleration or deceleration requirements meant that the increased inertia of the external rotor did not prohibit its use. The main concern was the mechanical construction of the machine, and whether a constant airgap could be maintained, as this is an important feature relating to acoustic noise and vibration. As a conclusion, the external rotor machine was chosen because of the save in end winding length and hence lower copper loss. It is also seen as a favoured solution in the fan industry and there was an interest in the design of such a unit, with low acoustic noise, despite the mechanical problems.

5.6.2 Electromagnetic Finite Element Analysis (FEA)

The primary tool for designing a modern electric machine is Finite Element Analysis. A computerised geometric model of the machine is created, which allows material properties, magnetic properties and conductor properties to be set. The model is then split into many small elements of triangular shape, all of which are connected. Electromagnetic equations are then solved for each individual element, thus eventually providing a solution for the entire model. The process can be computationally intensive, and work has been published on the trade-offs between computation time, mesh density and accuracy [48].

In the design of a lamination for a low acoustic noise flux switching motor Opera-2D software produced by Vector Fields Ltd has been used. This is a 2-dimensional, static analysis, finite element package that allows the user to create a parameterised model of the machine, whereby many different geometries can be quickly created and solved. More geometries can be investigated this way, and an optimised solution is more likely to be obtained. One disadvantage of this analysis is that it does not account for the effects of eddy currents and hysteresis losses.

This simulation tool was used to solve non-linear electromagnetic equations for different machine geometries and excitation states. From that, many output parameters can be calculated such as torque, force (Maxwell stress), energy and current density which are all used to decide whether one geometry will produce better performance than another. Making these decisions is where the skill and experience of a machine designer outweigh that of a computer although work on

Genetic Algorithms, to optimise designs for a given set of parameters within a design space, is ongoing to automate this process too [49].

5.6.3 Top Level Motor Design

The flux switching topology follows the same rules as the 2-phase switched reluctance motor when deciding how many poles to have on the rotor, N_r, and stator, N_s. A discussion of switched reluctance pole topologies is presented in [27]. From this, a summary of the common combinations of rotor and stator pole numbers for the flux switching machine is given in table 5.1:

Table 5.1: Common combinations of number of rotor and stator poles in the flux switching machine

N_r ↓ / N_s →	2	4	6	8	10	12
2		✔				
4				✔		
6		✔				✔
8						
10						
12				✔		

A machine with 8 stator poles and 4 rotor poles was chosen. The factors influencing this were the flux frequency, the number of connections required, end winding length, and availability of space for the end windings. Iron losses are proportional to

the flux frequency. In a machine with a greater number of stator poles than rotor poles, a low number of stator poles will give a low flux frequency and hence lower iron losses. A 4 pole stator was not selected because the windings would have to span 180° across the motor which makes the end windings very bulky and unnecessarily long.

An 8 pole stator can have either 2 field coils and 2 bifilar armature coils, each filling a whole slot, or 4 field coils and 4 bifilar armature coils, each filling half of one slot. The operation of the motor is not affected, but the end windings are very different. The 4 field and 4 armature coil configuration was selected because the end winding was evenly distributed around the stator. This configuration has 8 field terminations, and 16 (bifilar) armature connections.

The continuous working current density was considered next. The author assumes a conductor current density of $10A/mm^2$ to be a maximum. This is limited by the ability to transfer heat away from the stator, and this is more difficult in an external rotor machine. The FEA model assumes the current is flowing in 100% of the slot area. Assuming only 40% of a stator slot area is filled by conductors (carrying $10A/mm^2$), the current density in the stator slot is therefore $10*(40/100) = 4A/mm^2$.

The flux switching topology relies on the rate of change of mutual inductance to produce a back emf. The variation of inductance with position should be minimised to minimise fluctuations in the field flux. This equates to having wide rotor poles that may overlap two stator poles. This is very different from a switched reluctance machine design where the ratio of inductance between the aligned and unaligned

positions should be large (typically 8:1). In the switched reluctance motor this is a measure of the energy available for conversion per working stroke. To maximise the ratio, narrow poles are used to provide a low unaligned inductance, and minimise flux leakage paths.

Mechanical tolerances restrict how small the airgap, between rotor and stator poles, can be. To reduce the mmf dropped across the airgap, and improve the motor performance, a minimal airgap width is desirable. A typical airgap in a reluctance machine is 0.4mm. An airgap of 0.25mm was used in the design of this machine. It was felt that accurate machining, and the low power and speed of the machine would allow such an airgap to be used successfully.

5.6.4 Lamination Geometry Design

Given the top-level motor parameters described above, attention is now paid to the intricate design of the lamination for maximum performance, and minimum acoustic noise. The geometric parameters to be varied can be categorised as shown below.

- Rotor and stator back iron thickness
- Rotor and stator pole width at airgap
- Rotor and stator general pole shape
- Conductor slot area
- Radius of airgap
- Degree of saliency

Because the relationship between flux density, B, and magnetic field strength, H, is non-linear in machine steel, a characteristic curve must be used to identify how the material will behave when the phase coils are energised. Figure 5.4 shows part of the B-H curve for the iron. This closely resembles the grade of electrical steel used.

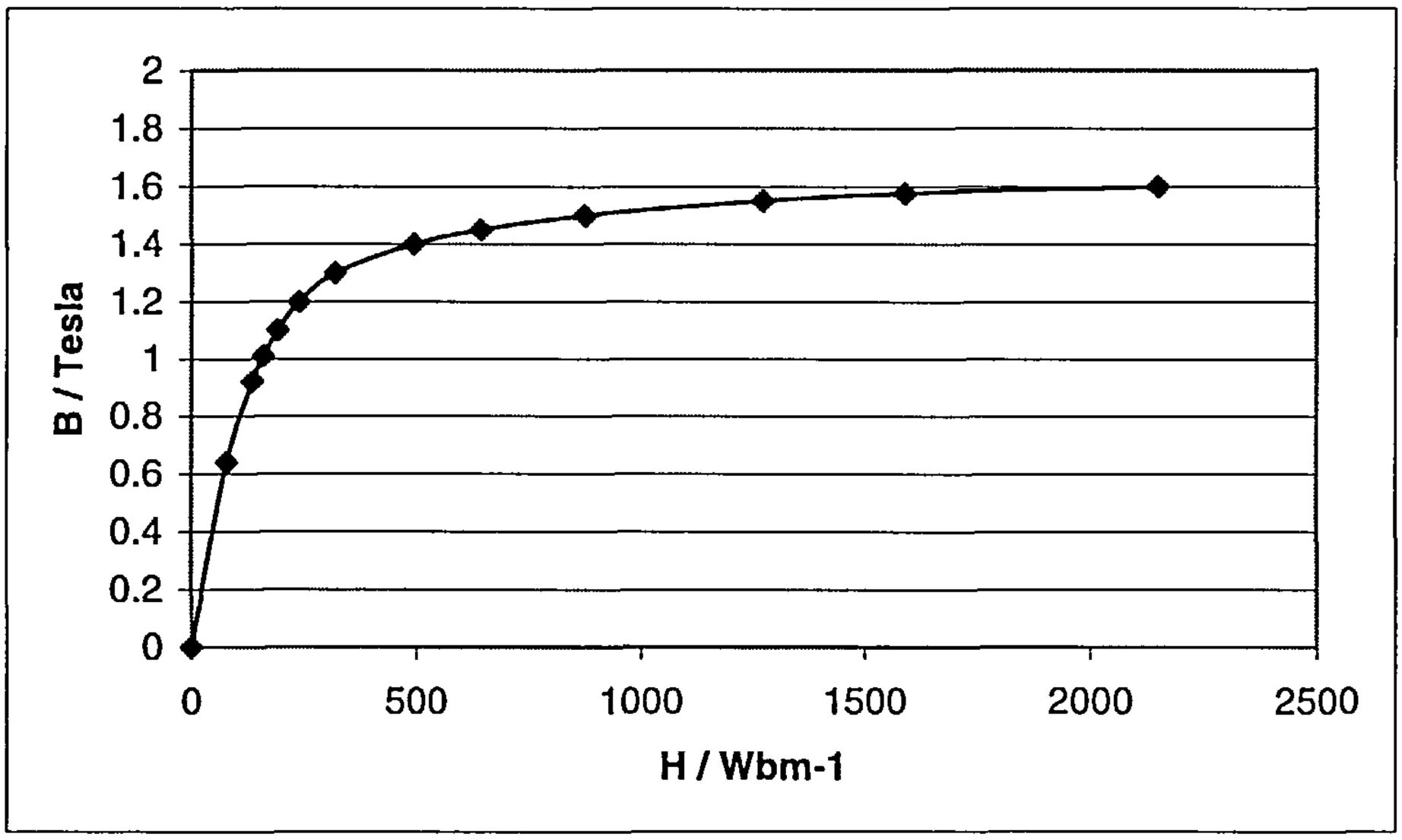

Figure 5.4: B-H Characteristic of Iron

Initially, models were created to analyse the relationship between back iron thickness and flux density. The rotor and stator poles were aligned, and basic geometries chosen and fixed. A constant current coil excitation was set at $4A/mm^{-2}$. The thickness of the rotor and stator back iron was then varied and the resulting flux density in those parts recorded. It was found that with a 3mm rotor back iron thickness, the maximum flux density achieved in it was only 1.3T. This thickness of back iron is likely to be mechanically weak, and so a 4mm thickness was felt to be the minimum. Ideally, the operating flux density would be around 1.5T, with a mechanically strong structure. This led to investigations of how to increase the

conductor slot area (hence the total excitation available), and find an appropriate back iron thickness. This was achieved by keeping the basic pole geometries and coil excitation constant, and varying the radius of the airgap (not the airgap width) to increase conductor area. This improved the level of flux in the machine and an appropriate rotor and stator back iron thickness of 4mm was used for the next stage of design, with a flux density in the iron of approximately 1.5T. Figure 5.5 shows the flux density distribution in the basic model.

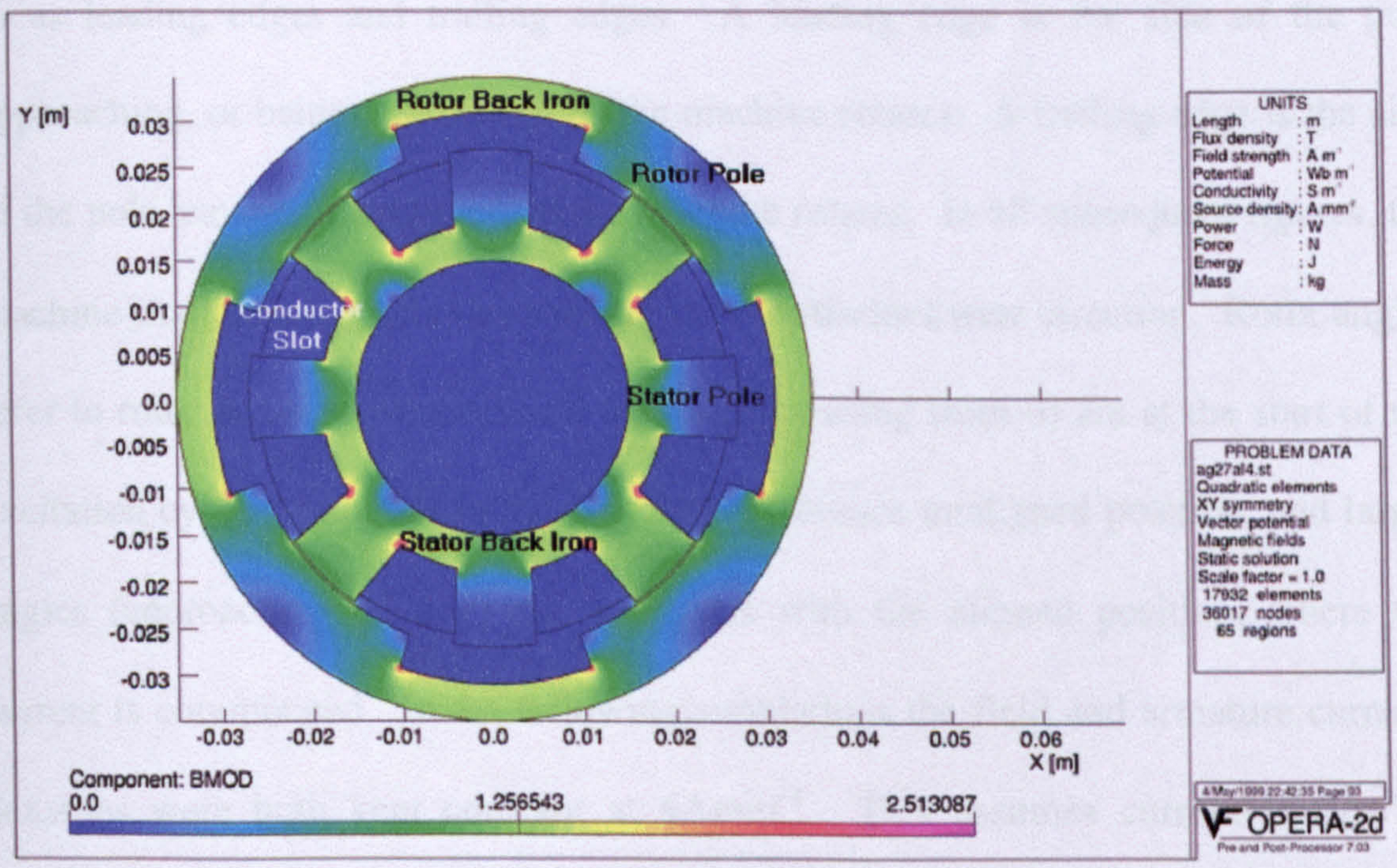

Figure 5.5: Predicted flux density distribution in early design model

Keeping the same current excitation in the conductor areas and the rotor and stator back iron thickness' constant, the width of the stator poles was varied to achieve a uniform flux density distribution through the pole and the back iron. A stator pole width of 15° was found to be optimal. Adding this to the parameters previously kept constant, the rotor pole widths were varied and motor torque predicted at various

rotor positions. It was found that a 50 degree rotor pole width gave the best torque profile with the minimum positions of zero or negative torque production.

Attention was then turned to the more detailed torque production profile of the machine. One important factor is that the machine must start at all rotor positions. This translates to positive torque being produced over a full 45 degrees of rotation for each commutation. The geometry of the rotor and stator poles must be shaped in order to achieve this. For purposes of this analysis, the pole edges shall be referred to as leading edges and trailing edges. A leading edge is the side of the pole approaching, or being approached as the machine rotates. A trailing edge is the side of the pole leaving or being left as the machine rotates. In all subsequent figures, the machine shall be assumed to be rotating in an **anti-clockwise** direction. Rotor angles refer to rotor positions where small angles (increasing from 0) are at the start of the excitation cycle, analogous to the switched reluctance unaligned position, and larger angles (approaching 45 deg) are analogous with the aligned position, where the current is commutated. In the following simulations the field and armature currents densities were both kept constant at $4Amm^{-2}$. This assumes current is flowing through one coil turn which fills the respective stator slot. The airgap, back iron and rotor and stator pole thickness' were also kept constant. Motor torque was calculated at various rotor positions assuming a 12mm stack length. A comparison of torque production between geometries was made.

The detailed geometry of the leading edge of the stator poles was investigated. It was found that by increasing the width of the pole at the airgap, positive torque production was achieved over the rotor positions at the start of a current cycle. This

increased width shall be termed "jut" and is measured in degrees. Figure 5.6 shows the stator pole with 9 degrees of jut added.

(a) without jut (b) with 9 deg. jut

Figure 5.6: Stator pole (a) without jut and (b) with 9 degree jut

Figure 5.7 shows how varying the width of the "jut" changed the torque profile.

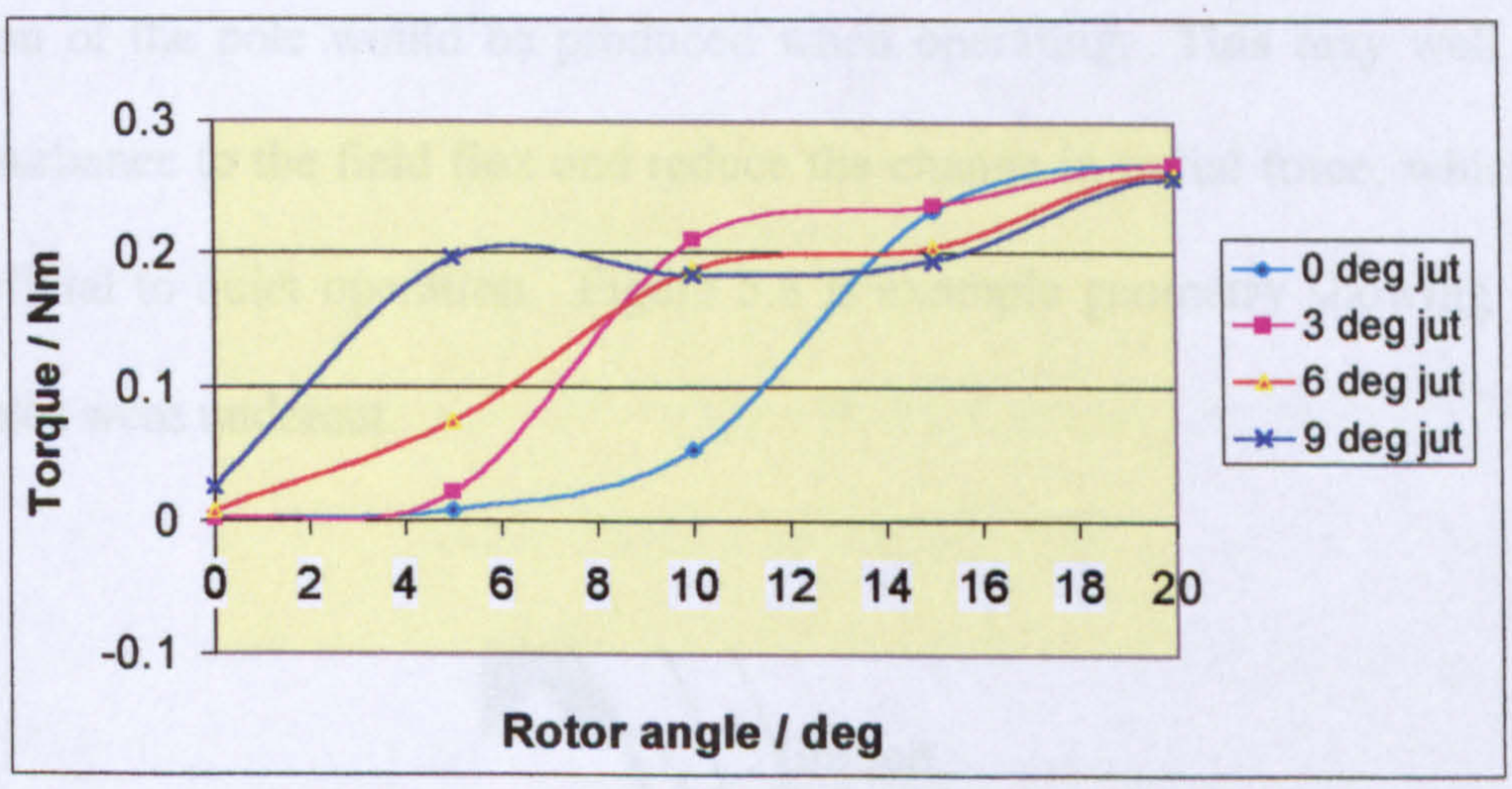

Figure 5.7: Predicted torque profile with varying widths of "jut"

Adding jut to the stator pole tip reduces the slot area and makes it more difficult to fit the coils, so the minimum jut width of 9° was selected to produce positive torque over the rotation angles shown. The depth of the jut was increased toward the stator pole to provide extra strength.

In an attempt to extend the production of positive torque at positions towards the end of the working stroke (approaching the "aligned" position), the effect of shaping the rotor poles was investigated. Methods for extending the range of torque production, such as grading the width of the airgap in the direction of rotation, are well published [29-31]. Grading the airgap reduces the overall performance of the machine because part of the machine always has a wider airgap, which increases the magnetic reluctance, reducing the total flux that can cross it.

Undercutting the rotor poles, by removing material between the back iron and the airgap face, may result in better machine performance than grading the width of the airgap. By grading the undercut on the pole, in the direction of rotation, graded saturation of the pole would be produced when operating. This may well provide less disturbance to the field flux and reduce the change in radial force, which would be beneficial to quiet operation. Figure 5.8 is example geometry showing how the rotor poles were undercut.

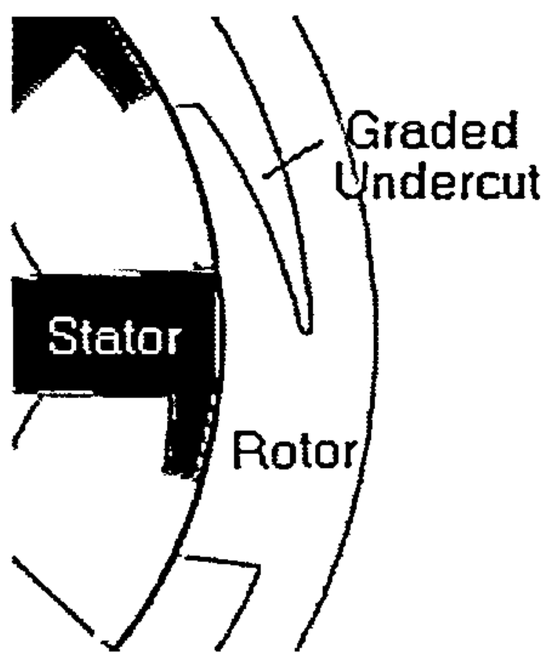

Figure 5.8: Example of a graded undercut rotor pole

Varying the amount by which the rotor pole was undercut had a significant effect on the magnitude and range of angles producing positive torque. It also had a

significant effect on the magnitude of radial force, between the rotor and stator poles, in the airgap. Although it is the sudden change in the rate of change of radial force that causes vibration in reluctance machines, minimising the magnitude of the radial force has a beneficial effect on reducing vibration. Figures 5.9 and 5.10 show how varying the rotor pole undercut changed the torque and radial force profiles at rotor angles nearing the aligned position.

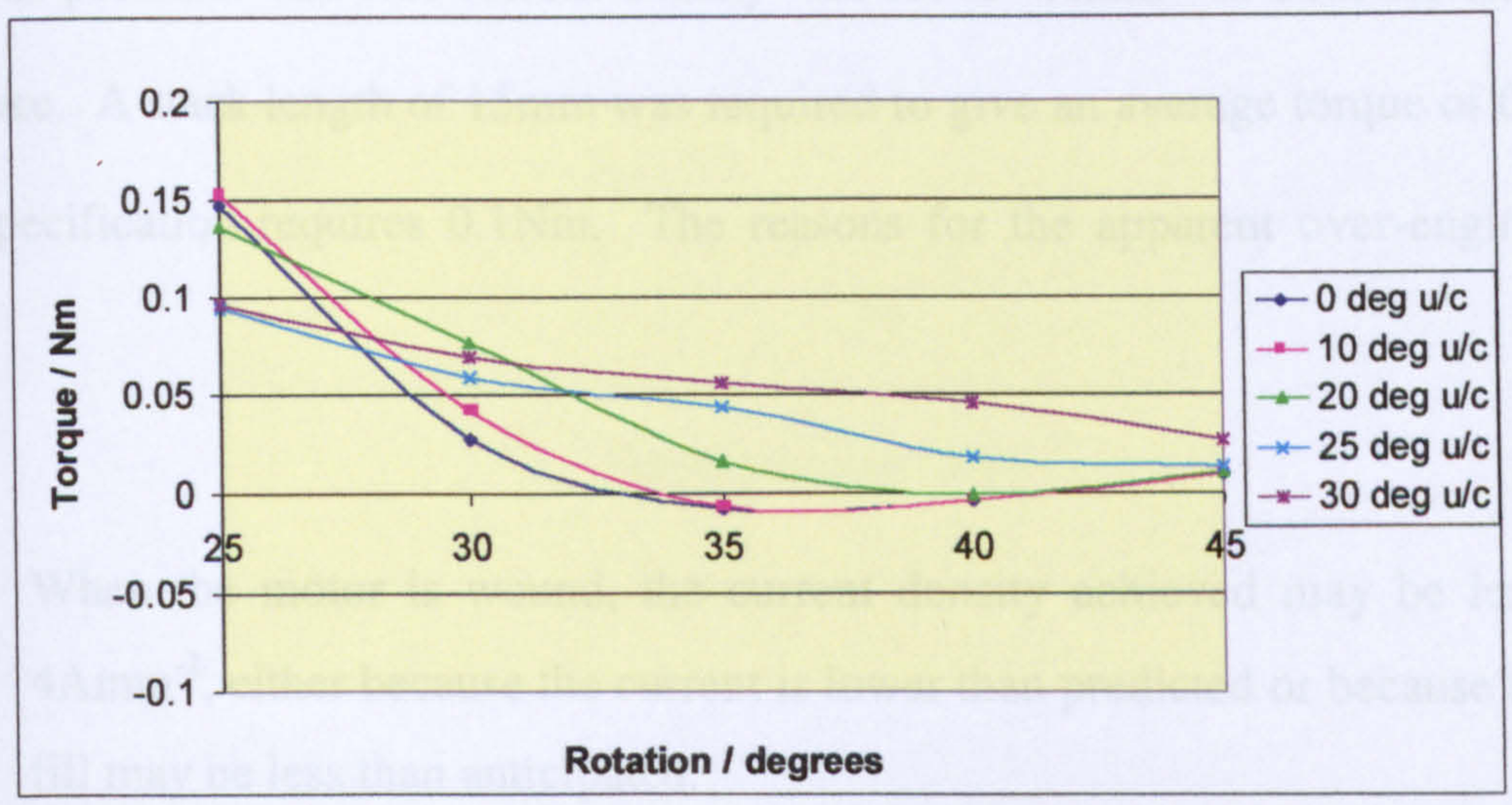

Figure 5.9: Predicted torque production approaching aligned position with varying rotor pole undercut

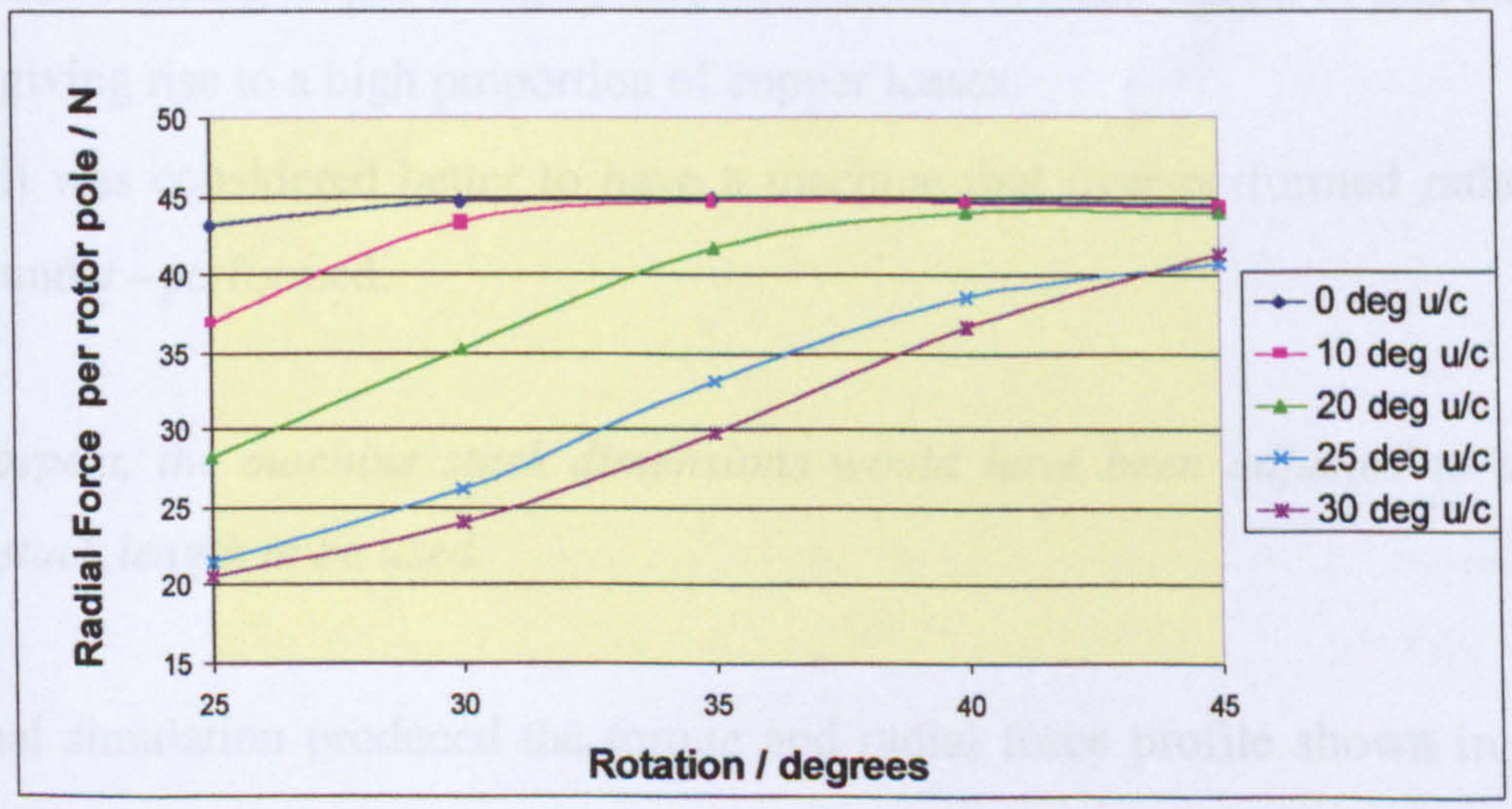

Figure 5.10: Predicted radial force approaching aligned position with varying rotor pole undercut

An undercut of 25 degrees (of the 50-degree rotor pole width) achieves positive torque at all rotor positions approaching the commutation point. This value of undercut also produced the minimum magnitude of radial force at 45° rotation, and its rate of change approaches zero.

Other small changes were made to the geometry to smooth the torque production as much as possible. The slot current density was set to $4Amm^{-2}$ in both the field and armature. A stack length of 15mm was required to give an average torque of 0.2Nm. The specification requires 0.1Nm. The reasons for the apparent over-engineering are:

- When the motor is wound, the current density achieved may be less than $4Amm^{-2}$, either because the current is lower than predicted or because the slot fill may be less than anticipated.
- The real excitation will not be constant – the armature current will build up from zero and reduce to zero every stroke, which will reduce the torque predicted.
- End winding length is highly disproportionate to stack length in this machine, giving rise to a high proportion of copper losses.
- It was considered better to have a machine that over-performed rather than under –performed.

In retrospect, the machine stack dimensions would have been adjusted to allow a longer stack length to be used.

The final simulation produced the torque and radial force profile shown in figures 5.11 and 5.12 respectively.

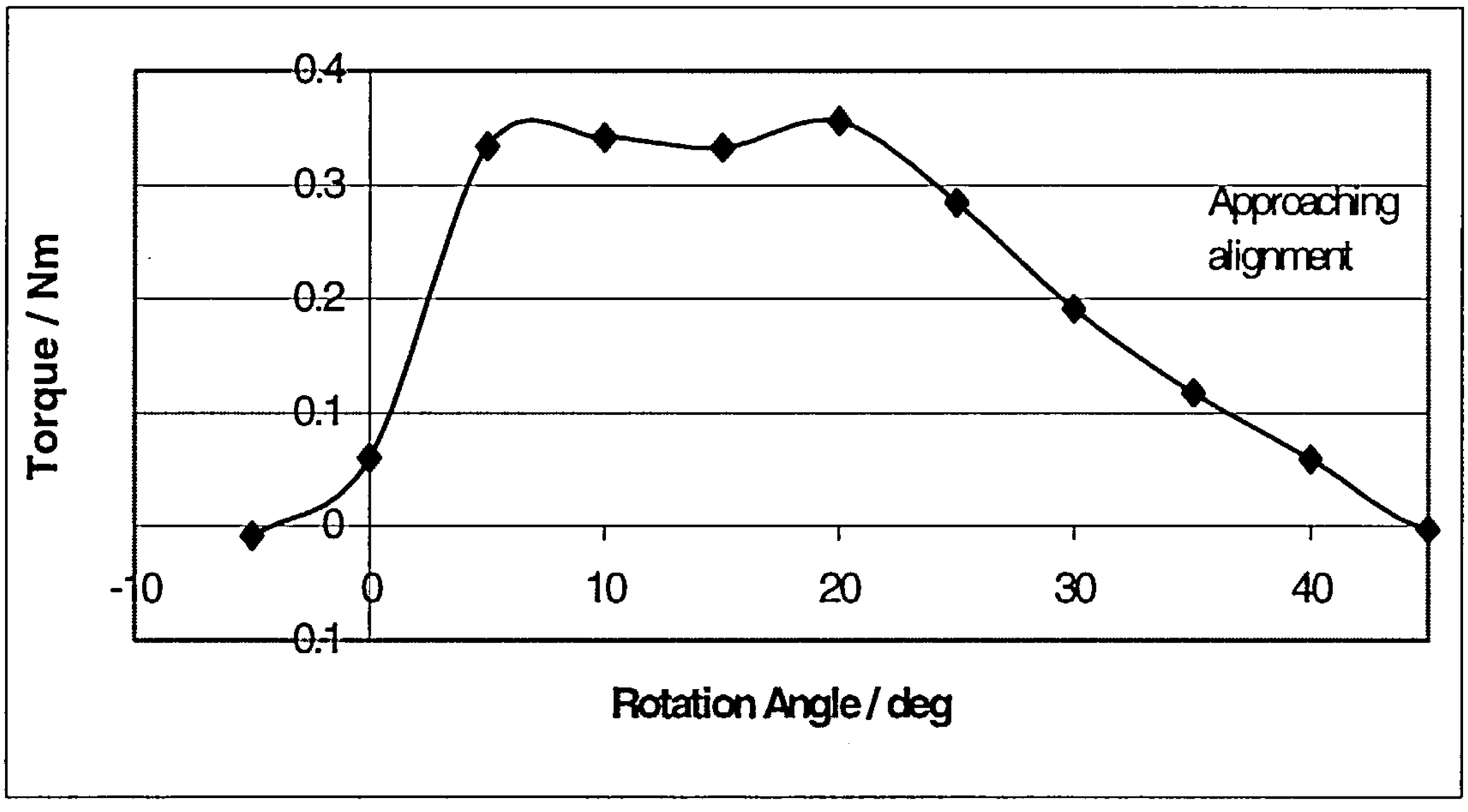

Figure 5.11: Predicted torque profile of final design

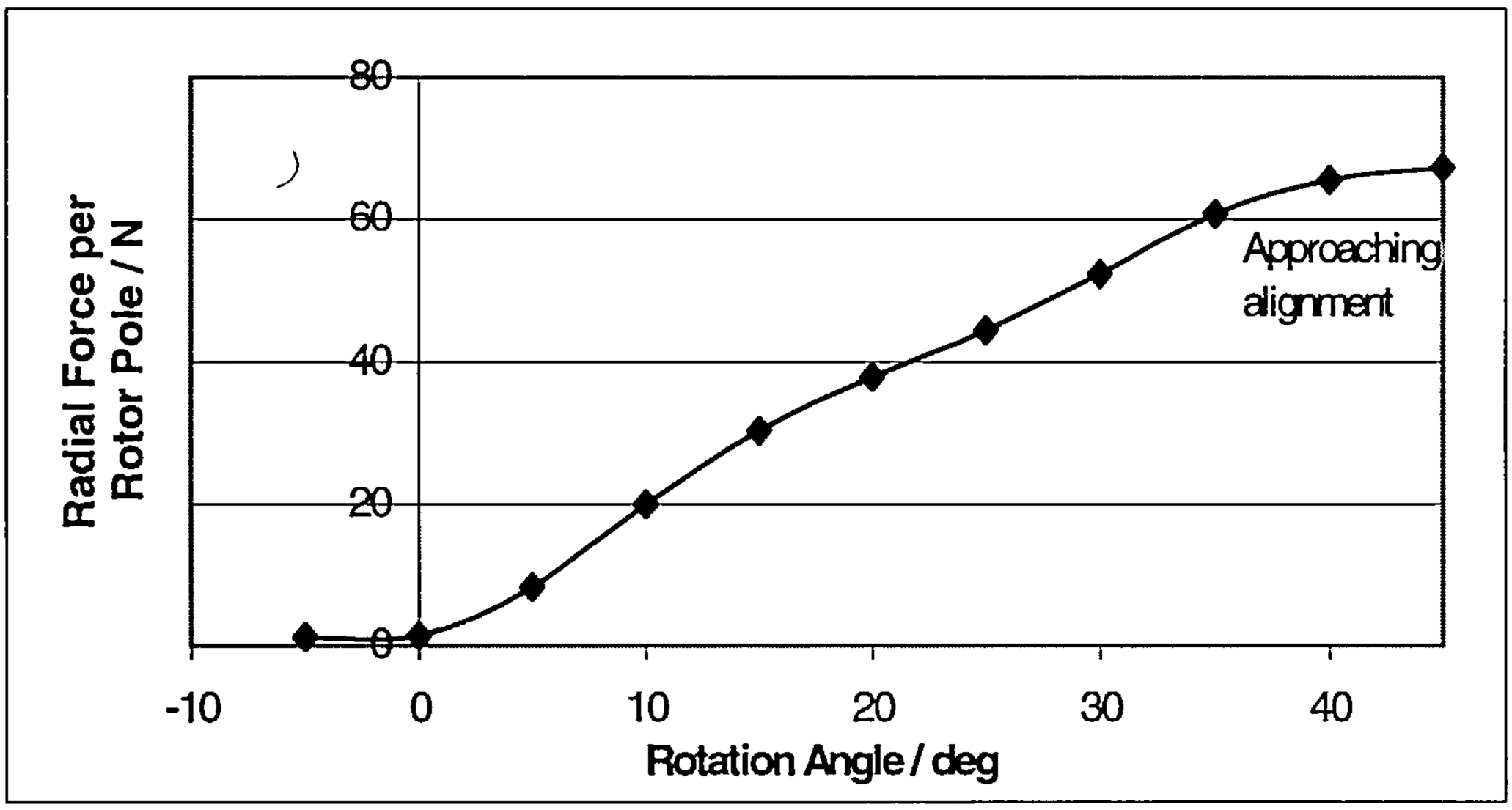

Figure 5.12: Predicted radial force profile of final design

The final lamination design, with aligning key-way and fixing holes is shown in figure 5.13 (not to scale):

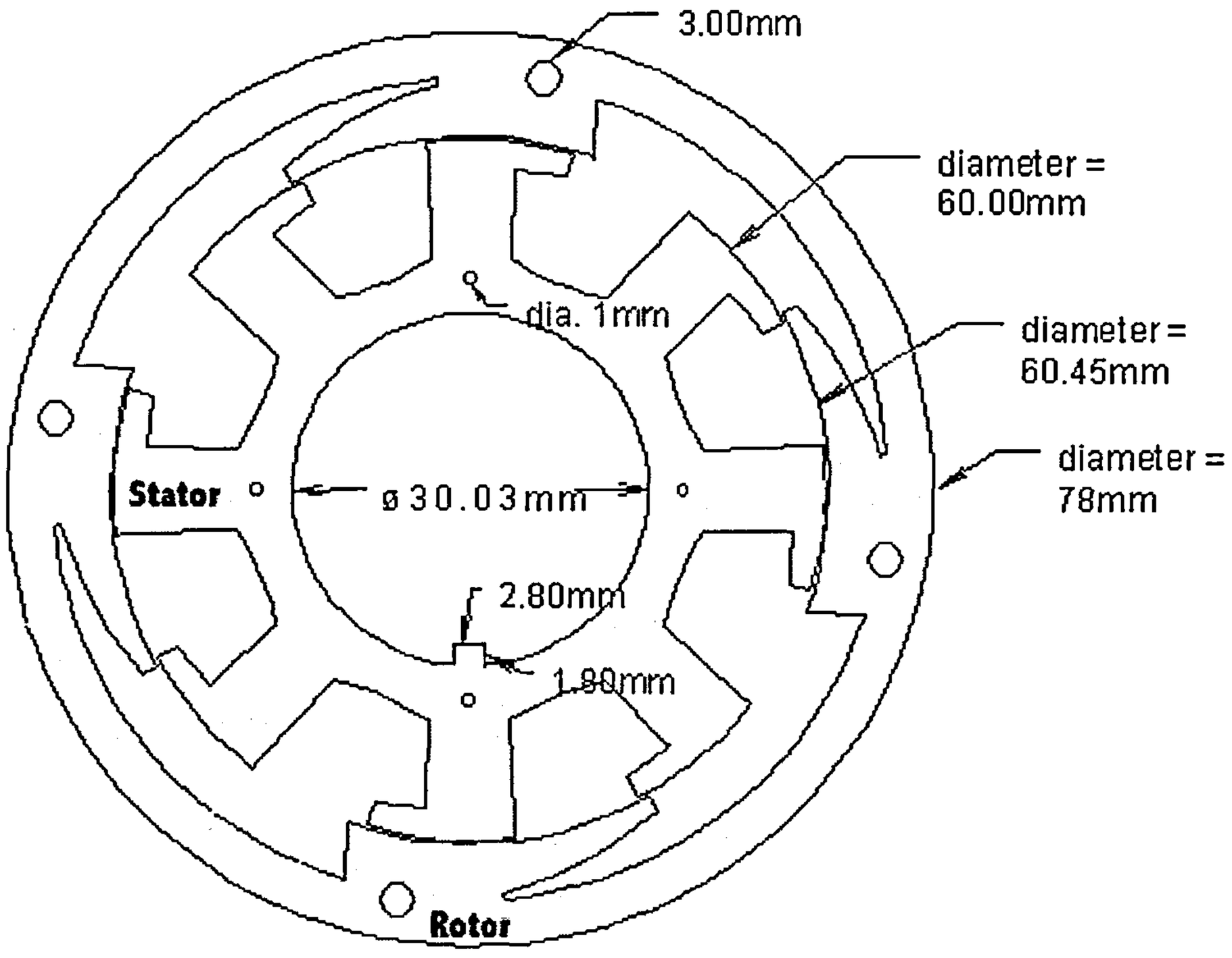

Figure 5.13: Final lamination design of external rotor flux switching motor

A simulation of field flux and armature flux with rotor position was performed on the final model, with the field coils excited only. This enables the amount of field flux linking the armature to be calculated and can be used in predicting the armature current as described in section 5.6.5. The field conductor slots were set to a current density of $4Amm^{-2}$, and the rotor position varied in 5 degree steps over 90°. Figure 5.14 shows how the field and armature flux varied with rotor rotation.

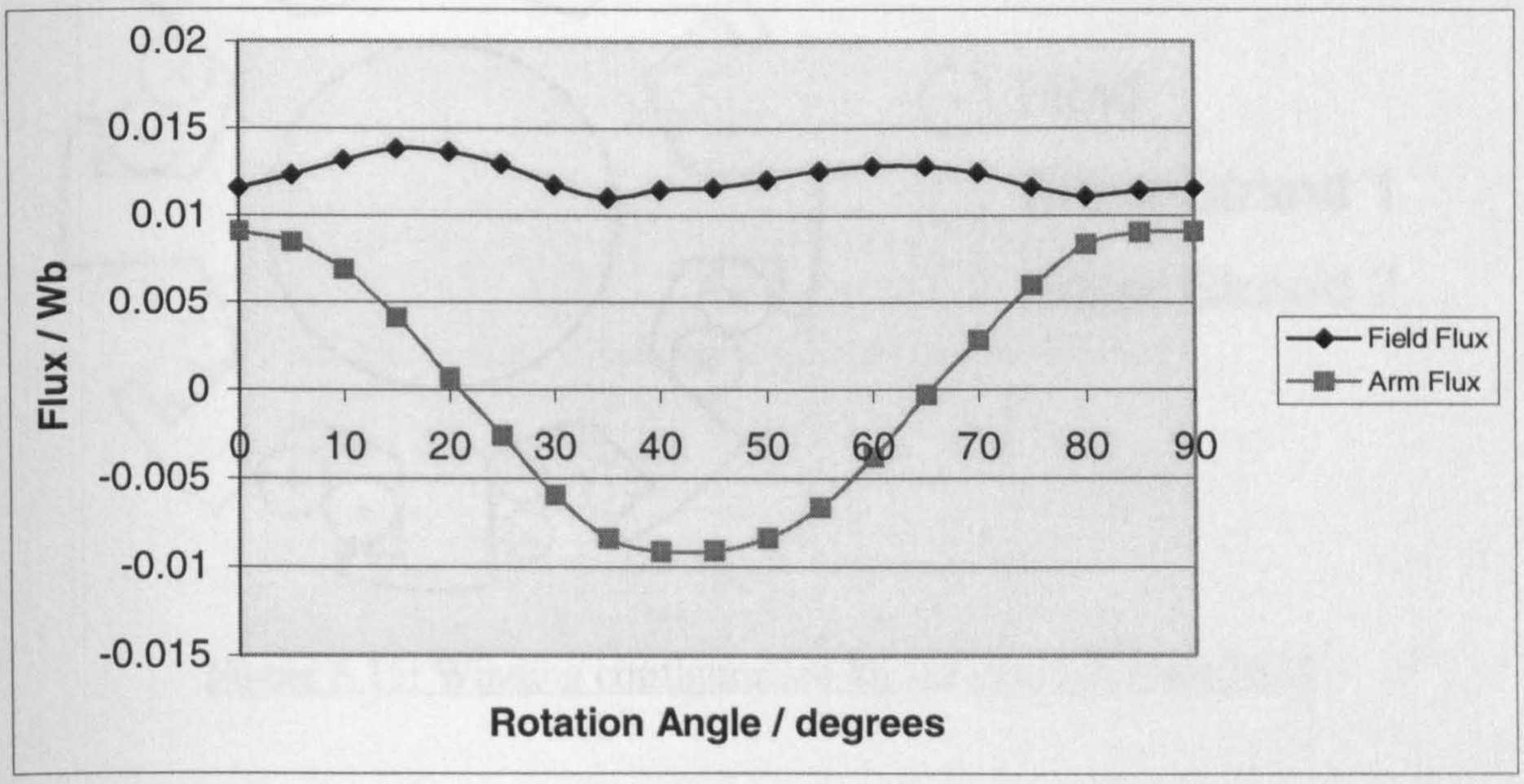

Figure 5.14: Simulated field and armature flux with field only excitation

The field flux varies very little with rotor position, as the change in ratio of maximum and minimum inductance is low. The armature flux varies smoothly between positive and negative values.

5.6.5 Winding Design

In this 8 stator pole, external rotor machine, the field and armature coils will be wound and connected according to figure 5.15, where the standard dot and cross convention has been used to denote current polarity.

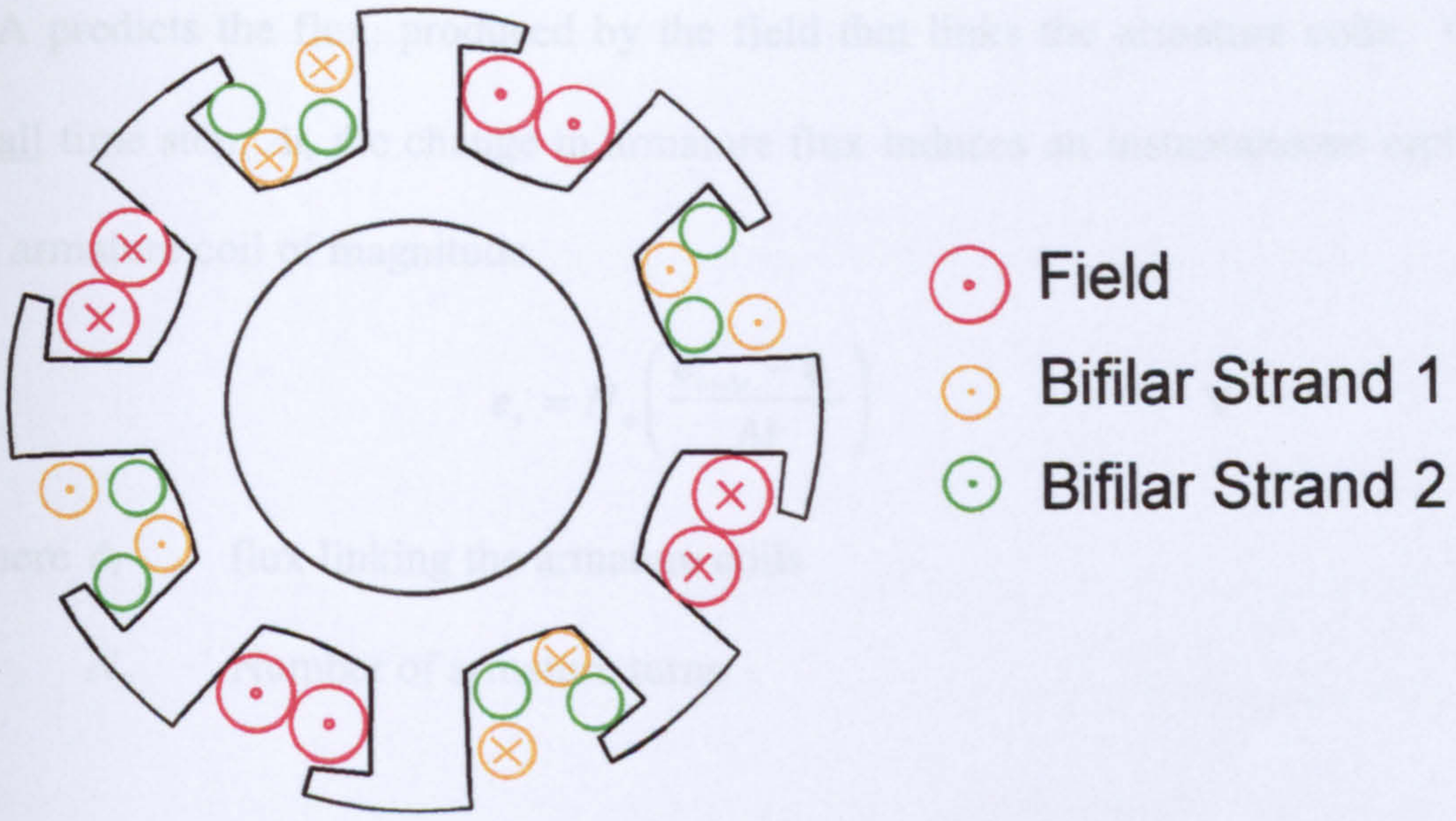

Figure 5.15: Winding configuration for the external rotor FSM

The principle of the flux switching motor is to inject current into the armature winding, to oppose the internal back emf set up by the field excitation, thus producing electromagnetic torque.

A spreadsheet based design tool has been created by the author, which solves electromagnetic motor equations to simulate motor performance for a given winding. It uses flux data from finite element analysis, based on a field only excitation pattern to calculate instantaneous values of armature current over a time stepped rotation of the rotor. Simulated performance data such as torque, mechanical power out, losses and efficiency are analysed to compare different winding designs. There are many assumptions made in the calculations and these will be listed later.

FEA predicts the flux, produced by the field that links the armature coils. Over a small time step, Δt, the change in armature flux induces an instantaneous emf, e_t, in the armature coil of magnitude

$$e_t = N_a\left(\frac{\phi_{t+\Delta t} - \phi_t}{\Delta t}\right) \qquad \text{V} \qquad (5.4)$$

Where ϕ_t flux linking the armature coils

N_a Number of armature turns

The polarity of the voltage applied to an armature winding, switches between positive and negative as the two armature circuits are energised alternately. With the field winding connected in series with the armature circuit, the magnitude of this voltage, v_a, is given by

$$v_a = V_s - i_f R_f \qquad \text{V} \qquad (5.5)$$

where V_s Supply voltage (can be positive or negative)

i_f Instantaneous current in field winding

R_f Resistance of field winding

The next time stepped value of instantaneous armature current, $i_{(t+\Delta t),}$ is given by

$$i_{(t+\Delta t)} = i_t + \left[(v_a - i_t R_a) - e_t\right]\left(\frac{\Delta t \Re_n}{N_a{}^2}\right) \qquad \text{A} \qquad (5.6)$$

where i_t previous instantaneous value of armature current

R_a Armature winding resistance

$\Re_n$ Reluctance of magnetic circuit

The instantaneous output power, p_t , is given by

$$p_t = i_t e_t \qquad \text{W} \qquad (5.7)$$

The average of these instantaneous values over a commutation cycle gives the mechanical power.

An estimate was made to allow for the effects of eddy currents and hysteresis. In such a small machine, these iron losses may make up a significant proportion of the input power. It was assumed that the iron losses would be around 10% of the output power of the motor, and so this was added to the input power.

The input power, P_{in}, is calculated from the available output power plus the copper losses from the field and armature windings, and the iron loss estimation and is given by

$$P_{in} = P_{out} + (I_f{}^2 R_f) + (I_a{}^2 R_a) + P_{iron} \qquad \text{W} \qquad (5.8)$$

where I_f RMS field current (although assumed to be constant)

I_a RMS armature current

R_f Field winding resistance

R_a Armature winding resistance

P_{iron} Iron losses

The average output torque of the machine ,T_{av}, is calculated from

$$T_{av} = \frac{P_{out}}{\omega} \qquad \text{Nm} \qquad (5.9)$$

where ω is the constant speed of the machine ($rads^{-1}$) from which Δt is derived. Because the machine was simulated at constant speed, a small time step of length Δt seconds, also corresponds to an angular rotation of the rotor. At 1800 rpm a 5° rotation corresponds to a 0.463ms (3 d.p.) time step.

Certain assumptions were made about motor conditions, and the calculations performed by the model. These are listed below:

- Motor is at constant speed, and Δt is small.
- Field current is constant (it actually varies with I_a and rotor position). This was set in the FEA model and is the basis for the flux data used in subsequent calculations.
- Iron Losses are 10% of the output power.
- A stack length of 15mm was assumed based on the crude values of torque calculated during early design, to meet the load specification.
- Mean length of a coil turn was estimated to be 0.14m.
- Packing factor of 0.4 was estimated for slot fill
- Resistance of windings increases by an estimated 20% due to temperature rise of the windings.
- An operating temperature of approximately 60° was assumed.

The wire diameter and number of turns for the field and armature windings were calculated, and the coils were wound and connected according to the specification given in Table 5.2:

Table 5.2: Field and armature winding specification

Attribute	Field Winding	Armature Winding
Number of Coils	4	4
Number of strands per coil	1	2 (bifilar)
Number of turns per coil	300	200
Wire diameter / mm	0.25	0.2
Connection	Series	Series
Resistance per coil / Ω (measured at 20°C)	11.4	11.7
Total Resistance / Ω	45.6	46.8

With this winding design, the model predicted the motor parameters given in Table 5.3, for a constant speed of 1800rpm. The supply voltage was fixed at 150V. A supply voltage of 340V d.c. was targeted, but the minimum available wire diameter limited the supply voltage.

Table 5.3: Summary of electrical design parameters calculated by the flux switching motor design spreadsheet model

Motor Parameter	Calculated Value
Input Power / W	72
Available Output Power / W	26.8
Total losses / W	45
Efficiency / %	37
Average Torque / Nm	0.14
RMS Armature current / A	0.558
Field Current / A	0.583

Figure 5.16 shows the field and armature flux data taken from the FEA model and used as an input to the spreadsheet model. Predicted values of predicted output power, induced armature voltage (back emf) and armature current are shown in figures 5.17-5.19 at time stepped instances, for the winding data given above.

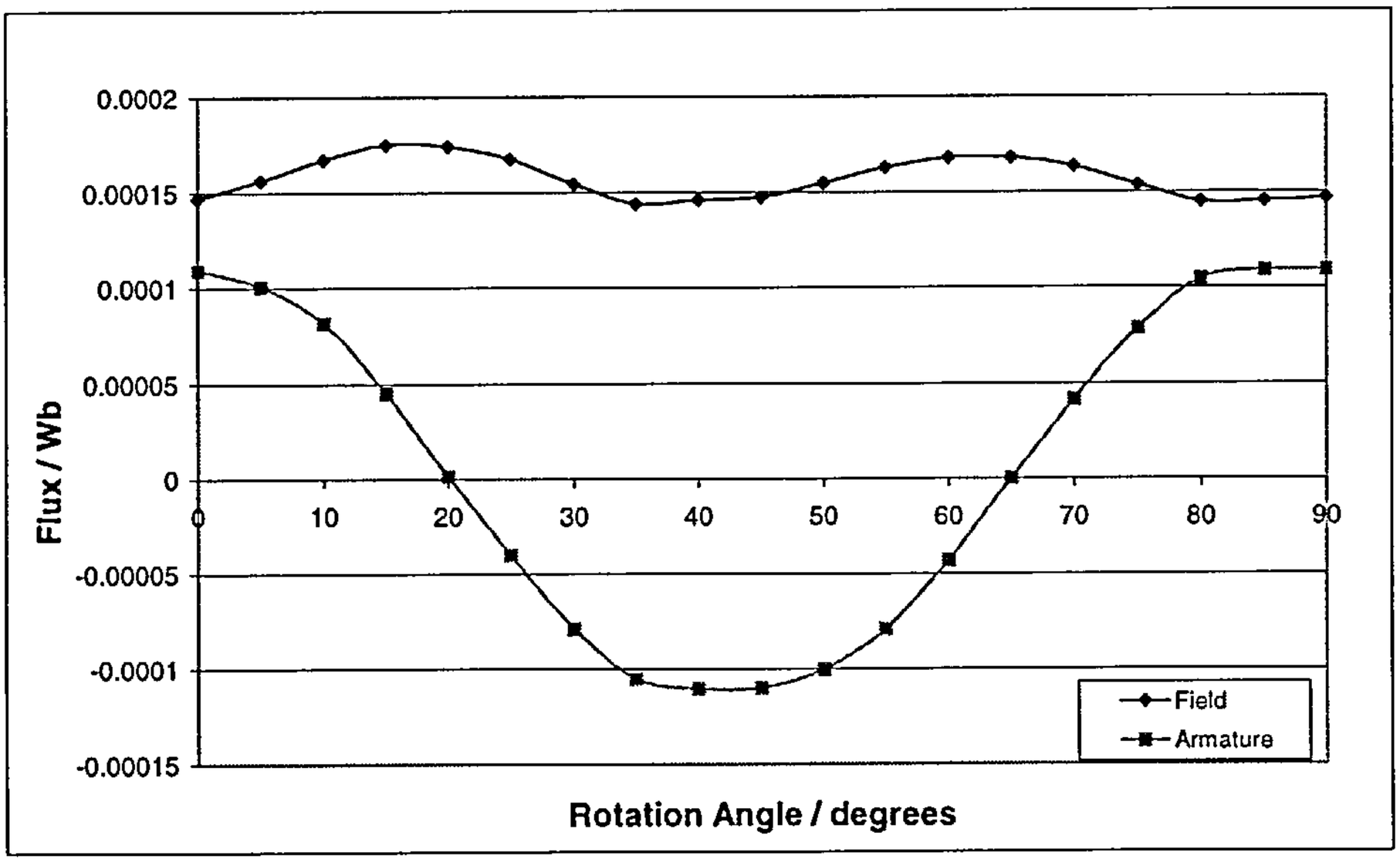

Figure 5.16: Predicted Instantaneous field and armature flux

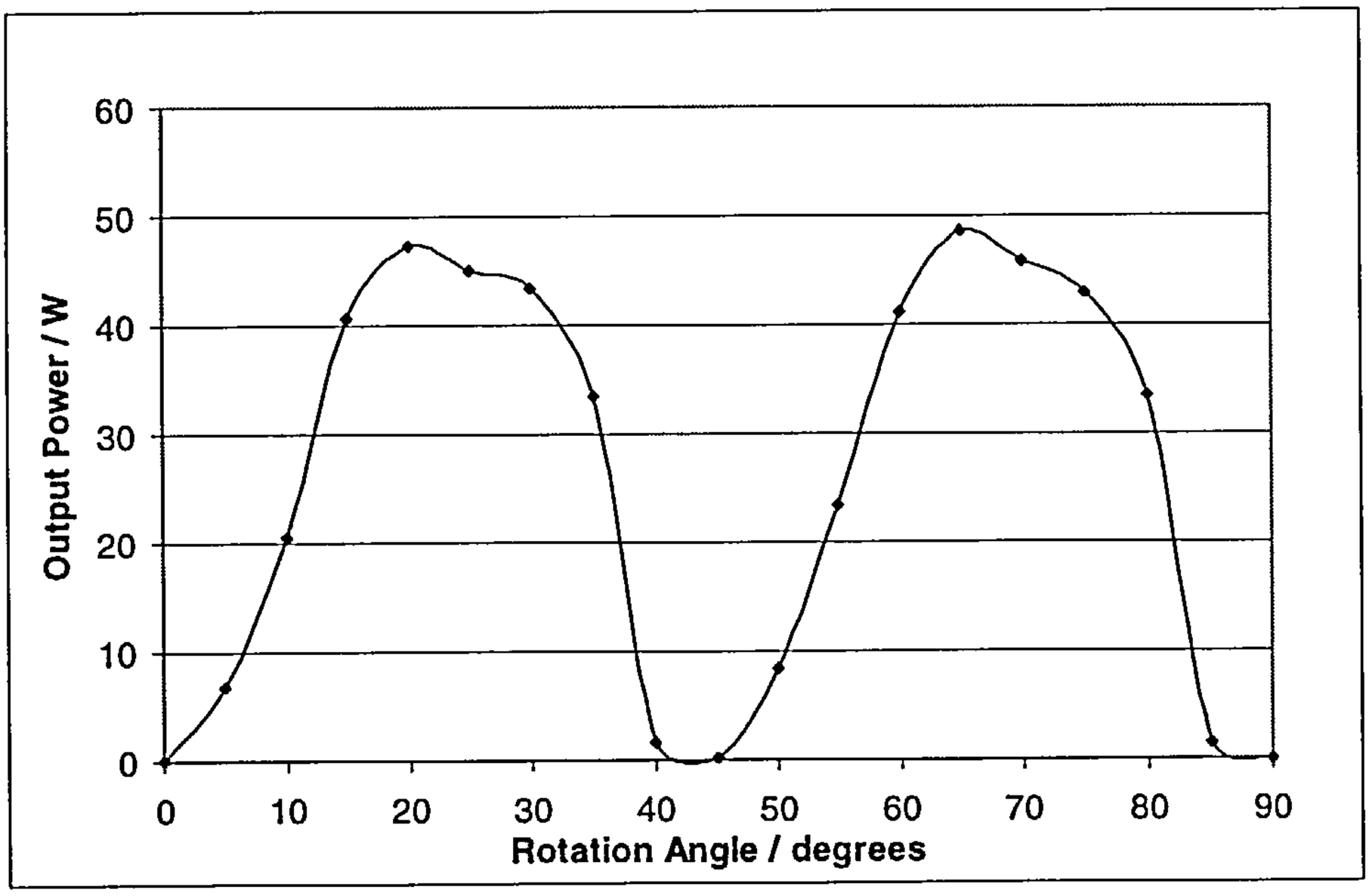

Figure 5.17: Predicted instantaneous output power

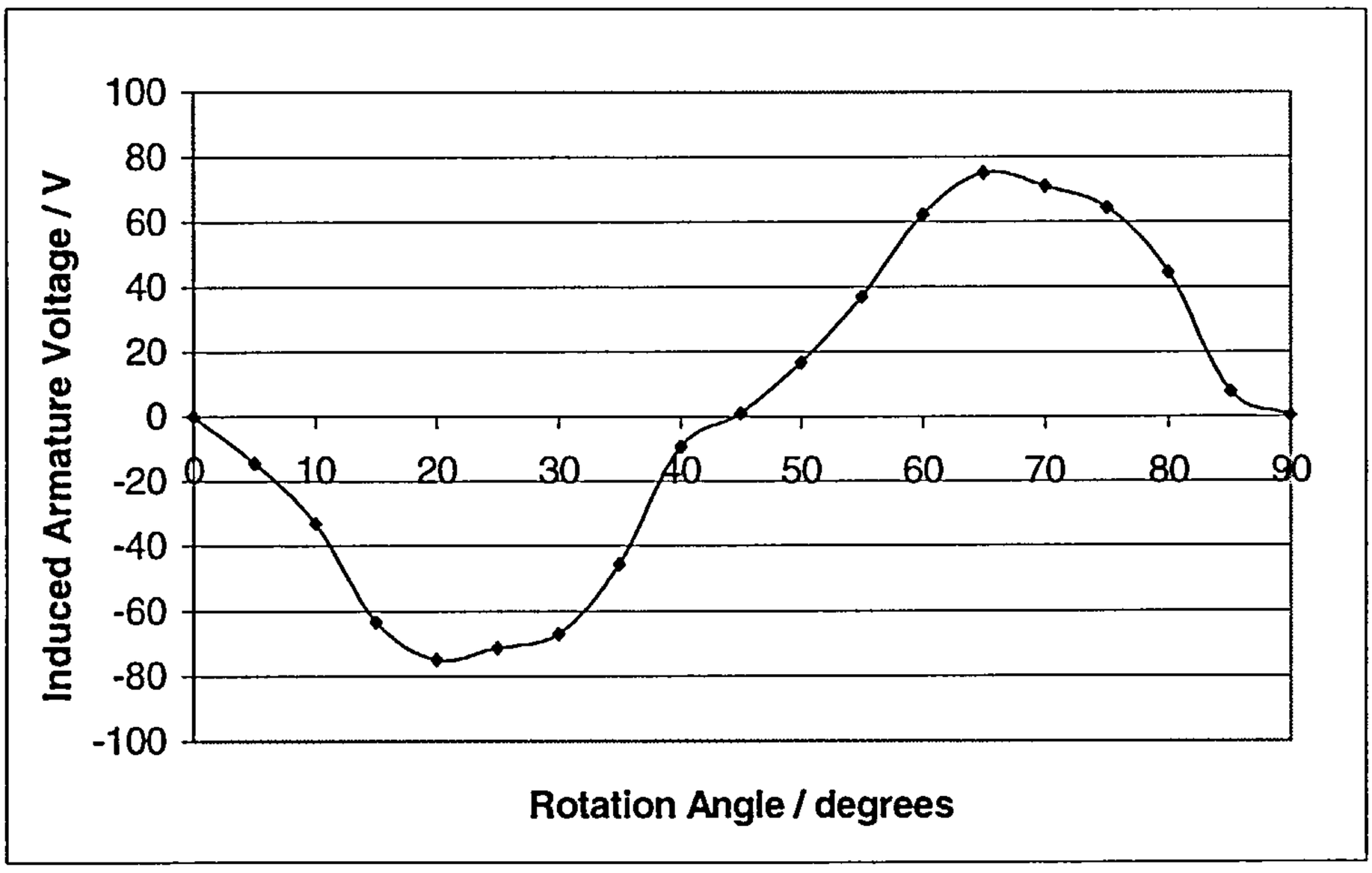

Figure 5.18: Predicted values of instantaneously induced armature voltage

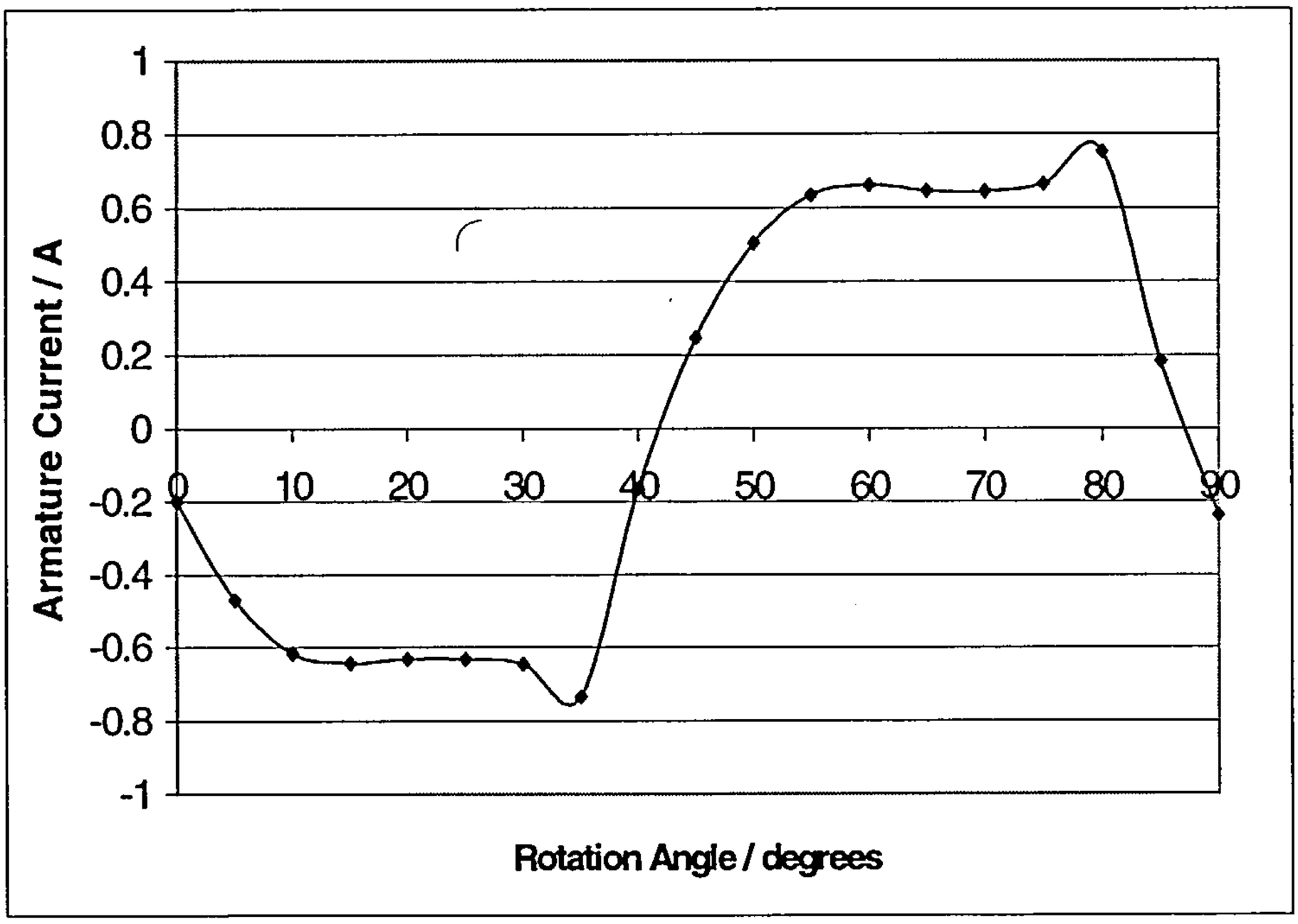

Figure 5.19: Predicted values of instantaneous armature current

This shows the armature current flowing into the back emf, generating torque (output power) twice per 90 degree revolution. One armature conducts for the first 45

degrees and then the other armature conducts (in the opposite direction) for the second 45 degrees. This is repeated as the rotor continues rotation.

5.6.6 Mechanical design

The mechanical design of the motor was completed with consideration given to some key factors:

- Concentricity of the rotor and stator (uniform airgap)
- Avoiding cantilever effect of rotor
- Housing the bearings
- Weight
- Alignment of rotor and stator laminations
- Space for on-board electronics
- Fit into existing product casing

Engineering drawings of the mechanical parts are given in appendix A. Three parts were manufactured. A stator stack support, a rotor stack support and a shaft. The bearings were housed in the stator support, as far apart as possible to reduce the cantilever effect of the rotor when moving. 8mm ball race bearings were used and were lightly pressed into position. The stator and rotor supports were manufactured from aluminium because of its lightweight properties. The shaft was manufactured from mild steel for strength. A slot was cut in the stator support to allow the stator laminations to be aligned. Four bolts were placed through the rotor support to align the rotor laminations. The rotor and stator supports were manufactured with the same centre on the same lathe, to sustain concentricity. Figure 5.20 shows the mechanical components used to build the prototype flux switching motor.

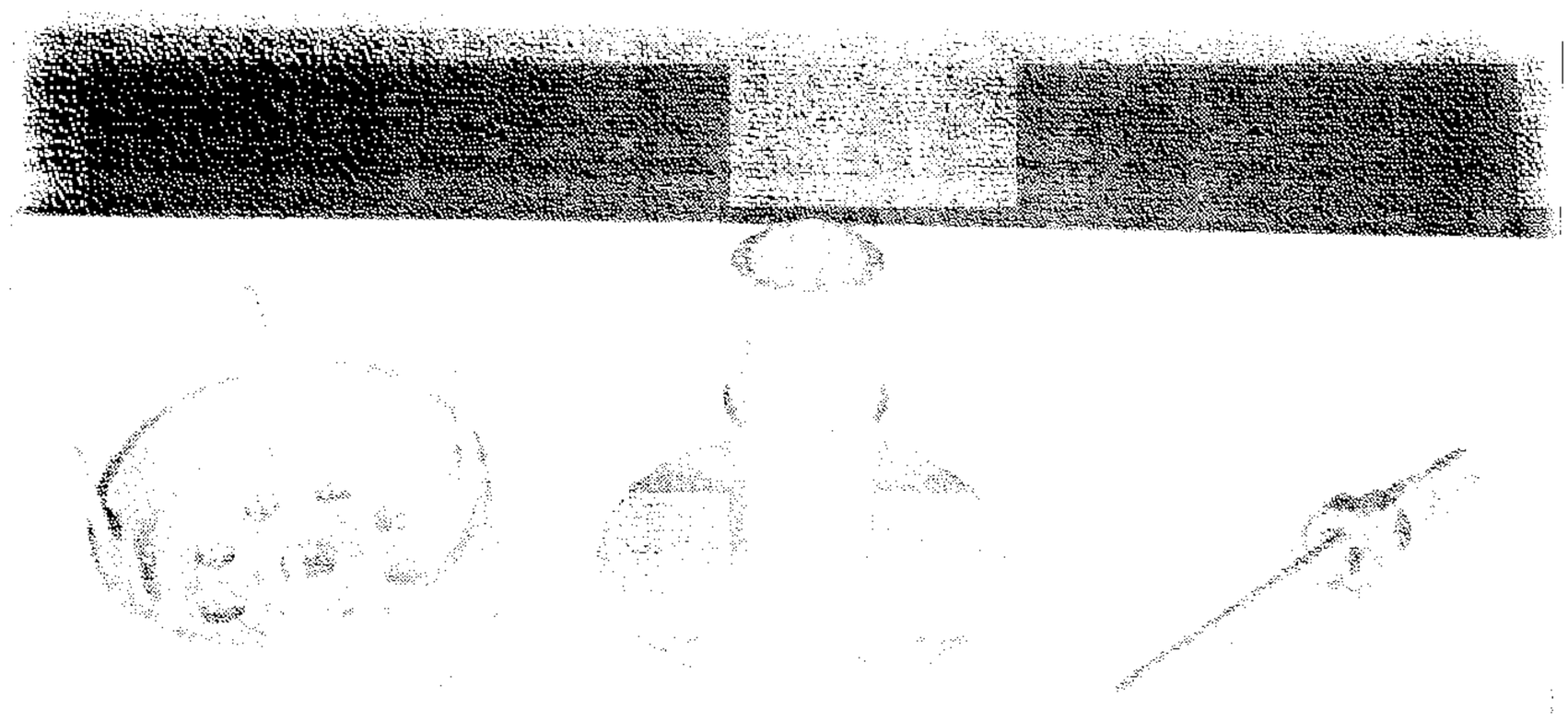

Figure 5.20: Manufactured mechanical components for the prototype external rotor Flux Switching motor

5.7 Experimental Verification of Simulated Flux

Having built and wound the prototype 8/4 external rotor flux switching motor based upon ideal characteristics and making many assumptions, experimental techniques were used to verify the design model. All the calculations performed were based on the FEA prediction of the amount of field flux that links the armature coils. Thus measuring this experimentally and comparing it to the FEA prediction should provide an indication as to the accuracy of the model.

5.7.1 Static Experimental Procedure

The motor was connected to a static test rig with a dividing head, allowing very accurate rotational position to be measured. To find a reference position, the field winding was excited with d.c. current. Eight parking positions were found, 4 with short flux paths and 4 with long flux paths. Figure 5.21 shows these two flux paths:

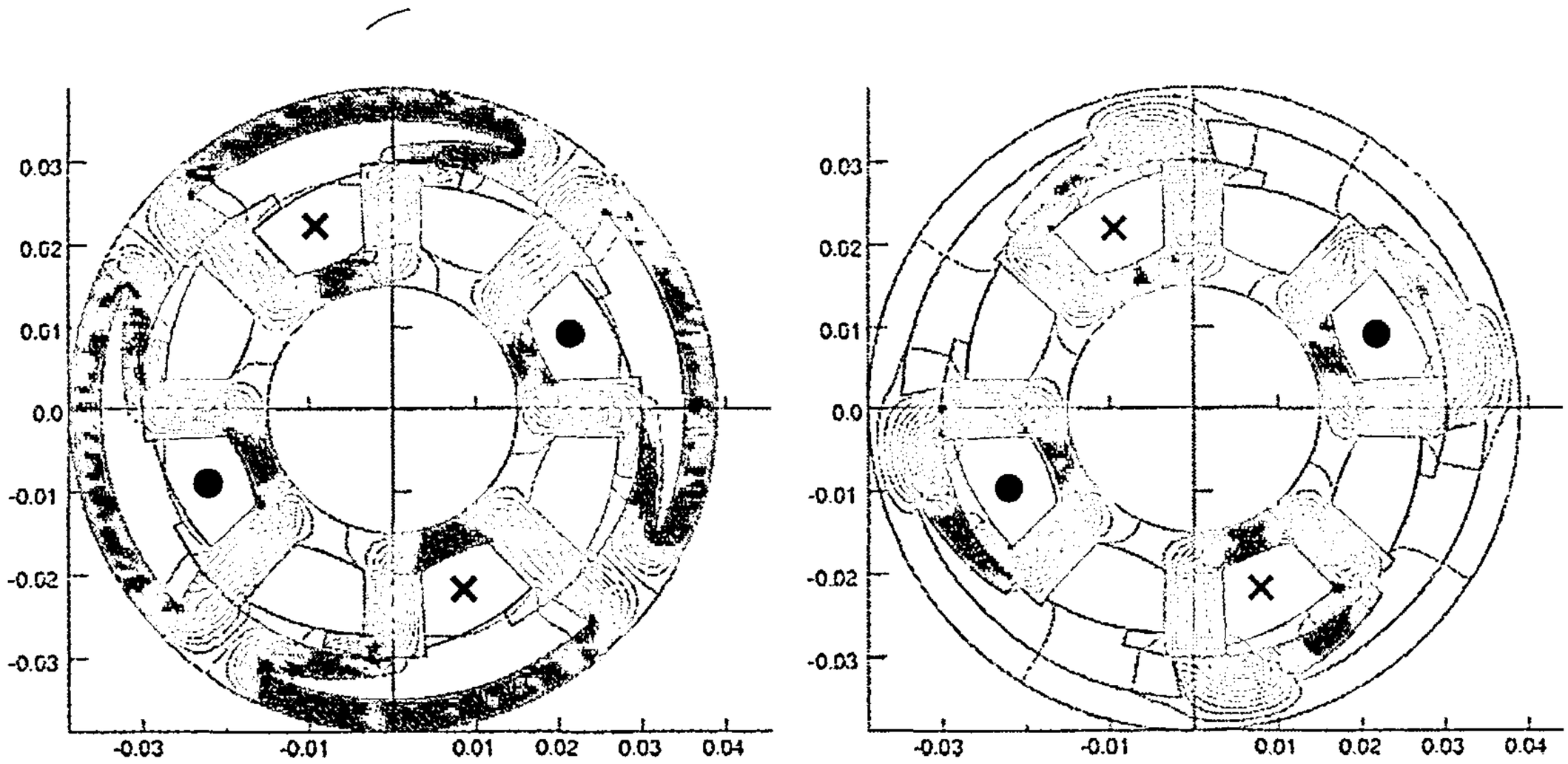

Figure 5.21: Parking positions with d.c. field excitation

The long flux path parking position was selected to be the experimental "0 degrees rotation" which corresponds to the FEA rotation position of 25 degrees. With the rotor locked to the dividing head, a sinusoidal excitation was applied to the field winding such that the motor went into a state of magnetic saturation. This provides flux in one direction and then the other and magnetises the motor over the complete B-H loop. The frequency of the sinusoidal excitation was 40Hz. By capturing one period of the sinusoidal voltage, v_f, and the sinusoidal current, i_f, on an oscilloscope, and measuring the resistance, R_f, of the winding immediately afterwards, the field flux linkage, ψ_f, can be calculated according to:

$$\Psi_f(t) = \int (v_f - i_f R_f) dt \qquad \text{Wb Turns} \qquad (5.5)$$

By appropriate choice of integration limits and initial conditions, the flux at a particular field current can be found. A frequency of 40Hz was chosen to minimise experimental errors, because a low frequency requires a lower voltage to achieve saturation, making the voltage drop $i_f R_f$ a higher proportion of V_f. This is therefore highly dependant on the measured value of R_f which is probably the least accurate of all the measurements. Equally a high frequency would yield high iron losses which would not be representative of the motor when operating.

By measuring the induced voltage, e_a, in one of the open circuit armature windings the amount of field flux which links the armature windings, ψ_a, can be calculated using

$$\Psi_a(t) = \int e_a(t) \; dt \qquad \text{Wb Turns} \qquad (5.6)$$

where T is one period of the induced armature voltage. The coupling coefficient, k, at this position, is the ratio of $\psi_f : \psi_a$

This procedure was carried out at rotor positions incrementing 5°. This provided a complete set of flux linkage versus current curves for the prototype flux switching motor. For comparison with the FEA data, the experimental data taken at the predicted field current (one point on the sinusoidal current trace) was extracted, and corrected for offsets. The FEA field and armature flux data was then converted to flux linkages by the respective number of turns, and plotted against the experimental data. Figure 5.22 shows the comparison of experimental flux linkage and predicted flux linkage in the field and armature windings at the predicted field current d.c. excitation.

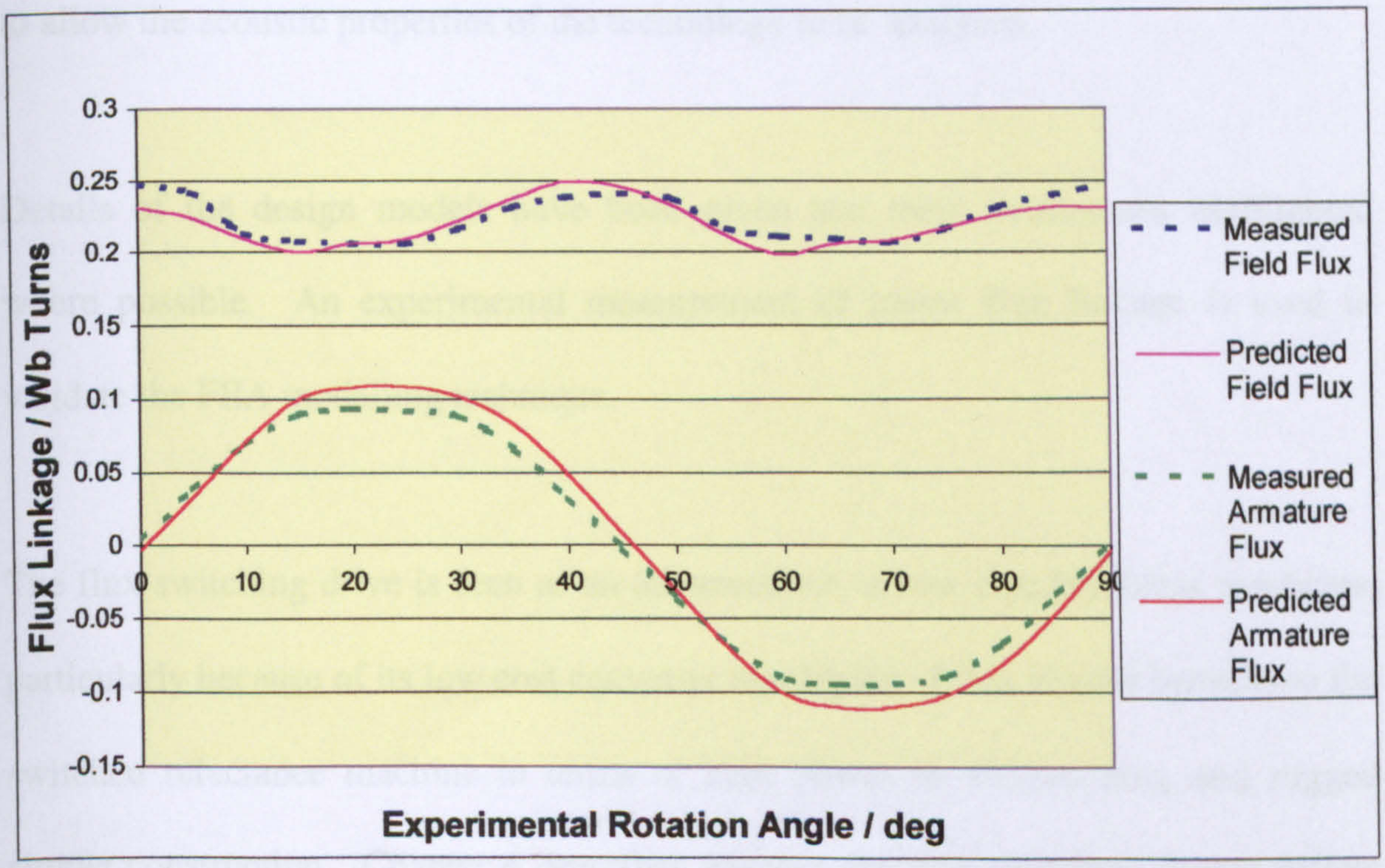

Figure 5.22: Comparison of experimental and predicted flux linkages

The average experimental field flux linkage was just 1.4% lower than the predicted flux linkage. The RMS experimental armature flux linkage was 13% lower than the FEA prediction. This means the coupling present in the motor is not as good as the

prediction. However, it should be remembered that FEA does not model eddy currents and hysteresis losses and therefore, taking this into consideration, the static model is a reasonably good approximation of the motor.

5.8 Conclusions

This chapter has introduced the new flux switching motor technology, explaining its construction, control, and converter topologies, along with the similarities it has with the switched reluctance motor. The detailed design of an external rotor flux switching machine has been presented. The machine was built for a fan application to allow the acoustic properties of the technology to be analysed.

Details of the design models have been given and their weaknesses highlighted where possible. An experimental measurement of motor flux linkage is used to validate the FEA modelling technique.

The flux switching drive is seen as an advancement in low cost brushless machines, particularly because of its low cost converter topologies. It has similar benefits to the switched reluctance machine in terms of high power to weight ratio, and rugged simple construction. Chapter 6 describes whether the flux switching motor suffers from the same disadvantage as the switched reluctance machine - high levels of acoustic noise.

CHAPTER 6

A COMPARATIVE ANALYSIS OF ACOUSTIC NOISE FROM THE FLUX SWITCHING MOTOR

6.1 Introduction

Chapter 5 presented the detailed design of an 8/4 external rotor flux switching motor for a fan application. As this is a new technology, little is known about the acoustic properties of the topology. The aim of this chapter is to outline the results of an experimental analysis of acoustic noise from the flux switching motor. In particular, it focuses on a comparison with a two phase switched reluctance motor, which is the nearest switched reluctance equivalent to the flux switching motor.

In chapter 1, a brief introduction was given to sound quantities and the general process and outputs obtained from measuring sound. In the author's measurement and analysis of the acoustic noise emitted from various motors, the experimental setup was based upon the Survey method, as detailed in EN ISO 3746 (1996) [50], using an enveloping measurement surface over a reflecting plane. Details of the experimental setup for measuring acoustic noise are given in section 6.1.1.

6.1.1 Measuring Acoustic Noise

Sound pressure levels are affected by the surroundings of a source, making the test environment critical to obtaining valid and repeatable results. A quiet room with sound absorbing material on the walls was used. The background noise in the room

had a consistent frequency content and the SPL was low in comparison with that of the test subjects. The solid floor provided a reflecting plane.

The microphone used in the tests was a Bruel & Kjaer ½ inch Electret microphone with cartridge type Mk224. It has a flat frequency response up to 16kHz (± 2dB) and the output was calibrated using a Bruel & Kjaer type 4231 calibrator which emits a 94dB tone at 1kHz. As the measurements were made indoors, a windshield was not required. The microphone was held in a tripod, having point contact with the floor.

The output from the microphone was captured using a standard PC sound card and processed by the SpectraPro software package from Sound Technology Inc. This allows the sound to be measured in real time, or recorded and post-processed at a later time. It has standard weighting functions (described in chapter 1) and averaging functions. As well as displaying the sound pressure level in dBA, the frequency spectrum in various 1/n octave bands can be displayed. This is useful for identifying discrete frequency noise that may be present.

The subjects were mounted on a heavy steel stand with 4 point contacts with the floor, to minimise the transmission of vibration. Some tests were performed with the subjects attached to a flat bed test rig which had resilient mountings.

When measuring the acoustic noise from the test subjects, a hypothetical measurement sphere, centring on the motor and with a radius of 1m, was used. 4 critical microphone positions and 4 additional positions were used in accordance

with the Standard. The sound pressure at each of these points is then averaged over the measurement surface using the following formula:

$$L'_{pA} = 10 \log\left[\frac{1}{N} \sum_{i=1}^{N} 10^{0.1 L'_{pAi}}\right] \text{dB} \qquad (6.1)$$

where L'_{pA} Surface averaged A-weighted sound pressure level

L'_{pAi} A-weighted sound pressure level measured at the ith microphone position

N Number of microphone positions

6.2 Selection and Description of Comparison Motors

For this investigation, the flux switching motor will be compared against two motors.

An external rotor 2-phase switched reluctance motor, and a standard induction motor.

Firstly the comparison with the switched reluctance motor is made to investigate the acoustic differences between the technologies, as the flux switching machine is seen to be an advancement in the reluctance motor field and has benefits over the conventional switched reluctance machine, particularly in the converter topology. Secondly, the flux switching motor will be compared to a single phase induction motor, which provides a bench mark to measure the overall acoustic performance of the flux switching motor.

6.2.1 2-Phase Switched Reluctance Motor

In order to compare the acoustic noise of a flux switching machine with that from a switched reluctance machine, a 2-phase switched reluctance motor was built. There are similarities between the flux switching machine and the switched reluctance machine. Both operate with doubly salient poles and neither employ permanent magnets. The main difference between the machines is the winding configuration and therefore the variation and distribution of magnetic flux. For this reason a 2 phase switched reluctance motor was constructed using *the same rotor and stator laminations as the flux switching motor* detailed in Chapter 5. The mechanical components, such as the stator support, bearings, shaft and rotor were also manufactured identically.

The switched reluctance motor was wound in a short pitched fashion with 8 coils in total, each coil wound around a stator pole. 0.315mm diameter copper wire was used and the number of turns was calculated to match the slot fill obtained with the flux switching motor. This gave 161 turns per coil. The coils were connected in series in two phase circuits. Phase one with coils around poles 1, 3, 5, 7, and phase two with coils around poles 2, 4, 6, 8. Figure 6.1 gives a schematic diagram of the this arrangement:

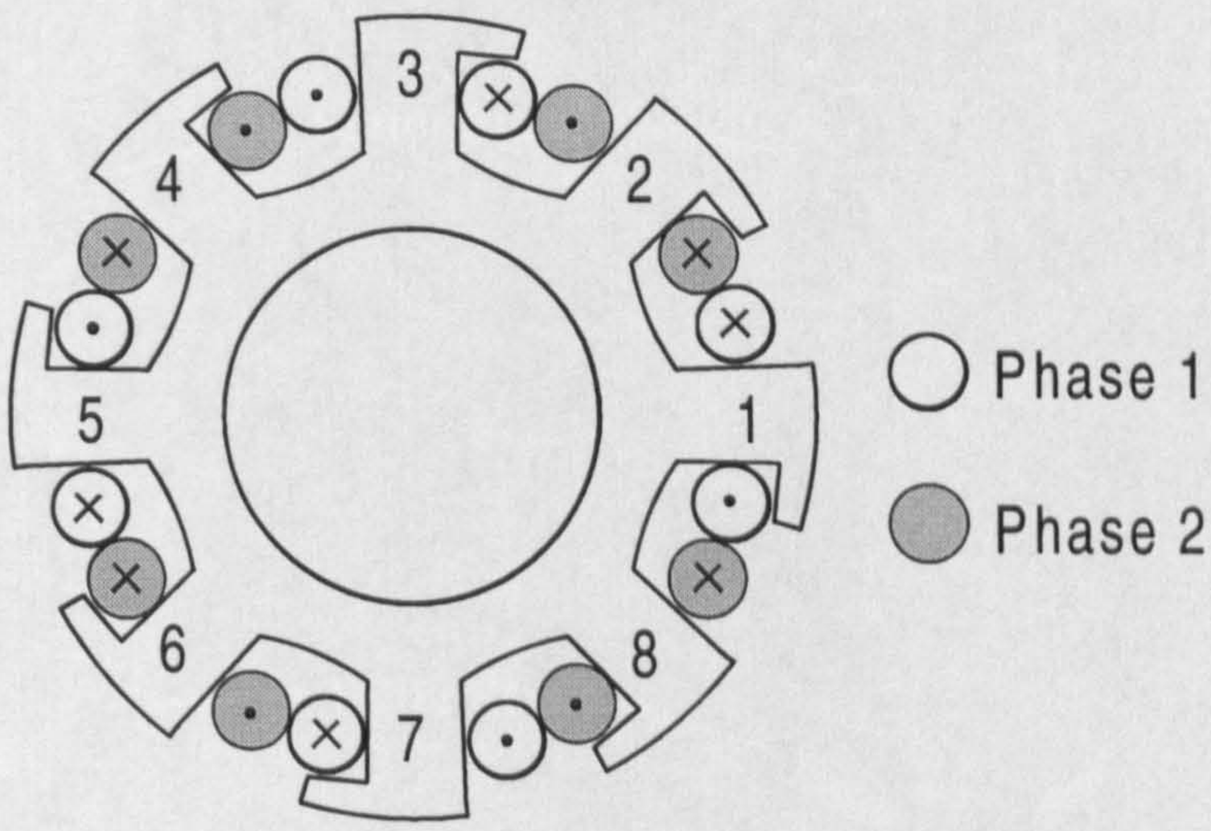

Figure 6.1: Coil arrangement in the 2-phase switched reluctance external rotor machine

When phase one is energised, the 4 external rotor poles will align with stator poles 1, 3, 5, 7. When phase two is energised the rotor poles will align with stator poles 2, 4, 6, 8.

Building the two motors from the same laminations, and with the same mechanical parts, allowed the fundamental difference in the flux control between the two machine topologies to be explored in terms of the acoustic noise production. It is accepted that because of the number of variables involved, there are other

comparisons that may be investigated. However because the author has found that mechanical configuration has the greatest effect on acoustic noise, particularly in small machines, maintaining mechanical similarity was prioritised. Figure 6.2 shows the prototype flux switching motor and the 2 phase switched reluctance motor side by side:

Figure 6.2: Flux switching motor and 2-phase switched reluctance motor built from the same components

6.2.2 Single-Phase Induction Motor

The application used for testing and comparing the different motor types is a commercial 9" window fan that currently employs an induction motor. This existing motor will be used as a bench mark for measuring the performance of the flux switching motor. It is a single-phase, 2 pole, mains fed machine. The stator stack is 31mm in length and has 12 teeth. The rotor is a cage design with 8 aluminium conductors running along its length. The stator is wound with a main winding and an auxiliary winding, the latter having a slightly higher number of turns. Three

operating speeds are available by connecting different capacitors in series with the auxiliary winding to boost or drop the voltage across it. The different capacitors also produce a change in the phase shift between the voltage on the main and auxiliary winding.

6.3 Analysis of the Flux Switching Motor

6.3.1 Optimisation of the Flux Switching Motor

Before running the flux switching motor, the optical position sensor must be aligned to allow current to flow at the correct time. This is done by exciting the field winding with a d.c. current, and turning the motor at constant speed by external means. This induces a back emf in the armature coils, which can be measured on an oscilloscope. To generate electromagnetic torque, the phase current is required to flow in opposition to this back emf. The sensor is therefore aligned such that the edge of the sensor signal occurs simultaneously with the zero crossing of the back emf.

The sensor position may be adjusted to provide a small phase shift between the sensor signal and the back emf. Normally this phase difference is quoted in mechanical degrees, and is called the advance angle. An advance angle of 0° is when the sensor signal edge occurs as the back emf passes through zero. If the edge occurs before the zero crossing the angle is advanced (+ve), and if it occurs after the zero crossing, the angle is retarded (-ve). This is the same as the firing angle commonly used in switched reluctance motors [29]. Figure 6.3 shows the position sensor, back emf, and field current for the external rotor flux switching motor, with 0° phase shift between the back emf and position sensor.

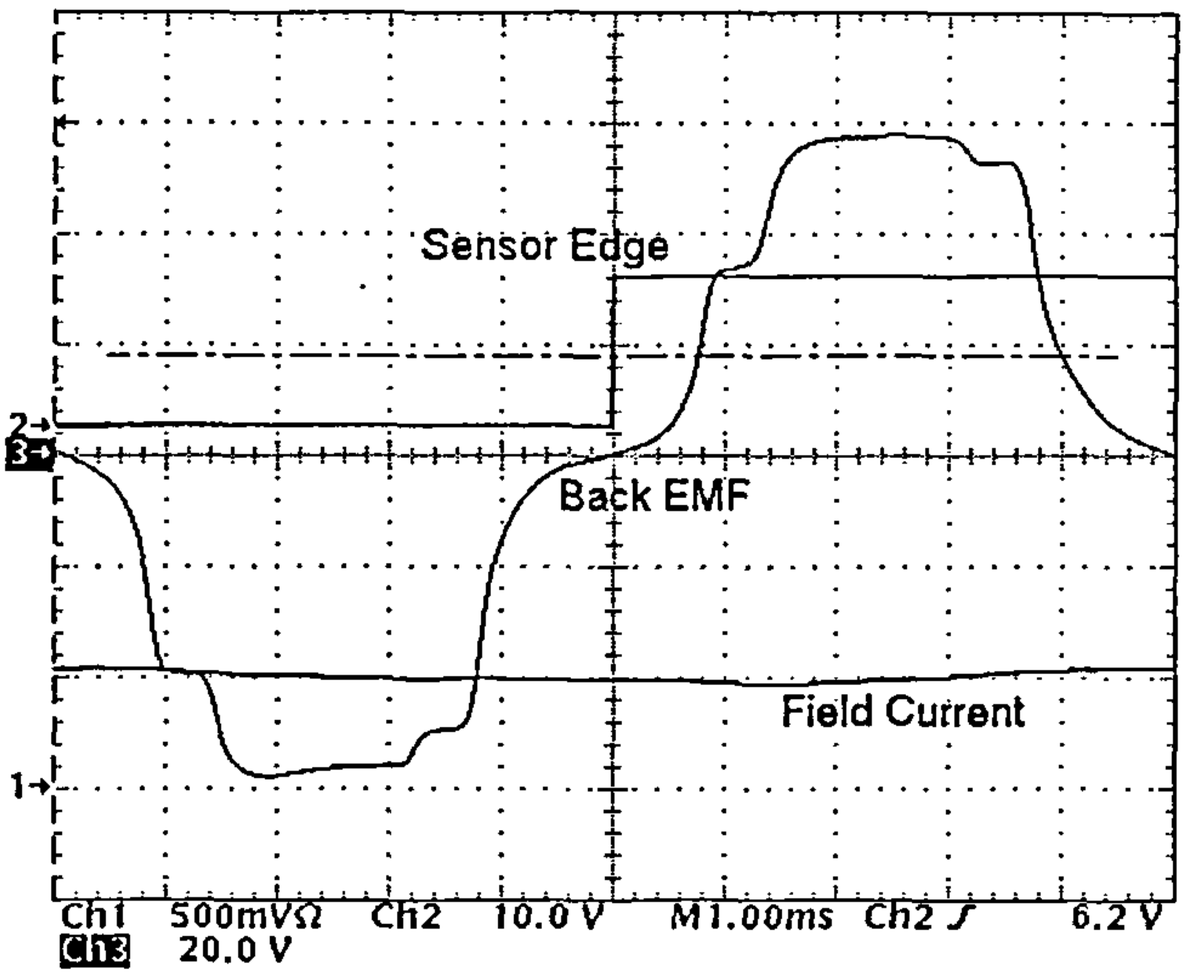

Figure 6.3: Sensor edge aligned with zero crossing on back emf

At higher speeds, advance angle becomes highly significant because the time available to reduce the phase current to zero, and establish the next phase current in the opposite direction, is shorter.

The power converter used to operate the flux switching motor was described in Chapter 5. Figure 6.4 shows a schematic of the circuit for reference.

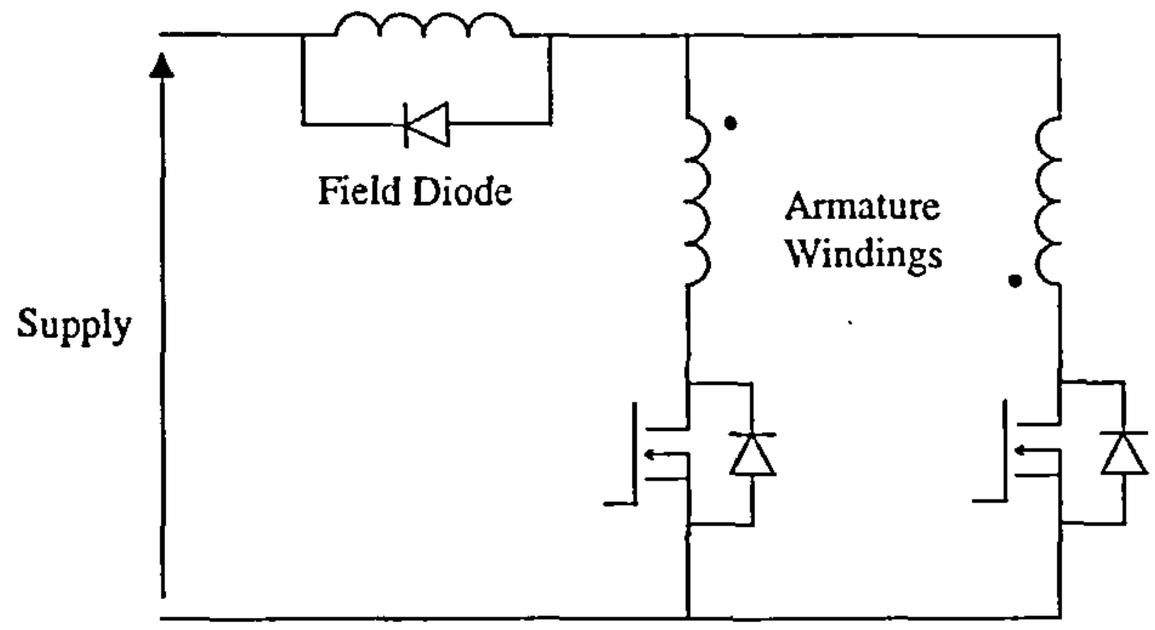

Figure 6.4: 2 switch converter for the flux switching motor

In the test motor, the two power MOSFETs were controlled by gate drive signals, derived from the position sensor, with each switch turning on for 50% of the time in turn. A short time delay was added to the gate control signals to avoid an overlap of the switch on-time, and therefore a short circuit current.

In order to operate the motor under its best conditions at rated speed, the input power and single point acoustic noise were measured for varying advance angles of commutation. The results of this are given in table 6.1. Each measurement was made with the fan load at 1800rpm.

Table 6.1: Optimisation of flux switching motor commutation angle for efficiency and low noise

Advance Angle / °	Input Power / W	Acoustic Noise SPL / dBA
0	76	65.21
2	74	64.98
4	**73**	**64.29**
6	75	65.18
8	80	65.64
10	89	65.87

A 4 degrees advanced commutation angle gives the highest efficiency and the lowest level of acoustic noise. Supply voltage reversal occurs before the back emf reaches zero allowing time for the current to decay before the back emf reverses.

6.3.2 Resonant Characteristics

Initial measurements were made to identify the natural resonant frequencies of the rotor and stator structures. This was achieved by fixing an accelerometer on the target surface and providing a force impulse. The impulse was generated electrically by pulsing current through the windings in a ramp-up ramp-down style. A current pulse was applied to the field and one of the armature windings of the motor, for duration 1ms, with the rotor and stator poles aligned. The resulting vibration was measured with an accelerometer placed on the stator support structure, just below the lamination stack. Similarly, vibration was measured on the external surface of the rotor laminations, behind a pole. Figures 6.5 and 6.6 show the voltage and current pulses, resulting vibration and frequency power spectrum for the stator support and rotor respectively.

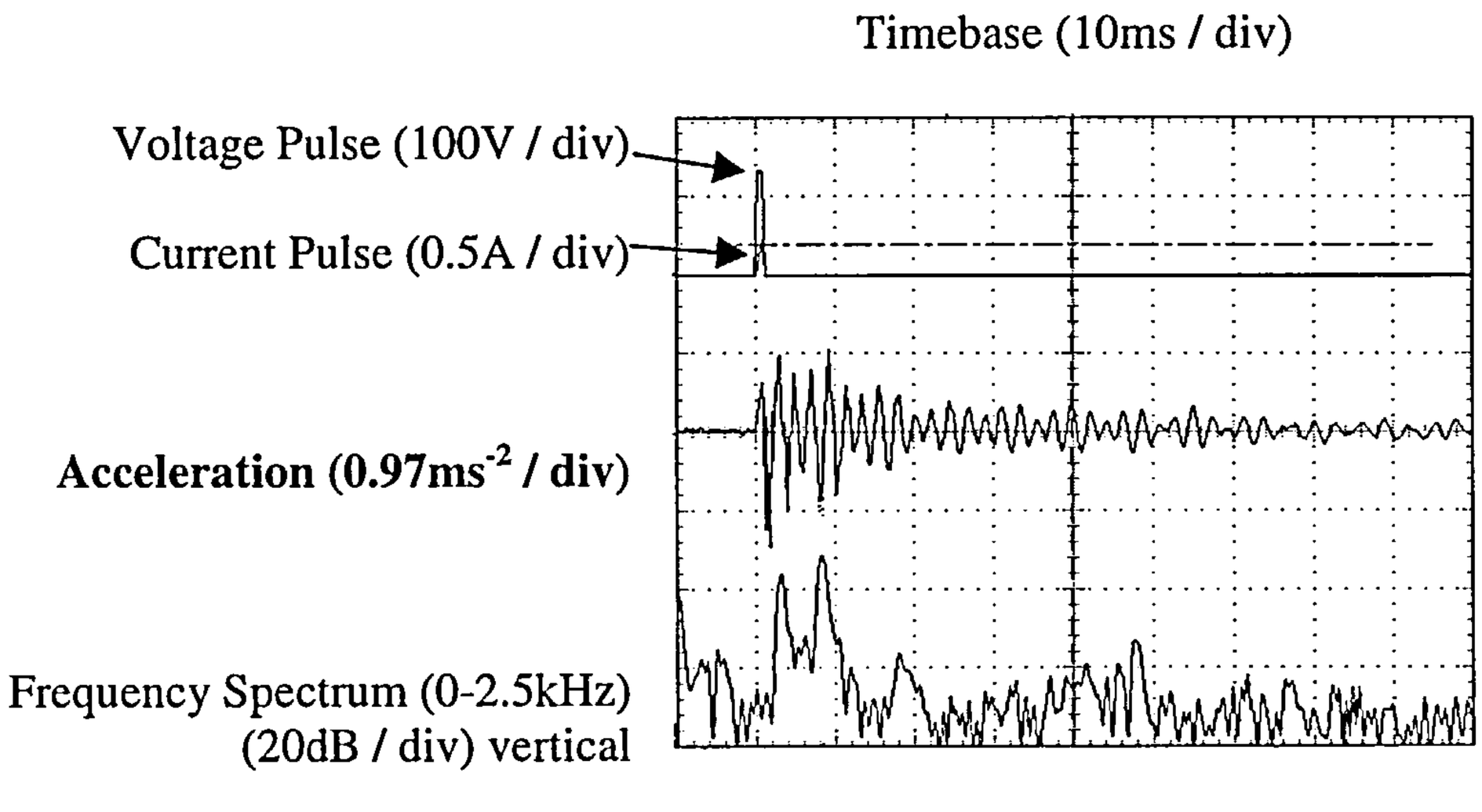

Figure 6.5: Acceleration and frequency spectrum of the stator support

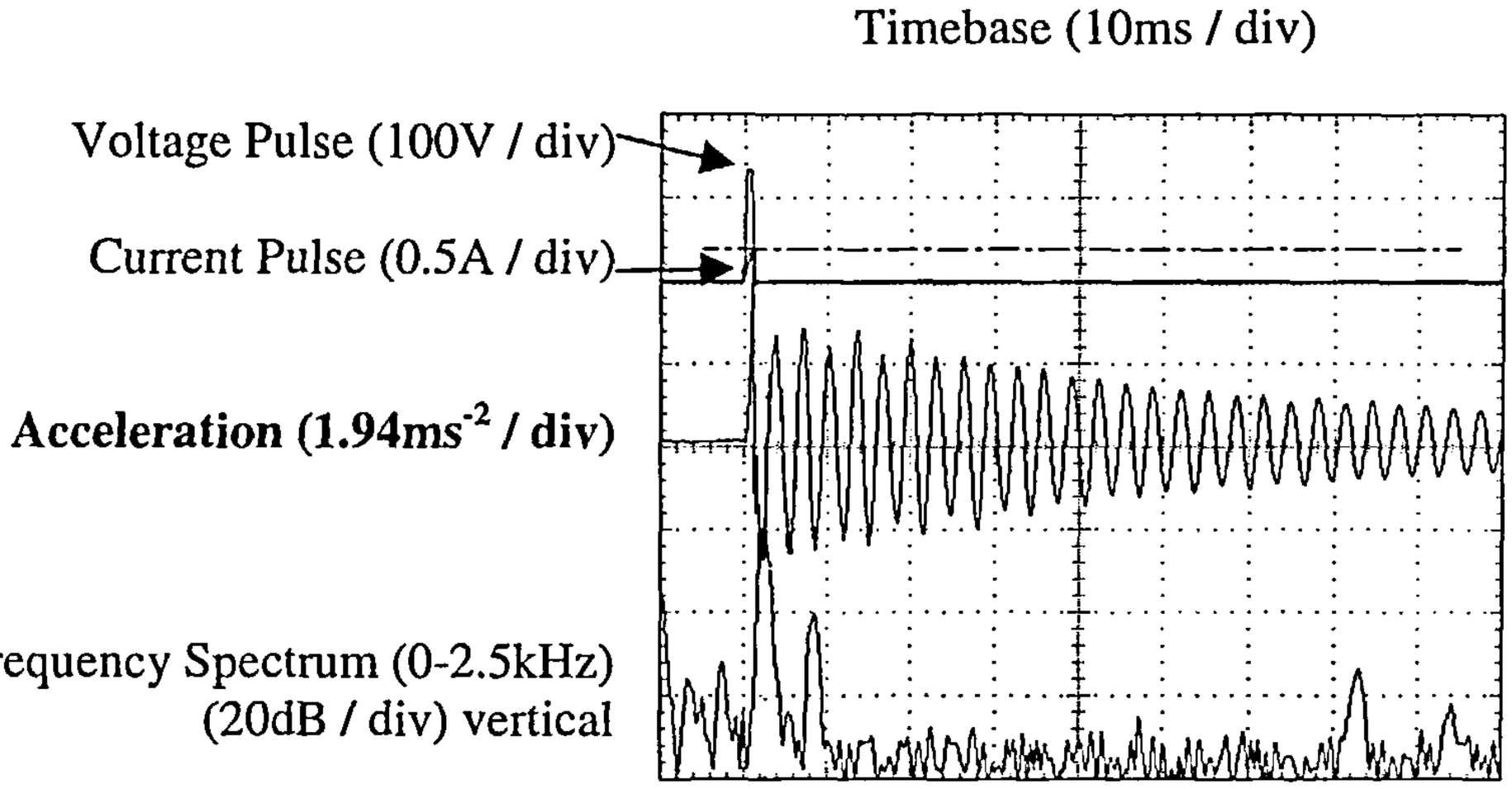

Figure 6.6: Acceleration and frequency spectrum of the external rotor

The dominant resonant frequency measured on the stator structure was found to be around 460Hz, with a further significant peak at 330Hz. The natural damping of this resonance was quite large as the vibration magnitude decreased quickly. The dominant resonant frequency measured on the rotor was found to be 315Hz and was significantly larger in magnitude than that of the stator. Other frequencies of significance were found to be 460Hz (possibly transmitted from the stator), 2.07KHz and 2.35kHz. The natural damping of the rotor was significantly less than that of the stator, with the 315Hz vibration magnitude not decreasing quickly with time.

It is reasonable to assume that the dominant source of modal resonant vibration would come from the external part of the machine, whether that is the rotor or stator, as this is the part with the least stiff shape.

6.3.3 Operating Vibration and Commutation

With the motor turning the fan at 1800rpm, the stator structure vibration was measured with an accelerometer. It was hoped that there would be an obvious correlation between commutation and vibration in the time domain. It is most likely that the less stiff, cylindrical rotor structure would see the effect of the changing radial force caused by commutation. Because the vibration was measured on the stator structure, and not on the rotor (which was turning), no conclusions could be drawn about the timing of commutation and vibration. However the order of magnitude of the vibration measured does give an indication of how acoustically noisy the motor is. Figure 6.7 shows the current excitation, stator structure vibration and vibration frequency spectrum for the flux switching motor at 1800rpm. The rms magnitude of acceleration was 4.656ms^{-2}.

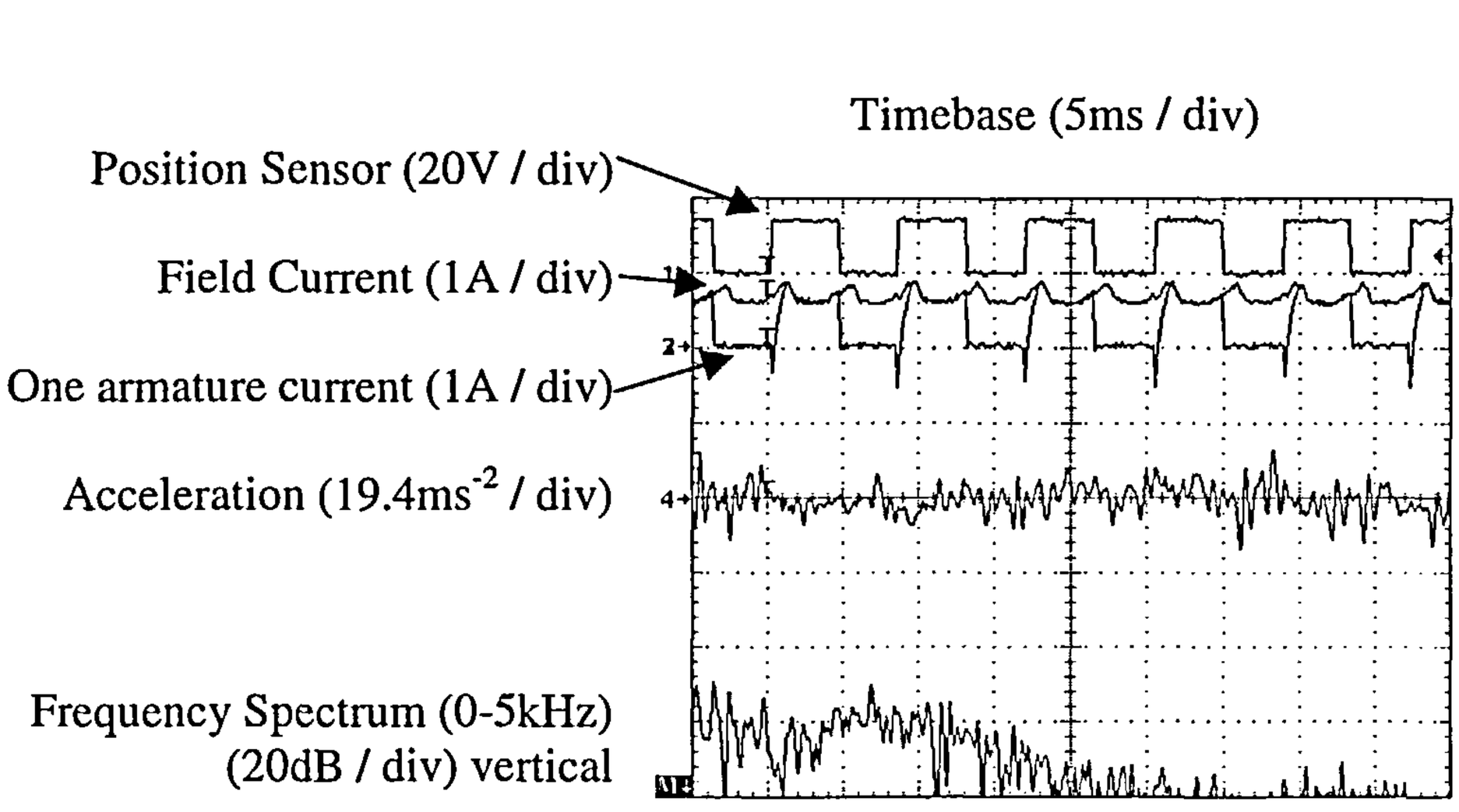

Figure 6.7: Flux switching motor stator structure vibration at 1800rpm

6.4 Analysis of the 2-Phase Switched Reluctance Motor

6.4.1 Optimisation of the 2-phase Switched Reluctance Motor

The same optical sensor arrangement was used as for the flux switching motor, with the sensor being aligned using a slightly different method. When d.c. current was applied to one of the phases, the rotor parked in the position of minimum reluctance (aligned position). The sensor position was then adjusted so that the output just changed state in the parked position. This corresponds to a 0° firing angle. Advancing the firing angle on this motor, by moving the sensor relative to the rotor, switches the phase off before the rotor reaches the position of minimum reluctance, and on before it reaches the position of maximum reluctance.

The power converter topology for operating the switched reluctance motor is described in Chapter 3. Because the test motor is a 2-phase machine, the power converter required for operation has 4 power switches and 4 power diodes. The complexity of this circuit immediately highlights one of the major advantages of the flux switching machine over its switched reluctance equivalent. Figure 6.8 shows a schematic of the power converter used to operate the 2-phase switched reluctance motor.

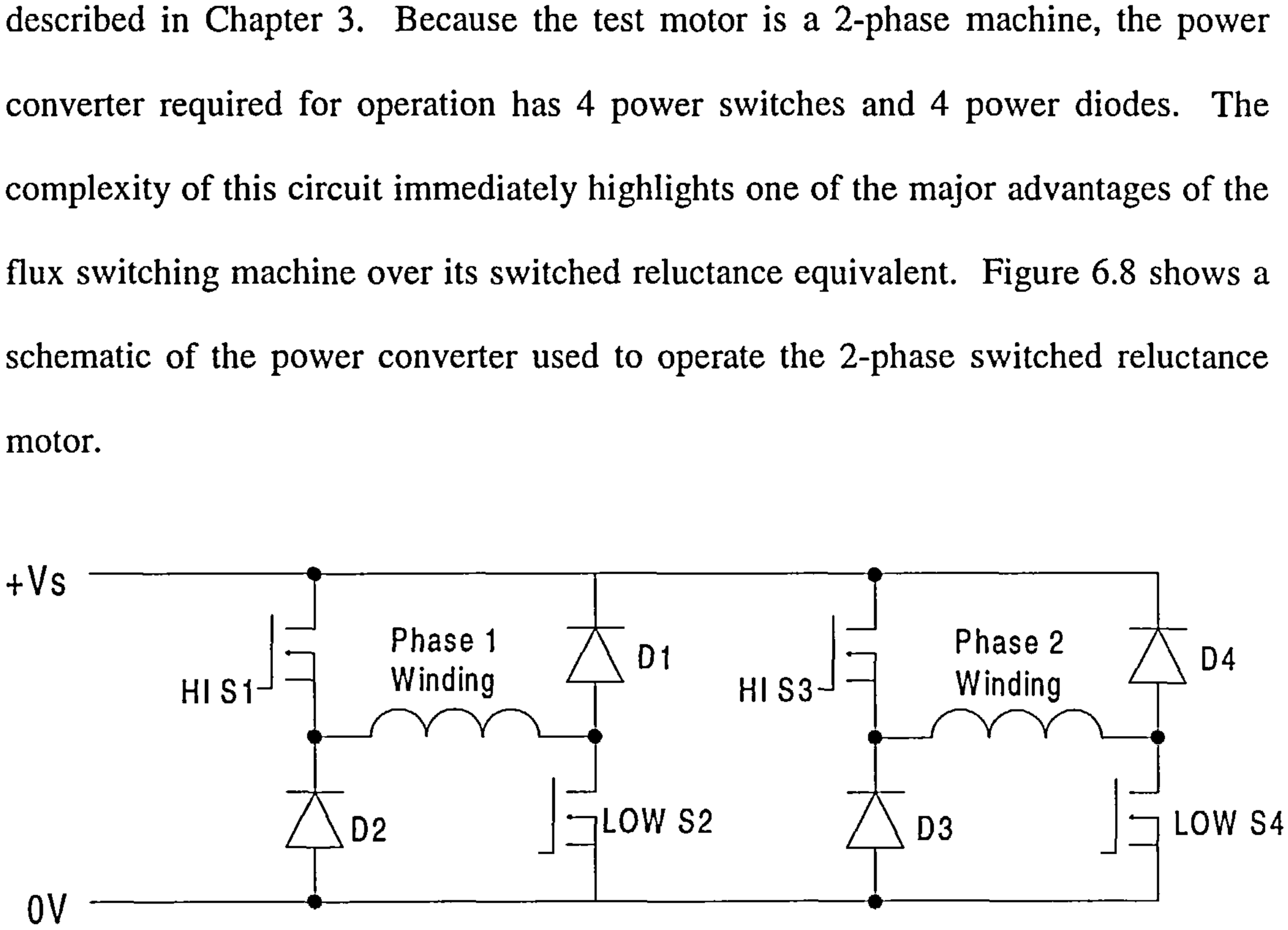

Figure 6.8: Power converter for the 2-phase switched reluctance motor

As with the flux switching motor, each phase will be on for 50% of the time. Again, the same time delay was added to the switch control signals to ensure that both pairs of switches are not on concurrently. In order to operate the motor under its best conditions at rated speed, the input power and single point acoustic noise were measured for various firing angles. The results of this are given in table 6.2. Each measurement was made at 1800rpm with the fan load attached.

Table 6.2: Optimisation of switched reluctance motor firing angle for efficiency and low noise

Firing Angle / °	Input Power / W	Acoustic Noise SPL / dBA
10	83	68.42
14	81	67.95
16	**78**	**67.27**
18	77	68.41
20	80	68.15
22	84	67.06

Although the lowest acoustic noise was achieved at a firing angle of 22° advanced, and the minimum input power at 18° advanced, it was felt that the best operating angle for the motor was 16° advanced, as a compromise between noise and efficiency. With an advance angle of 22°, the temperature of the motor was too high.

The flux switching and switched reluctance motors were optimised separately. Later investigation revealed that the firing angle selected for the two-phase switched

reluctance motor, and the advance angle selected for the flux switching motor were such that the rotor position at the time of commutation was the same in both cases.

6.4.2 Resonant Characteristics

As with the flux switching motor, measurements were made to identify the natural resonant frequencies of the switched reluctance rotor and stator structures. This was achieved by fixing an accelerometer on the target surface and pulsing current through the windings in short bursts. A 1A pulse was applied to one of the phase windings of the motor, for duration 1ms, with the rotor and energised stator poles aligned. The resulting vibration was measured with an accelerometer placed on the stator support structure, just below the lamination stack. Similarly, vibration was measured on the external surface of the rotor laminations, behind a pole. Figures 6.9 and 6.10 show the voltage and current pulses, resulting vibration and frequency power spectrum for the stator support and rotor respectively.

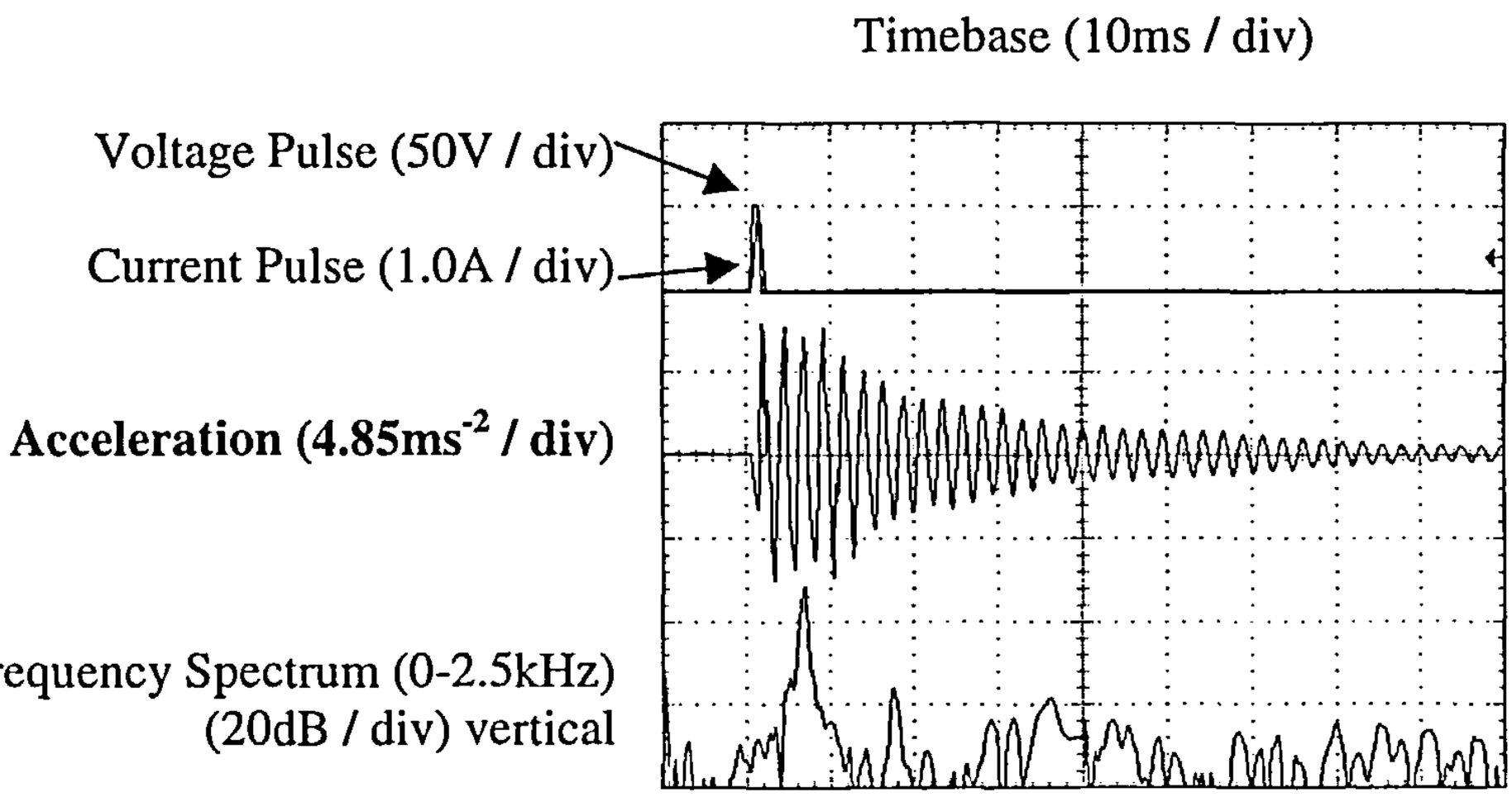

Figure 6.9: Acceleration and frequency spectrum of the stator support of the 2-phase switched reluctance motor

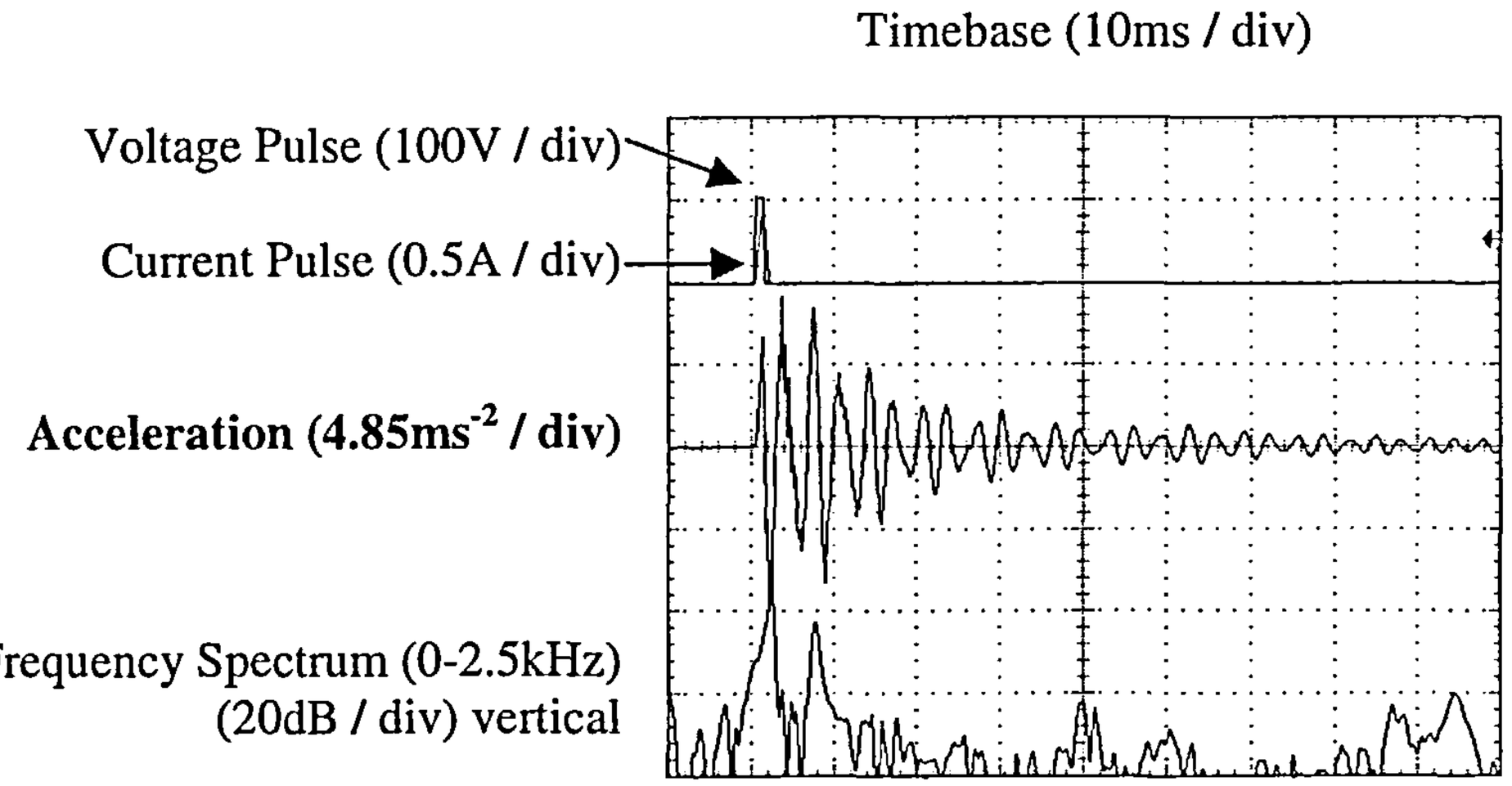

Figure 6.10: Acceleration and frequency spectrum of the external rotor of the 2-Phase switched reluctance motor

The dominant resonant frequency of the stator structure was found to be around 425Hz. The dominant resonant frequency of the rotor was found to be 310Hz but had a significant 445Hz component, again probably transmitted from the stator. The natural frequencies of the switched reluctance motor are close to those measured on the flux switching motor. Because they are designed and built from the same material, one would expect the resonant frequencies to be similar, but due to the slight differences in mechanical build, it is unlikely that the two motors would exhibit exactly the same characteristics.

6.4.3 Operating Vibration and Commutation

With the motor turning the fan at 1800rpm, the stator structure vibration was measured with an accelerometer, using the same method as was applied to the flux switching motor. For the same reasons, no correlation could be proved between the timing of motor commutation and induced vibration. Figure 6.11 shows the current

excitation, stator structure vibration and vibration frequency spectrum for the 2-phase switched reluctance motor at 1800rpm.

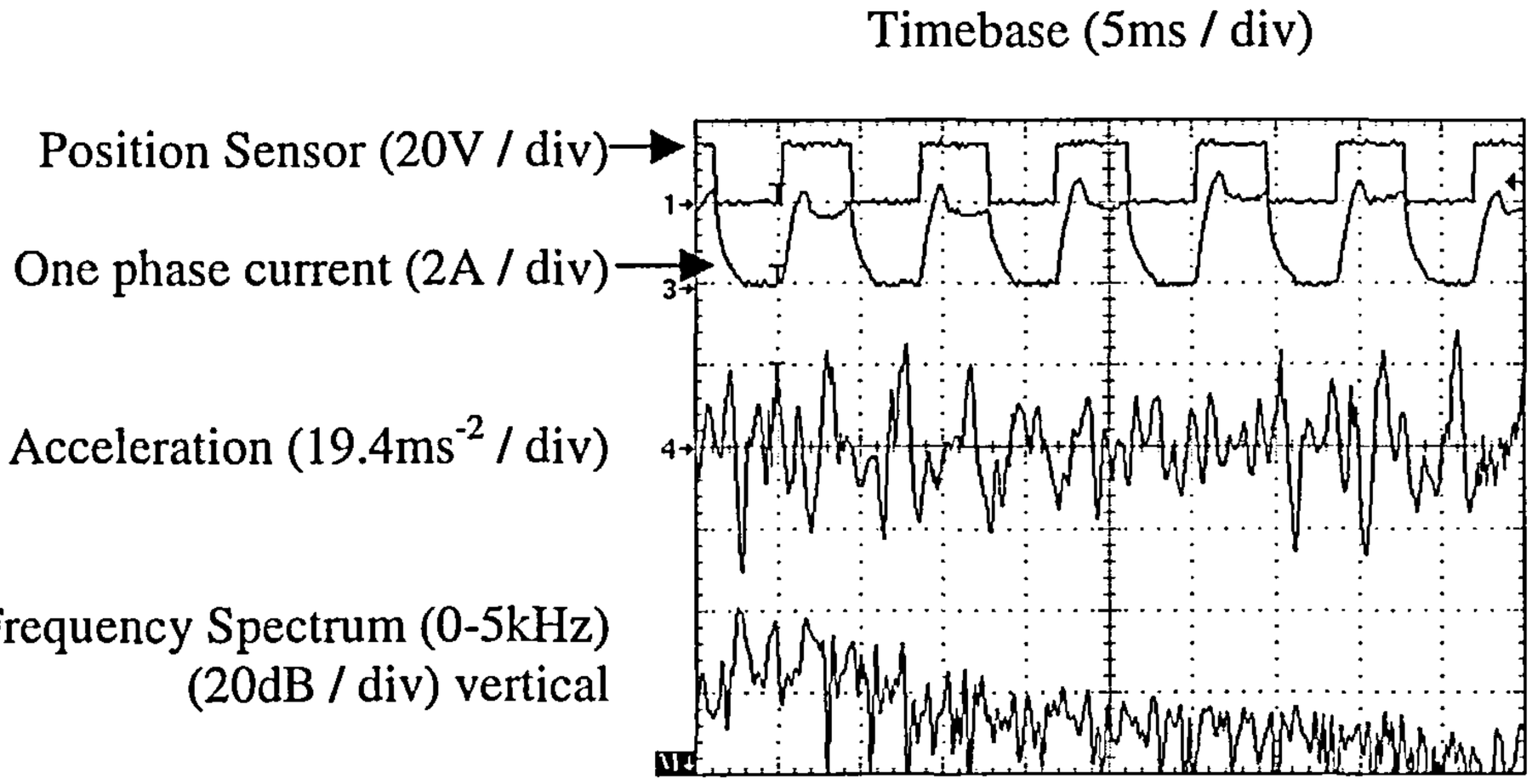

Figure 6.11: 2-phase switched reluctance motor stator structure vibration at 1800rpm

The rms magnitude of acceleration was 11.83ms^{-2}. This is approximately 2.5 times greater than the rms magnitude of vibration measured on the flux switching motor, at the same speed and same load.

6.5 Acoustic Noise Comparisons With Fan Load

The introduction to this chapter describes the setup and procedure used for measuring acoustic noise. The acoustic noise from three motors driving 9" fans at 1800rpm was measured. The air noise generated by the fan will be present in this analysis, revealing how the product would perform in the situation it was designed for.

The noise from each motor was measured at 8 sampling points, which remained constant for each of the tests. A time-averaged value of SPL was calculated by the processing software for each microphone position. The formula given in section 6.1 was used to calculate L'_{pA}, the average sound pressure level of the subject, from the eight position samples. Table 6.3 shows the acoustic data recorded for each motor tested, and the average sound pressure level. All tests were carried out at 1800rpm.

Table 6.3: Sound pressure levels measured with three motors driving fans at 1800rpm

Microphone Position	**SPL / dBA External Rotor Flux Switching Motor**	**SPL / dBA 2-Phase Switched Reluctance Motor**	**SPL / dBA Induction Motor**
Background	*39.36*	*40.59*	*39.89*
P1	65.29	68.30	62.13
P2	66.44	68.75	61.95
P3	64.89	67.44	61.66
P4	66.01	68.89	62.24
P5	66.02	68.78	62.28
P6	65.89	68.36	62.20
P7	65.89	68.2	62.22
P8	66.22	69.31	62.70
Average SPL L'_{pA}	**65.86**	**68.54**	**62.18**

The acoustic noise from the flux switching motor was found to be 2.68dB less than that from the switched reluctance motor running at the same speed and load. This

clearly shows that there is a difference in the acoustic noise production of the switched reluctance and flux switching motors. It also shows that the flux distribution and variation in the flux switching motor produces a lower average acoustic noise level compared to an equivalent short pitched wound 2-phase switched reluctance machine with the same lamination. The induction motor was the quietest overall with the flux switching motor producing 3.68dB more noise.

Although the differences in SPL provide a reasonably good indication as to which motor is "quieter", often, perceived noise is a larger factor and is affected more by the frequency content of the noise produced rather than its SPL. A motor with an identifiable pure tone may be considered unacceptable in many applications, even if its average acoustic noise is low.

Chapters 2-4 have shown that electronically commutated motors are more susceptible to discrete frequency acoustic noise than other motors, and for this reason the frequency content of the acoustic noise measured from each motor will be displayed. Figures 6.12 – 6.14 show the frequency content of the acoustic noise measured from the three motors with the background noise overlaid. A point measurement was picked that best represented the frequencies measured throughout the 8 test positions as they were found to be very similar.

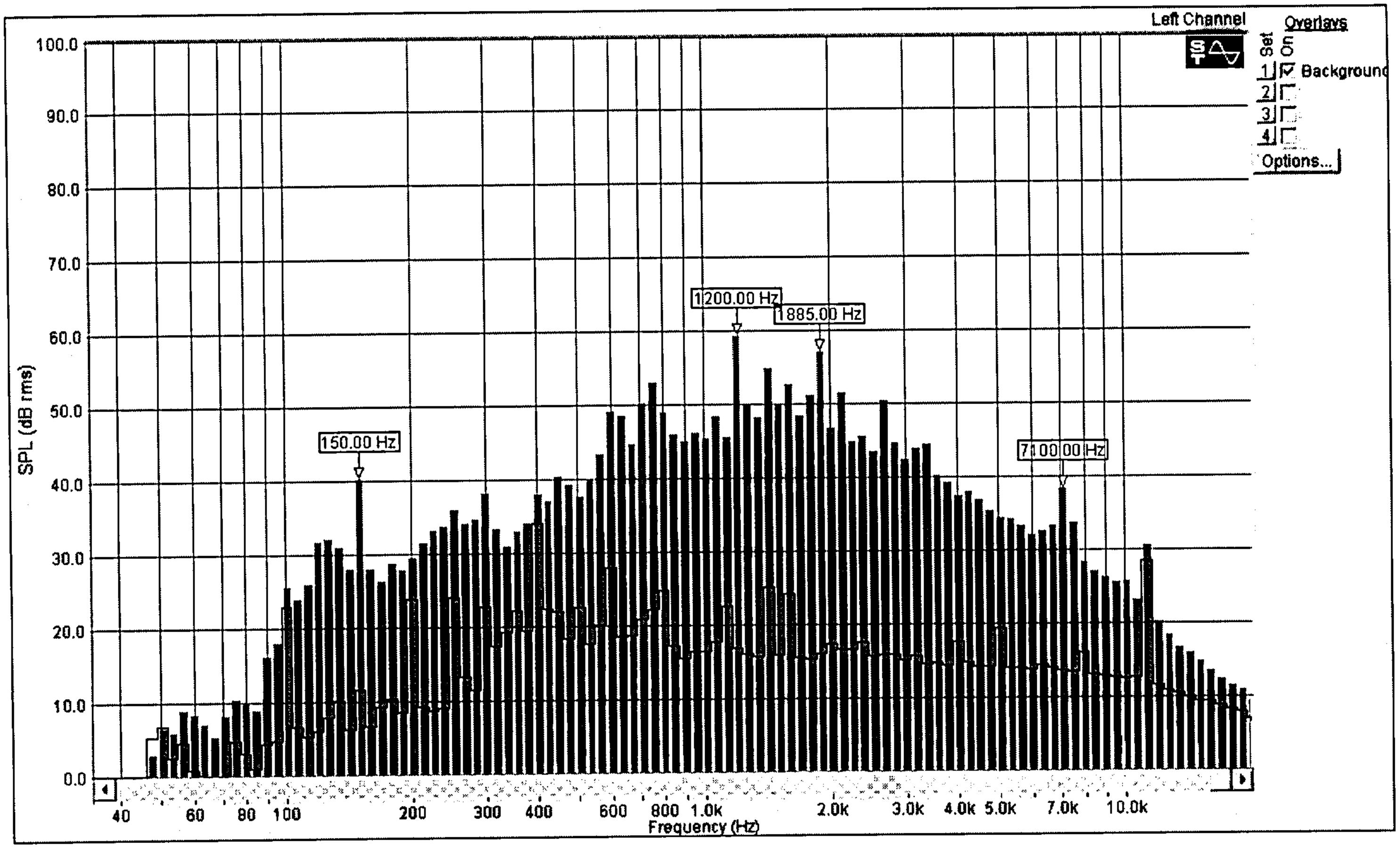

Figure 6.12: Frequency spectrum of acoustic noise from the external rotor flux switching motor while driving a 9" fan at 1800rpm.

Background levels are also shown

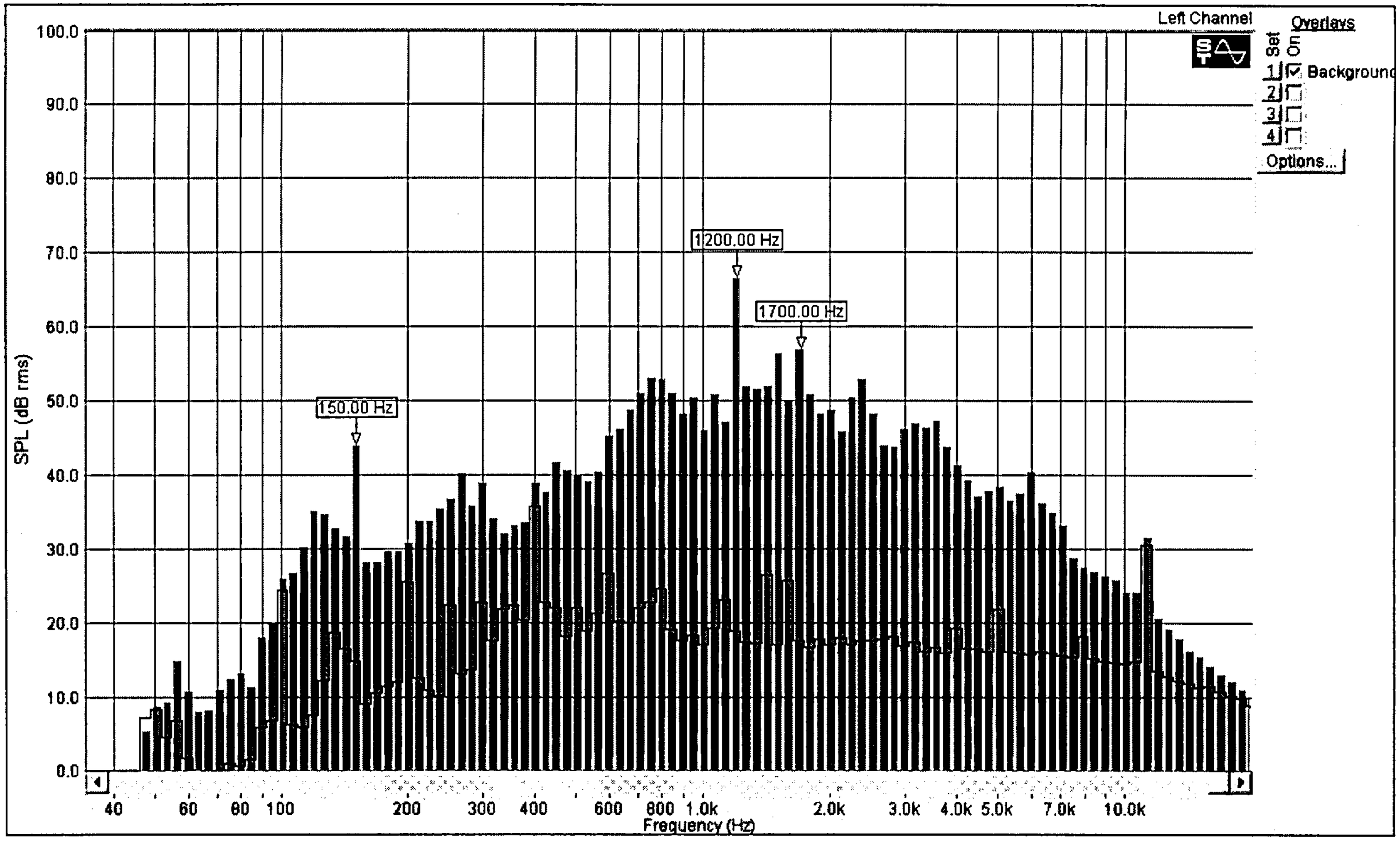

Figure 6.13: Frequency spectrum of acoustic noise from the external rotor 2-phase switched reluctance motor while driving a 9" fan at 1800rpm.

Background levels are also shown

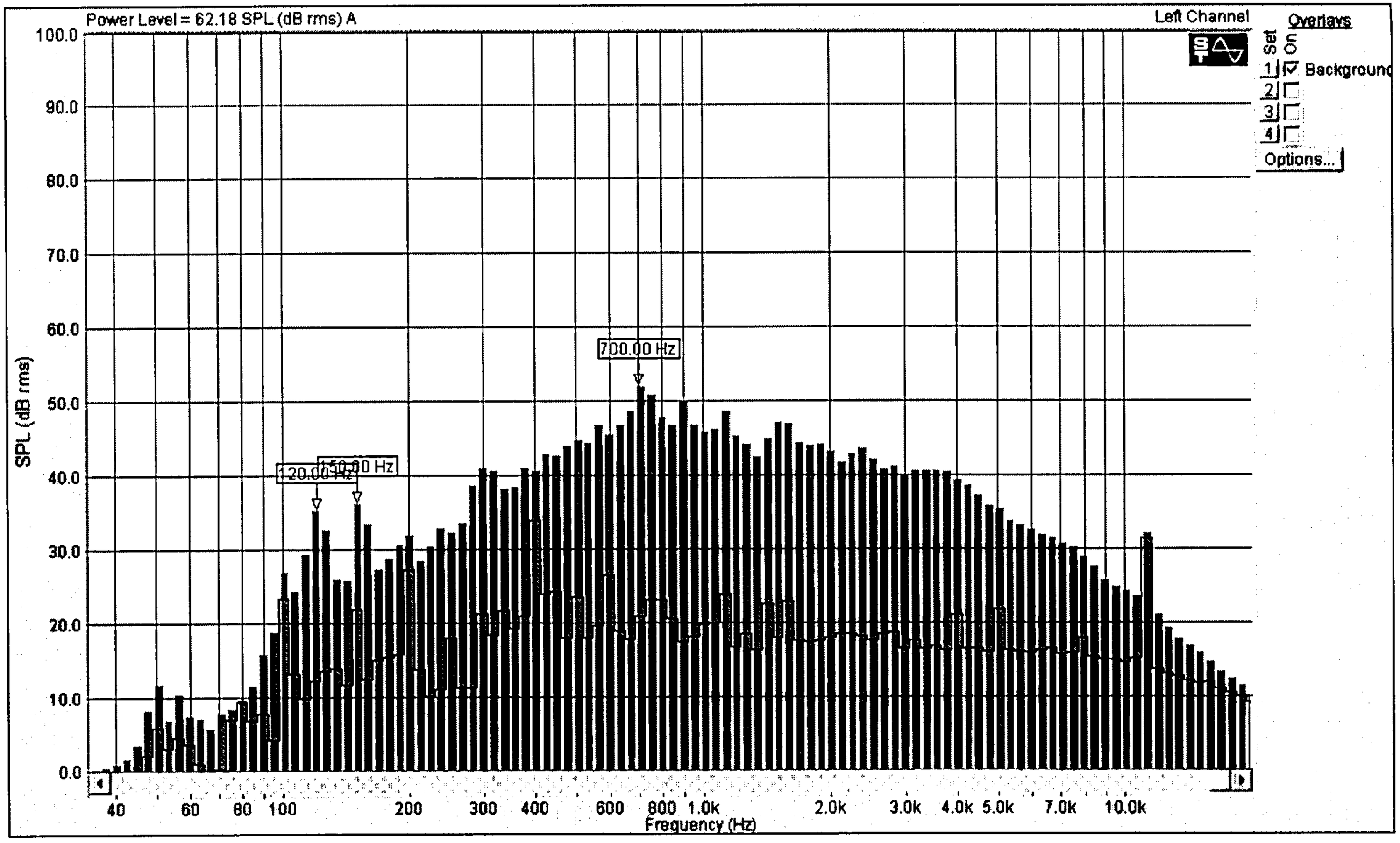

Figure 6.14: Frequency spectrum of acoustic noise from the induction motor with fan noise while driving a 9" fan at 1800rpm.

Background levels are also shown

Some notable frequencies are listed below:

150Hz	The fan blade passing frequency (speed dependent).
700Hz	Significant in all profiles. This may be a fan casing resonant frequency, or similar.
1200Hz	Present in both the flux switching and switched reluctance results, greater magnitude in the switched reluctance profile.
7100Hz	Particularly significant in the flux switching motor
11500Hz	Present in the background noise profile (irrelevant).

Clearly the induction motor has a much smoother acoustic profile than the two electronically controlled machines. The noise from the flux switching motor is fairly evenly spread across the spectrum, with some discrete peaks notably at 1200Hz and 1885Hz. These were not found to be speed dependent. The noise from the switched reluctance machine has a less smooth profile and is made up of groups of frequencies, particularly in the 2-7kHz range.

6.6 Acoustic Noise Comparisons Without Fan Noise

In order to focus on the acoustic noise generated by the motors, the fan load was replaced with a hysteresis brake, eliminating the air noise. Acoustic noise measurements were performed in an identical way to those above. The hysteresis brake was supplied with enough current to match the fan load at 1800rpm. Although there is some acoustic noise generated by the brake and coupling, it is very small,

making the brake a near silent load. Eliminating the effects of the air noise revealed a difference in the acoustic noise produced by the induction motor from that produced by the flux switching and switched reluctance motors. Table 6.4 shows the data recorded for each motor tested, and the average sound pressure level. All tests were carried out at 1800rpm.

Table 6.4: Sound pressure levels measured for three motors driving fans at 1800rpm

Microphone Position	**SPL / dBA External Rotor Flux Switching Motor**	**SPL / dBA 2-Phase Switched Reluctance Motor**	**SPL / dBA Induction Motor**
Background	*42.29*	*42.58*	*41.01*
P1	57.34	59.1	45.23
P2	58.98	60.76	44.42
P3	57.85	60.13	45.01
P4	58.42	60.43	44.42
P5	58.28	61.13	45.59
P6	57.38	59.72	44.88
P7	57.85	59.27	45.35
P8	58.60	60.06	45.57
Average SPL L'_{pA}	**58.12**	**60.12**	**45.08**

This shows that the induction motor is very quiet, with the average noise being close to the background average. Both the electronically commutated machines have higher levels of acoustic noise, with the flux switching motor being 2dB quieter than

the switched reluctance machine. This again reveals that under these test conditions, and with the same laminations, the flux switching motor has a quieter operation than the 2-phase switched reluctance equivalent.

Chapter 3 explained that switched reluctance motor commutation excites natural resonances in the motor stator and coupled components. By analysing the frequency content of the acoustic produced by the switched reluctance and flux switching motors, it is possible to identify if the same mechanism is true of the flux switching motor. Also, an analysis of the acoustic noise from the induction motor will reveal any system resonant frequencies that may be easily excited.

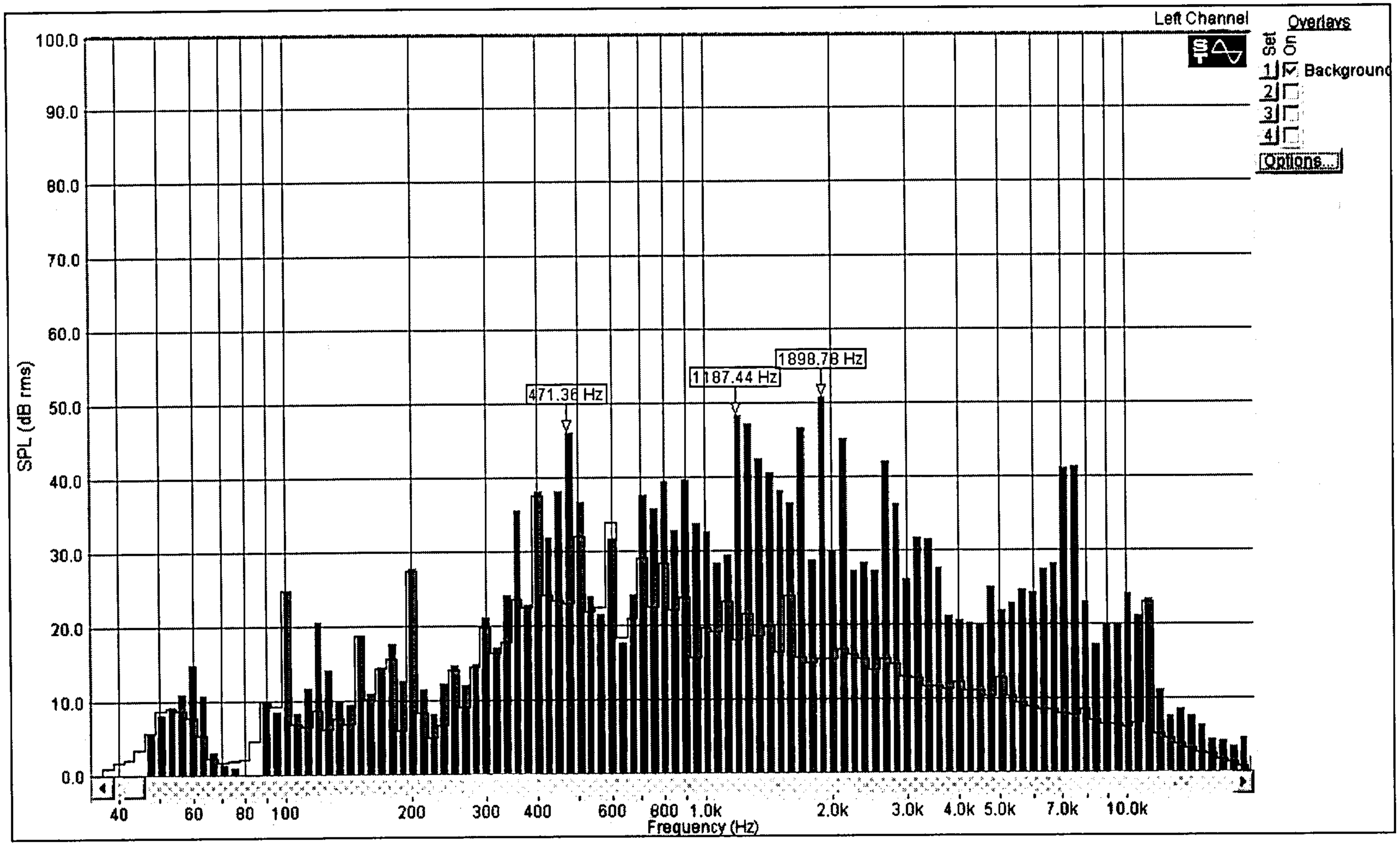

Figure 6.15: Frequency spectrum of acoustic noise from the external rotor flux switching motor while turning a hysteresis brake at 1800rpm

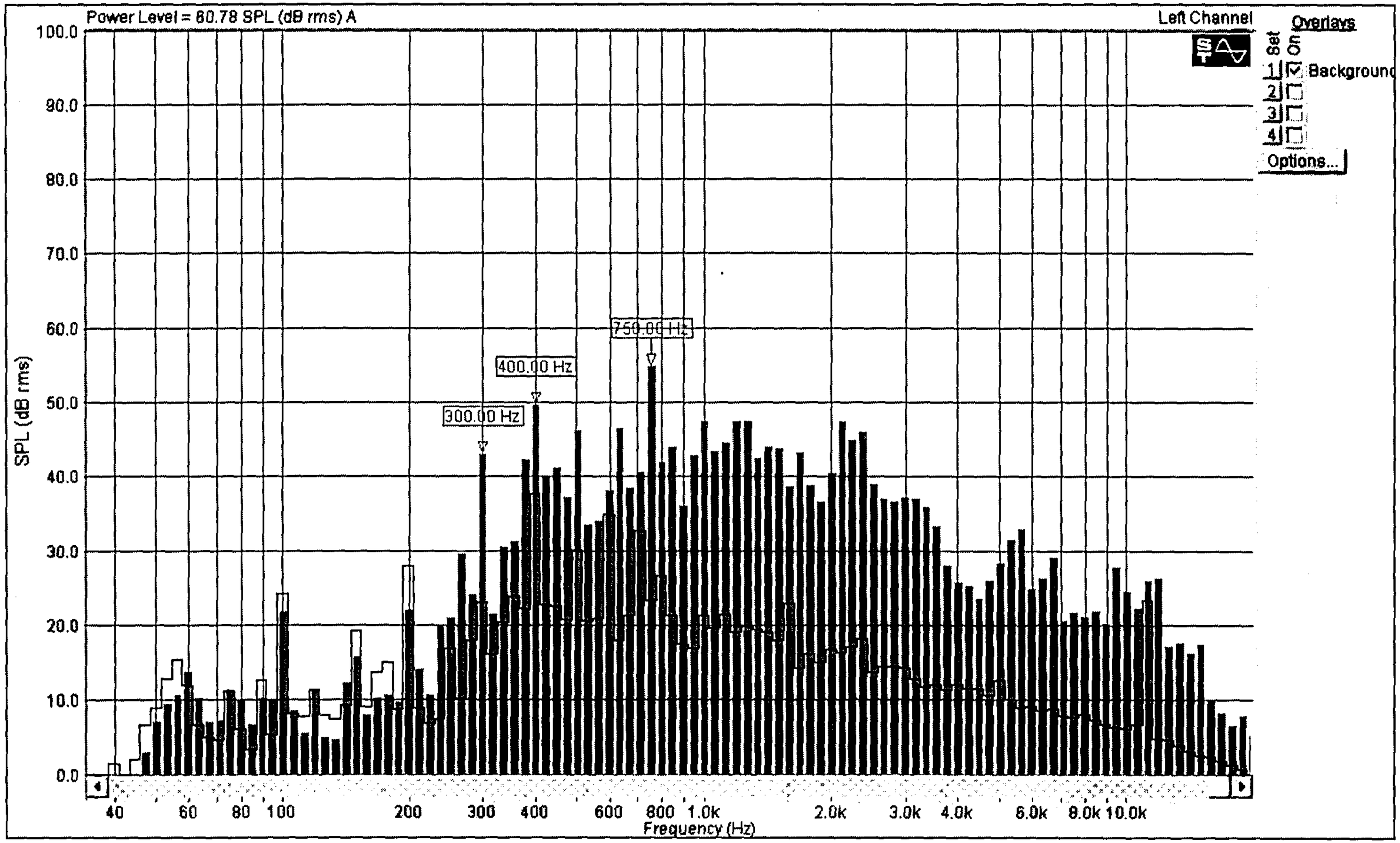

Figure 6.16: Frequency spectrum of acoustic noise from the 2-phase switched reluctance motor while turning a hysteresis brake at 1800rpm

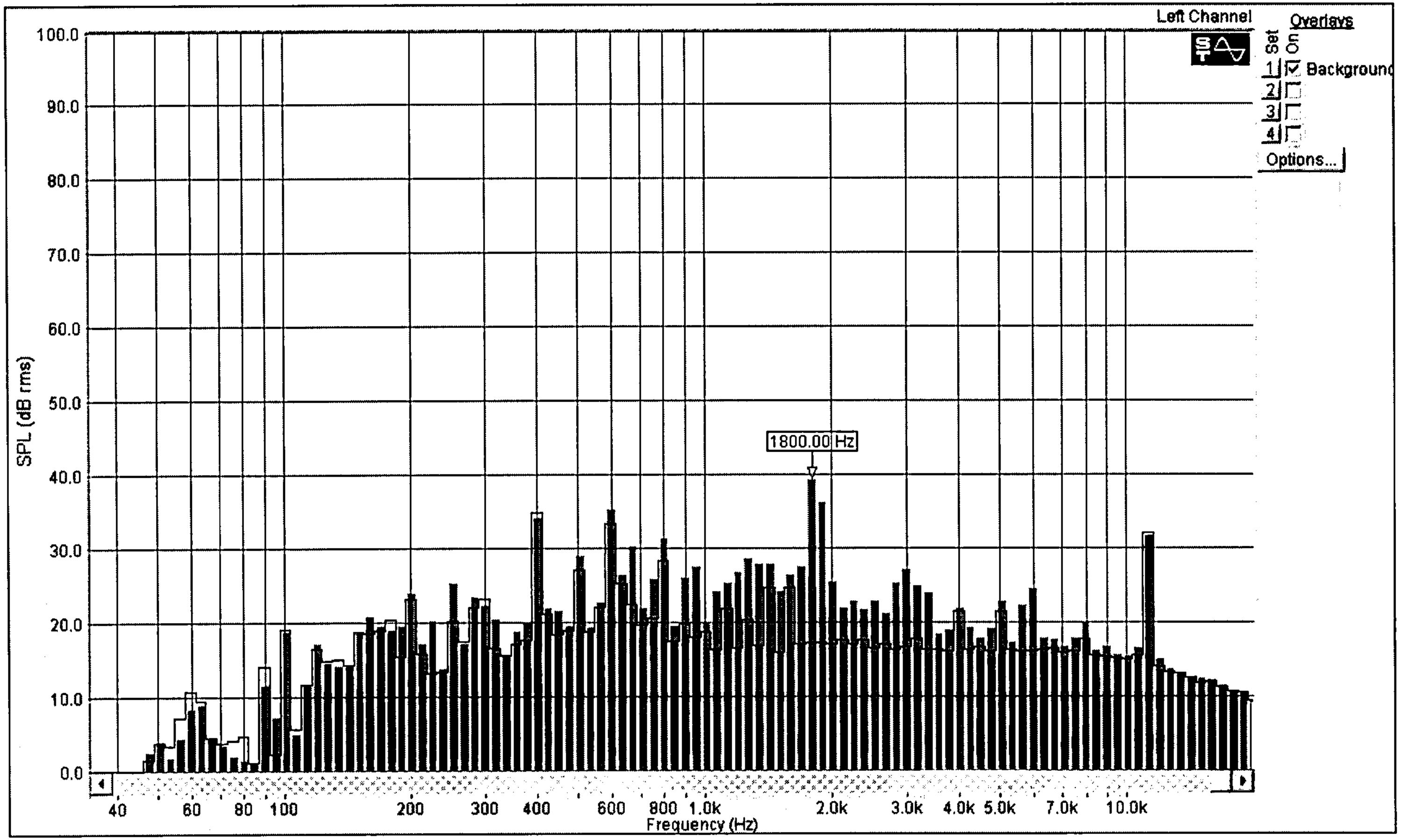

Figure 6.17: Frequency spectrum of acoustic noise from the induction motor while turning a hysteresis brake at 1800rpm

6.6.1 Discussion

The results presented were taken at a fixed speed (1800rpm). During the tests, the speed was varied and the significant frequencies that changed with speed and those that remained constant were noted.

At first glance, the flux switching motor appears to have more significant frequency peaks than the switched reluctance motor. However, when a more detailed comparison is made, it is revealed that this is due to the flux switching motor producing *less* noise than the switched reluctance motor at certain frequencies, leaving some frequencies at a similar level to those in the switched reluctance spectrum.

There are some interesting differences in the acoustic noise produced by the two motors. The significant frequencies are listed below:

Frequencies which are significant in the 2-phase switched reluctance machine analysis but not in the flux switching motor acoustic profile

300Hz	Very close to the rotor resonant frequency. Does not vary with speed.
400Hz	Close to the stator structure resonant frequency. Does not vary with speed.
750Hz	A motor or system resonance that is excited by the switched reluctance motor. Does not vary with speed.

Frequencies which are significant in the flux switching motor analysis but not in the 2-phase switched reluctance acoustic profile.

120Hz	Commutation frequency. Varies with speed.
360Hz	3rd Harmonic of commutation frequency. Varies with speed.

480Hz	Further related to the commutation frequency. Varies with speed.
1900Hz	A system resonance that is excited by the flux switching motor. Does not vary with speed.
7100Hz	High frequency noise – unlikely to be a mechanical resonance. Does not vary with speed.

The significant frequencies present in the acoustic profile of the switched reluctance motor do not generally vary with speed. They are motor or system resonant frequencies that are excited by motor commutation, particularly those of the rotor and stator structure.

The significant frequencies present in the acoustic profile of the flux switching motor are of more varied cause. Unlike the switched reluctance motor, the flux switching motor commutation causes acoustic noise at commutation (therefore speed) related frequencies. It does not, however, excite the resonant frequencies of the motor rotor and stator to the same extent as the switched reluctance motor commutation.

The presence of the high frequency acoustic noise in the flux switching motor was investigated further.

6.6.2 Removal of a Pure Tone Sound

The 7100Hz tone present in the flux switching profile is distinguishable to the human ear, unlike many of the other tones. When the converter was analysed, it was found that this high frequency acoustic noise was due to an electrical resonance effect

caused by the switching MOSFETs, which manifested itself in the voltage seen by the motor windings. The timing of the high frequency voltage transition was related to the frequency of the acoustic noise it caused. To eliminate the resonance, a polypropylene capacitor was added across the armature circuit as shown in figure 6.18.

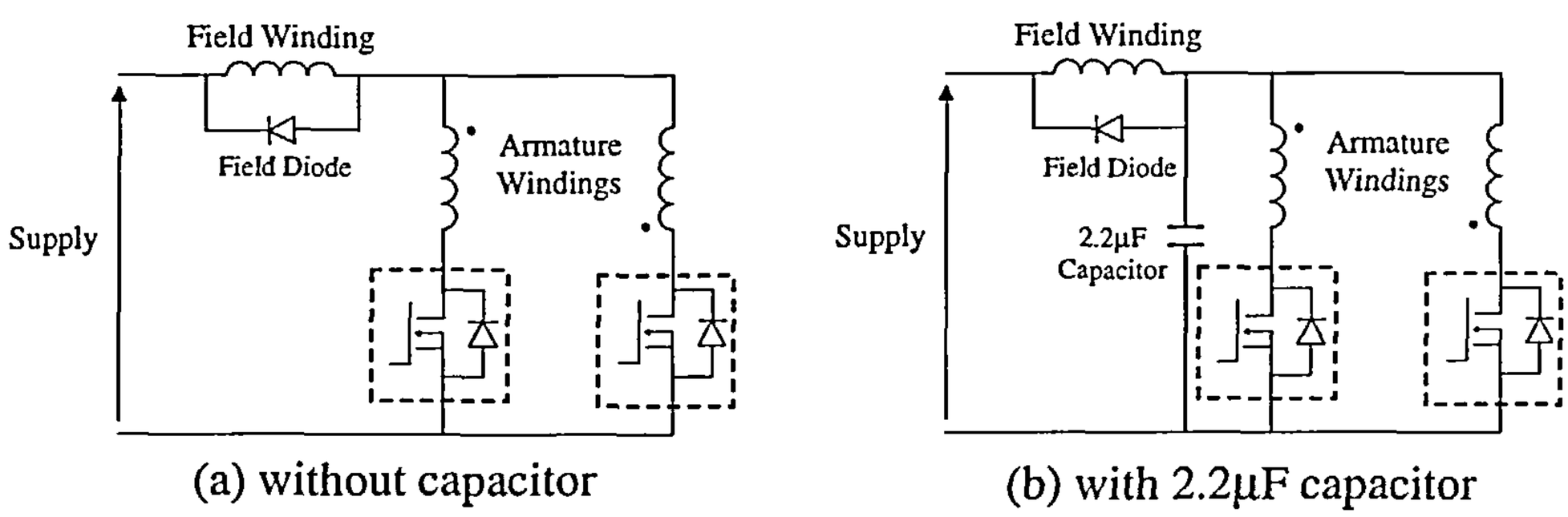

Figure 6.18: Control circuit (a) without and (b) with the addition of a 2.2μF capacitor

Figure 6.19 shows the armature voltage, undergoing a resonance effect in (a), which is removed by the addition of a 2.2μF polypropylene capacitor across the armature circuit in (b).

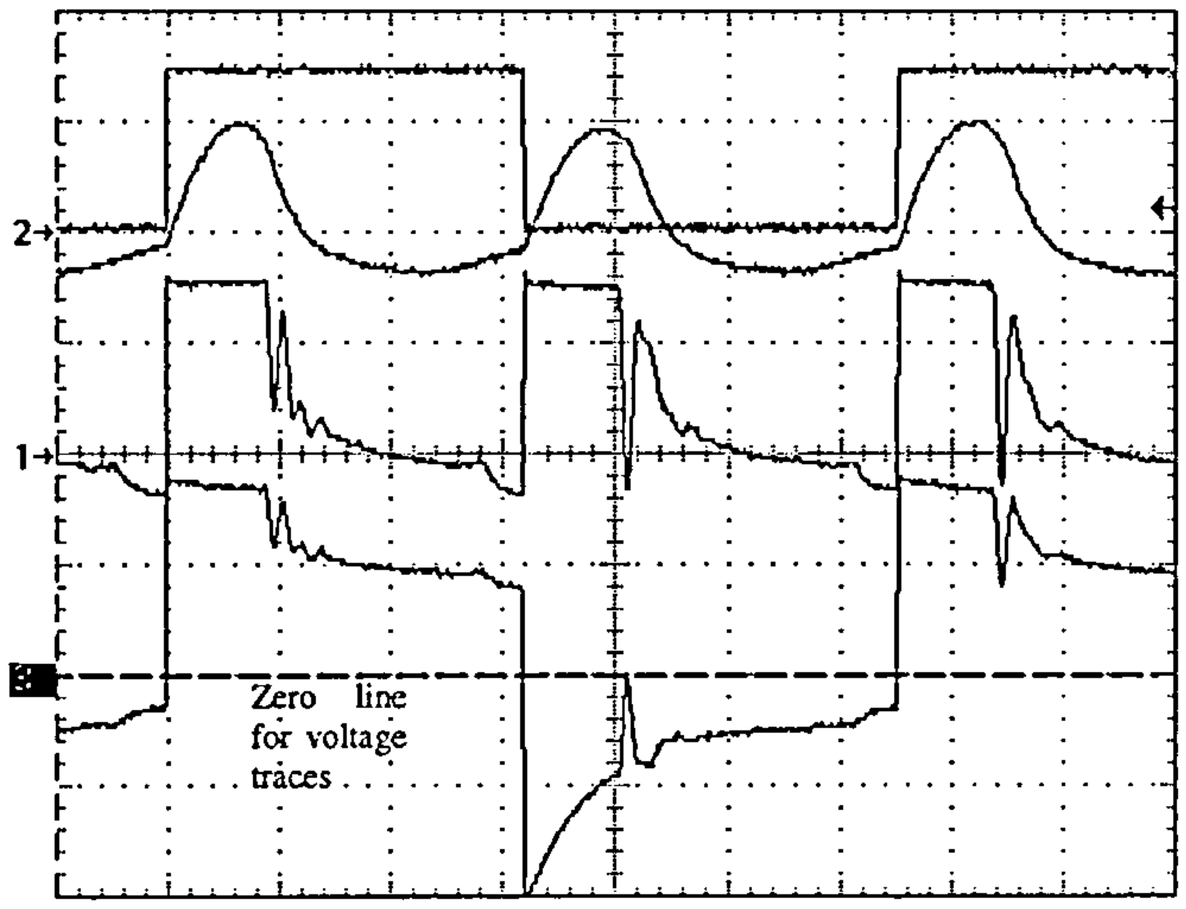

(a) without capacitor

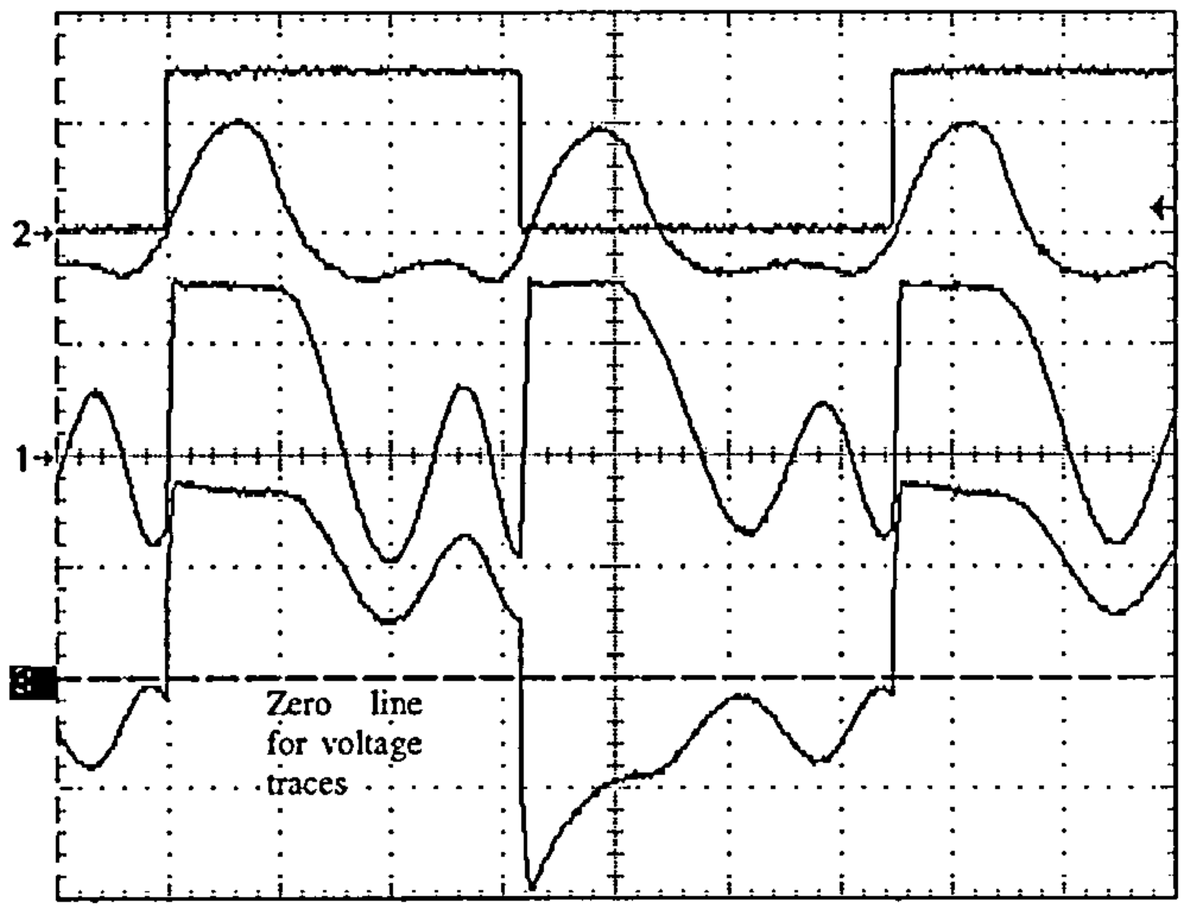

(b) with 2.2μF capacitor

Figure 6.19: Switching voltages (a) without and (b) with the addition of a 2.2μF capacitor

Adding a capacitor across the armature circuit eliminated the resonance effect and removed the audible high frequency acoustic noise.

6.6.3 Test Summary

Table 6.5 summarises the test conditions and results obtained from the comparison of the external rotor flux switching motor, the external rotor two-phase switched reluctance motor, and the internal rotor induction motor driving a fan load.

Table 6.5: Summary of test data for acoustic noise and performance comparisons under fan load conditions

	External Rotor Flux Switching Motor	**External Rotor 2-phase Switched Reluctance Motor**	**Internal Rotor Induction Motor**
Supply Voltage / V	135 d.c.	53 d.c.	230 a.c.
Volts per armature or phase turn	0.131	0.082	Unknown
Torque / Nm	0.103	0.103	0.103
Input Power to drive / W	73	78	71
Output Power at 1800rpm / W	19.5	19.5	19.5
Motor and Drive Efficiency	26.7 %	25 %	27.5 %
Weight / kg	0.835	0.740	2.150
Power : Weight	23.3	26.3	9.1
Average SPL L'_{pA} / dBA (with fan)	**65.86**	**68.54**	**62.18**

6.7 Electrical Performance Comparisons

The two motors were tested with a calibrated hysteresis brake at a variety of input voltages, to measure their performance. The hysteresis brake provides a constant torque for a given brake input current independent of speed, but as the brake characteristic maps a hysteresis loop, the value of torque is dependant on whether the brake current is increasing or decreasing.

6.7.1 Torque – Speed Performance

Figures 6.20 and 6.21 show the torque – speed characteristics of the external rotor flux switching and 2-phase switched reluctance motors, at various input voltages, respectively. The torque - speed load requirement of the fan was also and is shown.

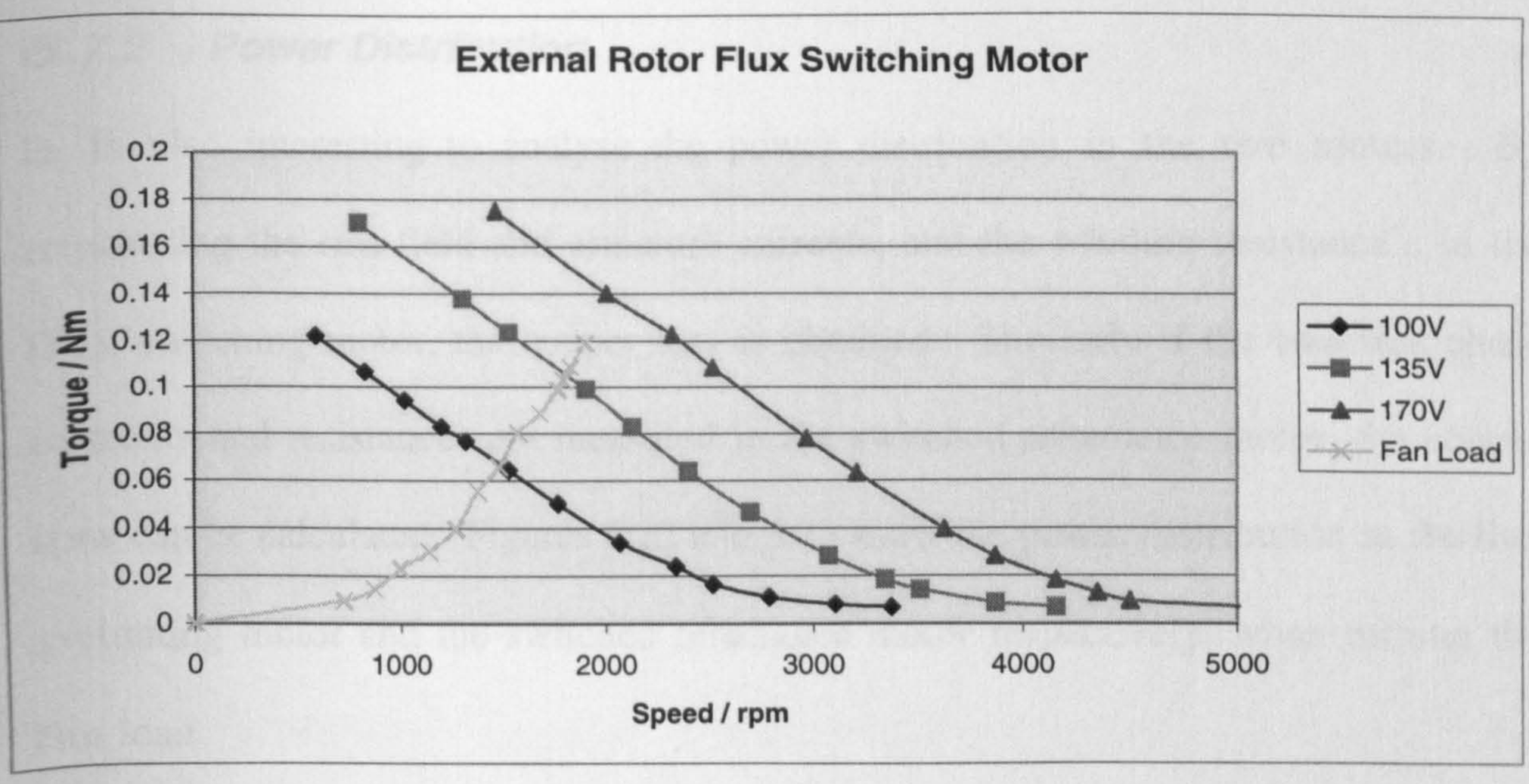

Figure 6.20: Torque – Speed characteristic of the external rotor flux switching motor at various input voltages

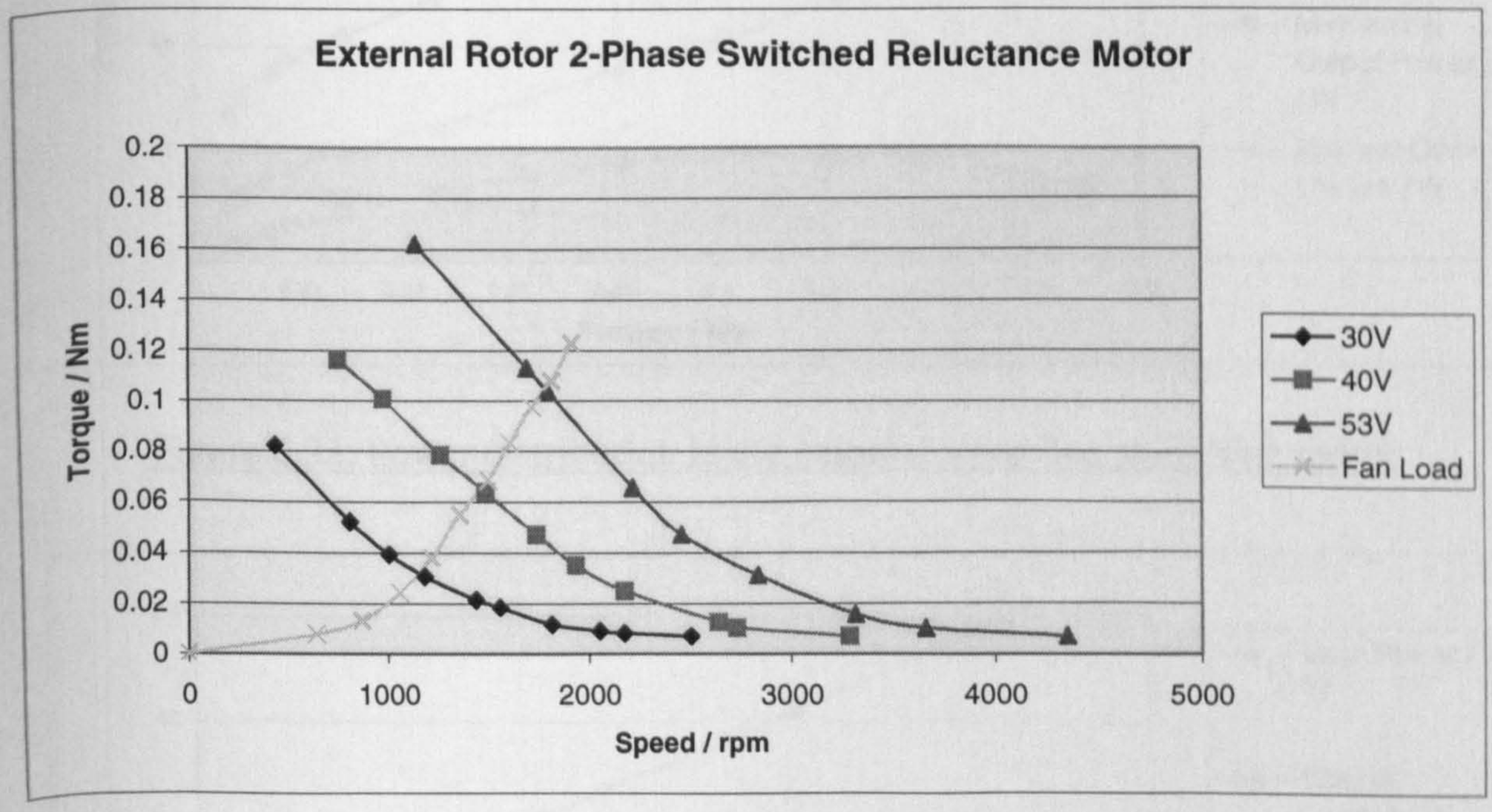

Figure 6.21: Torque – Speed characteristic of the external rotor 2-phase switched reluctance motor at various input voltages

6.7.2 Power Distribution

It is also interesting to analyse the power distribution in the two motors. By measuring the rms field and armature currents, and the winding resistance's in the flux switching motor, the copper loss is obtained. Similarly if the two rms phase currents and resistances are measured in the switched reluctance motor, the copper loss can be calculated. Figures 6.22 and 6.23 show the power distribution in the flux switching motor and the switched reluctance motor respectively, when turning the fan load.

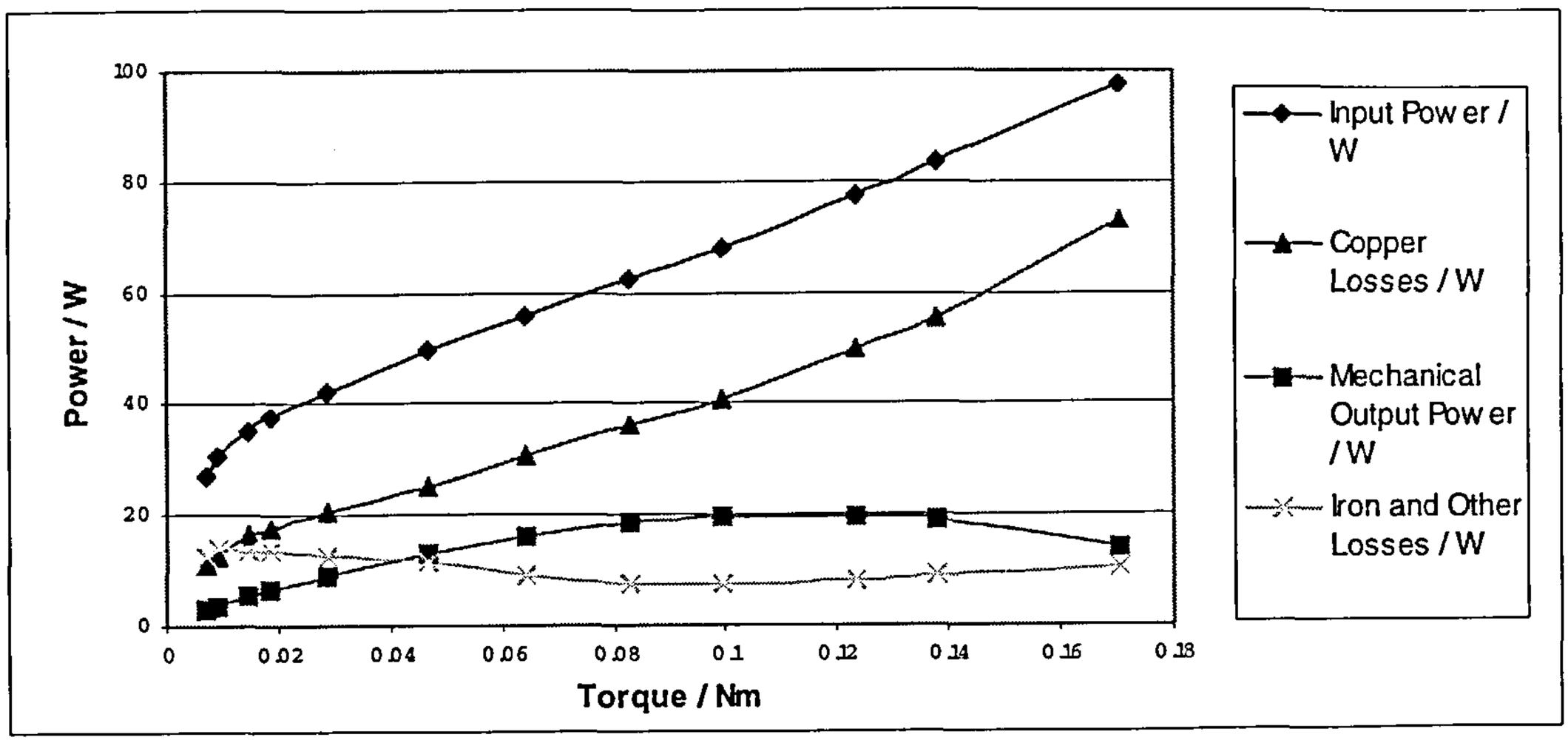

Figure 6.22: Power distribution in the external rotor flux switching motor

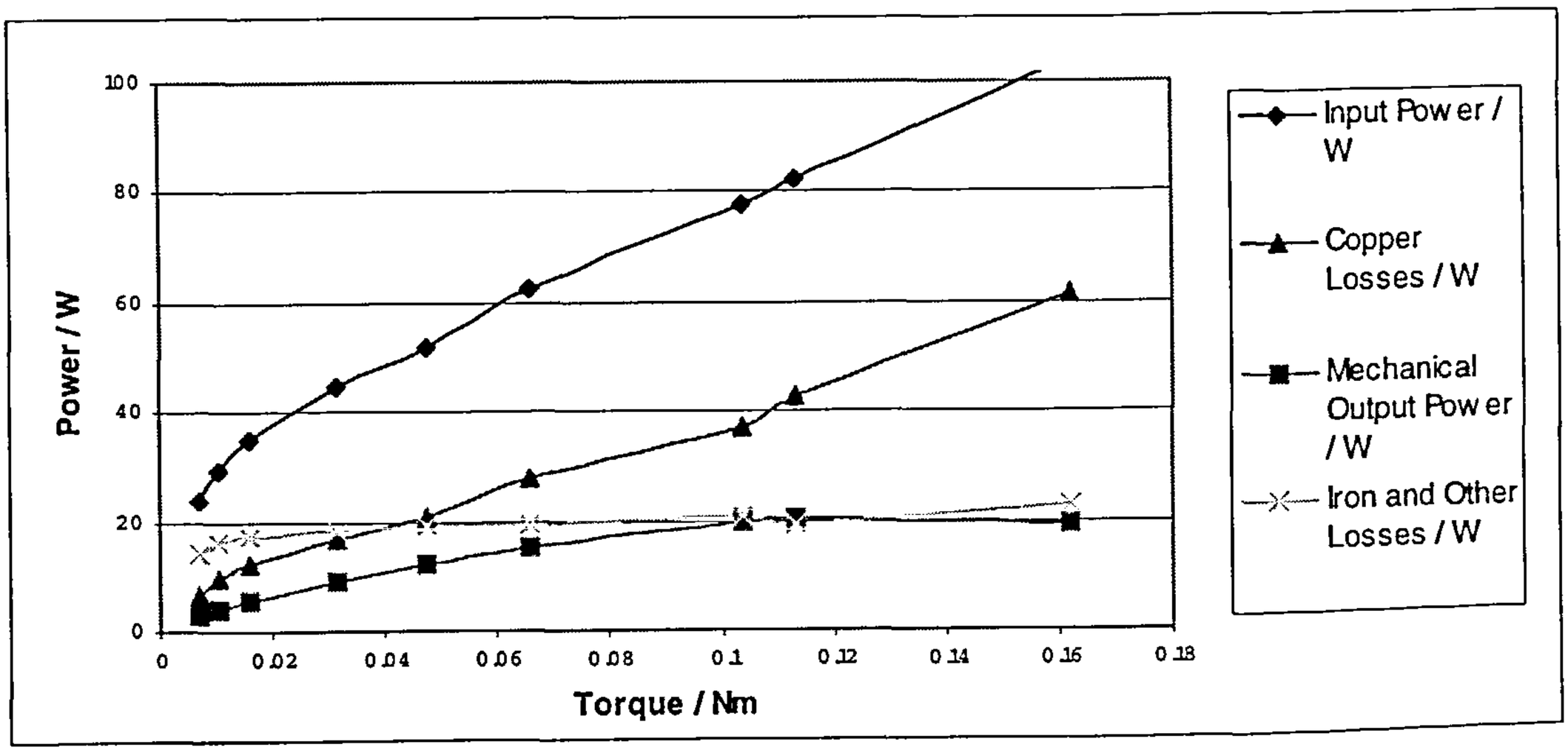

Figure 6.23: Power distribution in the 2-phase switched reluctance motor

The 2-phase switched reluctance motor has less copper loss than the flux switching motor. This is due to the d.c. excited field winding present in the flux switching motor and the greater end winding length. The proportion of iron / other loss is lower in the flux switching motor than in its 2-phase switched reluctance counterpart. In the flux switching motor there is d.c. flux present in half of the stator back iron sections and alternating (but not necessarily reversing) flux in the other half. This alternating flux is the cause of hysteresis and eddy current losses, and probably accounts for the difference in the iron / other losses measured.

It is concluded that lower iron losses are one advantage of the flux switching machine, over a switched reluctance machine, due to the difference in time varying flux in parts of the machine back iron. Conversely there is a disadvantage in the increased copper loss in the flux switching motor, due to the presence of the field winding and the greater end winding length created by the coil pitch.

6.7.3 Comparison of Flux Switching Motor Performance with Design Model Prediction

As a check as to the accuracy of the model used in the design of the external rotor flux switching motor, some comparisons will be drawn between parameters predicted by the model, and those measured on the bench.

The model used a 150V d.c. input voltage giving an rms field current of 0.583A and an rms armature current of 0.558A providing an average torque of 0.14Nm at 1800rpm. Bench tests reveal that at this speed, the motor delivered 0.10Nm of torque from 135V d.c. supply, with an rms field current of 0.65A and an rms

armature current of 0.85A. The motor did not quite achieve the performance predicted in the model, with a lower output torque and higher field and armature currents. However given the number of assumptions the model makes, it was felt that the model provides a sound basis for design

The input power was predicted in the model to be 72W with an overall efficiency of 37% at 1800rpm. The copper losses was predicted to be 42W and the iron/other loss 3W. Bench tests at 1800rpm, with a load torque of 0.1Nm, showed an input power of 74W, a copper loss of 42W, an output power of 20W, and iron/other losses of 12W. The overall efficiency was calculated as 27%. Clearly the model has predicted the input power and copper losses accurately, but the iron losses were measured to be much greater than predicted, reducing the output power (hence torque) available.

6.8 Internal Rotor Flux Switching Machine

The comparison between the external rotor flux switching machine and the external rotor 2-phase switched reluctance machine is fair - both being external rotor, of similar weight and of very similar mechanical build. However comparing the performance of an *external* rotor flux switching motor with an *internal* rotor induction motor of different mechanical build, and more than twice the weight, is perhaps unjust.

It has been shown that the flux switching motor is quieter than the switched reluctance motor. In order to make a fair comparison between the flux switching motor, and the induction motor, a new prototype motor was required. The main issues to address were the internal rotor arrangement, the mechanical design of the machine (endcaps, shaft, stator stack) and the weight of the machine.

6.8.1 Design of the Internal Rotor Flux Switching Machine

In order to provide a fairer comparison of the acoustic noise and performance of the flux switching topology with that of the single-phase induction motor, an internal rotor flux switching machine was constructed. To closely match the mechanical parameters of the two machines, a spare induction motor was dismantled and its mechanical parts re-used. The cage rotor was pressed from the shaft and replaced with a 6 (salient) pole reluctance rotor. An existing rotor lamination design was modified for use in this application. The 12 pole stator stack was stripped of its induction motor type winding and re-wound with a flux switching winding. The flux switching winding was designed using the tools and methods described in Chapter 5.

The original induction motor stator lamination and the reluctance rotor lamination are shown in figure 6.24.

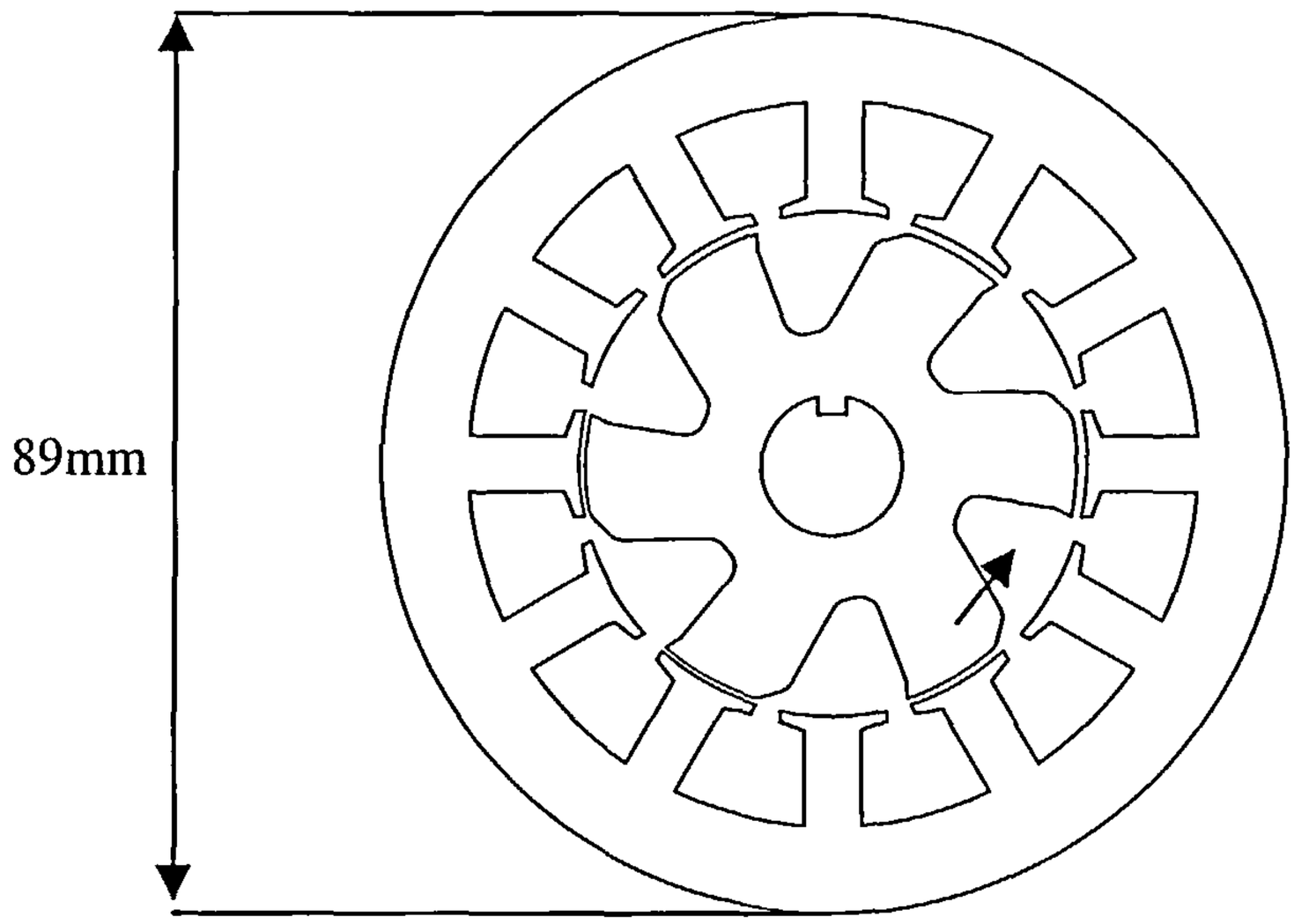

Figure 6.24: Original induction motor stator lamination and reluctance rotor lamination

The stator OD was 89mm the stack length 31mm, and the airgap 0.3mm. The internal rotor flux switching winding, wound on the original induction motor stator stack is summarised in Table 6.6.

Table 6.6: Internal rotor flux switching motor winding data

Attribute	**Field Winding**	**Armature Winding**
Number of Coils	6	6
Number of strands per coil	1	2 (bifilar)
Number of turns per coil	210	275
Wire diameter / mm	0.315	0.2
Connection	Series	Series
Resistance per coil / Ω (measured @ 20°C)	7.83	22.93
Total Resistance / Ω	47.0	137.6

The motor winding was designed to allow the motor to run at 1800rpm from a rectified mains (340V d.c.) supply.

The original induction motor endcaps were used to construct the motor. The only physical differences between the internal rotor flux switching motor and the induction motor were the reluctance and cage rotors, and the winding design and configuration. This allowed the acoustic noise produced by the two different magnetic flux variation and distribution schemes to be measured and compared.

A slotted optical position sensor was attached to the motor endcap. A sensor wheel on the protruding shaft was used to gauge rotor position. The sensor arrangement was optimised for efficiency at an advance angle of 10 degrees. This is a larger angle than was used with the external rotor machine, but the shape of the rotor teeth are very different, so comparison is difficult. Again, a 50% on time was used for each of the armature circuits alternately. In this 12/6 motor, there are 12 commutations per revolution. The 2-switch converter, previously used to control the external rotor motor, was used to control the internal rotor motor. A fairer assessment of the acoustic performance of the flux switching motor could now be achieved.

6.8.2 Resonant Characteristics

Measurements were made to identify the natural resonant frequencies of motor structure. As the rotor is internal in this machine, it was not possible to make a separate measurement for the rotor resonant frequency. An accelerometer was

placed on the external surface of the motor casing, adjacent to a stator. As before a current impulse of duration 1ms was applied through the field to one armature winding with the rotor in an aligned position. The resulting vibration was captured and analysed. Figure 6.25 shows the current pulse, resulting motor vibration (mode 2) and frequency power spectrum for the internal rotor flux-switching machine. A clear motor resonant frequency at 1.28kHz is revealed:

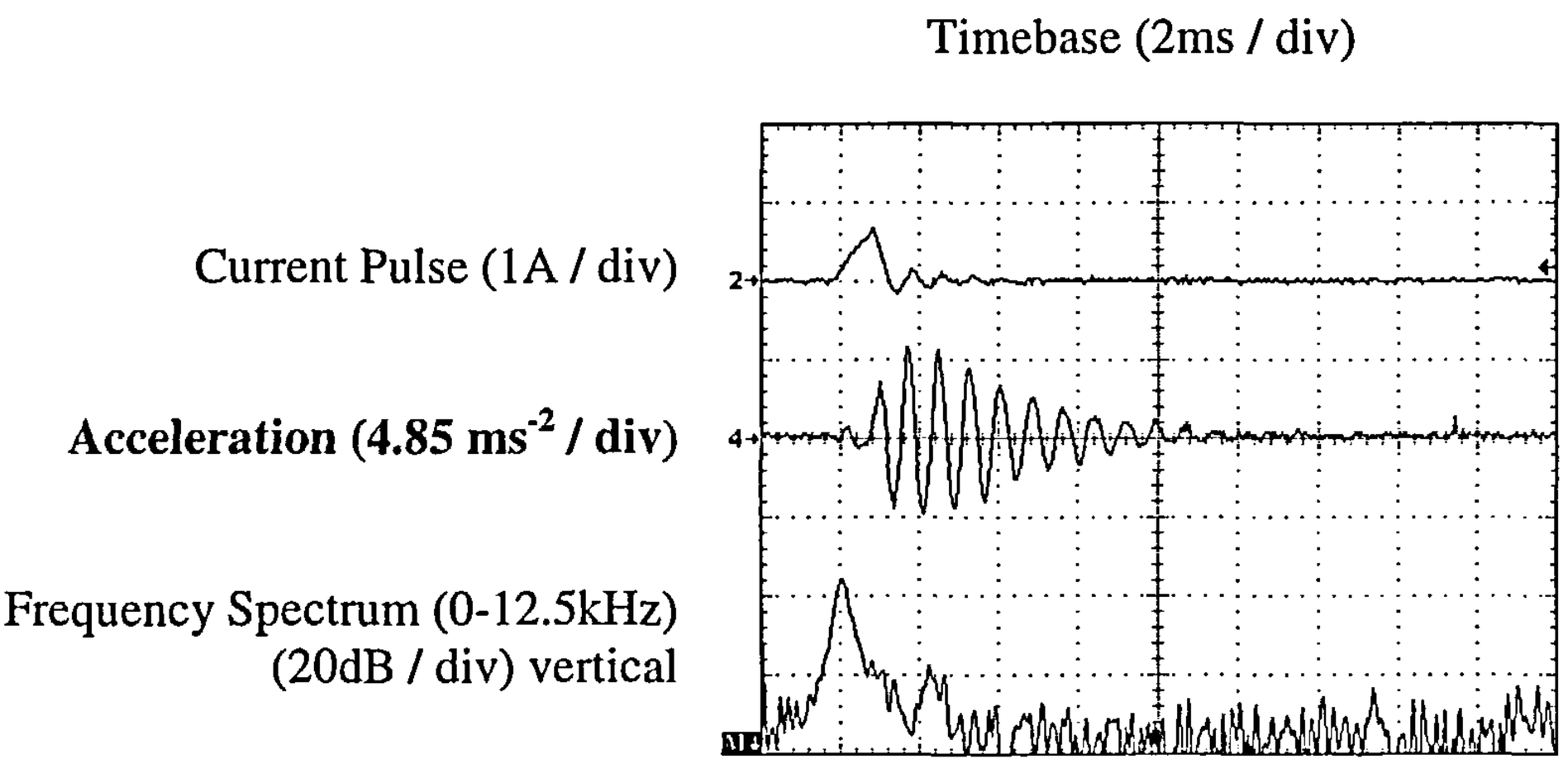

Figure 6.25: Acceleration and frequency spectrum of the stator support

6.8.3 Acoustic Noise Tests

The internal rotor flux switching motor was tested under the same conditions. The acoustic noise measurements were carried out with the fan load, and with the hysteresis brake. Table 6.7 shows a summary of the acoustic noise and performance results of the internal rotor flux switching motor and the induction motor at 1800rpm.

Table 6.7: Summary of test results from the internal rotor flux switching motor and the induction motor

	Internal Rotor Flux Switching Motor	**Internal Rotor Induction Motor**
Torque Delivered / Nm	0.103	0.103
Input Power / W	55	71
Output Power at 1800rpm / W	19.5	19.5
Efficiency	35%	27.5 %
Weight / kg	2.00	2.150
Power : Weight	9.8	9.1
Average SPL L'_{pA} / dBA (with fan load)	**63.21**	**62.18**
Average SPL L'_{pA} / dBA (with brake load)	**55.55**	**45.08**

The acoustic profile of the internal rotor flux switching motor was analysed to confirm whether the commutation frequency related noise was present in this motor. The peak spectrum values of the internal rotor flux switching motor and the induction motor with the brake and fan load are given in figures 6.26 and 6.27 respectively.

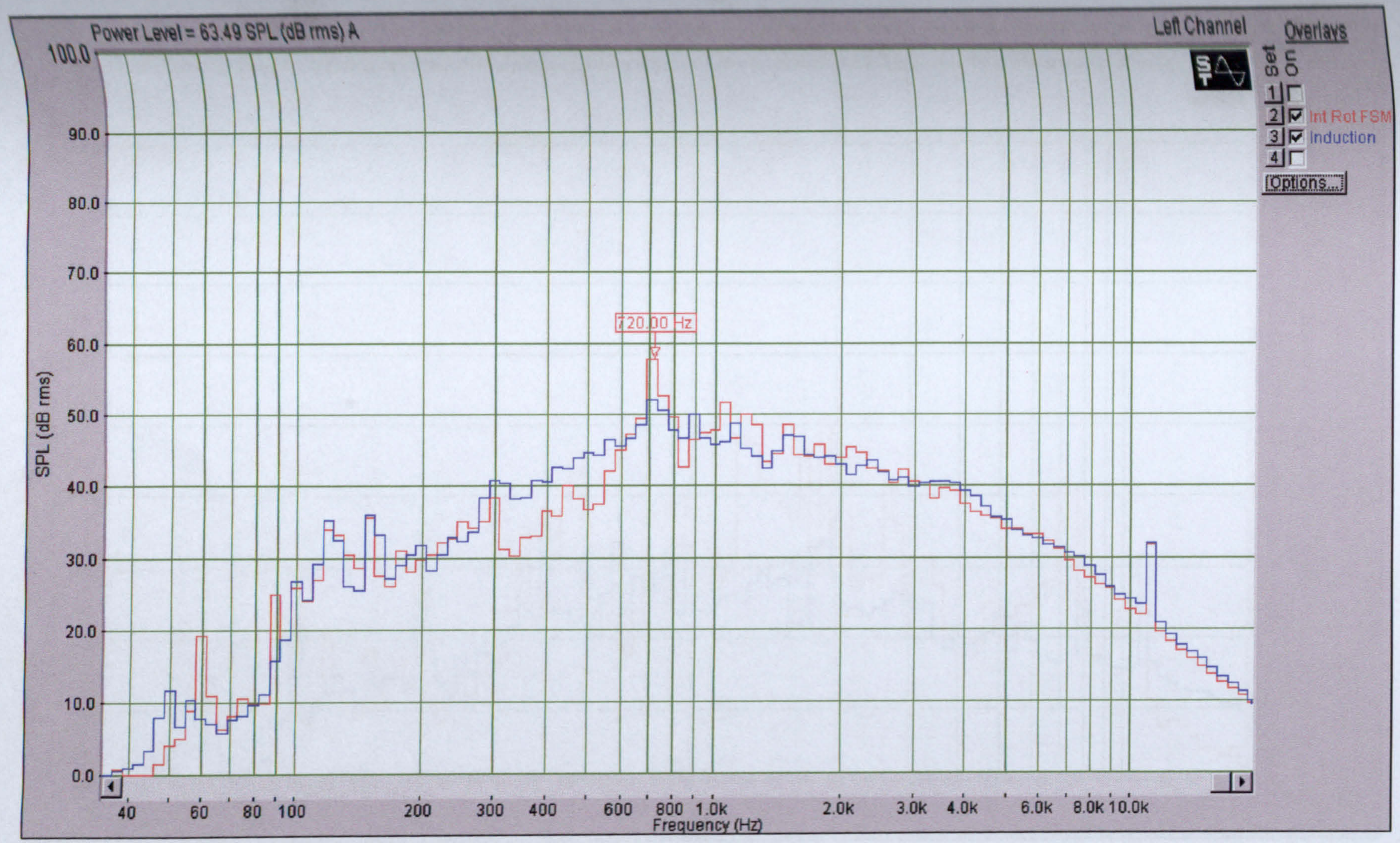

Figure 6.26: Acoustic profile of the internal rotor flux switching motor and the induction motor driving the fan at 1800rpm

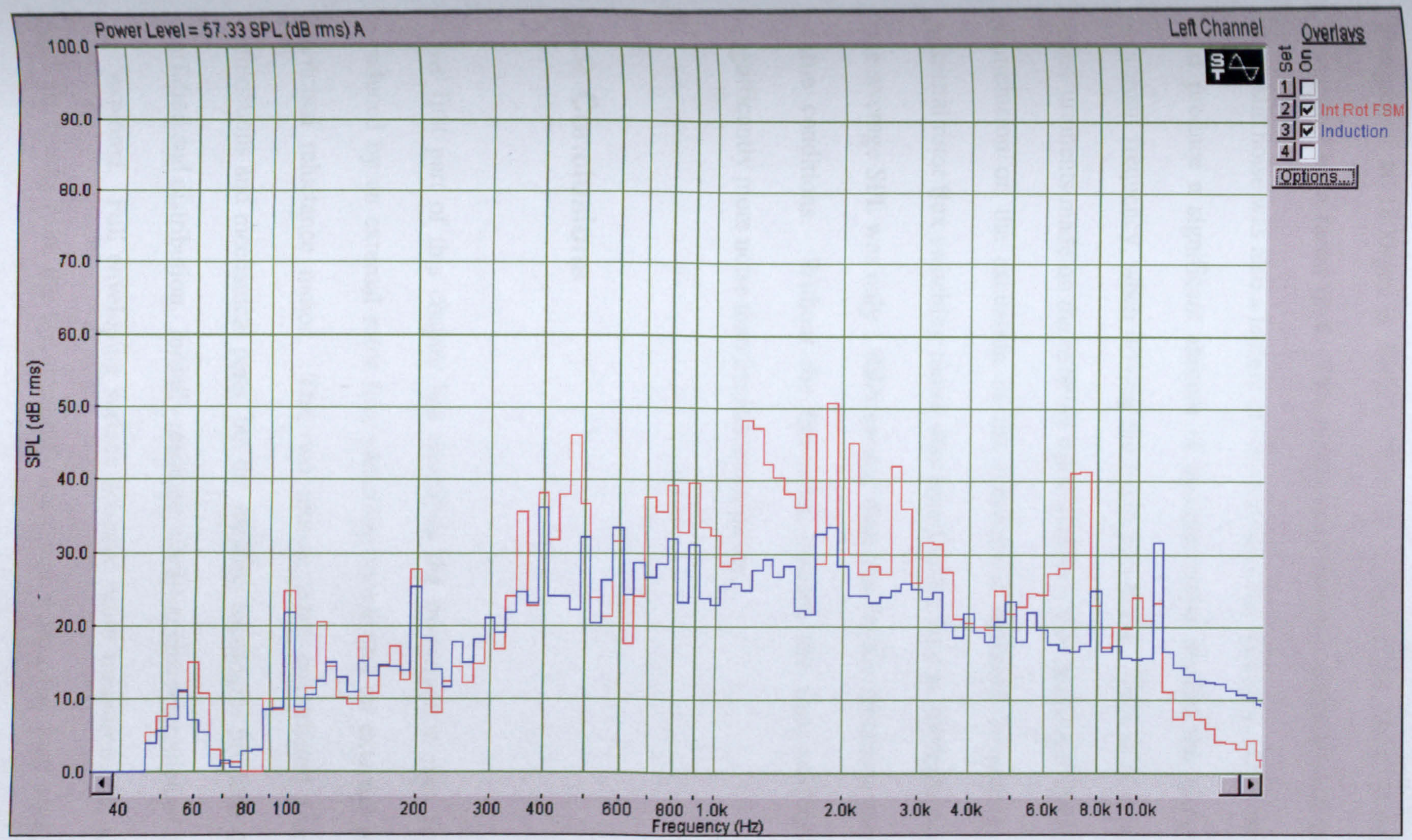

Figure 6.27: Acoustic profile of the internal rotor flux switching motor and the induction motor driving the hysteresis brake at 1800rpm

This confirms that the most significant frequency in the flux switching motor acoustic profile is 720Hz when driving the fan. In this 12/6 motor, the commutation frequency at 1800rpm is 180Hz. The most significant noise is related to this frequency by a factor of 4. This relationship between commutation frequency and acoustic noise was also a feature of the external rotor machine. The internal machine did produce a significant amount of acoustic noise around the motor mechanical resonant frequency, when driving the hysteresis brake. This is in conflict with the measurements made on the external rotor machine, thus making it difficult to draw a conclusion on the excitation of the mechanical resonant frequency. When the internal rotor flux switching motor was tested under load at 1800rpm driving the fan, the average SPL was only 1 dBA greater than that for the induction motor under the same conditions. Without the fan noise present, the flux switching generated significantly more noise than the induction motor.

6.9 Conclusions

This first part of this chapter has described the investigation into acoustic noise produced by an external rotor flux switching motor and an external rotor 2-phase switched reluctance motor. The two motors were constructed from the same laminations and mechanical parts, but the winding topologies produce different flux variation and distribution. Initially resonant vibration characteristics of the machines are explored. Full enveloping surface acoustic noise measurements are described and the results from the test machines are given with a fan load and a near silent hysteresis brake load. It was shown that the external rotor flux switching motor was approximately 2dB quieter than the 2-phase switched reluctance motor under the

same loading conditions. Furthermore, it was discovered that the external rotor flux switching motor produced acoustic noise at frequencies related to its commutation frequency, which vary with speed, whereas the switched reluctance motor did not. In addition to this it was noted that the external rotor flux switching motor did not excite motor stator and rotor resonant frequencies to the same extent as the switched reluctance motor.

A commercial 9" fan was used as a vehicle for this work. The product uses a single phase induction motor. This chapter further describes the construction of an internal rotor flux switching motor for a closer *physical* comparison with the induction motor. The internal rotor machine used the same stator stack, shaft, endcaps and bearings as the induction motor. The only physical differences between the machines were the cage and reluctance type rotors, and the winding configuration. It is accepted that there are inevitable operating differences.

The acoustic noise produced by the internal rotor flux switching motor was investigated and compared to that of the induction motor. When driving the fan load, the acoustic noise from the external rotor flux switching motor was only 1dB greater than the induction motor. The only significant frequency in the acoustic noise profile was 720Hz, which was related to the commutation frequency. Without the fan noise present, a band of acoustic noise, close to the mechanical resonant frequency was identified. No firm conclusion could be reached about its origin.

With the same mechanical build, and a less than optimal lamination design, the flux switching motor was shown to be 8.5% more efficient than the induction motor at

this speed. It also has the added benefits of more rugged and simpler components, shorter end windings and infinitely variable speed and controllability. In comparison with other low power electronically commutated motor drives, it requires only two power switches and one power diode for operation. With the field winding in series with the armature circuit, it can act as part of a filter for the high frequency electronic noise caused by the switching waveforms and reduces the need for additional components to comply with EMC requirements. These benefits are obtained at the cost of 1dBA of noise over the induction motor.

This chapter has shown that there is a significant difference in the level and type of acoustic noise produced by the flux switching and switched reluctance motor. It has shown that the flux switching motor can have benefits over the switched reluctance motor, in terms of acoustic noise and performance. Finally, it shows that the flux switching motor has the potential to rival the well established, quiet induction motor offering some significant benefits at the cost of 1dB of noise as measured in this fan application.

CHAPTER 7

COMPARATIVE SIMULATION OF RADIAL FORCE IN THE FLUX SWITCHING MOTOR

7.1 Introduction

Chapter 2 describes how the variation and distribution of magnetic flux in a motor airgap differs between machine topologies. It is well documented that the variation of radial force produced by this flux in a motor airgap results in acoustic noise. This chapter will review a proven simulation technique used for the modelling of the response of a switched reluctance motor stator caused by a change in radial force. It will go on to present a finite element simulation, comparing the radial forces in a flux switching machine and a 2-phase switched reluctance machine using measured current excitation at a constant speed.

7.2 Review of the Simulation of the Vibration of a Switched Reluctance Motor Stator

The work of C.Y. Wu models the vibration of a switched reluctance motor stator on a lumped parameter mass-spring-damper system [51]. By using radial force as an input to the system, he expressed the stator response using the general equation:

$$F_n = m\frac{d^2x}{dt^2} + c\frac{dx}{dt} + kx \tag{7.1}$$

where F_n radial force

m equivalent mass of stator

x displacement of stator

c viscous damping coefficient

k stiffness coefficient

Dividing (7.1) by m

$$\frac{F_n}{m} = \frac{d^2x}{dt^2} + \left(\frac{c}{m}\right)\frac{dx}{dt} + \left(\frac{k}{m}\right)x \tag{7.2}$$

This can be written as

$$\frac{F_n}{m} = \frac{d^2x}{dt^2} + 2\xi\omega_n \frac{dx}{dt} + {\omega_n}^2 x \tag{7.3}$$

where $\omega_n = \sqrt{\frac{k}{m}}$ is the undamped natural frequency

and $\xi = \frac{c}{2\sqrt{km}}$ is the damping ratio of the system.

Equation 7.3 describes the response of a stator to a force input. Wu solved the differential equation to obtain the simulated vibrational response of a switched reluctance motor stator. Further to this Wu went on to measure the acceleration of the stator of a real motor and showed a very strong correlation between his simulated and experimental results [52].

One of the conclusions from Wu's work was that the *larger the change in the gradient* of the radial force, particularly when the gradient changes from positive to negative, *the greater the resultant vibration* (acceleration) of the stator [53]. By analysing the rate of change of gradient of the radial force in the prototype motors, an comparative indication is provided as to the magnitude of vibrational acceleration produced by the radial force variation.

7.3 Finite Element Simulation of Radial Force

The objective of the author is to use analysis of the radial force waveforms to provide some evidence to account for the difference in acoustic noise production of the flux switching motor and the 2-phase switched reluctance motor, which was observed in the previous chapter. The radial force data was produced by finite element simulation.

An electromagnetic finite element model of the flux switching motor was used in the design of the test machine, as explained in Chapter 5. This was based upon ideal characteristics, which do not occur in practice. The authors approach to modelling the radial forces involved in the operation of the flux switching and switched reluctance motors was to measure the real winding currents in the two machines when running at the rated speed of 1800rpm. Using this data in the finite element model allowed a prediction of the radial force in the airgap, with rotor position, as the motor rotates.

The finite element software obtains a value for the radial force by calculating the Maxwell Stress over a line integral in the airgap. To calculate force in the radial and tangential directions to the airgap integral line, Maxwell Stress is resolved using normal and tangential unit vectors.

7.4 Sampling Current Data

The sampled current waveforms from the test external rotor flux switching and switched reluctance motors are given in figures 7.1 and 7.2. The measurements were made under the conditions described in table 7.1:

Table 7.1: Test conditions when sampling motor winding currents

Quantity	**External Rotor Flux Switching Motor**	**External Rotor 2-Phase Switched Reluctance Motor**
Speed / rpm	1800	1800
Torque / Nm	0.103	0.103
Input Power / W	73.3	77.7
RMS current / A	0.65 Field 0.85 Armature (total)	1.22 per phase 2.44 (total)
Total Number of Turns (Series Connected)	1200 Field 800 Armature	644 Phase 1 644 Phase 2

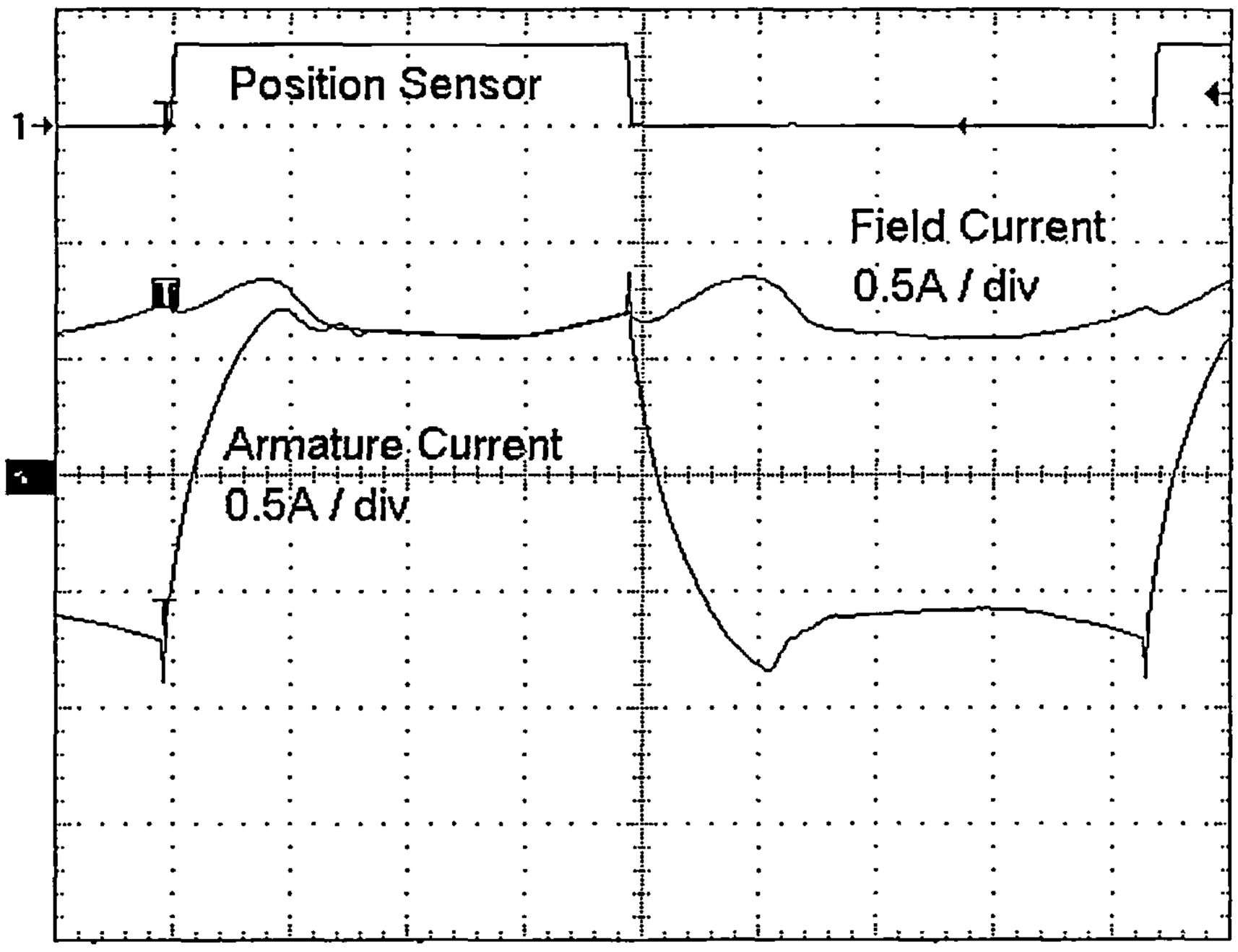

Figure 7.1: Flux switching motor winding current measurements for simulation

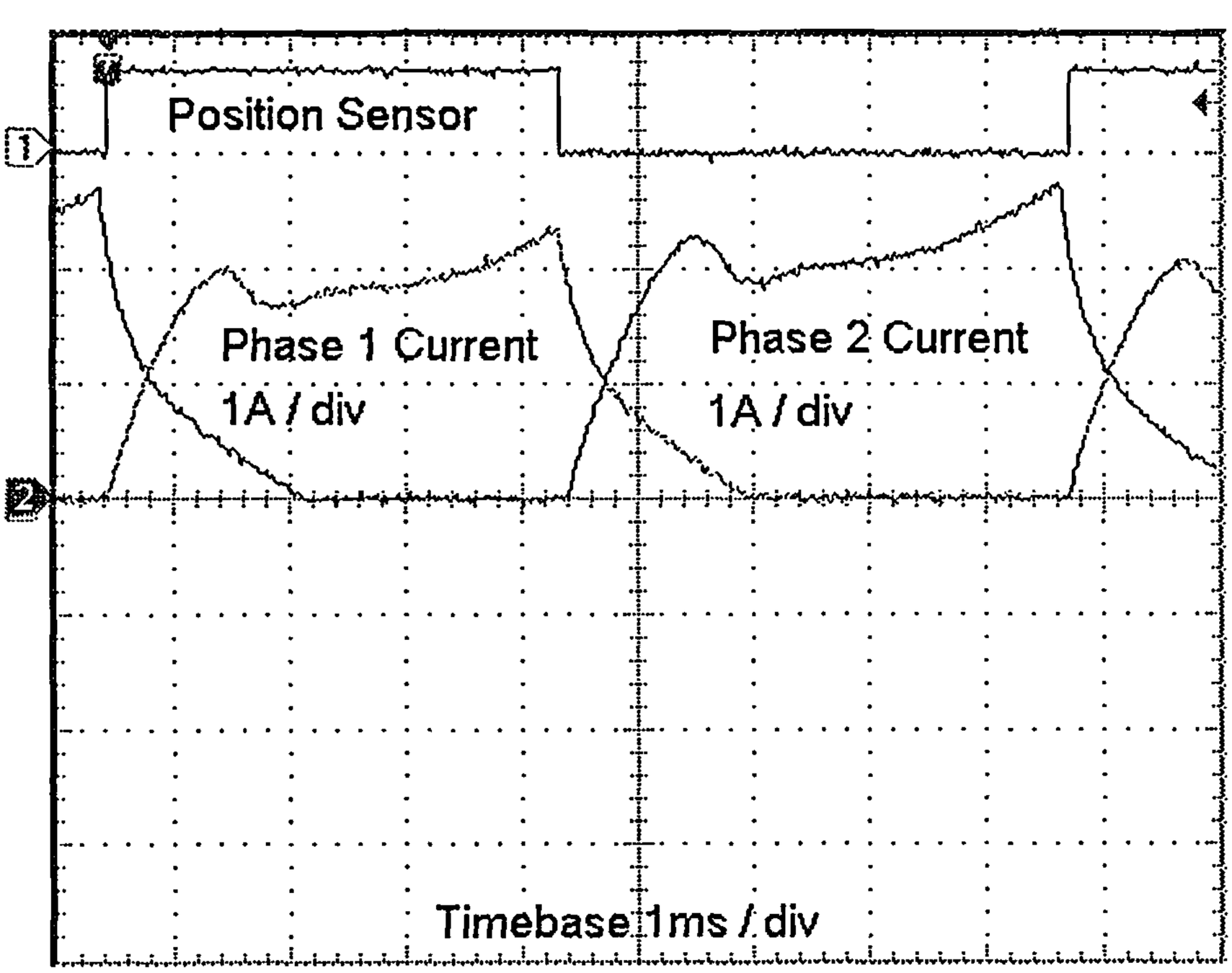

Figure 7.2: 2 Phase switched reluctance motor winding current measurements for simulation

The phase currents in the two phase switched reluctance motor were slightly imbalanced and the lower phase current was used. Samples were taken every 3 degrees of rotational position. Around the commutation point, the resolution was increased to single degree increments. The sampled points for the flux switching motor and the switched reluctance motor are displayed in figures 7.3 and 7.4 respectively.

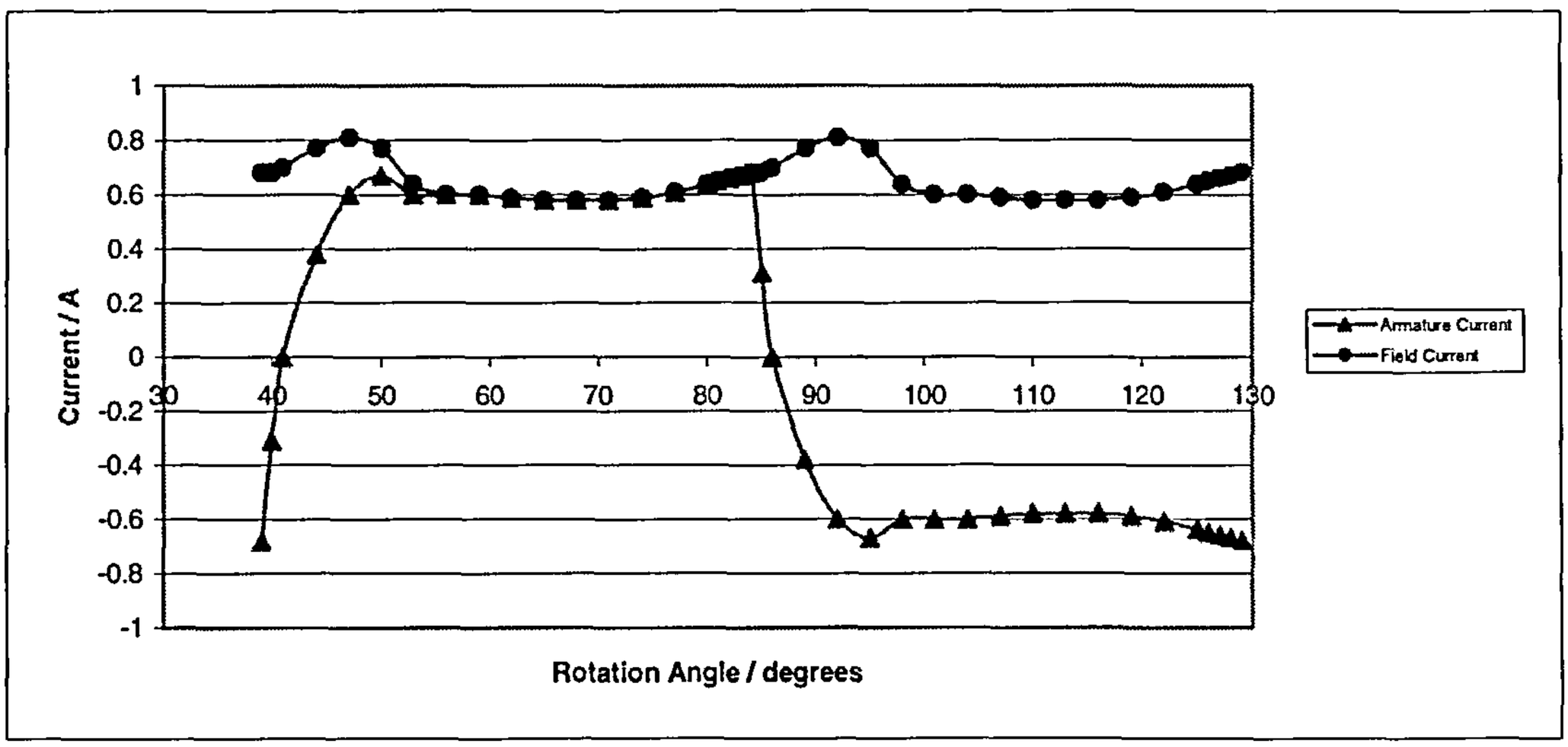

Figure 7.3: Flux switching motor winding current sample points

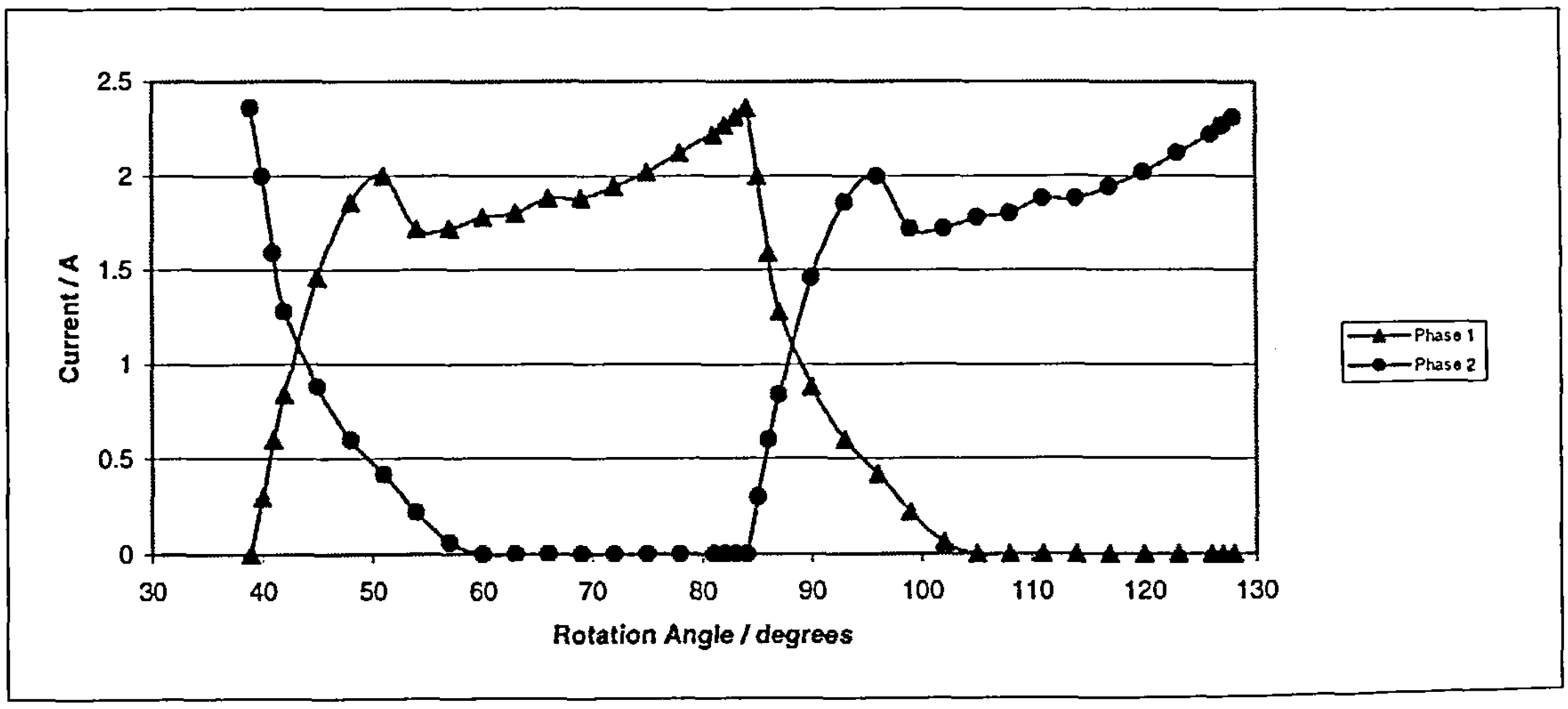

Figure 7.4: 2-Phase switched reluctance motor winding current sample points

This data was converted into current density for input into the simulation model, accounting for slot area and number of turns. Care was also taken to ensure the simulation rotor position and current information corresponded to the real rotor position and currents in each case. The two motors were commutated at the same physical rotor position. The flux switching motor firing angle was quoted with respect to the back emf, and the switched reluctance firing angle with respect to a position of minimum reluctance.

7.5 Simulation Results

7.5.1 Simulated Torque

Using the actual current in the windings of the flux switching and switched reluctance motors when under the same load at the same speed, a direct comparison can be made of the radial forces acting in the two motors. As a check as to the accuracy of the simulation, within its limits, the torque produced at each rotor position was also calculated using the Maxwell stress method. Although the actual value at each position may be different, due to the different current waveform shapes, the average torque over a commutation cycle should be the same for the two motors at the same load and speed.

The simulated torque profiles of the external rotor flux switching motor and the 2-phase switched reluctance motor are given in figure 7.5.

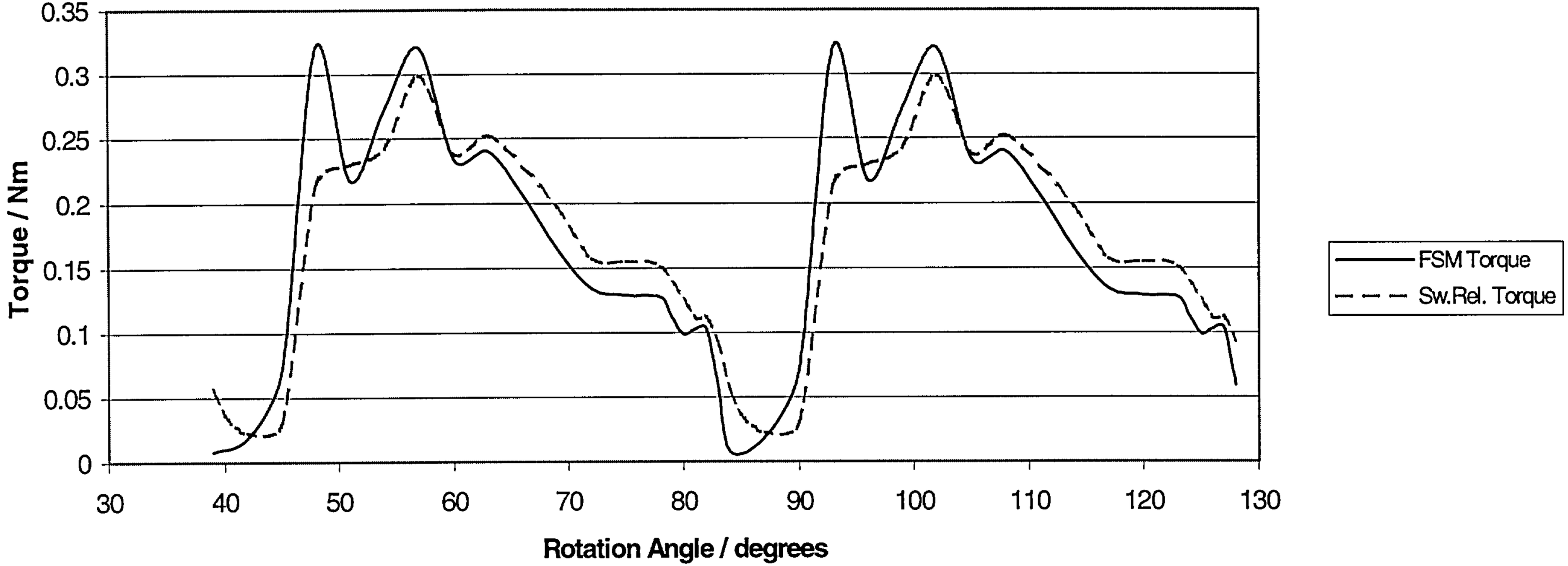

Figure 7.5: Simulated torque profile, over a 90 degree rotation, of the flux switching and 2-phase switched reluctance motors at 1800rpm

The torque profile of the flux switching motor is less smooth than that of the 2-phase switched reluctance motor. Acoustic noise produced by torque variation may therefore be worse in the flux switching motor. The average simulated torque for both the flux switching motor and the 2-phase switched reluctance motor was found to be 0.17 Nm. This torque is higher than was measured experimentally, and as a check to further validate the Maxwell Stress integration method, the energy per working stroke was calculated for one phase of the switched reluctance motor. The torque associated with this energy conversion was consistent with the 0.17 Nm predicted by the Maxwell Stress integral. Clearly the simulated flux is higher than has actually been achieved experimentally, but it is consistent to both motors. This can be attributed to eddy currents and hysteresis effects which are not modelled by FEA, which have a significant affect especially where the rate of change of flux is large at the motor pole tips.

7.5.2 Distribution of Radial Force in the Airgap

It has been shown that the radial force acting between rotor and stator poles across an airgap is confined to overlapping pole faces [51]. A brief analysis of this is presented to investigate the effects of the unusual pole geometries of the lamination used for the two test motors.

A line integral, in the airgap, encompassing two stator poles was used. The simulation was initialised and the radial force acting along that line was graphed as a rotor pole passed the stator poles. The force acts equally on the stator and rotor but since the external rotor is less stiff, the radial force is more likely to cause it to vibrate. Figure 7.6 shows the position of the integral line in the airgap with respect to the stator poles.

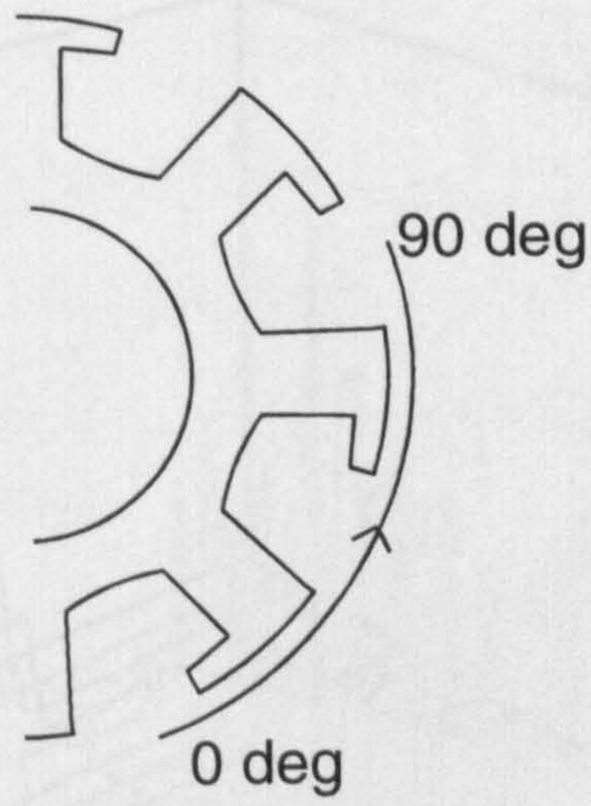

Figure 7.6: 90 degree integral line in the airgap

Figure 7.7 shows the position of the rotor with respect to the stator poles at the point at which a voltage is applied to the phase, and then removed.

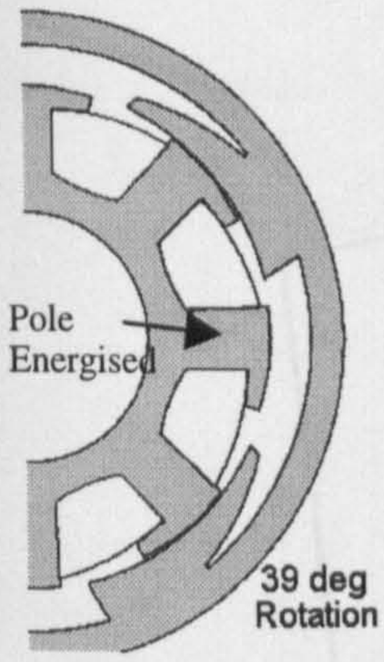

Start of current pulse

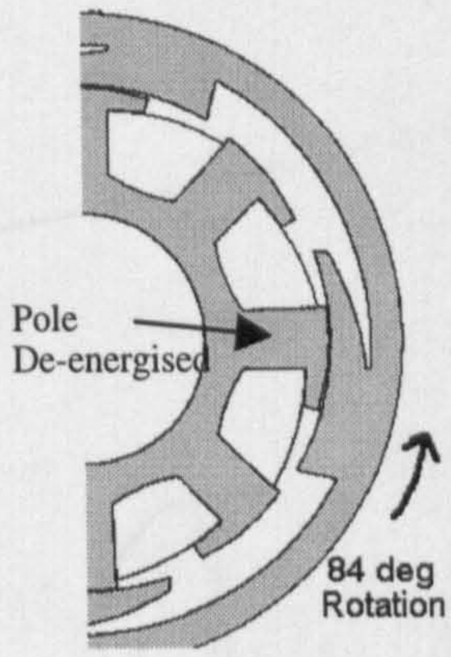

Voltage reversal across the windings

	FSM	Sw. Rel.
39 deg	V+ to Arm	V+ to Ph 1 V- to Ph 2
84 deg	V- to Arm	V- to Ph 1 V+ to Ph 2

Figure 7.7: Rotor position as voltage to phase is applied and removed

Figure 7.8 and 7.9 show how the per unit length (PUL) radial force distribution changes around the 90 degree integral arc, over a single operation cycle, for the flux switching motor and the 2-phase switched reluctance motor. An asterisk has been used to identify the position of the centre of a stator slots.

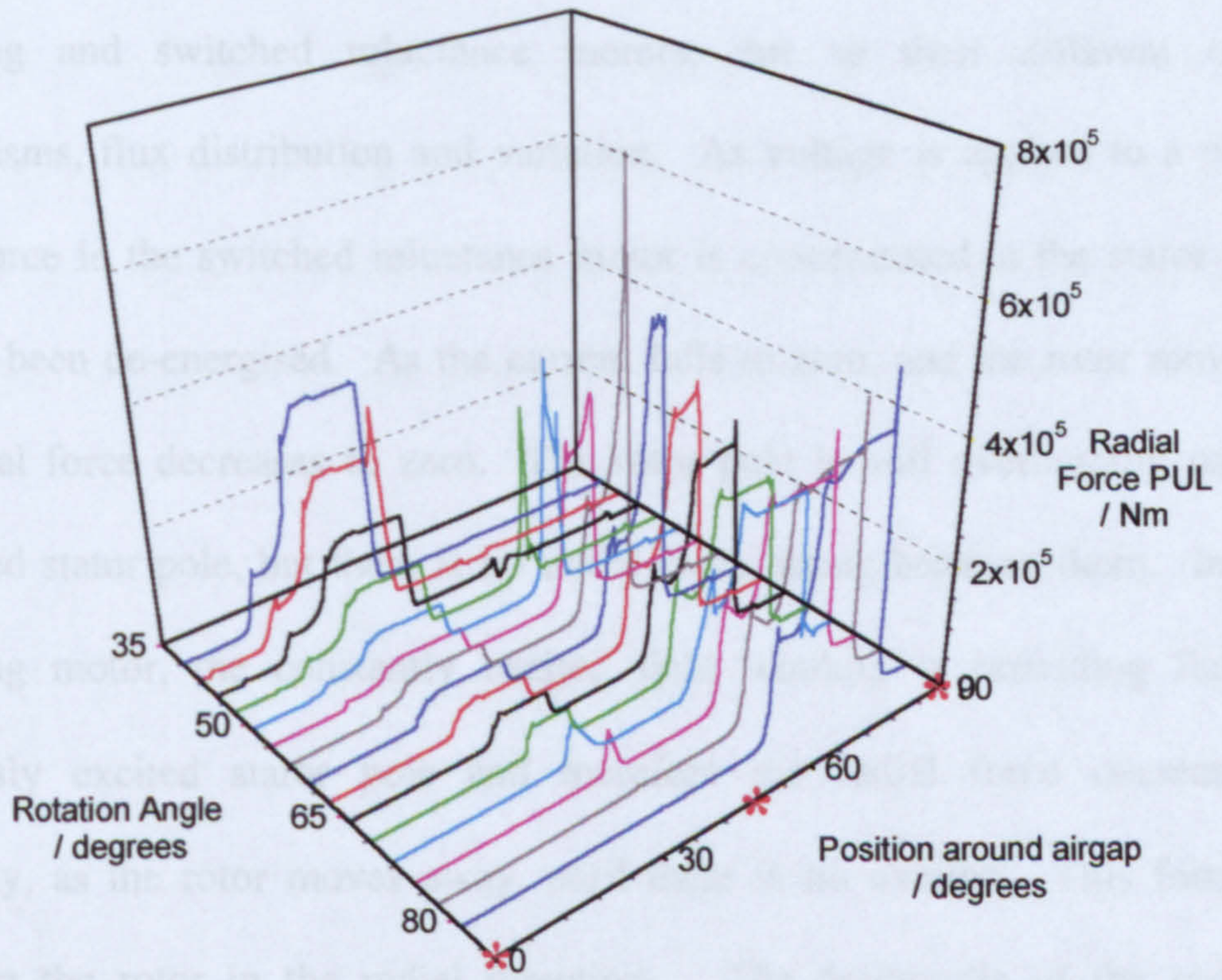

Figure 7.8: Simulated airgap radial force distribution with rotor position in the flux switching motor

Figure 7.9: Simulated airgap radial force distribution with rotor position in the 2-phase switched reluctance motor

There is a significant difference between the distribution of radial force in the flux switching and switched reluctance motors, due to their different excitation mechanisms, flux distribution and variation. As voltage is applied to a phase, the radial force in the switched reluctance motor is concentrated at the stator pole that has just been de-energised. As the current falls to zero, and the rotor moves away, the radial force decreases to zero. The rotor pole is still overlapping part of the unexcited stator pole, but there is no radial force acting between them. In the flux switching motor, the constantly excited field winding is providing flux in the previously excited stator pole and therefore the radial force decreases more gradually, as the rotor moves away, until there is no overlap. This force acts to constrain the rotor in the radial direction. The magnitude of the radial force concentrated at the energised stator pole at the commutation point, where the voltage to the phase is removed is significantly less for the flux switching motor. These results provide some evidence as to why there is a noticeable acoustic difference between the motors.

7.5.3 Total Radial Force

As well as considering the distribution of radial force around the airgap, the total radial force must be analysed. Rather than solve the equations in section 7.3 to obtain the individual motor response to a force input, a comparison will be drawn from the total radial force present in the flux switching and 2-phase switched reluctance motor. The second differential of radial force will be considered as this was shown, in section 7.2, to be an indication of acceleration produced by a change in radial force.

The total radial force has been calculated in the airgap, over a 90° arc. This encompasses the radial force between two stator poles (over a complete 90° commutation) and one rotor pole. The magnitude of the radial force is per unit stack length (PUL). Figure 7.10 shows the total simulated radial force, as described above, for the flux switching and 2-phase switched reluctance motors.

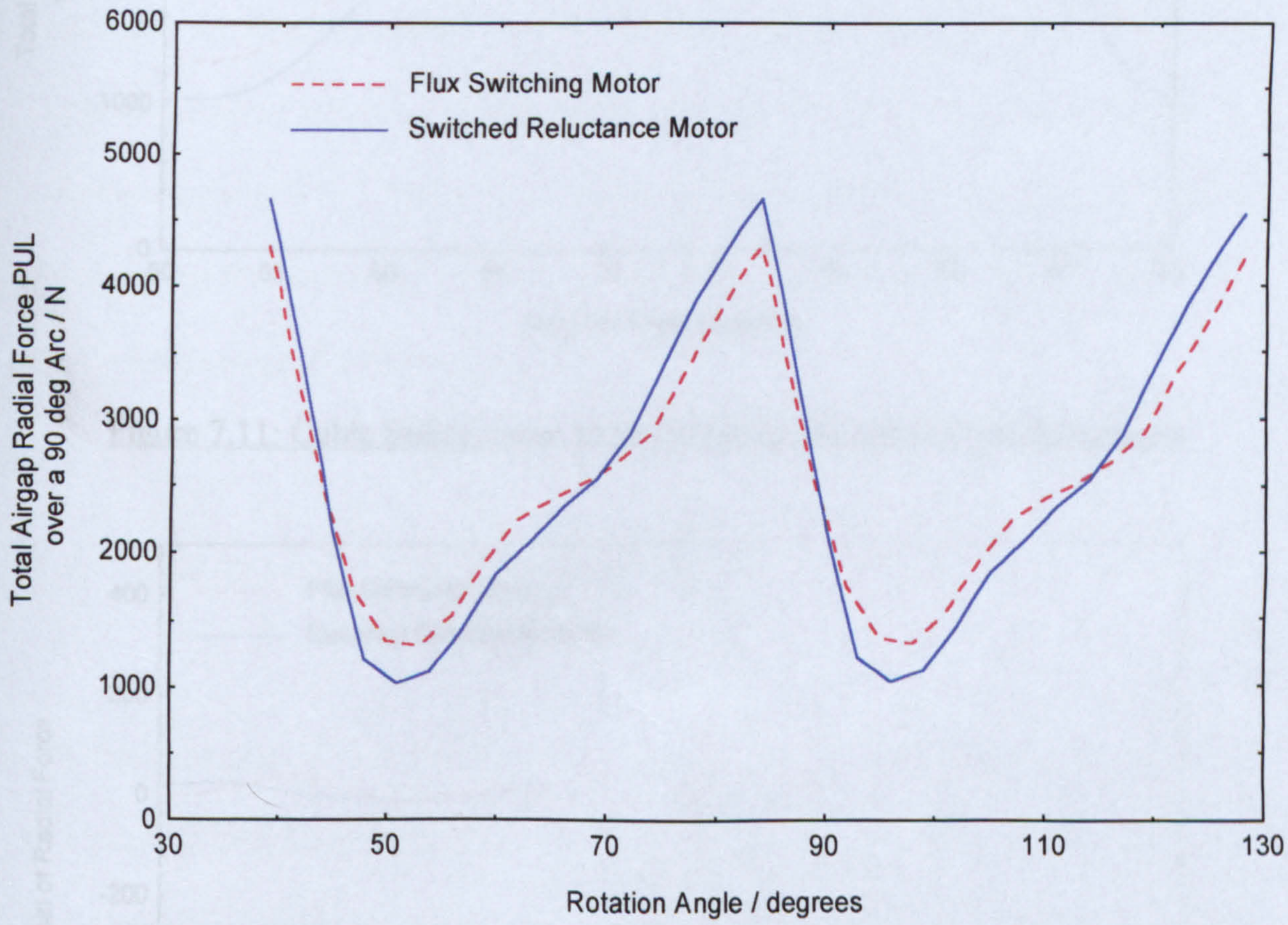

Figure 7.10: Total simulated radial force for the flux switching and 2-phase switched reluctance motor

The magnitude of the peak to peak radial force is less in the flux switching motor than in the switched reluctance motor. The largest change in the radial force occurs at the commutation point. A cubic spline curve fit was calculated for the radial force data over 3 periods. One period is shown in figure 7.11.

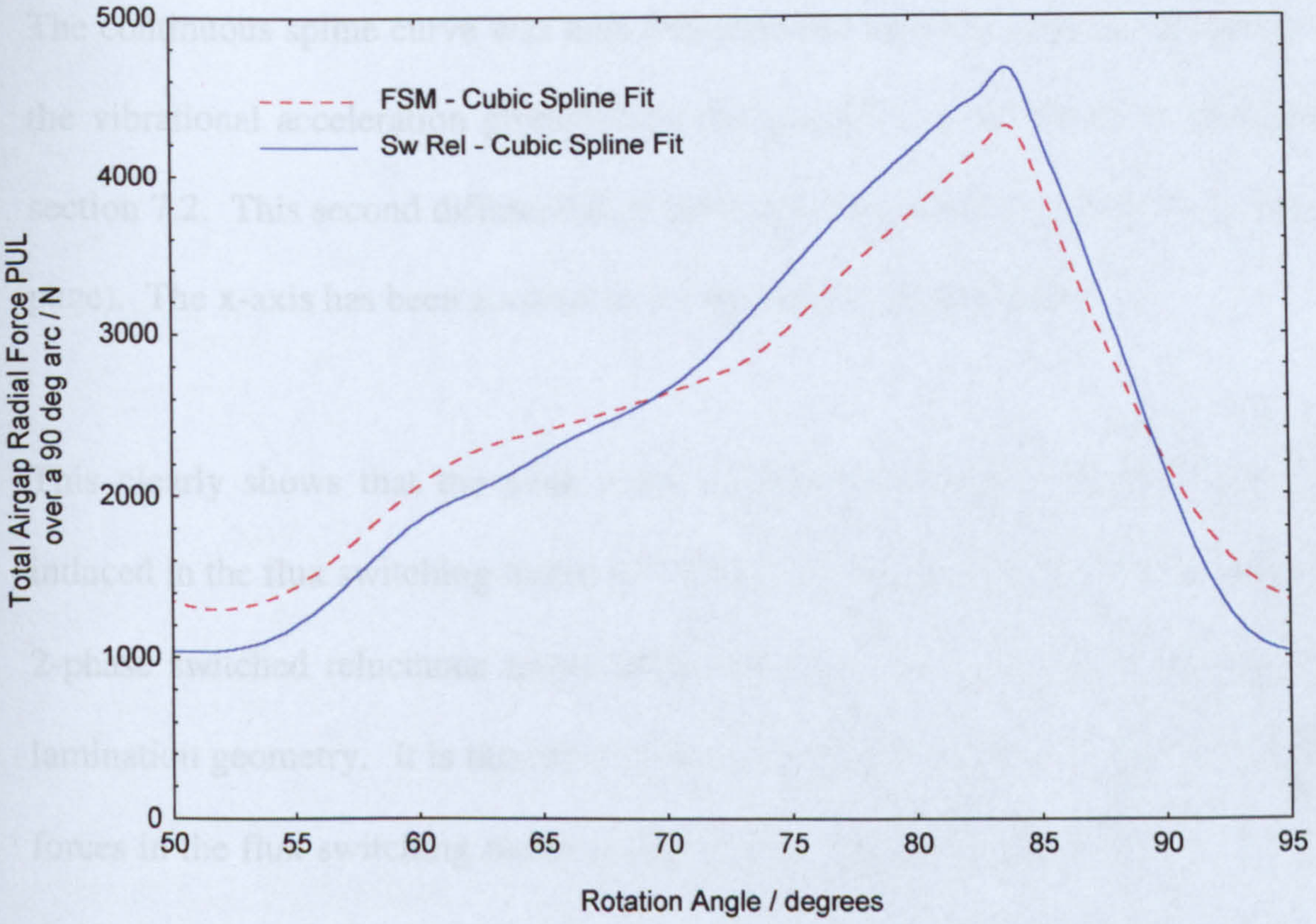

Figure 7.11: Cubic Spline curve fit to the simulated radial force data points

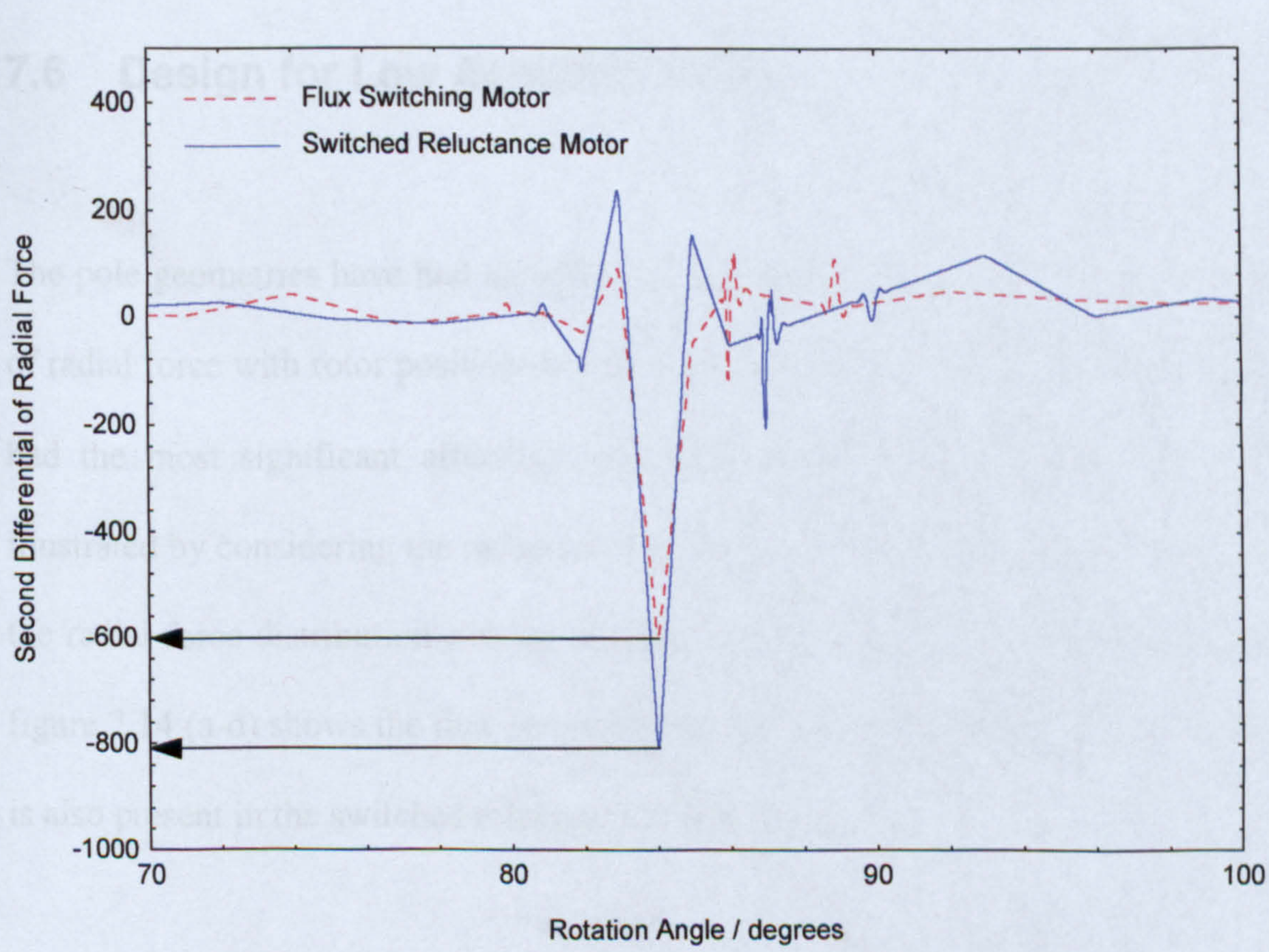

Figure 7.12: Second differential of cubic spline fit curve of radial force for the flux switching and switched reluctance motors

The continuous spline curve was then differentiated twice to give an indication as to the vibrational acceleration produced by the changing radial force, as described in section 7.2. This second differential of radial force is shown in figure 7.12 (previous page). The x-axis has been zoomed in on the point of commutation.

This clearly shows that the peak value of the second differential of radial force induced in the flux switching motor is 25% less in magnitude than that induced in the 2-phase switched reluctance motor under the same load and speed conditions and lamination geometry. It is therefore concluded that under these conditions the radial forces in the flux switching motor produces less vibration and acoustic noise than in the 2-phase switched reluctance motor.

7.6 Design for Low Acoustic Noise

The pole geometries have had an effect on the distribution of radial force. Analysis of radial force with rotor position reveals that the geometry of the stator pole tips has had the most significant affect on the distribution of the radial force. This is illustrated by considering the radial force at 4 key rotor positions. Figure 7.13 shows the radial force distribution over an energised pole in the flux switching motor, and figure 7.14 (a-d) shows the flux density in the motor and position of rotor. The trend is also present in the switched reluctance motor data.

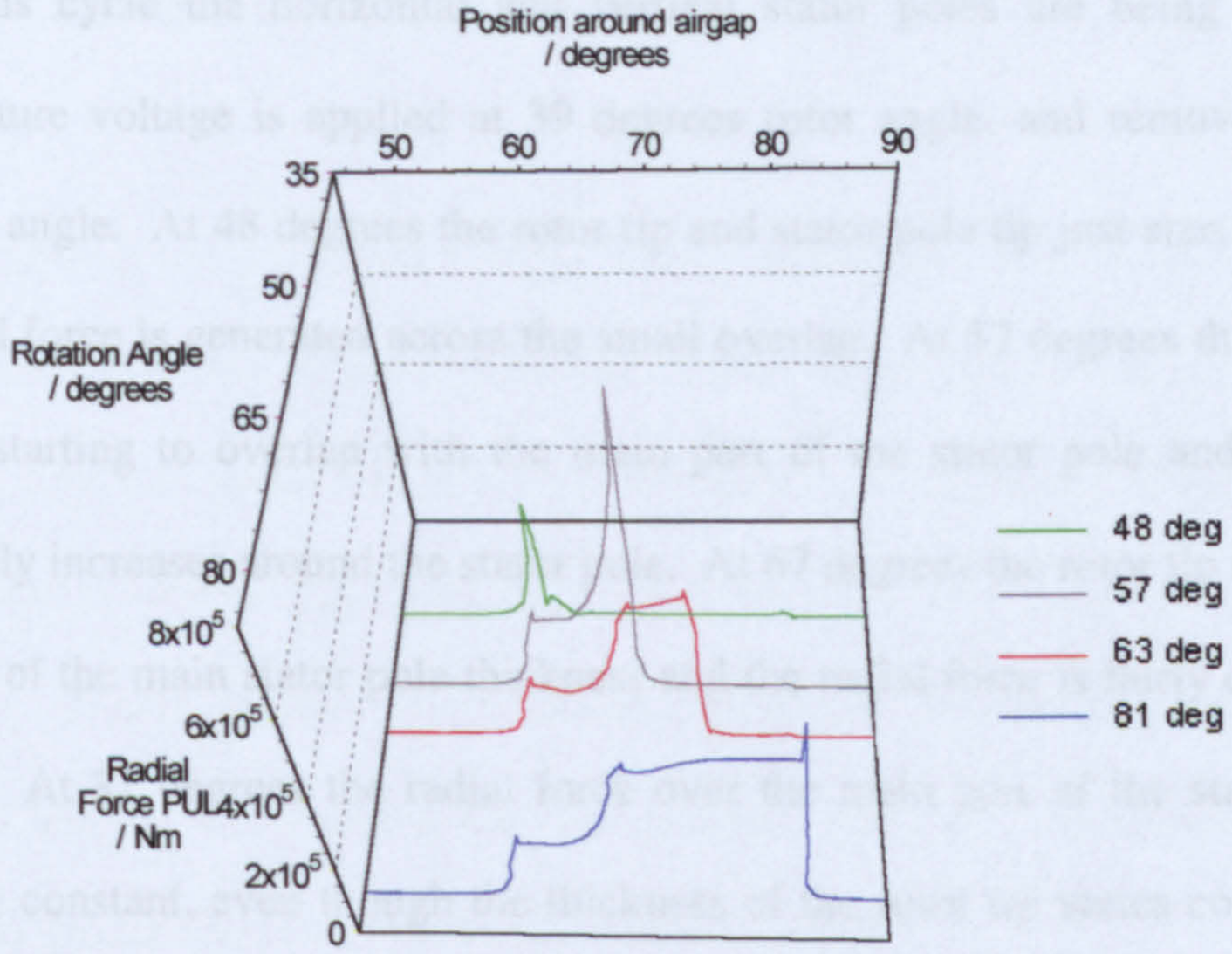

Figure 7.13: Radial force distribution over a stator pole in the flux switching motor

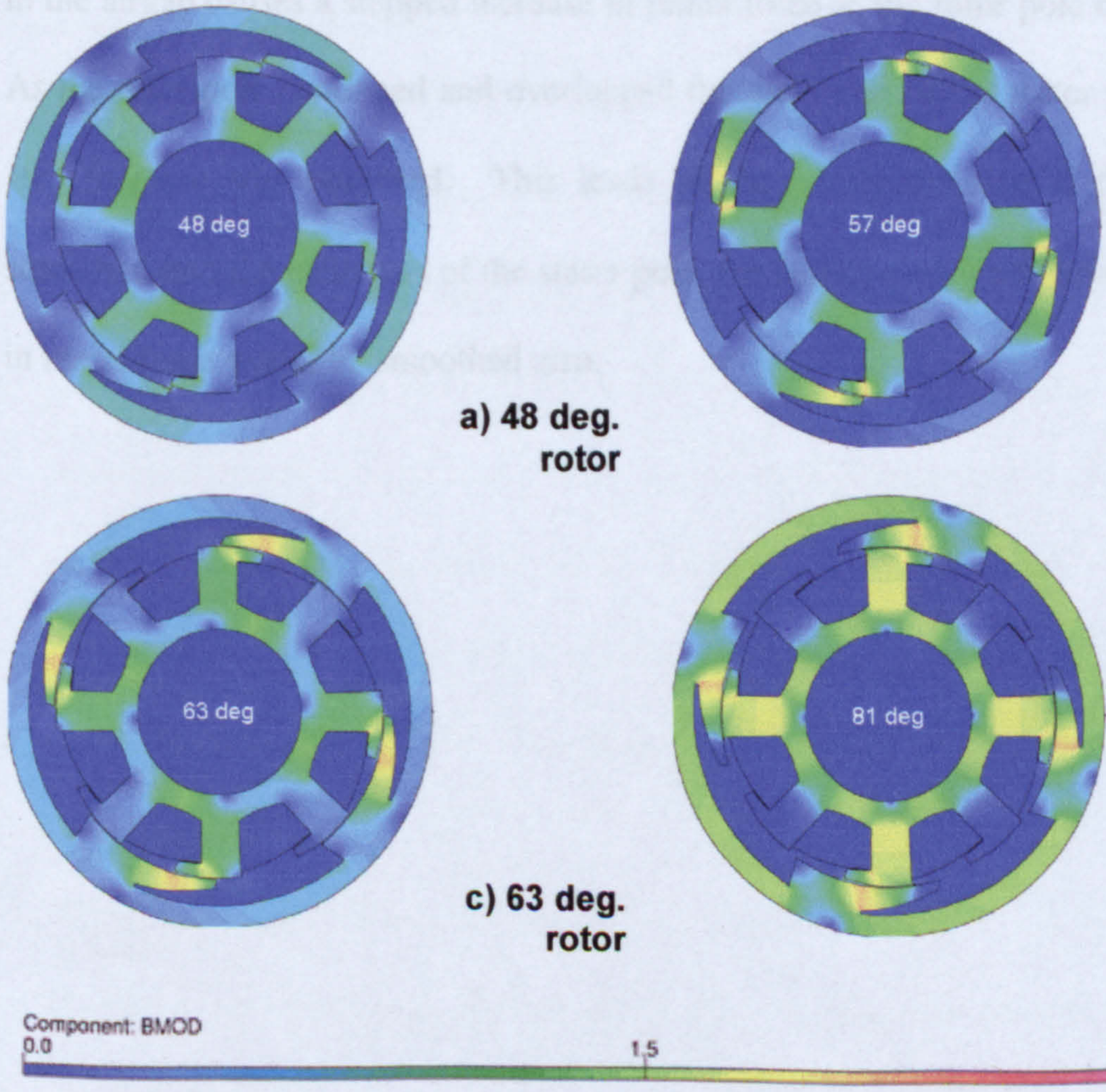

a) 48 deg. rotor

b) 57 deg. rotor

c) 63 deg. rotor

d) 81 deg. rotor

Figure 7.14: (a-d) Flux density in Tesla at various rotor positions

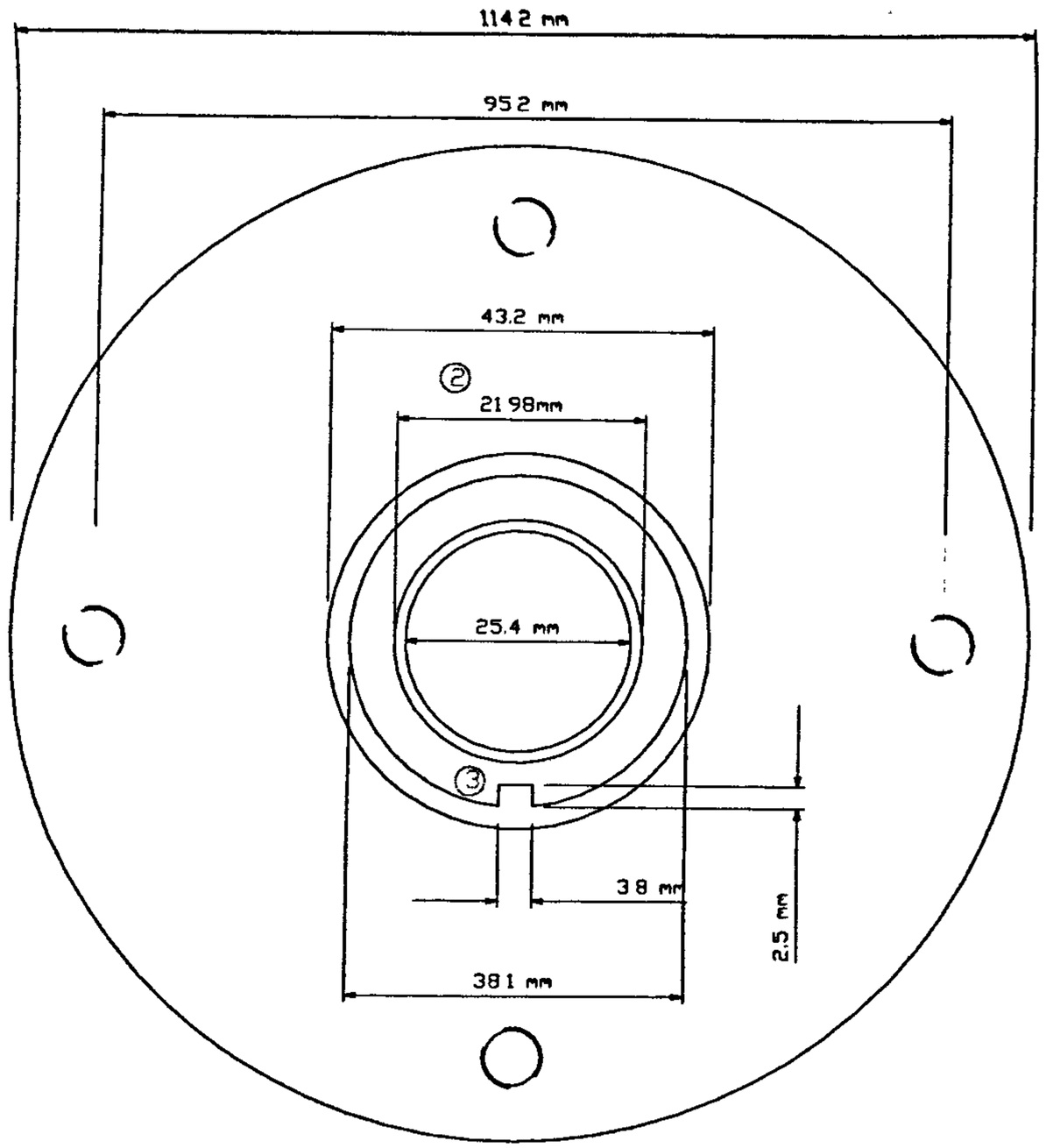

4 M5 Threaded holes on 75.0mm PCD

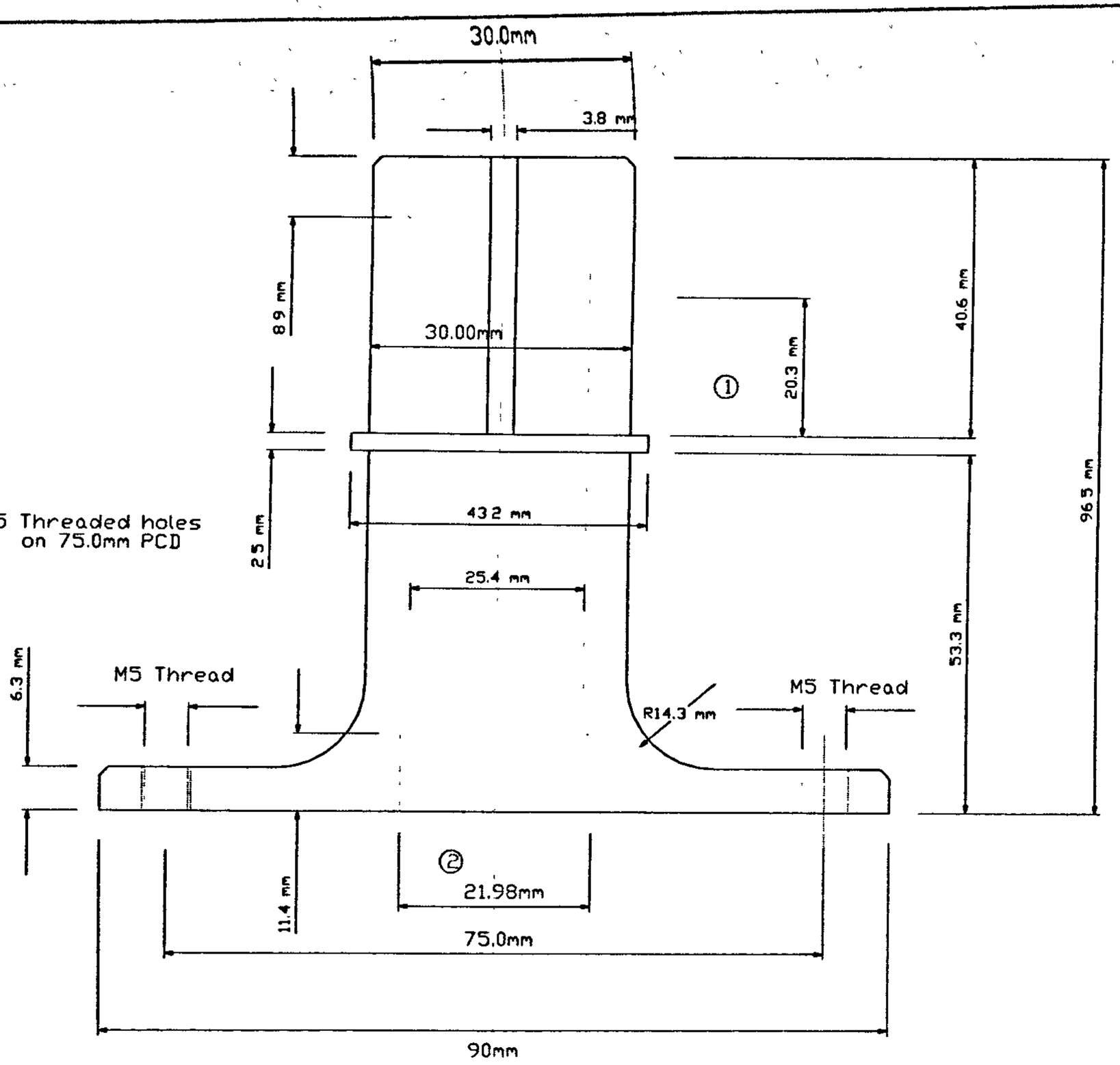

SPECIFICATIONS Material - Aluminium (one piece)	CONTRACT NO.	DATE	COMPANY Power Electronics & Drives Research Group A205 ext 22333		
① Maintain 30.00mm diameter over 16mm length for interference fit with laminations	DRAWN BY M. Brackley	22/2/99			
② Turn recess to 21.98mm diameter for interference fit for bearing	CHECKED BY		TITLE Stator Support for VASR MkI		
③ Keyway milled to allow laminations to locate on shaft without twisting.	DESIGNED BY M. Brackley		SIZE A4	FSCM NO.	DWG NO. / FILE NAME 1 / stator.skd
	DESIGN ACTIVITY				
	CUSTOMER		SCALE	DATE 23/6/99	SHEET 1 of 3

In this cycle the horizontal and vertical stator poles are being energised. The armature voltage is applied at 39 degrees rotor angle, and removed at 84 degrees rotor angle. At 48 degrees the rotor tip and stator pole tip just start to overlap, and a radial force is generated across the small overlap. At 57 degrees the rotor tip is now just starting to overlap with the main part of the stator pole and the radial force rapidly increases around the stator pole. At 67 degrees the rotor tip is well passed the edge of the main stator pole thickness and the radial force is fairly constant over that part. At 81 degrees the radial force over the main part of the stator pole remains fairly constant, even though the thickness of the rotor tip varies considerably across the overlapping segments. This suggests that the rotor pole undercut has had no real affect on the radial force distribution in the motor. The 'jut' added to the stator poles in the airgap causes a stepped increase in radial force as the rotor pole overlapped it. As the rotor pole continued and overlapped the main part of the stator pole, another step increase was observed. This leads to the conclusion that if the 'jut' was smoothed into the main part of the stator pole, the increase (and potentially decrease) in radial force would be smoothed also.

7.7 Simulation Conclusions

This chapter has presented a finite element simulation of a flux switching motor and a 2-phase switched reluctance motor, with the same laminations, operating under the equal load and speed. Real current waveforms were measured for each motor, and sampled at various rotor positions. This information was used to generate a sequence of static electromagnetic finite element models. The chapter goes on to show how radial force is calculated in the finite element program, and presents the results of a torque production analysis to validate the data used.

The simulated distribution of radial force in the airgap was analysed, and the following conclusions reached:

1. In the switched reluctance motor the radial force across the previously commutated stator pole reduces to zero when the current falls to zero. In the flux switching motor, the radial force across the previously commutated stator pole continues to act until the rotor pole is no longer overlapping it. A constraining effect, caused by this radial force, acting on the rotor in the inward radial direction is present in the flux switching motor after commutation, but not in the switched reluctance motor. This does not however, reduce the torque output of the motor.
2. This constraining effect, caused by the presence of radial force, is transferred between stator poles as the motor rotates. A smoother transfer induces less vibration.

3. The unusual profiling of the stator and rotor geometries revealed that the shape of the stator pole had a significant effect on the distribution of the radial force. The 'jut' added to the stator poles in the airgap caused a stepped increase in radial force as the rotor pole overlapped. As the rotor pole overlapped the main part of the stator pole, another step increase was observed. This led to the hypothesis that if the 'jut' was graded more smoothly into the main part of the stator pole and added to both edges of the stator poles, the radial force would potentially increase and decrease in a smoother fashion.
4. The width of the undercut of the rotor poles did not have a significant effect on the distribution of radial force as the rotor moved past the main section of the stator pole.

The total radial force in the airgap (acting on a rotor pole) was analysed and the following conclusions reached.

1. The flux switching motor had a lower peak to peak value of radial force than the switched reluctance motor. The total change in radial force in therefore less in the flux switching motor.
2. When the second differential of radial force was analysed, to give an indication of the vibrational acceleration, the flux switching motor exhibited a peak value which was 25% less than the 2-phase switched reluctance motor with the same lamination.

Overall, the radial force characteristics of the flux switching motor indicated that it induces less vibration and therefore radiates less acoustic noise than the switched reluctance motor under the same operating conditions and lamination design. This was due to the fundamental difference in flux variation and distribution in the two motors, caused by their different operating topologies.

CHAPTER 8

CONCLUSIONS AND FURTHER WORK

8.1 Conclusions

With increasing demand for low cost high efficiency variable speed drives, and the decrease in cost of semiconductor devices, electronically controlled motors hold huge potential for domestic, industrial and commercial products in the future. Chapter 2 describes the flux distribution and variation in various types of common machines, and shows that electronically commutated motors produce more vibration and acoustic noise than those operated by other methods. For this reason, the vibration and acoustic noise produced by these types of machine must be analysed, understood and minimised to allow the advantages of the technology to be exploited.

The third chapter of this thesis provided a detailed analysis of the mechanism of acoustic noise production in the switched reluctance motor. When a switched reluctance motor is commutated, a force impulse is produced by the reversal of the phase voltage, which induces vibration at the resonant frequency of the motor stator. This vibration is usually the dominant cause of acoustic noise. Prior art has been described which reduces the vibration and acoustic noise at the motor stator resonant frequency. This is known as active cancellation. The chapter went on to show how the force impulses, generated by motor commutation, can excite resonant frequencies of other components coupled to the motor. An example of a fan housing resonance is given, where the acoustic noise it produces is far greater than that from the motor stator. The author extends the application of the cancellation technique by altering

motor commutation, to cancel the resonant vibration of the fan housing, achieving a significant reduction in the vibration and acoustic noise it produces at its natural resonant frequency. This work has extended the powerful acoustic noise reduction technique, from the stator of a switched reluctance motor, to any coupled component that has resonance excited by the commutation of the motor.

Chapter 4 showed that the brushless d.c. motor, commutated with square wave current, is susceptible to similar acoustic noise production as the switched reluctance motor. A case example was given of a 3-phase brushless d.c. motor and fan unit which emits increased levels of acoustic noise at one particular speed in its operating range. Further analysis revealed that the frequency of motor current commutation, at this speed, matched the natural mechanical resonant frequency of the motor endcap. A technique was described whereby the pattern of current commutation was altered electronically, in the time domain, to avoid the excitation of the endcap resonance. The results of the study show a dramatic decrease in the vibration of the endcap at its resonant frequency, and the associated acoustic noise was eliminated. A low cost implementation was also described using discrete components.

A new class of electric motor, known as flux switching, was introduced in chapter 5 and its main features and converter topology described. A detailed design of a low noise flux switching motor for a fan application was presented.

Chapter 6 described the comparison of the acoustic noise generated by an external rotor flux switching motor with that from an external rotor 2-phase switched reluctance motor, constructed from the same mechanical parts and laminations. Also

a comparison of an internal rotor flux switching motor and an induction motor, of similar mechanical build, was presented.

The conclusions drawn from this experimental work were that the acoustic noise measured from the external rotor flux switching motor was at least 2dB less than that from the external rotor 2-phase switched reluctance motor (with the same laminations) under the same conditions. An analysis of the power loss distribution in the two motors revealed that the flux switching motor had a lower iron loss, but a higher copper loss, than the 2-phase switched reluctance motor.

When turning a fan load at 1800rpm, the acoustic noise from the internal rotor flux switching motor was only 1dB greater than that from the induction motor, which was of similar size. At this speed the flux switching motor, with a less than optimal design, had an efficiency of 35% compared to 27.5% measured from the induction motor.

The dominant frequencies in the acoustic noise power spectrum of all the machines were analysed and it was discovered that those from the flux switching motors generally varied with speed, whereas those from the switched reluctance motor did not. In relation to this, the external rotor flux switching motor did not excite the natural resonant frequency of its rotor or stator parts to the same extent as the switched reluctance motor, although it could not be conclusively said that the natural resonances were not excited at all. There is still a fundamental difference in the acoustic noise production mechanism between the two motors. The only significant frequency in the acoustic noise power spectrum of the internal rotor flux switching

motor, with the fan load, varied with speed and was a multiple of the commutation frequency.

Chapter 7 presented a finite element simulation of the distribution and variation of radial forces present in the external rotor flux switching and 2-phase switched reluctance motors. The real motor winding currents were measured at 1800rpm, and using this excitation data, a static time stepping simulation was initiated in FE. A Maxwell stress force integral was performed around a portion of the airgap. The simulation revealed that the peak to peak radial force present in the flux switching motor was approximately 20% less than that in the 2-phase switched reluctance motor. At the point of commutation, common to both motors, the peak value of the second differential of radial force in the flux switching motor is 20% less than that in the 2-phase switched reluctance motor with the same laminations.

Analysis of the distribution of radial force showed that in the flux switching motor, the previously commutated stator pole continues to provide an attractive radial force to the departing rotor pole until there is no overlap. This is due to the fundamental operation of the motor, where the constantly excited field winding provides flux in the motor at all times. The same radial force in the 2-phase switched reluctance motor reduces to zero as the previously commutated phase current reduces to zero, with the rotor pole overlapping. The force constraining the rotor is therefore spread over the pole face and is transferred more smoothly as the rotor position changes.

The final chapters of this thesis have shown that there is a significant difference between the acoustic noise produced by the switched reluctance motor and the flux switching motor with the same laminations. A time stepping simulation of radial

force in the two motors has revealed differences in the magnitude of radial force at the point of commutation, the variation of the radial force with rotor position and the distribution of radial force with rotor position. This is due to the fundamental differences in flux control in the two motors, which have the same laminations and are commutated at the same rotor positions.

8.2 Areas for Further Work

In this comparison of the flux switching motor and the 2-phase switched reluctance motor, the lamination geometries were kept the same to highlight the differences between the differing methods of flux control. A future analysis might consider separately designing a performance optimised flux switching motor and switched reluctance motor for a single test application, and measuring the resultant vibration and acoustic noise. In most cases, a motor is designed for electrical performance and the acoustic noise produced is subsequent.

The scope of the analysis could be extended by comparing the acoustic noise from a flux switching motor with a similar brushless d.c. (bldc) motor. The bldc motor has been shown to be susceptible to acoustic noise problems, and it is a potential rival to the flux switching motors in many areas.

This work has shown that although the flux switching motor has the potential to be an improvement over switched reluctance motor in terms of acoustic noise production, it is still not silent. Work could be undertaken to reduce the remaining acoustic noise from the flux switching motor by using electronic cancellation techniques, similar to those used on switched reluctance motors. Also further work

could be carried out on the design of the rotor and stator pole geometries in light of the conclusions reached in chapter 7.

To provide more evidence for the findings of this thesis, a similar analysis could be carried out with machines of greater power, to confirm that the trends carry forward to larger motors.

As the flux switching motor is a new technology, a lot of work needs to be done to improve the design model, and control techniques.

REFERENCES

[1] J.D. Turner and A.J. Pretlove, "Acoustics for Engineers", *MacMillan*, 1991

[2] S.J. Yang and A.J. Ellison, "Machinery Noise Measurement", *Clarendon Press, Oxford*, 1985

[3] S.P. Verma and A. Balan, "Experimental Investigations on the Stators of Electrical Machines in Relation to Vibration and Noise Problems", *IEE EMD Conference Publication"* No. 444, pp 74-85, 1997

[4] S.P. Verma, "Noise and Vibrations of Electrical Machines and Drives; Their Production and Means of Reduction", *Record of the International Conference on Power Electronics, Drives and Energy Systems"*, pp 1031-1037, 1996

[5] S.C. Chang, "Electrical Noise in Small Electrical Motors", *IEE EMD Conference Publication"* No. 444, pp 391-395, 1997

[6] P.L. Timar, "Noise and Vibration of Electrical Machines", *Elsevier,* 1989

[7] C. Picod, M. Besbes, F. Camus and M. Gabsi, "Influence of Stator Geometry upon Vibratory Behaviour and Electromagnetic Performances of Switched Reluctance Motors", *Proceedings of the IEE 8th International Conference on Electrical Machines and Drives,* No.444, pp 69-73, 1997

[8] S.P.Verma, R.S.Girgis, "Resonant Frequencies and Vibration Behaviour of Stators of Electrical Machines as Affected by Teeth, Windings, Frame and Laminations", *Proceedings of the IEEE Power Engineering Society summer meeting*, 1978.

[9] S.J. Yang "Low Noise Electric Motors", *Clarendon Press, Oxford*, 1985

[10] A.K. Wallace, R. Spee and L.G. Martin, "Current Harmonics and Acoustic Noise in AC Adjustable-speed Drives", *IEEE Transactions on Industry Applications,* Vol 26, no.2, pp 267-273, 1990

[11] V. Ostovic and G. Boman, "Radial Air Gap Force as a Source of Audible Noise in a Sinusoidally Fed Induction Machine", *Proceedings of the IEEE 30th Industrial Applications Society Annual Meeting"* Vol 1, pp 591-598, 1995

[12] S. Onodera and K. Yamasawa, "Electromagnetic Vibration Analysis of a Squirrel-cage Induction motor", *IEEE Transactions on Magnetics,* Vol. 29, No.6, pp 2410-2412, 1993

[13] S. Garcia-Otero, M.Devaney, "Minimization of Acoustic Noise In Variable Speed Motors Using Modified PWM Drives", *Proceedings of the IEEE Applied Power Electronics Conference*, pp126-131, 1992.

[14] N. Toshihiro, N, Mutsuo and M. Toru, "Reduction of Vibration and Acoustic Noise in an Induction Motor Driven By Three-phase PWM AC Chopper Using Static Induction Transistors", *IEEE Transactions on Power Electronics,* Vol. 4, No.3, pp 313-318, 1989

[15] P.C. Sen, "Principles of Electric Machines and Power Electronics", *Wiley,* 1989

[16] S. Hwang and D.K. Lieu, "Electromagnetically Generated Acoustic Noise in DC Machines", *Design Engineering Technical Conference,* Vol. 3, Pt C, pp 561-570, 1995

[17] M. Yoshida, Y. Murai and M. Takada, "Noise Reduction by Torque Ripple Suppression in Brushless DC Motor" *Proceedings of the IEEE 29th Annual Power Electronics Specialist Conference"*, Vol 2, pp 1397-1401, 1998

[18] D.C. Hanselman, "Effect of Skew, Pole Count and Slot Count on Brushless Motor Radial Force, Cogging Torque and Back EMF", *Proceedings of the IEE Electrical Power Applications"*, Vol. 144, No.5, 1997

[19] M. Brackley and C. Pollock, "Analysis and Reduction of Acoustic Noise from a Brushless D.C. Drive", *IEEE Transactions on Industry Applications,* Vol 36, No.3, pp 772-777, 2000

[20] D.E. Cameron, J.H. Lang and S.D. Umans, "The Origin and Reduction of Acoustic Noise in Doubly Salient Variable-Reluctance Motors *Proceedings of the IEEE Industrial Application Society Annual Meeting"*, Vol. 1, pp 108-115, 1989.

[21] D.W. Pulle, J.C. Lai, J.F. Milthorpe and N. Huynh, "Quantification and Analysis of Acoustic Noise in Switched Reluctance Drives", *European Power Electronics Conference,* pp 65-70, 1993

[22] M.L. Stanley (GEC), "Skewing of pole laminations of a switched reluctance machine to reduce acoustic noise", *US Patent no. 5,266,859*, Nov 1993

[23] C.Y. Wu and C. Pollock, "Analysis and Reduction of Acoustic Noise in the Switched Reluctance Drive" *IEEE Transactions on Industry Applications,* Vol 31, No.1, pp 91-98, 1995

[24] C. Pollock and C.Y. Wu, "Acoustic Noise Cancellation Techniques for Switched Reluctance Drives" *IEEE Transactions on Industry Applications,* Vol 33, No.2, pp 477-484, 1997

[25] A. Michaelides and C. Pollock, "Reduction of Noise and Vibration in Switched Reluctance Motors: New Aspects", *Conference Record of the IEEE Industrial Applications Society 31st Annual Meeting,* Vol 2, pp 771-775, 1996

[26] M.N. Anwar and I. Husain, "Radial Force Calculation and Acoustic Noise Prediction in Switched Reluctance Machines", *Proceedings of the IEEE Industrial Applications Society 34th Annual Meeting"*, Vol 4, pp 2242-2249, 1999

[27] C. Pollock and A.Michaelides "Switched Reluctance Drives: A Comparative Evaluation" IEE Power Engineering Journal, pp 257-266, December 1995

[28] R. Arumugam, J.F. Lindsay and R. Krishnan, "Sensitivity of Pole Arc/Pole Pitch Ratio on Switched Reluctance Motor Performance", *Proceedings of the IEEE Industrial Application Society 23rd Annual Meeting"*, Vol. 35, No. 6, pp 50-54, 1988

[29] T.J.E. Miller, "Switched Reluctance Motors and Their Control", *Clarendon Press*, Oxford, 1993

[30] M. Moallem, C.M. Ong and L.E. Unnewehr, "Effect of Rotor Profiles on the Torque of a Switched Reluctance Motor", *Proceedings of the IEEE Industrial Application Society 25rd Annual Meeting"*, Part 1, pp 247-253, 1990

[31] A. Pelikant and S. Wiak, "Influence of the Rotor Pole Shape on the Static and Dynamic Characteristics of the Switched Reluctance Motor", *IEEE Transactions on Magnetics,* Vol. 31, No. 3, pp 1529-1532, 1996

[32] D.S. Reay and B.W. Williams, "Sensorless Position Detection using Neural Networks for the Control of Switched Reluctance Motors", *Proceedings of the IEEE Conference on Control Applications*, Vol 2, pp 1073-1077, 1999

[33] C. Pollock, "Power Converter Circuits for Switched Reluctance Motors", *PhD Thesis*, Heriot-Watt University, 1989.

[34] S. Vukosavic and V.R. Stefanovic, "SRM Inverter Topologies: A Comparative Evaluation", *IEEE Transactions on Industry Applications,* Vol.27, No.6, pp 1034-1047, 1991

[35] D.E. Cameron, J.H. Lang and S.D. Umans, "The Origin and Reduction of Acoustic Noise in Doubly Salient Variable-reluctance Motors", *IEEE Transactions on Industry Applications,* Vol 28, No.6, pp 1250-1255, 1992

[36] R.S. Colby, F.M. Mottier and T.J.E. Miller, "Vibration Modes and Acoustic Noise in a Four-phase Switched Reluctance Motor, *IEEE Transactions on Industry Applications,* Vol 32, no.6, pp1357-1364, 1996

[37] R. Krishnan, P. Vijayraghavan, "State of the Art: Acoustic Noise in Switched Reluctance Motor Drives, *Proceedings of the IEEE Industrial Electronics 24th Annual Conference"*, Vol 2, pp 929-934, 1998

[38] P. Pillay and W. Cai, "An Investigation into Vibration in Switched Reluctance Motors", *IEEE Transactions on Industry Applications,* Vol. 35, No. 3, pp 589-596, 1999

[39] M. Brackley and C. Pollock, "Electronic Cancellation of Acoustic Noise in a Fan System Driven by a Switched Reluctance Motor," *Proceedings of the EPE 8th European Conference on Power Electronics & Applications*, Lausanne, CD-ROM 1999.

[40] R.E. Kier, "Method and Apparatus for Noise-Quietening in Brushless DC motors" *UK Patent no.8527959,* Nov 1985.

[41] T.I. Minoo and M.G. Nishinomiya, "Brushless DC motor" *US Patent no. 5,144,209*. Sept 1992.

[42] K.F. Raby, "Inductor alternators for 10 KC/S", Technical Monograph, Engineering Department, The British Thomson-Houston Company Ltd., 27th April 1950.

[43] B.C. Mecrow, "New Winding Configurations For Doubly Salient Reluctance Machines", *IEEE Transactions on Industry Applications*, vol. 32, No.6, pp. 1348-1356, 1996

[44] Y. Li, J.D. Lloyd and G.E. Horst, "Switched Reluctance Motor with DC Assisted Excitation", *IEEE Transactions on Industrial Applications*, vol. 32, No. 2, pp 801-807, 1996

[45] F. Liang, Y. Liao and T.A. Lipo, "A New Variable Reluctance Motor Utilizing an Auxiliary Commutation Winding", *IEEE Transactions on Industrial Applications*, vol. 30, No. 2, pp 423-432, 1994

[46] R.P. Deodhar, S. Andersson, I. Boldea and T.J.E. Miller, "The Flux-Reversal Machine: A New Brushless Doubly-salient Permanent-Magnet Machine", *IEEE Transactions on Industrial Applications*, vol. 33, No. 4, pp 925-934, 1997

[47] C.Pollock and M. Wallace "The Flux Switching Motor, a DC Motor without Magnets or Brushes", *Proceedings of the IEEE Industrial Application Society 34th Annual Meeting"*, Vol. 3, pp 1980-1987, 1999.

[48] J. Sheppard, "Finite Element Analysis of Electrical Machines", Kluwer Academic Publishers, 1995

[49] D.E. Goldberg, "Genetic Algorithms in Search, Optimisation and Machine Learning", Addison –Wesley Longman, 1989

[50] BS EN ISO 3746:1996 "Acoustics- Determination of Sound Power Levels of Noise Sources Using Sound Pressure – Survey Method Using an Enveloping Measurement Surface over a Reflecting Plane.

[51] C. Y. Wu, "Analysis and Control of Switched Reluctance Drives to Reduce the Vibration and Acoustic Noise", *PhD Thesis*, University of Warwick, 1994

[52] C. Y. Wu, "Analysis and Control of Switched Reluctance Drives to Reduce the Vibration and Acoustic Noise", *PhD Thesis*, University of Warwick, 1994, pp 120-124.

[53] C. Y. Wu, "Analysis and Control of Switched Reluctance Drives to Reduce the Vibration and Acoustic Noise", *PhD Thesis*, University of Warwick, 1994, pp 139-140

APPENDIX

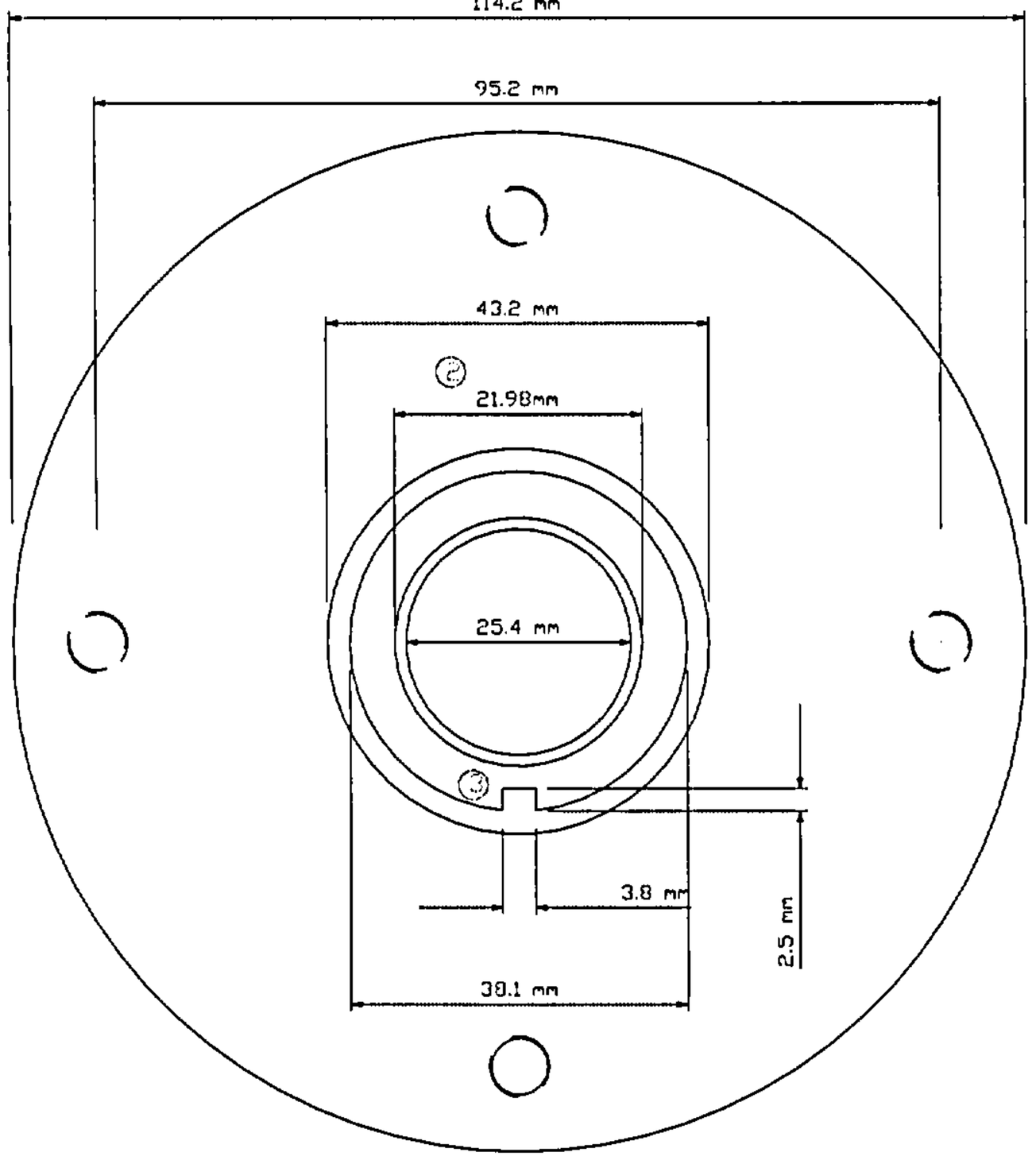

4 M5 Threaded holes on 75.0mm PCD

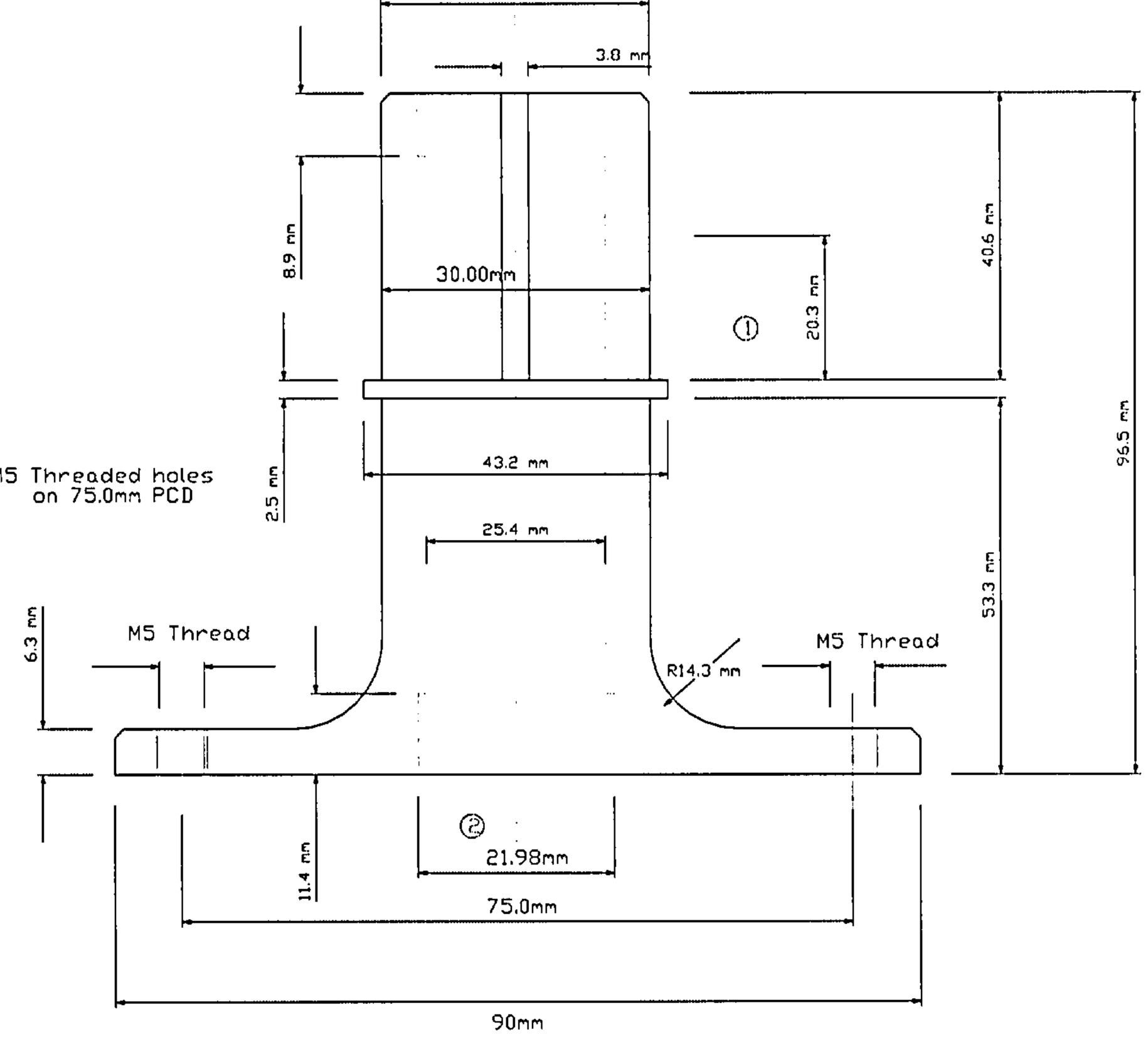

SPECIFICATIONS Material - Aluminium (one piece)	CONTRACT NO.	DATE	COMPANY Power Electronics & Drives Research Group A205 ext 22333
① Maintain 30.00mm diameter over 16mm length for interference fit with laminations	DRAWN BY M. Brackley	22/2/99	
② Turn recess to 21.98mm diameter for interference fit for bearing	CHECKED BY		TITLE Stator Support for VASR MkI
③ Keyway milled to allow laminations to locate on shaft without twisting.	DESIGNED BY M. Brackley		SIZE A4 / FSCM NO. / DWG NO. / FILE NAME 1 / stator.skd
	DESIGN ACTIVITY		
	CUSTOMER		SCALE / DATE 23/6/99 / SHEET 1 of 3

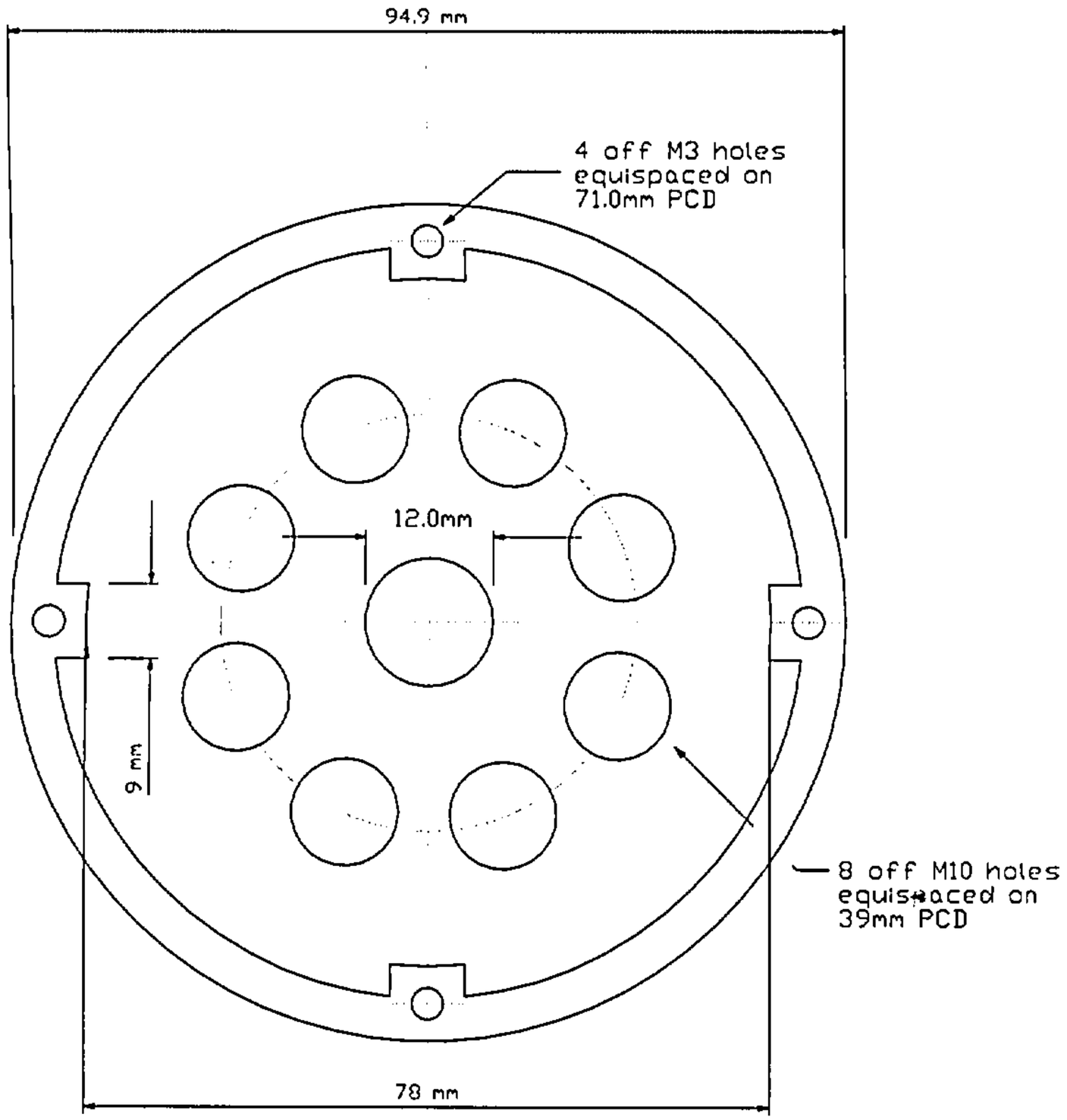

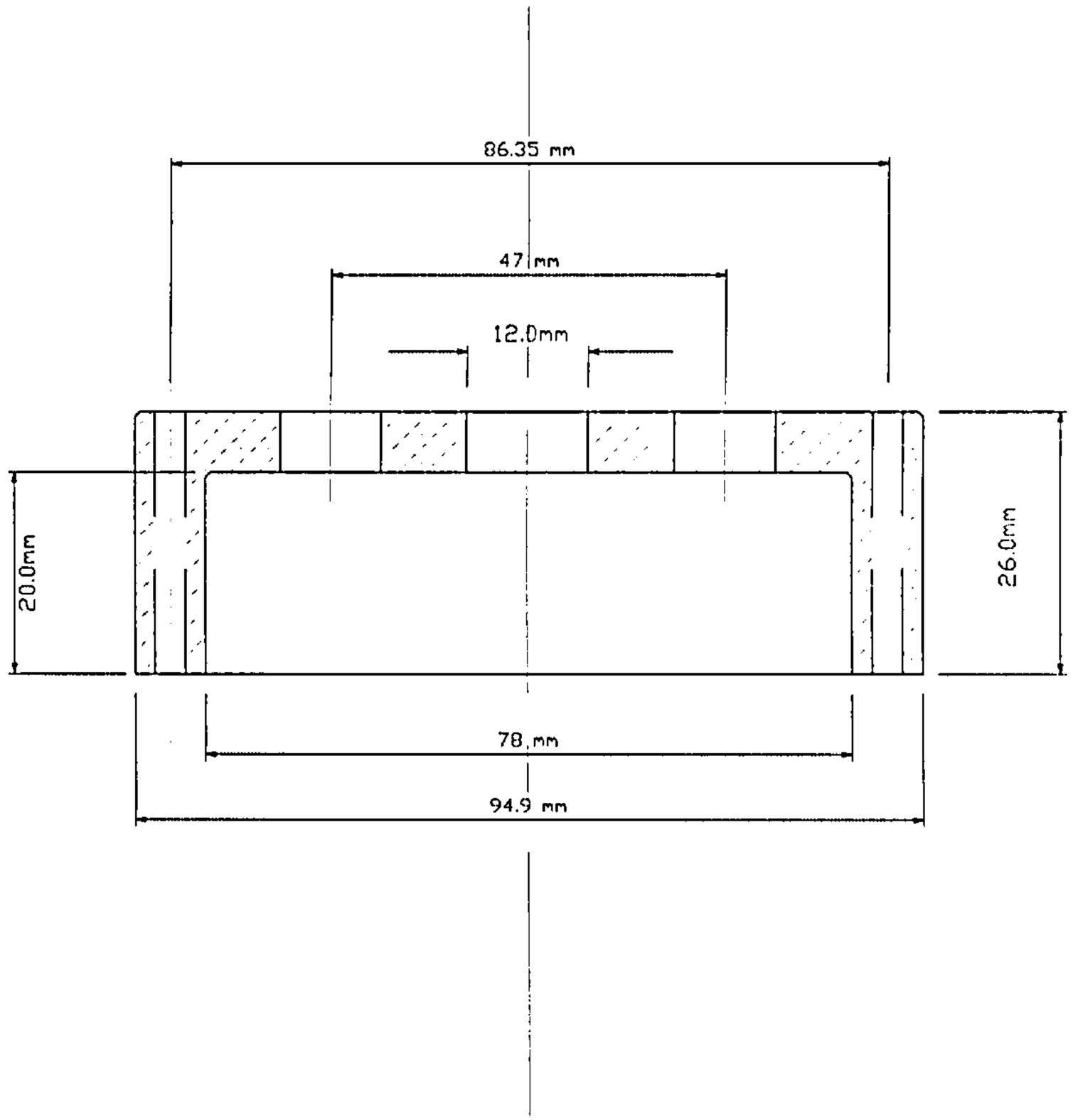

SPECIFICATIONS	CONTRACT NO.	DATE	COMPANY Power Electronics & Drives Research Professor C. Pollock
Material - Aluminium	DRAWN BY M. Brackley	15/3/99	
	CHECKED BY		TITLE VASR MkI Rotor Arrangment
	DESIGNED BY M. Brackley		
	DESIGN ACTIVITY		SIZE A4 / FSCM NO. / DWG NO. / FILE NAME 2 / rotor.skd
	CUSTOMER		SCALE / DATE 21/6/99 / SHEET 2 of 3

SHAFT

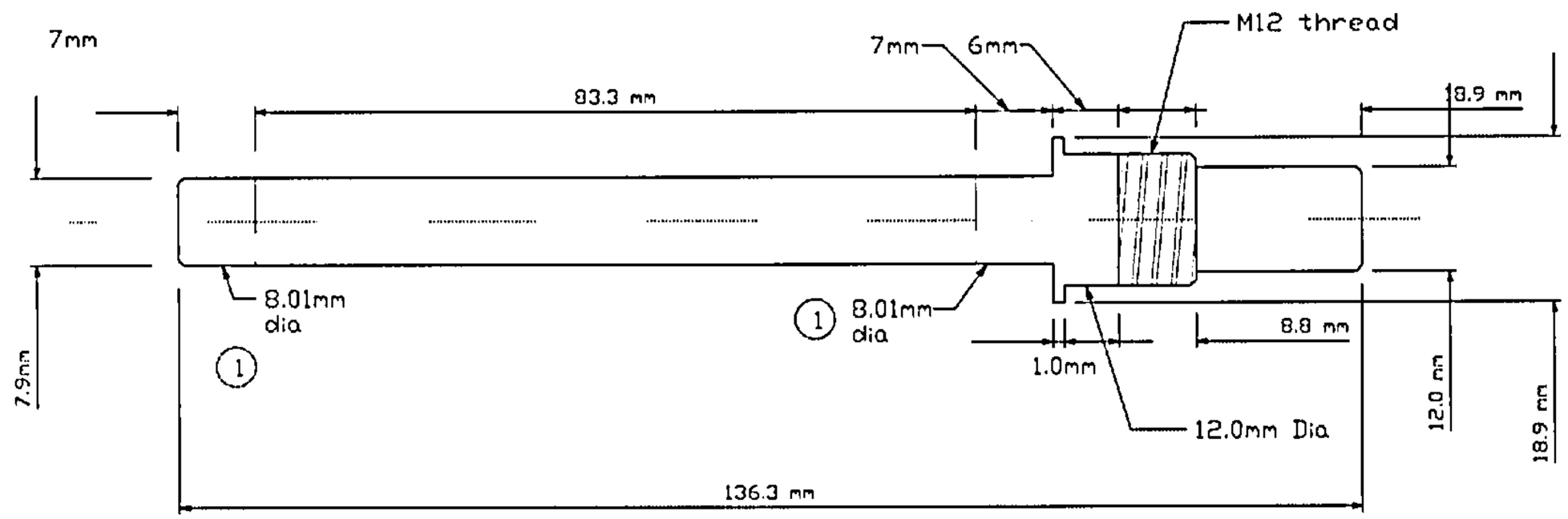

LOCATING PINS

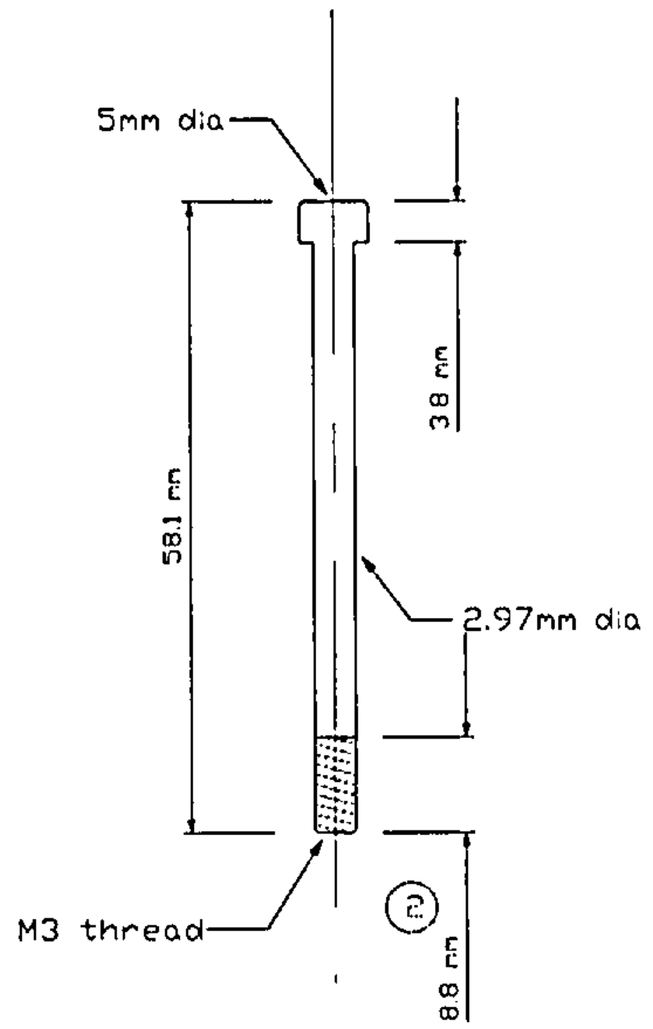

SPECIFICATIONS Material - Mild Steel

(1) 8.01mm diameter to provide interference fit with 8mm I/D bearing

(2) Please manufacture 4 of these pins

CONTRACT NO.	DATE	COMPANY	Power Electronics & Drives Research Prof. C. Pollock
DRAWN BY M. Brackley	16/3/99		
CHECKED BY		TITLE	VASR MkI Shaft and locating pins
DESIGNED BY M. Brackley		SIZE A4	FSCM NO.
DESIGN ACTIVITY			DWG NO. / FILE NAME 3 / Shaft.skd
CUSTOMER		SCALE 1mm = 1mm	DATE 23/6/99 SHEET 3 of 3